Development of Microfluidic Instrumentation for Application in the Diagnosis of Rare Anaemias

NIAMH AINE KILCAWLEY

Development of Microfluidic Instrumentation

for

Application in the Diagnosis of Rare Anaemias

Niamh Áine Kilcawley

Thesis submitted in partial fulfilment of the requirements for the degree of

Doctor of Philosophy

Supervisors: Dr. Margarita Staykova, Prof. John Girkin – Durham University

Dr. Timothy Ryan – Epigem, North Yorkshire

Department of Physics

Durham University

November 2022

Abstract

Globally, the number of children born every year with a rare anaemia exceeds 500,000. The symptoms of rare anaemias range, depending on the mutation, from mild to severe, and in many cases prove to be fatal. The geographical prevalence of rare anaemias is concentrated in developing countries where resources available for diagnosis and treatment are scarce. The gold standard diagnosis of rare anaemia requires a three-tier investigation which is costly and not readily available in the areas most afflicted. As such, there is a need for a low-cost and user friendly method of diagnosis for these diseases.

This thesis investigates the diagnostic abilities of a bio-chemical assay that exposes red blood cells to a low pH shock using microfluidic techniques. This involved the development of a novel low-cost microfluidic instrument, which has been named MeCheM, to run Lab-on-a-Chip devices. The experimental techniques and protocols developed are critically reviewed using healthy blood samples as the control. The results from the control population establish baselines for comparison against the diseased samples. Subsequently, the developed methods are investigated for diagnostic capabilities using rare anaemia blood samples.

The results from these investigations suggest that there are observable differences for the developed Flow Test in the case of the Thalassaemia and Hereditary Spherocytosis disorders. Similarly, the developed Cell-Surface Adhesion measurements highlighted significant differences among the Sickle Cell samples. Additionally, secondary investigations indicated correlations between the gold standard Red Blood Cell Count and the RBC Count as measured using MeCheM, and Mean Corpuscular Volume and Average Cell Projected Area (pre-acid addition). The development of MeCheM, a novel microfluidic instrument, as a stand-alone device is a key output from this body of work.

Research output

US Patent application number: *16604400*

Title: Microfluidic Device and Apparatus

Link: http://surl.li/dorsu

Description: A microfluidic test apparatus including a microfluidic device having a first reservoir for receiving a first fluid containing a sample of cells, a microfluidic test region, a first microfluidic pathway provided between the microfluidic test region and the first reservoir; and a port for connection to a pump, the apparatus including a first pump connected to the port and configured to pump a priming fluid into the port, a second pump connected to the port and configured to apply suction at the port when operated and a controller configured to control operation of the first and second pumps, where the controller operates the first pump to prime the microfluidic device and operates the second pump to draw a test volume from the first reservoir into the microfluidic test region.

"Once you make a decision,

the universe conspires to make it happen"

– Ralph Waldo Emerson

Declaration

The work presented in this thesis was conducted under the joint supervision of Dr. Margarita Staykova, Prof. John Girkin and Dr. Timothy Ryan. The experimental work was conducted on-site at Epigem Limited, United Kingdom; University of Zürich, Switzerland; Ha'Emek Medical Centre, Israel; and University Medical Centre, Utrecht. The results, analysis, figures, and text are all my own unless otherwise stated. None of the work in this thesis has been submitted for any other degree or qualification.

Acknowledgements

Whilst it has been a thoroughly enjoyable process, it has also been a lengthy one, so buckle up for these acknowledgements!

The first thanks must go to my supervisors; Dr. Timothy Ryan – thank you for three wonderful, busy, and ultimately inspiring years at Epigem. Your scientific optimism knows no bounds and I am grateful for all the conversations we've had over the years. Dr. Margarita Staykova and Prof John Girkin – thank you both for accepting me as a student and for always believing that this thesis would come to fruition! Your advice, particularly in the later stages of this project, has been invaluable and I have thoroughly enjoyed my time as a student at Durham University.

I would like to thank the team at Epigem for their engineering help with the project. In particular, I would like to express my sincere gratitude to my bio-lab partner, Simon Allen. Thank you for all your advice, scientific and life, during the years I was with Epigem, and for always being a calming influence during the busier times! Thanks to Saqib Ali in North Umbria University for the design and 3D printing of MeCheMs outer 'shell'!

A special mention must go to the wonderful Brenda Burns. Thank you for all the kindness you showed me (and continue to show me) while I was in Redcar. We have memories to last a lifetime and I feel incredibly lucky to have made such a wonderful friend.

I am incredibly grateful to the Marie Skłodowska-Curie Actions Fellowship Program for funding the work carried out in this thesis.

A massive thanks goes to the RELEVANCE family – without which none of this would be possible. Thanks to Anna Bogdanova and Asya Mahkro for their guidance, hospitality (and whiskey) during secondments to the University of Zürich.

Thanks to Prof. Ariel Koren for the opportunity to work and learn at the Ha'Emek Medical Centre, Israel. Thanks to Dr Carina Levin for graciously hosting me during my time in Israel – your kindness and generosity was greatly appreciated, I felt like part of

your family! Thanks to my colleagues Leonid and Etedal for showing me different sides to the region and making sure I didn't get into too much trouble!
Thanks to Dr Richard Van Wijk for inviting me to research at the group at University Medical Centre, Utrecht, and thanks to the many patients and volunteers who donated their blood to this work.

A special mention to Ario Sadafi who helped to develop the high magnification detection program used for cell analysis in this thesis – I will forever be indebted to you!

Thanks to all my fellow ESRs – you added a great element of fun and light-heartedness to all of the secondments, meetings and conferences that we attended together.

To Virginia Pretini who became, and still remains, a close friend throughout this project. Karaoke nights, video chats and weddings – you were there for them all. I'm so grateful for all the memories we have together – and looking forward to making some new ones too!

To Natasha Day (!), we have seen each other through all the milestones! Our coffee catch ups in Durham became zoom calls across waters and you have been the most wonderful confidante and friend throughout this process. Thank you for all your advice over the past few years and for always believing in the completion of this document – it meant more to me than you know!

My PhD journey began long before I realised that was the path I was going to take and there is really only one person to blame for that – Dave Kinahan! Dave, thank you for all the advice and friendship over the years. I firmly believe that had I not been so invested in the exciting research you were conducting in the microfluidics group in DCU I might not have considered further research after my undergrad at all. So really, this is all your fault! A 'wise' man once said "the only part of any thesis that's worth reading is the acknowledgements" … But I will quiz you on a random chapter of this someday.

A massive mention must go to Éadaoin Carthy! We started our journeys together in Physics and we have seen each other through all of the highs (and some lows!) of life, the universe and everything. You have always been someone I could turn to for advice when needed and I am so happy for you and all of your achievements – you must stop achieving someday so that someone else can have a go! I am very much looking forward

to whatever shenanigans we will get ourselves into next – might I suggest we involve some macrofluids this time!

I want to thank all my friends, and I am lucky to have so many. Each of you have helped me finish this thesis in some way, whether it was sending a text to check that I was still alive or bringing me out into the world to re-socialise me. Nothing has gone unnoticed or unappreciated. I would especially like to thank the best group of friends I could ask for – Méabh, Emily and Marie. You have seen this process from beginning to end and have always been so supportive and encouraging. We are all on our own journeys and I am so proud and excited for each of you. Thank you for being there for me, particularly in the last couple of years. I'm looking forward to many celebrations with you!

To my family – thank you for not asking too many questions and for nodding enthusiastically when I explained some abstract part of this thesis without any background context!

To my parents, Mary and Brian, thank you for always believing in me and for encouraging me to pursue research. In particular, thank you for pushing me to finish this thesis when its completion seemed almost impossible! I am incredibly grateful to you both for everything you have done for me over the years, and I am very lucky to have such wonderful parents. I promise I will leave college now…

To my brothers, Liam and Eoin, thank you both for your encouragement over the years and for bringing me back down to earth when I needed it (even if you didn't know I did!).

To my sister, Sinéad, who gets a separate mention because she demanded it (!!). Thank you for listening to me when I went on rants about all things science related and for generally being the best sister. I am so proud of everything you have achieved so far and am very excited to see where this next chapter of your life takes you – dancer extraordinaire!!

To my wonderful gran, Nen, thank you for the great advice you have given me over the years and for your continued patience with my questionable baking skills!

To Frank, Patricia, Anna, Feargus, Charlie and Georgia. Thank you all so much for the kindness and compassion that you've shown me over the years. I am looking forward to

celebrating with you all and encouraging/discouraging Charlie and Georgia from doing PhDs in the future!

And finally, to my husband Michael. We met in the middle of all of this madness, and you have been the *most* supportive and understanding person. There aren't enough words to describe how grateful I am to have had you by my side throughout this process, particularly in the last couple of years. You have seen all the highs and the lows and have always encouraged without ever putting pressure on me. You have been and continue to be my biggest supporter, and I can't thank you enough for everything you've done for me. I could not have finished this without you. I am so excited to see what the next few years brings, and even more excited to have you with me on this crazy journey. This thesis is dedicated to you xxx

List of abbreviations

BTI	β-thalassaemia Intermedia.
BTM	β-thalassaemia Major.
BTm	β-thalassaemia Minor.
CAD	Computer Aided Design.
CBC	Complete Blood Count.
EMA	Eosin-5'maleimide test.
FOV	Field of View.
G6PD	Glucose-6-Phosphate-Dehydrogenase Deficiency.
Hb	Haemoglobin.
HS	Hereditary Spherocytosis.
HX	Hereditary Xerocytosis.
LHS	Left Hand Side.
LoaC	Lab-on-a-Chip.
LoaD	Lab-on-a-Disc.
MCH	Mean Corpuscular Haemoglobin.
MCV	Mean Corpuscular Volume.
OFT	Osmotic Fragility Test.
PKD	Pyruvate Kinase Deficiency.
POC	Point-of-Care.
RBC	Red Blood Cell.
RBC count	Red Blood Cell count.
RDW	Red cell Distribution Width.
RHS	Right Hand Side.
SCD	Sickle Cell Disease.

Contents

Chapter 1 Introduction

1.1 Anaemia

Globally, anaemia affects approximately 1.93 billion people, with Iron Deficiency Anaemia (IDA) being the most common form of this blood disorder.[1,2] Typically, iron deficient red blood cells (RBCs) are smaller in size, with lower levels of haemoglobin (oxygen carrying protein) and ferritin (iron carrying protein). Most forms of IDA are mild and can be treated with dietary changes and iron supplements. Blood transfusion is also a treatment option in more severe cases.[3]

However, there is an uncommon sub-group of anaemias described as 'rare', 'hereditary', or 'inherited', that are much more complicated with respect to both their diagnosis and treatment. These hereditary anaemias range from mildly symptomatic to fatal and their prevalence largely dominates in developing countries.[4]

1.2 Rare anaemia in developing countries

Although the prevalence of rare anaemias is increasing in Europe due to immigration, most cases are found amongst the ethnic populations of Sub-Saharan Africa, Mediterranean countries, Southeast Asia and India.[4–8]

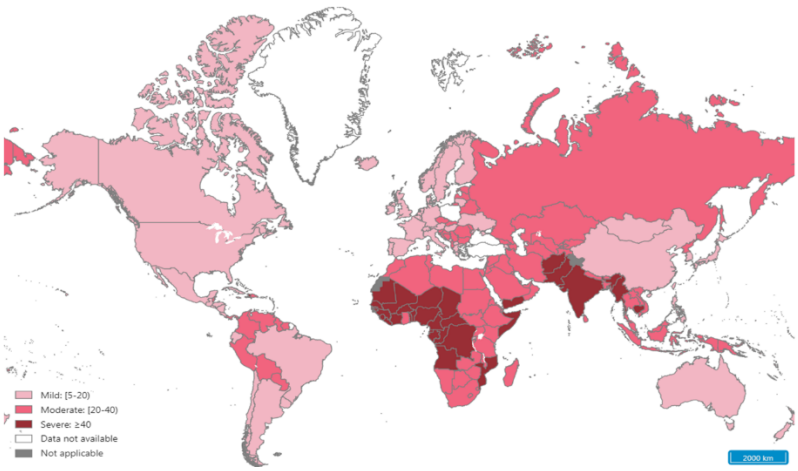

Figure 1-1 Data from the World Health Organisation (WHO) on the global prevalence of iron deficiency and inherited anaemia in women of reproductive age shows that >40% of the cases are found in Sub-Saharan Africa, the Middle East and India.[9] Data is described as percentage. Image sourced from WHO website, 2021.[10]

The predominance of RBC disorders in these regions is related to the following factors; (i) the association between consanguineous relationships and genetic disorders, and (ii) the protection afforded against Malaria by the heterozygous sickle cell trait.[11,12]

1.2.1 Consanguineous relationships

A consanguineous relationship is described as a union with a close family member such as a first or second cousin.[13] Such close relationships do not provide enough gene heterogeneity. Elevated gene homogeneity increases the risk of autosomal recessive gene mutations.[14] Many inherited diseases can be traced back to consanguineous relationships.[14,12]

Inbreeding is almost non-existent in Europe due to the prohibition of marriage if the individuals are within 4 degrees of consanguinity by Roman civil law, with the notable exception of European nobilities.[15] There is a high prevalence of consanguineous marriage in regions, such as Sub-Saharan Africa, the Middle East and Southeast Asia, that are the most effected by inherited anaemia.[16]

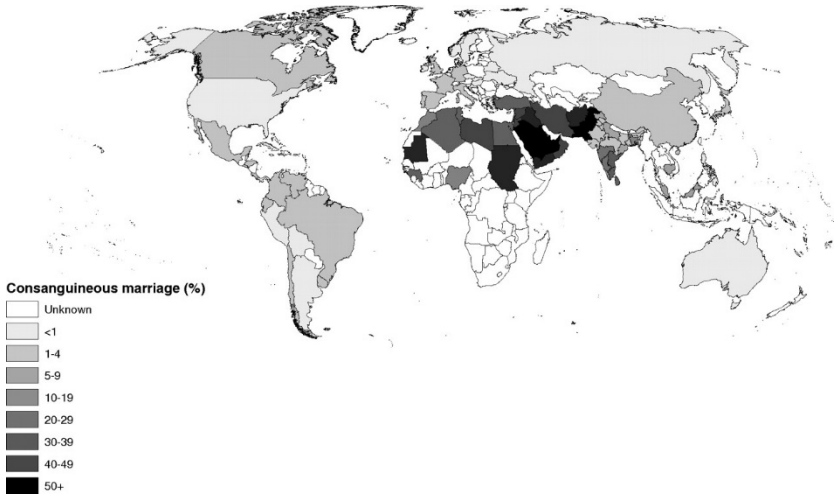

Figure 1-2 Worldwide distribution of consanguineous relationships from Bittles and Black shows high percentages in regions most affected by anaemia.[16] Reprinted with permission from Bittles and Black.

The low socio-economic status of these localities also contributes to the issues of the inherited disorders and consanguinity.[7] In developing countries, there is often less access to education, particularly for females, and it is characteristic that couples will marry and become pregnant at an early age.[16] The insufficient education means that, in many cases, people are not aware of the risks associated with consanguineous relationships, owing to their prevalence in developing countries.

1.2.2 Malaria paradox

Malaria is a life-threatening disease caused by the bite of a female mosquito infected with the parasite *Plasmodium Falciparum*.[17] According to the *World Malaria Report 2019* by the WHO, 93% of worldwide Malaria cases were recorded in the Africa region, with 19 countries in Sub-Saharan Africa and India carrying almost 85% of those cases.[18]

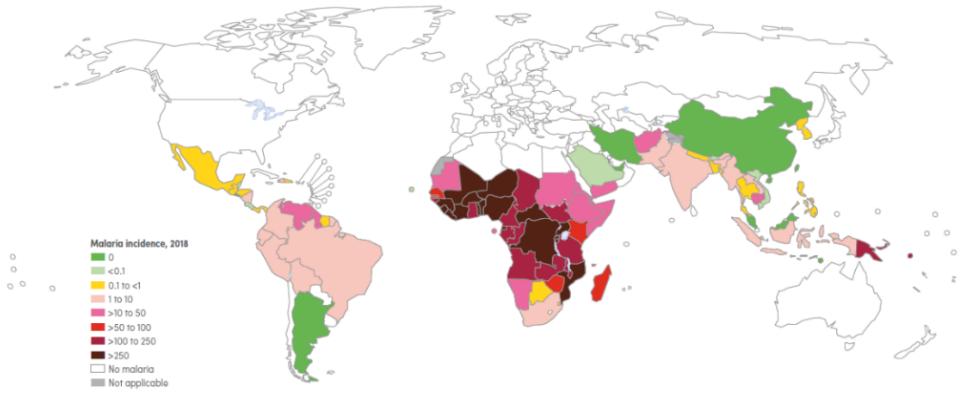

Figure 1-3 Global incidence of Malaria, from the World Malaria Report 2019, shows the case incidence rate per 1000 at risk population.[18] Source: WHO estimates.

Interestingly, the regions with high incidence of Malaria also show a high rate of infants born with Sickle Cell Disease (SCD).[19]

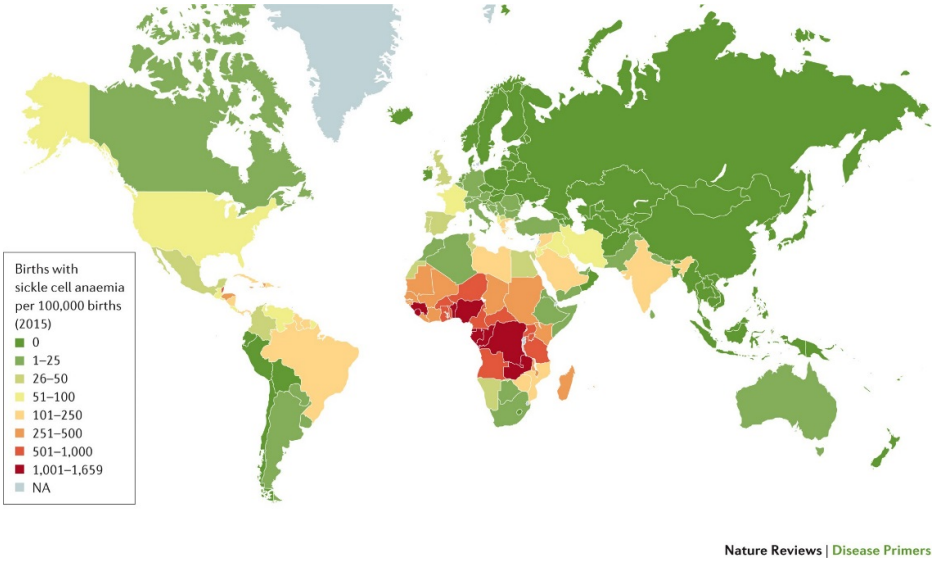

Figure 1-4 Incidence of infants born with Sickle Cell Disease show the majority of cases are found in Sub-Saharan Africa and India.[19] Reprinted with permission from Springer Nature.

The correlation between SCD and Malaria is not coincidental. In fact, links between both diseases have been reported in multiple studies.[20–22] For carriers of the sickle cell trait, HbS, it has been found that the HbS gene mutation affords some protection against Malaria upon infection.[17,23]

Whilst individuals with the HbS trait can succumb to Malaria, it is rare that the contraction of Malaria will prove to be fatal.[23] Research conducted by *Archer et al.* reports that the polymerization of HbS upon deoxygenation is responsible for the growth arrest of the *Plasmodium Falciparum* parasites.[21] It is suggested that this is the mechanism responsible for the protection afforded against Malaria by the HbS trait.

1.3 Sub-divisions of Rare Anaemia

Rare anaemia is an umbrella term that covers a range of mutations of the red blood cell. These mutations can be classified into haemoglobinopathies, membranopathies and enzymopathies.

Any mutation associated with the haemoglobin protein is categorized as a haemoglobinopathy. Mutations of the red blood cell membrane are classified as membranopathies and, similarly, mutations associated with the enzymes of a red blood cell are referred to as enzymopathies.

1.3.1 Haemoglobinopathies

Haemoglobin (Hb) is the most abundant protein the in red blood cell and is vital for oxygen transport around the body.[24] For a healthy individual, the adult haemoglobin molecule consists of 4 protein sub-units; 2 sub-units of α-globin and 2 sub-units of β-globin.

Each of these 4 sub-units are attached to haeme which contains an iron atom in its centre.[25] One iron molecule will bind to one oxygen molecule and there are approximately 270 million haemoglobin molecules per red blood cell.[26] The optimal functioning of haemoglobin is absolutely critical for oxygen delivery. Abnormalities in this protein will diminish the oxygen-carrying capacity of the RBC which can result in serious and life-threatening conditions.

Approximately 7% of the global population carries a trait for a mutant haemoglobin making it the most common form of inherited anaemia worldwide.[27] Haemoglobinopathies are divided further into 2 sub-categories; (i) Thalassaemias, and (ii) Sickling disorders.[28]

(i) Thalassaemias

Thalassaemias are caused by mutations of the α and/or β-globin sub-unit of the haemoglobin molecule.

α-Thalassaemia

Alpha-thalassaemia is caused by anomalies (reduced; α^+ and/or absent; α^0) in the production of the α-globin chains of haemoglobin[29]. The severity of anaemia varies from mild (if only one gene is involved) to severe (no expression of α-genes).

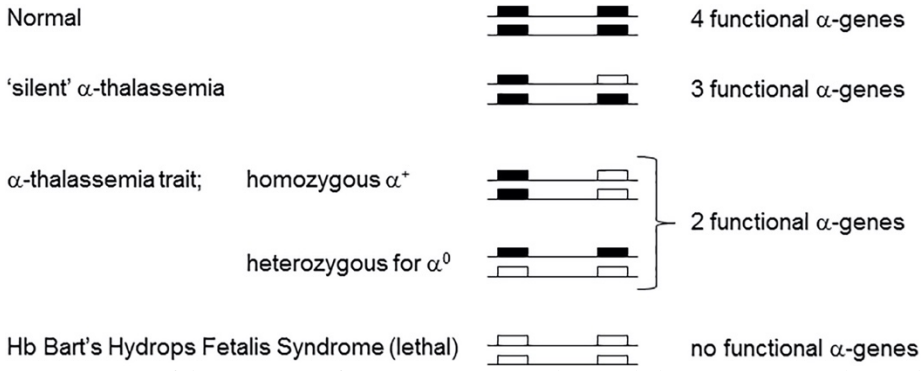

Figure 1-5 Categorization of the variations of α-gene mutations. 'Silent' α-thalassaemia is termed as such due to the mild anaemic clinical presentation. α-thalassaemia trait is characterised by microcytic anaemia and is often misdiagnosed as iron deficiency anaemia. Hb Bart's Hydrops Fetalis Syndrome is fatal if not treated immediately. If the child survives birth, it will have irreversible abnormalities and will require lifelong transfusions.[29] Reprinted with permission: © 2018 The Authors. Published by Elsevier Inc.

The α-Thalassaemia trait can be misdiagnosed as iron deficiency anaemia due to both disorders displaying microcytic red blood cells.[30] Undiagnosed α-deletion types can increase the risk of carrying a foetus with Hb Bart's Hydrops Fetalis Syndrome which often results in foetal demise by the third trimester.[31] In addition to miscarriage, women carrying a foetus with Hb Bart's Hydrops Fetalis Syndrome have a heightened chance of developing severe pre-eclampsia throughout the pregnancy.[32]

Correct and early diagnosis of the α-Thalassaemia trait is essential to provide the individuals/families with information about the risks of this inherited disease.

β-Thalassaemia

Beta Thalassaemia is characterised by reduced (β^+) or absent (β^0) synthesis of the β-globin chains on the haemoglobin molecule.[33] β-thalassaemia is a heterogeneous disease with over 200 mutations identified thus far.[34] The disease can be further divided into 3 sub-categories; (i) β-Thalassaemia Minor, (ii) β-Thalassaemia Intermedia, and (iii) β-Thalassaemia Major.

As the name might suggest, β-Thalassaemia Minor (BTm) is the least severe of the 3 sub-categories. In this condition, there is one mutated or deleted β-globin gene alongside one fully functional β-globin gene[33]. Affected individuals typically display mild anaemic symptoms and often don't require a treatment plan.[35]

However, despite the relatively benign presentation of BTm, the correct diagnosis of the disease is essential as parents carrying the β-Thalassaemia Minor trait have a 25% chance of conceiving a child that will suffer from the fatal β-Thalassaemia Major.[36]

β-Thalassaemia Intermedia (BTI) is a homozygous disease of moderate severity caused by 2 defective β-globin genes which results in decreased function of the red blood cell.[37] The clinical presentation of BTI is generally more pronounced than BTm with patients sometimes displaying retardation of growth and development.[33] Individuals affected by BTI are also at risk of facial deformities and osteoporosis, among other bone abnormalities, due to hypertrophy of erythroid marrow.[38]

Treatment of BTI is dependent on the clinical manifestation of the disease in the patient and can include splenectomy, drug therapies and blood transfusions.[39]

β-Thalassaemia Major (BTM) is a life-threatening homozygous disease caused by 2 defective β-globin genes.[34] With a predicted survival rate of only 50% for patients suffering with BTM by aged ~29, it is essential that this disease is diagnosed as early as possible to increase patient quality of life.[40]

Frequent blood transfusions are the most common form of treatment for BTM. If a patient does not undergo transfusion often, it is likely they will die from high-output heart failure.[33]

Unfortunately, there are many complications associated with frequent blood transfusion such as; growth retardation in children, failure to reach sexual maturation, liver fibrosis, hypersplenism among others.[41,42,43]

As mentioned previously, carriers of the β-Thalassaemia Minor trait are at risk of conceiving a child with BTM. Genetic screening for BTm is an option available to some

families, however, it is not a universal solution. Most of the affected areas are located in the developing world and genetic screening is often not financially possible.[44] The lack of genetic screening results in significant numbers of infants born with BTM which puts a severe burden on the patients, their families and health services.[45]

(ii) Sickling disorders

Healthy RBCs have a specific biconcave morphology which is optimal for oxygen transport and delivery.[46] The discus shape of the RBC allows for the compression required for its passage through the small capillaries and vessels of the body.[47] Any shape which deviates from this disc-like architecture will result in reduced oxygen delivery.[48] Such is the case for sickling disorders.

Sickling disorders, more commonly referred to as Sickle Cell Disease (SCD), is a blanket term which covers a range of haemoglobin mutations that result in the loss of the biconcave shape referred to as sickling of the RBC.

SCD was first reported in 1910 by *James Herrick* with the observation of irregularly and sickled shaped cells, as such, the term 'sickle cell' was coined.[49] The specific mutation which generates SCD is caused by a single amino acid substitution (glutamic acid for valine) in the β-globin sub-unit of Hb.[19] This substitution produces the mutant HaemoglobinS (HbS). Upon deoxygenation, HbS crystallises creating polymers of haemoglobin which give the sickle cell its characteristic sickle shape.[50]

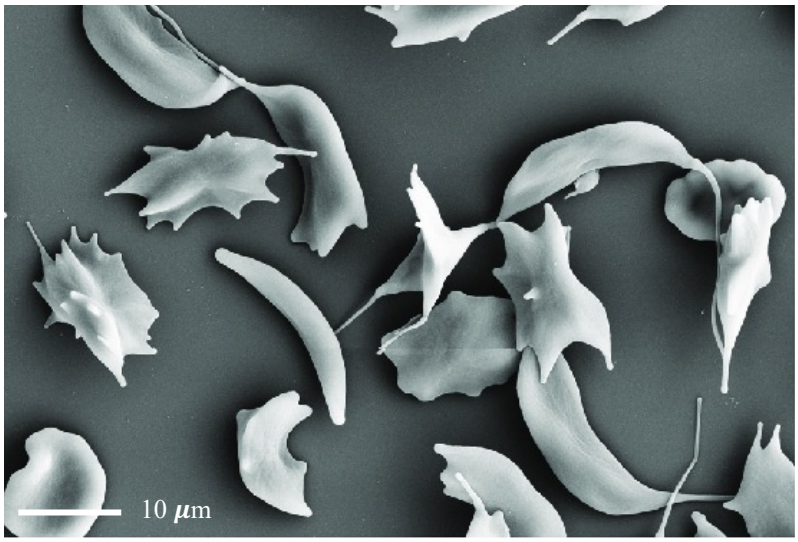

Figure 1-6 Scanning electron microscope image of sickled RBCs adapted from Abay et al.[51]Reprinted with permission: © 2019 Abay, Simionato, Chachanidze, Bogdanova, Hertz, Bianchi, van den Akker, von Lindern, Leonetti, Minetti, Wagner and Kaestner.

Sickled RBCs show a great reduction in cell deformability which limits their travel through the narrow capillaries of the body.[52] This reduces oxygen delivery to tissues and can result in acute vaso-occlusive pain.[53]

Patients suffering with SCD also have a range of other associated complications and comorbidities including chronic pain, heart failure, kidney problems, liver disease, delay in growth and puberty, increased risk of stroke, and premature death among many others.[54,55,56]

SCD can present itself as homozygous (HbSS) or heterozygous (HbS), where HbS is a carrier of the trait and HbSS is severely clinically symptomatic.[57] There are other variations of HbS which can also induce sickling such as; HbSC, HbSE, HbSβ, and others.[58]

SCD can be cured by the patient undergoing allogeneic haematopoietic stem cell transplantation (HSCT).[59,60] However, this procedure is not frequently conducted due to difficulties in finding matched donors, the procedural risks involved and the overall associated expense.[60,61,62] More generally, the primary treatments of SCD are regular blood transfusions and drug therapy (Hydroxyurea).[54]

Parents carrying the HbS trait also have a 25% of conceiving a child with homozygous SCD. Although there are screening tests for SCD, they are not readily available in Sub-Saharan Africa where the disease is most prevalent resulting in high numbers of infants born with the hetero/homozygous sickle cell disease.[63,64,65]

1.3.2 Membranopathies

The erythrocyte membrane is ~8 μm in diameter, ~2 μm in thickness and adopts a discocyte shape.[66] This biconcave architecture allows for optimal flow through the small vessels of the body.[67] The geometry of the RBC is maintained by a complex 2-dimensional membrane structure, consisting of a cytoskeleton anchored to a lipid bilayer via membrane proteins.[68,69,70] RBCs have unique and extraordinary membrane properties which allow their deformability along a linear axis up to 250%. However, just a 3 – 4% increase in surface area will result in haemolysis.[71]

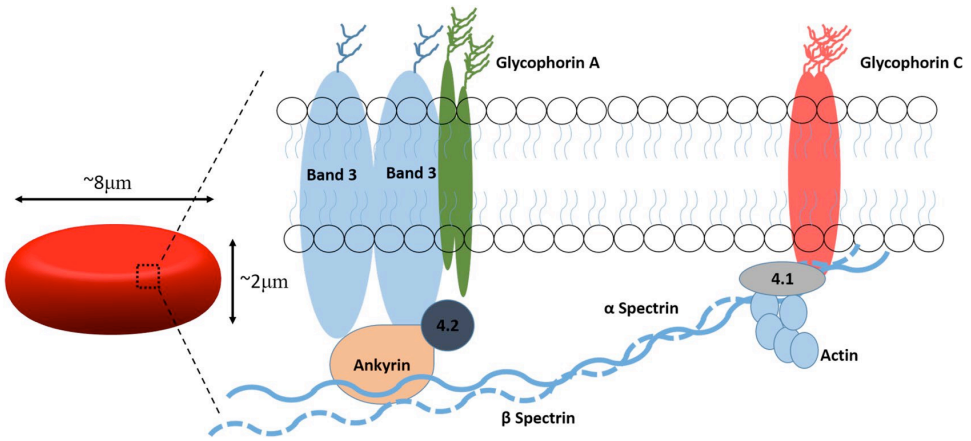

Figure 1-7 Schematic diagram from Paradkar and Gambhire[72] of the RBC membrane structure displaying the peripheral (spectrin, 4.1R) and integral (Band 3, Rh complex) proteins. Reprinted with permission from Springer Nature.

RBC membrane proteins are classified into 2 distinct groups; (i) peripheral membrane proteins, and (ii) integral membrane proteins.[73] A filamentous network of peripheral proteins (Spectrin, Actin, protein 4.1R, to name a few) are located on the cytoplasmic surface of the phospholipid bilayer.[68]

These proteins are commonly referred to as the membrane skeleton and are responsible for the membrane elasticity and mechanical stability of the RBC.[68] Integral proteins (Band 3, Aquaporin-1, glycophorins) are anchored into the lipid membrane through hydrophobic, electrostatic and other non-covalent interactions with lipids in the bilayer.[74]

These proteins are responsible for the transport of anions across the cell surface.[75] Abnormalities of these membrane proteins can result in fatal diseases such as Hereditary Spherocytosis (HS)[76,77,47] and other RBC disorders.[48]

(i) Hereditary Spherocytosis

Hereditary spherocytosis (HS) is an umbrella term referring to a group of heterogeneous inherited membrane defect disorders which result in the spherical appearance of the RBCs.[78] HS is the most common red cell membrane disorder with a prevalence of 1:2000-5000 in people of Northern European descent.[79] Deformities in the membrane proteins band 3, spectrin, ankyrin and/or protein 4.2 are typically found as the cause of HS and there is a multitude of isolated gene mutations encoding these membrane proteins.[80]

HS can range in disease severity from asymptomatic to the patient requiring regular blood transfusions.[6] Early diagnosis is advantageous as delays in treatment can cause long-term complications such as gall stones and severe anaemia.[81] The most common laboratory diagnostic tests for HS are; (i) Complete Blood Count (CBC), (ii) Eosin-5'-maleimide (EMA) Test, (iii) Plasma Membrane Protein Electrophoresis, and (iv) Osmotic Fragility Test (OFT).

Although a general diagnosis of Hereditary Spherocytosis can be inferred from the CBC, OFT and EMA tests, specific diagnosis involves a more complex and expensive test.[81,82] A low-cost test with specific mutation diagnosis would be very beneficial for the patients and for future research of Hereditary Spherocytosis.

(ii) Elliptocytosis

Hereditary Elliptocytosis (HE) refers to a group of red cell membrane disorders which are characterised by the elliptical shape of the RBCs.[83] Like Hereditary Spherocytosis, HE is highly heterogenous with genetic mutations found in the spectrin, band 3 and protein 4.1 membrane proteins of the RBC.[69] HE can be classified into the following sub-categories; (i) HE trait, (ii) typical HE, (iii) Pyropoikilocytosis, and (iv) Neonatal Poikilocytosis. In the case of HE trait and typical HE the symptoms are rare, however, for Pyropoikilocytosis the anaemic effects are severe and patients will require regular blood transfusions to improve quality of life.[76]

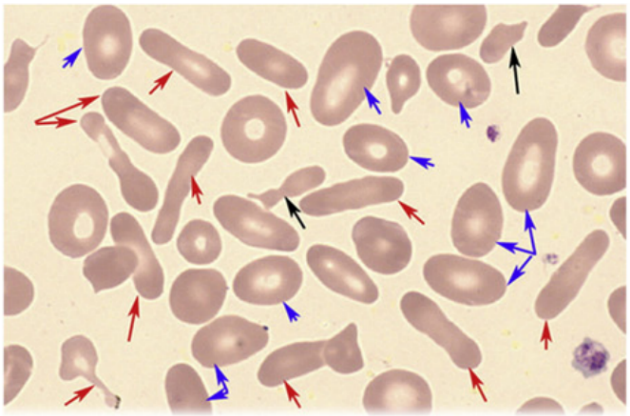

Figure 1-8 Pyropoikilocytosis blood sample image from Da Costa et al.[83] with characteristic elliptical cells (red arrows), ovalocytic cells (blue arrows) and fragmented cells (black arrows). Reprinted with permission: © 2013 Elsevier Ltd. All rights reserved.

Neonatal Poikilocytosis presents clinically as severe haemolytic anaemia in the first year of life and often requires regular blood transfusions throughout that period. Typically by

the second year, the symptoms will have subsided and the infant will experience mild Hereditary Elliptocytosis.[83,84]

The clinical diagnosis of HE is similar to HS with a focus on aberrant RBC morphology, protein 4.1R deficiency and spectrin variants.[76]

1.3.3 Enzymopathies

Lacking a nucleus and other cytoplasmic cell organelles, the mature RBC requires 3 fundamental metabolic pathways to carry out transport and delivery of oxygen around the body; (i) anaerobic glycolysis, (ii) anti-oxidant pathways, and (iii) nucleotide metabolism.[85]

Anaerobic oxidation of glucose (glycolysis) is the exclusive source of energy for the RBC. Glycolysis is responsible for maintenance of RBC structure and function.[86]

Anti-oxidant pathways are essential to maintain cellular oxidant and anti-oxidant homeostasis.[87] Although oxidants serve an important role in the RBC, an excess can lead to damage of cellular components.[88] Thus, the role of the anti-oxidant pathways is to preserve the balance of oxidants within the RBC thereby allowing for the protection of the RBC components.

Nucleotide metabolism supports the production of ATP and guanosine triphosphate (GTP) by providing the substrates adenine monophosphate (AMP) and adenine diphosphate (ADP).[89] The optimal functioning of these enzymes is critical for the maintenance of the RBC membrane.

Enzymopathies are inherited disorders of the red cell enzymes which can emerge as point mutations, insertions, deletions or splice defects.[90] These abnormalities are the cause of inherited anaemias termed ‘hereditary non-spherocytic haemolytic anaemia’.[91] Unlike haemoglobinopathies and membranopathies, enzymopathies often show no visible morphological abnormalities rendering them difficult to diagnose via conventional clinical methods.[90,92] The 2 most commonly observed enzymopathies are Pyruvate

Kinase Deficiency (PKD) and Glucose-6-Phosphate-Dehydrogenase Deficiency (G6PD).[90]

(i) Pyruvate Kinase Deficiency

Pyruvate Kinase Deficiency is a chronic haemolytic anaemia whereby the patient's blood cells undergo premature haemolysis.[93] PKD is caused by a recessive enzyme defect of the glycolytic pathway.[94] The Pyruvate Kinase enzyme regulates glycolysis which is essential for ATP production in the RBC thus a mutation in this enzyme will result in an ATP shortage.[95] This ultimately affects the deformability of the RBC which results in a shortened life span. PKD can present a range of clinical manifestations from asymptomatic to hydrops fetalis.[96,97]

The haematological indices of PKD are similar to those observed in other red cell disorders.[98] These similarities give rise to challenges with discerning one disorder from another using the standard clinical testing.

As the haematological indices of PKD are non-specific, the diagnosis typically follows exclusion of any other red cell disorders.[99] For specific diagnosis, there must be a demonstration of decreased enzyme activity and/or the identification of mutations in the PKLR gene.[97]

There are 2 gold standard methods for diagnosing PKD at present; (i) measurement of PK enzyme activity in RBC lysates with confirmation by DNA sequence analysis of PKLR, (ii) screening by NGS panels.[100–102]

Although these approaches are the most widely used, they have some drawbacks. The assay for the detection of PK enzyme activity may give false results due to a high number of immature red blood cells (reticulocytes) and interference of donor RBCs from transfused individuals. Confirmation by DNA sequencing analysis has many advantages such as relatively rapid time to achieve results (2-10 working days) and low cost with high sensitivity and specificity. However, DNA sequencing is unable to differentiate between homo/heterozygous carriers and can face interference from the same issues mentioned above for the detection of enzyme activity.[99]

Recent advances in Next Generation Sequencing (NGS) has been showing success for genetic mutation diagnosis.[92,103,104] However, although NGS can give highly accurate diagnosis, there is a lot of data complexity caused by a large number of variants of unknown clinical significance.[103]

(ii) Glucose-6-Phosphate-Dehydrogenase Deficiency

Glucose-6-Phosphate-Dehydrogenase is an enzyme located in the RBC cytoplasm which holds a crucial role in the prevention of damage to the RBC due to reactive oxygen species (ROS). ROS is an unstable oxygen-containing molecule which reacts with other molecules in a cell. Premature haemolysis of the RBC can be caused by oxidative stress due to abnormally high levels of ROS.[105] Deficiencies or mutations of the G6PD enzyme can generate an acute haemolytic anaemic response throughout the production of ROS.[106]

Most carriers of the G6PD deficiency are asymptomatic.[106] For symptomatic individuals, a jaundice complexion is present along with haemolytic anaemia occurring shortly after the onset of an infection, exposure to a new chemical or drug, and/or ingestion of fava beans.[105] Typically, individuals with G6PD deficiency will not require treatment beyond the removal of oxidative stressors from their diet. Iron and folic acid supplements can be helpful during a haemolytic episode but are generally not necessary.[106]

Diagnostic tests for G6PD deficiency are akin to those of the aforementioned PKD with the initial testing of the enzyme activity levels, followed by confirmatory DNA sequence analysis and, if appropriate, NGS sequencing.[106]

1.4 Diagnosis of rare anaemias

1.4.1 Clinical practices for diagnosing rare anaemias

Multiple rare anaemia disorders can present similar clinical features upon preliminary evaluation of a complete blood count (CBC). The implication of this is that the specific diagnosis of these inherited blood disorders can require several lines of investigation comprising; (i) clinical investigations, (ii) biochemical testing, and (iii) molecular analysis.[107]

(i) Clinical investigations

Complete blood count analysis includes a battery of tests used as the first investigative layer in diagnosing a rare anaemia.[4] Typically, the initial focus is on the following parameters; (i) Red Blood Cell Count (RBC Count), (ii) Haemoglobin Concentration (Hb), (iii) Mean Corpuscular Volume (MCV), (iv) Mean Corpuscular Haemoglobin Concentration (MCHC), (v) Red Cell Distribution Width (RDW), and (vi) Reticulocyte Count.[108]

Test	Description
RBC count	The average healthy human will have an RBC count between 3.92 – 5.61 x 10^{12}/L.[109] Decreased RBC counts may suggest premature removal of RBCs from the circulatory system which could be indicative of their health status and suggest the presence of anaemia.
Hb concentration	Hb concentration quantifies the amount of Hb per RBC. Low levels of Hb are typical in patients with both iron deficiency and inherited anaemia.[110,33]
MCV	MCV results indicate the average size of the RBCs in a sample. A low MCV result could suggest microcytic anaemia, which is common in iron deficiency anaemia or Thalassaemia.[111]
MCHC	MCHC considers the amount of Hb per unit volume of the RBC. It is not unusual for a patient with hereditary spherocytosis to show a high result for MCHC.[112] MCHC is also observed in theThalassaemias.[113]
RDW	RDW measures the size distribution of the RBC sample. Patients with Sickle Cell Disease often display higher values in contrast to a healthy sample.[114]
Reticulocyte count	Reticulocytes (immature RBCs) are produced at a higher rate if the body requires compensation for premature RBC destruction, indicating the presence of a haemolytic anaemia. Contrary to that, reticulocytes are produced at a lower rate if the anaemia is caused by erythropoietic insufficiency.[4]

Table 1-1 Preliminary investigations to decipher whether the patient has anaemia are carried out via CBC analysis. Although these can point a clinician towards an anaemic diagnosis, the results are not disease specific and further testing is required to determine the type of anaemia.

In addition to a CBC, peripheral blood smears (PBS) can also give an insight into the possible cause of anaemia through visual examination. This is particularly important for rare anaemias that display morphological deformities, for example, SCD where the RBCs are abnormally sickle shaped.[115]

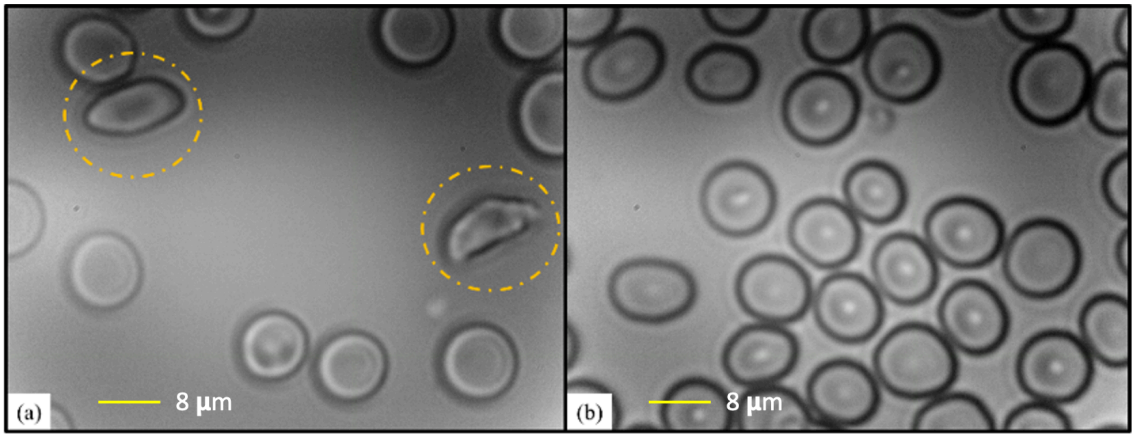

Figure 1-9 Peripheral blood smear of a blood sample from a patient positive for SCD, (a), and a healthy control, (b). The abnormally shaped cells in (a) are highlighted with a yellow circle. Image obtained from work conducted within this thesis.

CBC and PBS coupled with knowledge of the familial history help to point clinicians in the right direction for more in-depth rounds of testing.

(ii) Biochemical testing

Biochemical testing is used to further reduce diagnostic ambiguity by either eliminating or highlighting certain disease phenotypes. Clinicians will carry out a variety of biochemical tests depending on the suspected anaemia, some of which are described in *Table 1-2* below.

Method	Description
Sickling test	HbS will tend to sickle under low oxygen conditions. The Sickling test introduces an oxygen depletion chemical to the blood sample to induce sickling of the RBCs if HbS is present. This sicking can be observed with the use of a microscope.[116]
Solubility test	For a blood sample containing HbS, incubation with sodium dithionate will produce a turbid solution due to precipitation of HbS. In contrast, a healthy control (HbA) will appear clear, albeit with a red colouring.[117]
Electrophoresis	Electrophoresis is based on the principle that proteins contain either a positive or negative charge which is determined by their amino acid sequence. Upon the application of an electric field, the migration of proteins will either be in favour of the cathode (positively charged proteins) or the anode (negatively charged proteins). A stain is applied to visualise the locations of the Hb bands. For the typical HbA, there is a characteristic band, and this will differ in the case of a mutated Hb (HbS, HbE, Hbα, Hbβ).[118]
EMA binding test	The Eosin 5-Maleimide (EMA) binding test is used in the diagnosis of HS. EMA is a dye that binds to the Band 3 protein on the RBC membrane. For HS and other membranopathies the levels of Band 3 binding will be reduced in comparison to a healthy blood sample. The samples are analysed via their fluorescent intensity output during flow cytometric investigations.[76]
AGLT test	The Acidified Glycerol Lysis Test (AGLT) uses acidified glycerol to lyse RBCs. A spectrophotometer measures the turbidity of the solution, and thus, the cell lysis over time. Output results are analysed as the time taken to achieve 50% lysis. Results showing < 5 minutes are typically classed as pathological and suspect for HS.[119]
OFT	The principle behind the Osmotic Fragility Test (OFT) is that healthy RBCs will lyse within a certain timeframe upon exposure to a hypotonic solution. For a patient with HS, the osmotic fragility of the cells will be increased thus they will lyse quicker than a healthy sample. In comparison, the dehydrated sickle cell will take longer to complete lysis.[120,121]

Table 1-2 Listed above is a non-exhaustive list of tests conducted following preliminary haematological testing. The results of the investigations list in the table above are used as good indicators for disease type, but samples will still require confirmatory testing.

High-performance liquid chromatography

High-performance liquid chromatography (HPLC) is the favoured laboratory method due to its high sensitivity and specificity for detection of the most prevalent haemoglobin

variants and its fast turnaround time (< 3 minutes). The basic principle behind HPLC is that proteins with a greater charge will move more slowly through a chromatography column. The time taken for this passage is termed the 'retention time'.[116] HPLC allows for the separation and quantification of the various types of haemoglobins as each Hb protein will possess a different charge and therefore the retention times should also differ.

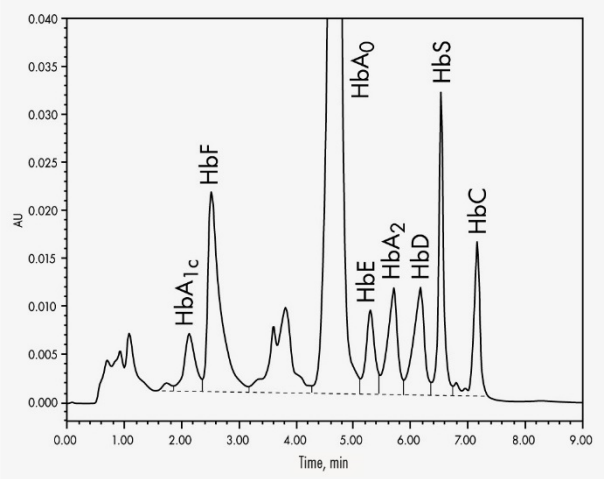

Figure 1-10 Chromatogram output adapted from ChromSystems showing the characteristic retention times for various haemoglobin types. HbA_0 is normal, healthy adult Haemoglobin and should be the most prevalent Hb in a healthy adult individual.[122] *© 2023 Chromsystems Instruments & Chemicals GmbH.*

A disadvantage with this method is that some haemoglobin variants will have a retention time in a similar or identical range.[123] This is clearly a problem as clinicians could misdiagnose a patient based on HPLC results. Thus, a confirmatory test must be conducted to ensure the reliability of the diagnosis.[116]

As previously mentioned, biochemical testing is not used for conclusive diagnostic purposes. Clinicians are required to analyse the results from the preliminary clinical investigations and the biochemical testing to determine a possible diagnosis and take this knowledge forward to the final stage of testing: molecular analysis.

(iii) Molecular analysis

The final, and confirmatory, step in diagnosing an inherited anaemia is the application of molecular diagnostic techniques such as DNA sequencing, Polymerase Chain Reaction (PCR), and Next Generation Sequencing (NGS). These methods are highly sensitive and require trained personnel for their operation.[124–126]

Polymerase chain reaction

PCR is a widely utilised laboratory technique for the amplification of short DNA sequences from a relatively low number of copies.[127] PCR techniques have been transformative in molecular diagnostics for a range of areas including forensics, infectious diseases and, of course, inherited disease diagnosis.[128,129]

Although PCR is a highly sensitive and specific method for highlighting known mutations,[124] the heterogeneous nature of the inherited RBC disorders would likely provide previously undiscovered gene sequence mutations. As PCR is dependent on some knowledge of the DNA sequence of interest, unknown sequences would present a diagnostic challenge.

Next Generation Sequencing

NGS is a method by which the nucleic acid sequence of a sample is determined.[126] It is a relatively recent technological advancement but its ability to detect a range of genetic variants has already transformed the diagnostic field. As such, it is clear to see that this technique is imperative for not only the confirmatory diagnosis of rare anaemias, but also for new genetic mutation discovery.

Agarwal et al. have successfully demonstrated NGS as a highly sensitive molecular diagnostic approach for hereditary anaemias.[92] However, the use of NGS is not a universal solution in many cases considering the expense (£6000 - £7000) and time (~ 4 hours) required to obtain results.[130,131] Particularly, employing NGS remains unrealistic in many countries where these blood disorders are most prevalent.[132,133,134]

With the vast majority of rare anaemias predominant in developing countries, a low-cost, point-of-care device would be invaluable in the diagnosis of these diseases.[135]

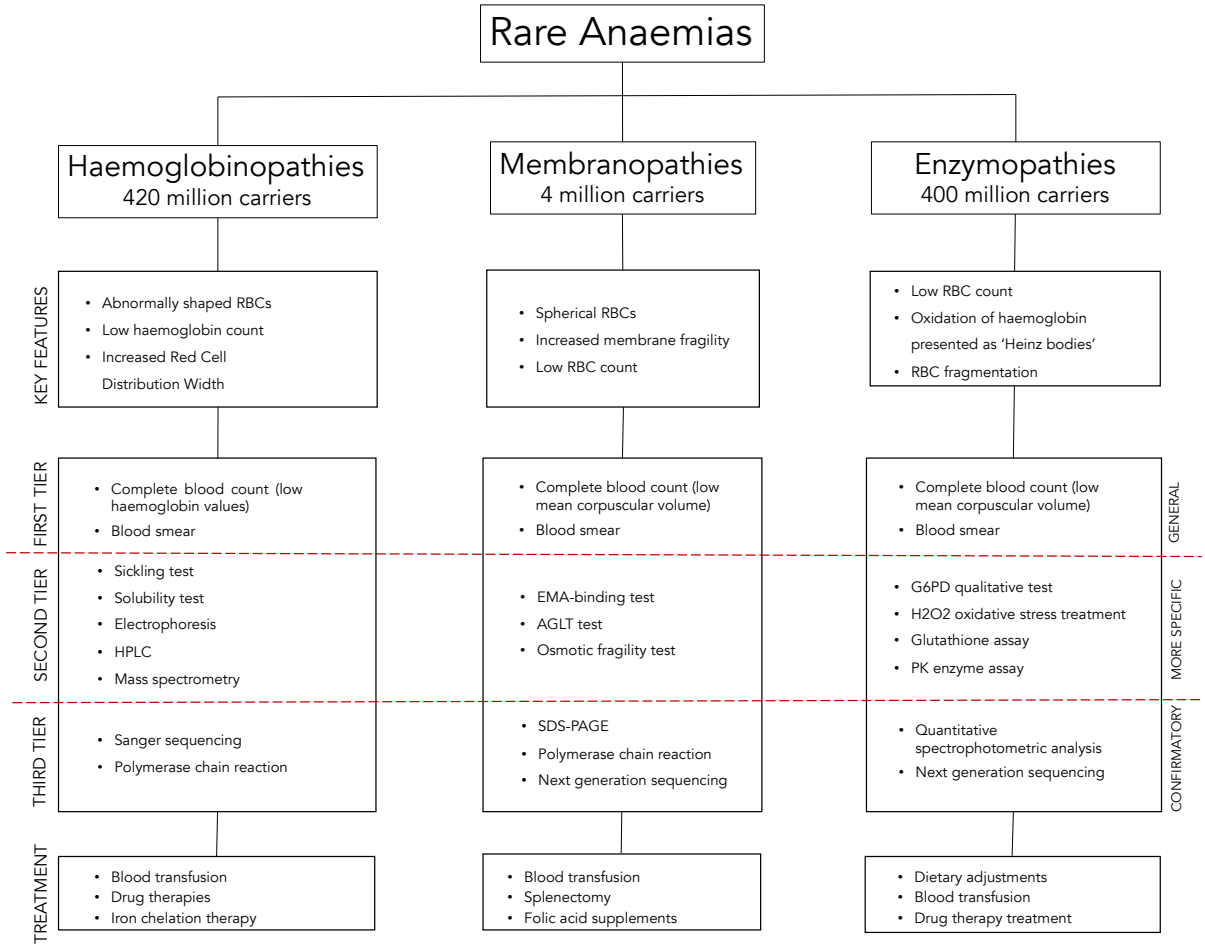

Figure 1-11 A summary diagram of the different categories of Rare Anaemia, their clinical characteristics, investigative tests and treatment options.

1.4.2 Diagnosis in developing countries

Developing countries face major obstacles with respect to their diagnostic and screening resources. Few clinics are equipped to execute genetic diagnostics and there is a lack of available resources for the general population due to inadequate expertise, facilities and financial limitations.[134,136] As a result, inherited anaemias can be misdiagnosed, if diagnosed at all, resulting in either incorrect, or a complete absence of, treatment.

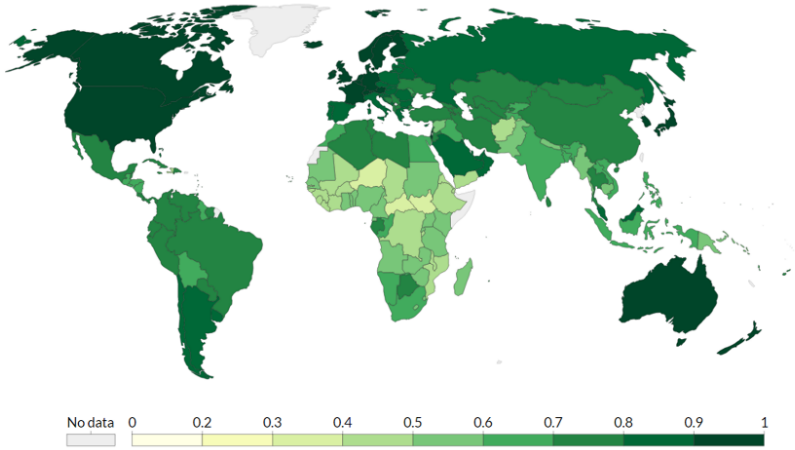

Figure 1-12 The socioeconomic status of countries can be defined by the Human Development Index (HDI). The HDI scale goes from 0-1, with 1 being the most developed. The above map from 'Our World in Data' allows a visual representation of the regions that have a mid (0.55-0.7) to low (<0.55) score on the HDI scale.[137] *These countries also have the highest prevalence of anaemia and malaria, see maps in previous sections. Reprinted with permission: © 2020 Heidt, Siqueira, Eersels, Diliën, Grinsven, Fujiwara, and Cleij.*

With approximately 750,000 anaemic related deaths per year in Africa and India alone, it is fair to say that anaemia is a severe burden to the health systems of the aforementioned and other developing countries.[8]

1.4.3 Challenges for current point-of-care diagnostics for rare anaemia

As previously mentioned, one of the biggest constraints on the testing and diagnosis of inherited anaemia in developing countries is the lack of financial resources with respect to laboratory equipment and trained personnel. Though a considerable effort has been made to develop low-cost and point of care solutions.[138–140]

Paper-based haemoglobin solubility assays and or lateral flow immunoassays have been developed for detection of SCD and sickle trait and G6PD deficiency.[141–144] For the Thalassaemias and Spherocytosis, NESTROFT (Naked Eye Single Tube Red cell Osmotic Fragility Test) was developed for disease detection. NESTROFT exploits the knowledge that the aforementioned disorders will display resistance or increased susceptibility to environmental osmotic changes.[76,145,146]

However, although these developments are continuing to progress in the hereditary anaemia diagnostic field, thus far, there are no gold standard confirmatory point of care diagnostic tests available. A brief description of the advantages and challenges associated with current point of care (POC) technologies is given in the following sections.

(i) Haemoglobin solubility

The Hb solubility assay is used in low resources settings as a screening technique for HbSS, HbS, HbSC and HbS-β. The objective of this assay is to identify the presence of HbS in a blood sample.[141]

The principle of this test relies on the dissolvability of haemoglobin in a blood sample upon mixture with a solubility (phosphate) buffer. A drop of the blood sample mixed with the solubility buffer is placed on chromatography paper. Healthy Hb will disperse and form an evenly distributed pale red circle around the drop whereas the insoluble HbS will precipitate and become trapped in the fibres of the paper. This will form a concentrated dark red circle in the centre of the paper which is clearly distinguishable from the evenly distributed pale red of the normal Hb.[147] Results can be obtained visually by the user or digitally by a custom image analysis program as demonstrated by *Piety et al.*[143]

An advantage of this test is its low-cost (< $0.25 per sample), and although this technique reports good sensitivity and specificity for detection of HbS (94.8% and 87.8% respectively[148]), it does not give information about other possible Hb mutations within the sample or any indication of disease severity. Thus, this test cannot be used for confirmatory diagnosis of disease or specific Hb mutations.

(ii) Lateral flow

The first commercial application of the lateral flow test (LFT) was used for the detection of the hormone hCG in urine, which is produced in the early stages of pregnancy.[149] Since then, lateral flow tests have been transforming the diagnostic field due to their ease of use. The principle of LFTs is the detection of a molecule of interest (antibody, antigen, hormone etc.) through specific bio-recognition molecules which are immobilised on to the surface of a porous membrane, typically chromatography paper.[150]

In 2016, *McGann et al.* presented a paper on a lateral flow immunoassay (Sickle SCAN) for the diagnosis of common Hb mutations which lead to Sickle Cell Disease. The paper reports very high sensitivity (98.3-100%) and specificity (92.5-100%) for the detection of; HbA, HbS, and HbC.[151]

Although the sensitivity and specificity of Sickle SCAN is quite high, there is a potential risk of overlooking less common mutations as the test concentrates on screening for the most prevalent mutations.

In effect, there is no 'one size fits all' approach when it comes to POC screening and diagnosis where the tests currently available are searching for a few specific mutations that are not inclusive of all the mutations that cause rare anaemia.

(iii) Osmotic fragility

The osmotic fragility of erythrocytes has been a topic of interest since the initial observations of *William Hewson* (1773) when he reported swelling or shrinking of RBCs dependent on the salt concentration of their dilution media.[152,153]

There is an osmotic pressure in RBCs that is attributed to a concentration difference of solutes across the cell membrane. In a hypotonic solution, a pressure difference is created due to the change in salt concentration of the solution surrounding the RBC. This pressure difference causes the cell membrane to become more permeable to water due to osmosis.[154]

Parpart developed the Osmotic Fragility Test (OFT) in 1946 to measure the degree of haemolysis of red blood cells when subjected to osmotic stress and this was later optimised by *Kattamis et al.* (1981) to be used for screening of β-thalassaemia trait, and other anaemias, in the one tube osmotic fragility screening test.[155,156]

The principle of the one tube osmotic fragility test is to dilute RBCs in solutions of different salt concentrations to induce haemolysis. The rate at which haemolysis occurs provides information about the hydration status of the RBC or it's membrane stability and may suggest the presence of a rare anaemia.

For this test, 0.02 mL of whole blood is pipetted into Eppendorf tubes containing a 0.36% saline solutions. The results are visually interpreted as negative if the sample solution appears as clear and red following a 5 minute incubation time at room temperature with a 0.36% saline solution, and positive if the sample displayed a turbid solution following the same conditions. *Kattamis et al.* reported high sensitivity for detection of β -

thalassaemia trait (>96%) using a 0.36% saline solution with a 5-minute incubation time, however, the test is unable to distinguish between the various β-thalassaemia mutations.

Further evaluations of the one tube osmotic fragility test for detection of β-thalassaemia trait, later termed NESTROFT (Naked Eye Single Tube Red cell Osmotic Fragility Test), have been conducted and all observe high sensitivities between 91 and 100% for detection of β-thalassaemia trait.[146,157,158] NESTROFT specificities have a wider range from 66 – 100% as outlined in the review by *Piplani et al.*[158]

Unfortunately, this test does not give any definitive information regarding specific mutations or disease severity and other types of anaemias present in the sample, for example, it has been reported that iron deficiency anaemia can produce false positives using the NESTROFT method.[158,159]

NESTROFT is incomparable to more advanced and commonplace laboratory techniques however, due to the prevalence of rare anaemias in developing countries, a low cost solution like NESTROFT is ideal where laboratory facilities are lacking.[160]

1.5 Haemolysis by low pH

1.5.1 Proposed mechanism for acid haemolysis

The most abundant protein in the RBC membrane is the Band 3 protein which is responsible for cell volume maintenance, HCO_3^-/Cl^- exchange, and conservation of the RBC architecture.[161–164]

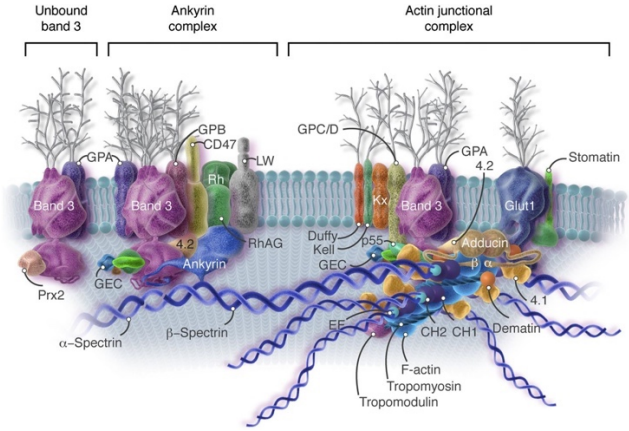

Figure 1-13 Schematic diagram of the RBC membrane structure displaying the peripheral (spectrin, 4.1R) and integral (Band 3, Rh complex) proteins. Reprinted with permission. © 2016 American Society of Hematology.

The transport of HCO_3^- is critical for the maintenance of cellular pH and the Band 3 protein facilitates this by exchanging intracellular HCO_3^- for extracellular Cl^- across the RBC membrane.[165]

Upon entering a low pH environment, the HCO_3^-/Cl^- channel is activated and Cl^- enters the cell. In the case of the acid stress test, the additional Cl^- ions present in the sample is due to the dissociation of HCl to H^+ and Cl^- ions.

The increase of negatively charged intracellular chloride ions also causes a rapid change in the RBCs membrane potential which causes the opening of Na^+ gated ion channels.[166] This leads to an influx of Na^+ ions via either the Na^+/H^+ antiporter or sodium channel.[161]

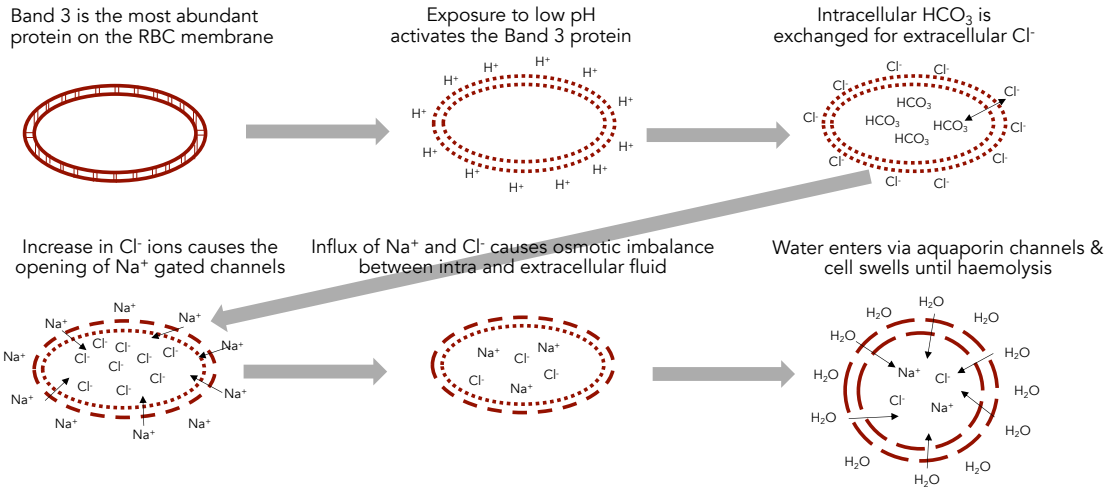

Figure 1-14 Proposed mechanism for haemolysis by low pH shock. Water enters the RBC via aquaporin channels in the membrane of the RBC after the RBC has been exposed to a low pH shock causing swelling of the RBC membrane and, finally, haemolysis.

In an effort to maintain the osmotic balance between the *intra* and *extra* cellular fluid, water will also enter through aquaporin channels resulting in cell swelling.[167,168] In the absence of any counteracting method, the cell will continue swelling until reaching its critical volume causing cell necrosis by haemolysis, see above in *Figure 1-14*.[169]

Past studies have shown that the pre-treatment of RBCs with DIDS (4,4′-diisothiocyanato-stilbene-2,2′-disulfonic acid), a HCO_3^-/Cl^- exchanger (Band 3 protein) inhibitor, prevents the effects of acid haemolysis.[170,171] Inhibition of the Band 3 protein with DIDS suggests that this protein is responsible for the influx of extracellular Cl^- ions into the cell upon exposure to a low pH environment. Band 3 function is reported as reduced, and in some cases, severely reduced, in all Rare Anaemias. It is considered that

applying a low pH shock to RBCs with known Band 3 impairments may highlight a novel diagnostic factor. [172,173,174]

1.5.2 Microfluidics for point-of-care diagnostics in low resource settings

Microfluidics is the science of fluid flow on the microscale, concerned with volumes in the nano to microlitre ranges.[175] The sub-categories of microfluidics include Lab-on-a-Disc (LoaD), droplet-based microfluidics, and Lab-on-a-Chip (LoaC).[176–178]

There are many advantages to using microfluidic technology. One such benefit is that the sample and reagent consumption are significantly reduced in comparison with the accepted gold standard methods in many cases. For example, due to low concentrations of bacteria in the blood of a patient suffering with life-threatening sepsis, high sample volumes (10 – 30 mL) are required for detection using standard protocols.[179] There are other indicative diagnostic factors for sepsis, such as measurement of neutrophil dysfunction in a blood sample. *Ellet et al* reports a microfluidic platform which measures the phenotype of neutrophils from only one droplet of blood (~ 35 μL) with 97% sensitivity and 98% specificity for identification of sepsis.[180]

For comparison, standard haematological analysis requires a blood volume of ~120 μL.[181] Whilst this volume is not typically a significant loss for the average adult, it could prove to be critical in the case of neonates.[182,183] Thus, the reduction of sample requirements would be particularly beneficial for neonatal screening and diagnosis.

Importantly, another advantage of microfluidics is the decreased sample reaction time due to reduction of length scales, thus a reduction in diffusion times. Time from test to result is especially important for high throughput of samples and reducing these times is highly advantageous for on-site testing in rural villages.

Pumping systems for microfluidic devices can be both passive (non-mechanical) and active (mechanical). The obvious benefit to a passive system is that there is no requirement for external instrumentation.[184]

Passive flow techniques include but are not limited to; Gravity-Driven, Capillary Action, Osmosis, and Vacuum Driven. Each of these have their advantages but also have limitations, see *Table 1-3*.

Passive Flow System	Principle	Limitations
Gravity Driven	Fluid flow assisted by gravity	Can only generate continuous flow, requires constant solution replenishment
Capillary Action	Fluid flow through a narrow space caused by the intermolecular forces between the liquid and the surrounding solid surfaces	Backflow, poor flow control and inconsistent flow rates
Osmotic Flow	2 solutions of differing solute concentrations are separated by a semi-permeable membrane which creates a chemical potential difference across the membrane	Requires a complicated structure
Vacuum Driven	Gas permeability of polydimethylsiloxane (PDMS) is used to drive liquid through the chip	Low flow rates from limited air diffusion, typically single use, PDMS material is hydrophobic

Table 1-3 Examples of non-mechanical, or passive, microfluidic flow techniques, their general principle and limitations.

Contrastingly, active, or mechanical, flow systems require the use of external instrumentation, like syringe pumps, external motors for centrifugal microfluidics, and electroosmotic pumps. [184,185] An example of some common types of active flow systems are described below in *Table 1- 4*. Although the requirement for external instrumentation may be considered a drawback for active pumping systems, the precision of the flow within the microchannel is greatly increased.

Active Flow System	Principle	Limitations
Pressure Driven	Syringe pump used to push fluid through microchips	Unidirectional flow, system dimensions are determined by syringe pump size
Centrifugal Driven	Uses an external motor to create centrifugal force on a Lab-on-a-Disc system	Testing is limited by the amount of storage available on the microfluidic disc, fabrication process can be complex
Electro-Osmotic Flow	Fluid flow is generated with a microchannel by application of an electric field	Complex fabrication process, only polar liquids can be pumped, sensitive to temperature and gas variations

Table 1- 4 Examples of active flow techniques. Each technique requires the use of external instrumentation, but overall system flow control is greatly increased in comparison to the passive flow techniques.

However, despite the increased flow control, instrumentation required to run microfluidic chips can be bulky and the experimental setup can be labour intensive.

To run a LoaC device, the user will require at the very least a syringe pump and a microscope.[186] The sample will be loaded into the syringe and infused at a flow rate determined by the user. Reactions within the chip can be visualised on a microscope and recorded for further probing if the setup includes a camera.

The requirement for a new syringe per test to prevent cross contamination adds a costly element to an otherwise inexpensive test. Replacing the syringe also increases the time per test reducing test throughput. Although most laboratories are equipped with a bench-top microscope, this is not always true in the case of developing countries where facilities are lacking.[187]

Thus, there is a need for a user-friendly, low-cost and compact microfluidic testing kit that has a high throughput ability for rapid diagnosis of blood mutations from minute samples of blood.

1.6 Thesis overview

As detailed in this review, the requirement for a low-cost, point of care test with high sensitivity and specificity for distinguishing between the different types of rare anaemias is essential. The current gold standard diagnostic tests comprise a 3-tier investigation from clinical investigations to molecular analysis. These investigation methods are expensive, time consuming and require trained personnel and advanced technology.

Often rural villages in localities where these blood disorders are most prevalent do not have the facilities for such investigations. In addition to diagnosis, a low-cost pre-marital screening test would be of great benefit for prevention of unions between carrier parents.

This section has outlined the different types of hereditary anaemias, the current methods of diagnosis and a potential new application of the acid haemolysis test in rare anaemia diagnostics. The acid haemolysis test has been mostly used to date in Eastern Europe and Russia for monitoring the resistance of erythrocytes to chemical haemolysis. The acid haemolysis test gives a measure of Band 3 functionality, which is markedly reduced in Rare Anaemic red blood cells, particularly for Haemoglobinopathies and Membranopathies.

The adaptation of the acid resistance test in a user-friendly microfluidic setup and investigation of acidic lysis on various hereditary anaemias is the forefront of the research aim.

Chapter 2 outlines the materials used throughout this work.

Chapter 3 describes the development of a microfluidic cartridge and operational instrumentation. This chapter also details the development of the system and experimental protocols. The work conducted in this chapter directly relates to the patent, see *Appendix A.5*.

Chapter 4 investigates the application of the developed instrument and methods for repeatability within a healthy population. This chapter will give a comprehensive view of the advantages and disadvantages of each method highlighting the successful tests.

Chapter 5 compares rare anaemic samples with the healthy population for the previously determined successful methodologies.

Finally, Chapter 6 summarises the main findings of Chapters 3 – 5 and future recommendations for system optimisations is discussed here.

Chapter 2 Materials

2.1 Materials

BSA (Bovine serum albumin, CAS no: 9048-46-8) was purchased from Sigma Aldrich, UK. 0.9% NaCl (Sodium chloride, CAS no: 7647-14-5) was purchased from Fisher Scientific, UK. EDTA (ethylenediaminetetraacetic acid, catalog no: 12967666) coated vacutainers for blood collection were purchased from Fisher Scientific, UK. 37% HCl (hydrochloric acid, CAS no: 7647-01-0) was purchased from Sigma Aldrich, UK and diluted to a stock solution of 25% HCl.

2.2 Dilution medium preparation

A stock solution of BSA and 0.9% NaCl was prepared by adding 50 mg of BSA to 50 mL of 0.9% NaCl. Gentle mixing by hand aided the dissolving of the BSA powder. The stock solution was stored at 4ºC until required for testing. This solution was used as the dilution medium for both the blood sample and the acid sample.

2.3 Ethics for blood collection

Informed consent was given by all volunteers and patients who donated blood for this research. Donor anonymity was protected by using codes for each sample. Each volunteer and patient was informed of the right to withdraw consent at any point during this research.

2.4 Blood preparation

Fresh whole blood samples from all donors were collected in the EDTA coated vacutainers unless otherwise stated. Samples were stored at 4°C in the vacutainers. Samples were used within 2 hours of collection, unless otherwise stated.

8 µL of whole blood was measured by pipette (P10) and diluted in 800 µL of the dilution medium (1% BSA, 0.9% NaCl). This diluted sample was used as the working sample for all tests unless otherwise stated.

2.5 Acid preparation

25% hydrochloric acid, HCl (CAS no: 7647-01-0, Merck, UK) was diluted in 1% BSA and 0.9% NaCl to achieve a pH of 0.7 ± 0.1 and made up to a volume of 2 mL.

2.6 Microfluidic cartridge

The microfluidic cartridge was manufactured using both standard SU-8 photolithography and proprietary bonding methods. The dimensions of the microfluidic channel were as follows:

- Width of (a)-channel: 0.5 mm
- Width of (b)-channel (b): 0.25 mm
- Width of the merged channels: 0.75 mm
- Channel depth: 0.04 mm
- Channel length: 30 mm

The microfluidic channel used was referred to as the Y-channel due to its shape.

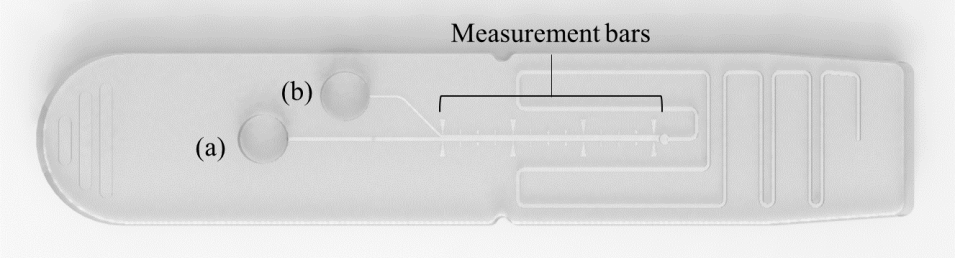

Figure 2-1 The microfluidic channel designed used for comparative testing between healthy and diseased samples was the Y-channel. Diluted blood was stored in reservoir (a) and diluted acid sample was stored in reservoir (b).

2.7 Experimental protocols

Design and development of all systems and experimental protocols described in this section is thoroughly discussed in *Chapter 3*.

All experiments were carried out at room temperature ~ 20°C ± 2°C. Fresh blood (used within 2 hours of extraction) was used unless otherwise stated and all whole blood samples were stored at 4°C. Once diluted, samples were used immediately.

2.7.1 Flow test

Sample preparation

1. Blood diluted in 1% BSA and 0.9% saline to a concentration of 15%. Final volume in Eppendorf tube should be 50 μL.
2. HCl added to Eppendorf tube by drop until pH is 0.7 as read by pH meter.

Experimental setup

1. Chip is inserted into holder on MeCheM and is secured to microfluidic circuit board.
2. MeCheM is switched on via the switch at the back of the instrument.
3. User opens up operating programme on laptop and uses the real-time view to adjust the focus if required using the z-focus wheel.
4. System is primed by initiating the priming step via the operating programme which primes the channel with the priming solution at a flow rate of 1.8 mL/min for a volume of 0.8 mL.
5. Upon completion of priming step, a pipette is used to remove excess priming solution from the sample reservoirs.
6. User pipettes 50 μL of the blood and acid sample into their allocated reservoirs.

MeCheM operation

1. User runs the testing phase via the operating programme which includes pre-set ‘fast’ flow rate of 5 μL/min for a volume of 1.5 μL followed by the testing flow rate of 0.5 μL/min for a volume of 1.5 μL.
2. User starts a timer for 120 seconds for flow stabilization.
3. Immediately after 120 seconds, user begins image and video capture.
4. The first position to be captured is in the blood sample channel prior to the intersection with the acid sample channel and is unmarked.
5. User should use the multi-capture function to capture 10 images per position.
6. User should move the XY-stage manually to the next marked position for image capture.
7. Upon completion of positional image capture, user should scan along the channel and image any areas of interest (cell adhesion to surface).

System reset

1. Following the completion of the testing phase, the user employs the 'Empty syringe' function on the operating programme.
2. Once this function has been completed, the user removes the chip and disposes of it in a biohazard bin.

2.7.2 Low magnification drop test

Experimental setup

1. Microscope slide placed on top of MeCheM holder.
2. MeCheM switched on via switch at back of instrument.
3. User pipettes 5 µL of dilute blood sample on to the microscope slide and allows ~ 90 seconds for cells to settle into the plane of focus.
4. User opens up operating programme on laptop and uses the real-time view to adjust the focus as required using the z-focus wheel until the cells come into view.

Low magnification drop test protocol

1. User initiates video recording via the MeCheM operating programme.
2. User pipettes 2.5 µL of HCl stressor on top of the diluted blood sample.
3. User concludes video recording when cell lysis has been completed *or* the test time had reached 3 minutes.
4. User disposes of microscope slide in biohazard bin.

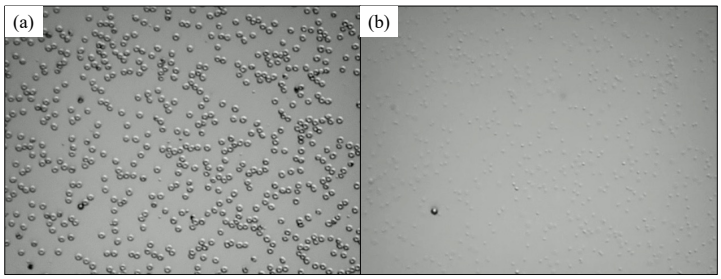

Figure 2-2 (a) Typical image of the LMDT prior to acid addition, (b) example of complete haemolysis by HCl exposure. The remaining artefact was debris on the microscope slide. Faint spherical structures can be seen in (b). These are referred to as 'ghosts' and are the remains of the RBCs after their contents have been evacuated from the cytoskeleton.

2.7.3 High magnification drop test

Experimental setup

1. HMS is switched on via the switch at the back of the instrument.
2. User pipettes 100 µL of blood sample into well and allows ~ 90 seconds for cells to settle.

3. User opens up operating programme on laptop and uses the real-time view to adjust the focus as required using the z-focus wheel until the cells come into view.

High magnification system protocol

1. The manual XY-stage is used to navigate through the well to capture image of the cells prior to acid addition.
2. User initiates video recording using the operating programme.
3. 50 µL of HCl stressor is carefully added to the well plate by angling the pipette tip to make contact with the side of the well surface.
4. Upon lysis of the last cell in the FOV, or if the test time had reached > 3 minutes, the video recording is stopped and the test is considered completed.
5. Once the well plate is full, it is disposed of in a biohazard bin. No further system reset is required.

2.8 Analysis

Graphs and analysis were carried out using Microsoft Excel and GraphPad Prism.

2.9 Haematology analyser measurements

The haematology analyser used for blood measurements within this body of work was the CELL-DYN Sapphire Haematology Analyser. The CELL-DYN Sapphire Haematology Analyser measures peripheral blood cells in whole blood samples by way of impedance for Red Blood Cell count (RBC), Mean Corpuscular Volume (MCV), and Red Cell Distribution Width (RDW). The optical scatter method is also an option which can be utilised for RBC count. Haemoglobin concentration is measured by spectrophotometry.

2.10 Patient RBC indices

	Sample code	*Disease*	*RBC, 10^{12}/L*	*MCV, fL*	*MCH, fmol*	*RDW, %*
Sickled Diseases	S1	HbSS	4.74	58.1	1.17	22.1
	S2	HbSS	2.83	97.8	2.08	20.1
	S3	HbSS	3.46	80.5	1.69	24.4
	S4	HbS/BT	2.70	116.0	2.60	17.3
	S5	HbS/BT	2.88	86.9	1.69	28.7
	S6	HbS/BT	4.42	71.3	1.40	20.6
	S7	HbSC	4.75	64.9	1.43	19.1
Thalassaemias	S8	BTM	3.01	84.6	1.74	15.6
	S9	BTM	3.10	76.2	1.73	24.5
	S10	BTI	2.42	83.9	1.59	28.1
	S11	BT_m	5.77	53.4	1.05	16.3
	S12	HbH	5.68	59.6	0.86	26.1
	S13	HbA/HbH	4.31	72.6	1.55	28.1
	S14	HbE/HbH	4.90	75.6	1.64	12.2
Membranopathies	S15	HS	4.41	83.5	1.86	16.8
	S16	HS	3.20	82.0	1.79	21.6
	S17	HX	3.15	101.0	2.16	11.3
	S18	HX	4.25	87.7	2.04	12.9

Table 2-1 Compilation of all patient samples with their haematological values reported for; Red Blood Cell Count (RBC), Mean Corpuscular Volume (MCV), Mean Corpuscular Haemoglobin (MCH), and Red cell Distribution Width (RDW), for the investigations carried out in this thesis.

Chapter 3 Microfluidic platform development

3.1 Introduction and justification

Microfluidic point of care (POC) devices have been altering the diagnostic field since the emergence of the technique in the 1980s.[175] As the name suggests, microfluidics is the study of fluid on the micro-scale, that is, in the region of nano to microlitres.[188] Operating with fluid on the micro-scale allows for faster experimental reaction times with much smaller volumes of sample and reagents.[189] This makes microfluidics an attractive solution for neonatal screening and diagnosis, particularly in developing countries where large reagent consumption could be expensive.

The World Health Organization have defined a set of criteria for the development of diagnostic technologies for low-middle income countries. Their recommendations report any such devices should be user-friendly, low-cost and robust, and provide rapid and accurate results.[190] Microfluidic technology satisfies many of these requirements thus it is an appealing option for diagnostic test development.

There have been many successful outputs of microfluidics devices including but not limited to; the pregnancy test and, most recently, the COVID-19 antigen tests, both of which utilise lateral flow paper-based microfluidic technology.[191,192]

However, microfluidic technology is not without its challenges. Whilst microfluidic devices independently tend to be small and easily portable, the instrumentation required for operation can often be bulky and difficult to transport.[193] Although this is not problematic for a standard working laboratory, developing countries typically lack many of the resources necessary for operation and analysis of these devices.[194] As such, it would be beneficial for low-middle income countries to have a user-friendly and relatively portable microfluidic instrumentation setup for rapid testing.[140]

As outlined in *Chapter 1*, the diagnosis of rare anaemias requires multiple laboratory tests prior to disease confirmation. An example of this is the diagnosis of α-thalassaemia whereby a clinician is required to carry out a 3-tier investigation including; complete

blood count with iron studies, haemoglobin electrophoresis and genetic testing before confirmation of a diagnosis is achieved.[195] Currently, this amalgamation of tests is necessary, but it is far from an ideal single test that gives clinicians a definitive yes or no answer.

For the success of a novel diagnostic instrument, it must be, at the very least, as accurate as the current laboratory standards. Following that, it should have notable advantages such as reduced sample volume and reagent consumption, faster testing times, ease of use, potentially novel useful information output, and reduced overall cost[196]. Another imperative function of a new instrument is ease of use. This is especially important for developing countries where minimal training on diagnostic devices is a necessity.[197]

The aim of this chapter describe the development of the research instrumentation to investigate the value of the analytical methods and their readouts. This is a necessary step towards developing a machine prototype with the ultimate aim of commercialisation.

This chapter will describe; (i) the operation of the novel microfluidic instrument, (ii) the microfluidic chip, and (iii) the optimisation of the proposed biochemical assay for detection and diagnosis of rare anaemias.

3.2 Instrument specifications

In the interest of developing an optimised platform for the proof-of-principle biochemical assay, it was critical to consider the user requirements. The areas of most importance for the integration of a bioassay on to a Lab-on-a-Chip device are; (i) ease of use of the system, and (ii) chip to chip repeatability.

A conventional setup requires the use of standard equipment including a microfluidic chip, a syringe pump and a commercial microscope. This equipment is expensive, requires training to operate and a suitable laboratory environment. We need a low-cost, mobile, user-friendly screening and diagnostic device for developing countries. As such, the first challenge to be addressed was combining the necessary components into a portable instrument that required minimal training.

3.2.1 Technical requirements

The specifications for the proposed instrument were centred on the 2 main system requirements; (i) flow, and (ii) imaging capabilities.

(i) Flow requirements

A popular syringe pump that is used in Lab-on-a-Chip setups is the Mirus-Evo-1311-02 (Cellix Limited, Ireland). This pump, shown below in *Figure 3-1*, permits connection to 8 microchannels simultaneously, it has automatic syringe refill and boasts an incredibly low flow rate (100 nL/min – 20 µL/min with 100 µL syringe). This pump comes with an impressive capability, however, it is costly at €9,595 (priced February 2022).

Figure 3-1 Mirus Evo syringe pump from Cellix Limited.

One of the selling points of the pump, automatic syringe refill, is, in fact, a disadvantage when multiple samples require testing. One of the aims in developing this system was to run multiple samples as required. The Mirus Evo pump would require a new syringe and system clean each time a new sample was tested to avoid contamination between samples, increasing testing time and decreasing the ease of use of the system. For the proposed assays the flow precision of the Miro Evo pump was not required.

The requirements for the new pumping system were; (i) low flow rate capabilities, and (ii) removal of any potential areas for system contamination.

(ii) Imaging requirements

In a typical microfluidic setup, the imaging system uses a standard upright light microscope. The microfluidic chip is attached to an XY-stage and the user manually moves the stage to image the points of interest on the chip. This requires training on the

mechanics of the microscope and the software for image capture. While it is fair to note that this is not particularly taxing for the user, the insertion and removal of the microfluidic chip and the necessary microscope refocusing all increase assay testing time. To fully understand the challenges of a standard microfluidic setup, its recreation was attempted at *Epigem* with a low precision syringe pump.

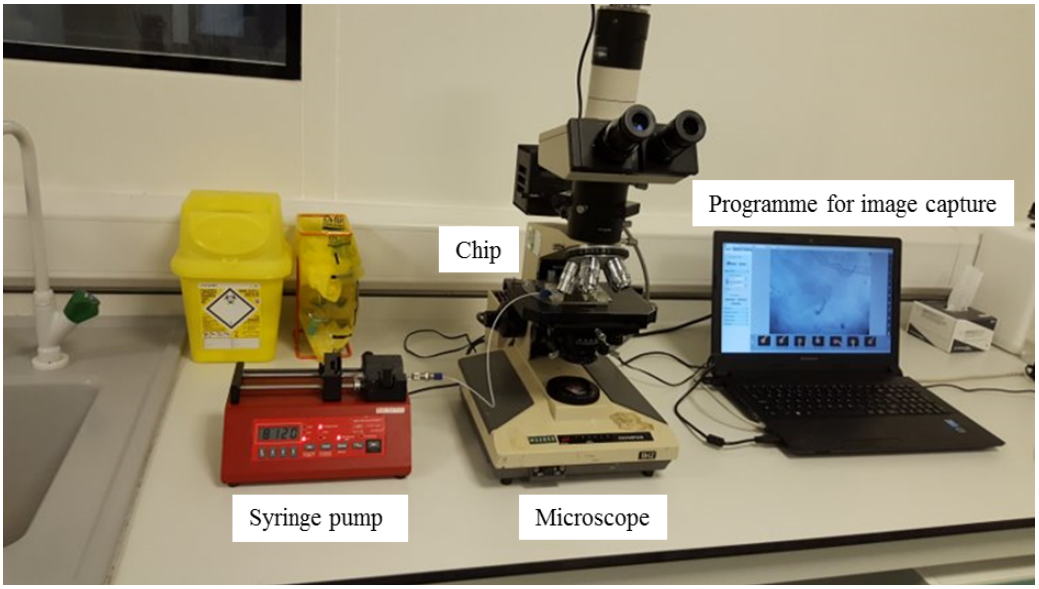

Figure 3-2 The original setup was clearly not easily portable requiring a syringe pump, microscope and computer to conduct the assay. Access to such equipment is taken for granted in well-equipped laboratories. It is important to realise that this is not always the case in the laboratories of developing countries.

The main disadvantages of this imaging system was the lack of portability and the total bench space it consumed, along with the necessity for training on any microscope and pump control software.

The requirements for the imaging system were simple; the RBCs travelling down the microchannel needed to be imaged. It was not important to have high magnification or resolution for this as the test output was a cell count verses position along the channel, monitoring cell survival over time with exposure to the chemical challenge, namely acid. It would be advantageous to simultaneously capture image and video footage, and this should be stored in a file format that is suitable for analysis in any standard programme (Microsoft Excel, GraphPad Prism etc).

(iii) Essential system

Following many trial runs of the initial setup, a list of essential and desired system requirements was determined.

Component	Requirement
Flow	Multi-use. Inexpensive syringe pump. Portable.
Image capture	Multi-use. Inexpensive imaging system. Portable. Sufficient magnification to see the RBCs travelling through the microchannel. Image capture essential. Video capture desired.
Image analysis	Analysis of captured data should give the diagnostic output. This will be given in terms of cell count per position along the channel.
Cartridge	Single-use, disposable. Inexpensive. Portable.

Table 3-1 Essential requirements for instrumentation.

As can be seen from the above *Table 3-1* the system requirements are simple. The fundamental steps in the protocol were agreed to include the following;

- **Microfluidic chip insertion:** the single-use chip is inserted and secured in place to couple it to the instrument.

- **Sample input:** user is required to insert pre-made sample/reagent solutions into respective sample reservoirs.

- **Sample flow:** the low flow pump is initiated, and sample/reagent are withdrawn from their respective reservoirs through the microchannel.

- **Image capture and analysis:** user should capture images of cells at distinct distances along the microchannel which correspond to the time of the reaction. Appropriate analysis should be conducted.

- **Results reporting:** results of image analysis are utilised to report the test results.

- **System clean and cartridge disposal:** low flow syringe should be reset to its zero position and chip can be disposed of appropriately.

3.3 Instrument development

Flow through a microfluidic chip can be achieved by various methods including pressure driven flow and, more commonly in a standard laboratory setup, positive displacement pumping.[198]

Positive displacement pumping uses a syringe pump to execute fluid flow through microchannels.[199]

With aims of establishing a device that is economically accessible for developing countries, the syringe pump is an attractive solution given that it is a relatively inexpensive instrument.[200]

3.3.1 Fluidic components

The pump used in the microfluidic setup in *Figure 3-2* was an Aladdin Syringe Pump (AL-1000; World Precision Instruments, USA) costing ~ €1,000 (priced June 2022). While the specifications of this pump were as required and it was programmable, the additional manual settings increased the cost of this pump. The Aladdin pump was also quite bulky, which would increase final instrument dimensions. In an effort to keep instrument dimensions and costings as low as possible, it was decided to source lower cost and smaller original equipment manufacturer (OEM) pump. The syringe pumps chosen for instrument development were positive displacement pumps (New Era NE-500 OEM, Pump Systems Inc. USA) which cost ~ €500.

To remove the requirement for thorough system cleaning, the application of negative displacement pumping, or withdrawal mode, was investigated. Withdrawal mode would allow the samples to be stored on a single use chip, thus removing the requirement for intensive system cleaning.

(i) Proof of principle for use of syringe in withdrawal pumping mode

An initial concern for using the syringe pump in withdrawal mode was that there would not be sufficient suction within the system to pull the samples through the microchannel at a low flow rate. To test the validity of this option, the microfluidic chip was redesigned to have 2 reservoirs in which the samples would be stored and a tube fitting at the end of the microchannel which would connect the chip to the syringe pump.

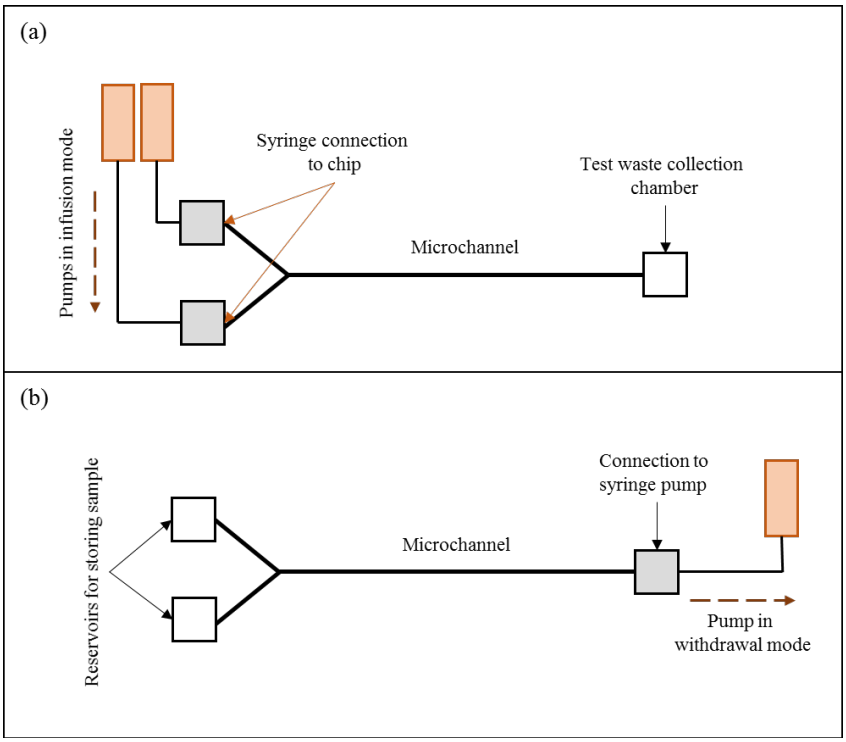

Figure 3-3 (a) original chip setup with 2 separate syringe connections to the microfluidic chip. Syringes were filled with sample and syringe pump infused samples at the same flow rate into the microfluidic chip. The test waste was collected in a reservoir at the end of the microchannel on the chip. (b) Re-design of the chip included reservoirs to store the samples, meaning that the syringes were no longer required to store the sample and reagents. This configuration was used in withdrawal mode which moved the samples from their reservoirs through the microchannel.

To achieve the low flow rates required, the syringe that was chosen for these investigations was a gas tight glass 100 µL syringe (Kloehn, part no: 17593; IMI Precision, USA). The flow rates that were investigated were between 0.1 and 10 µL/min.

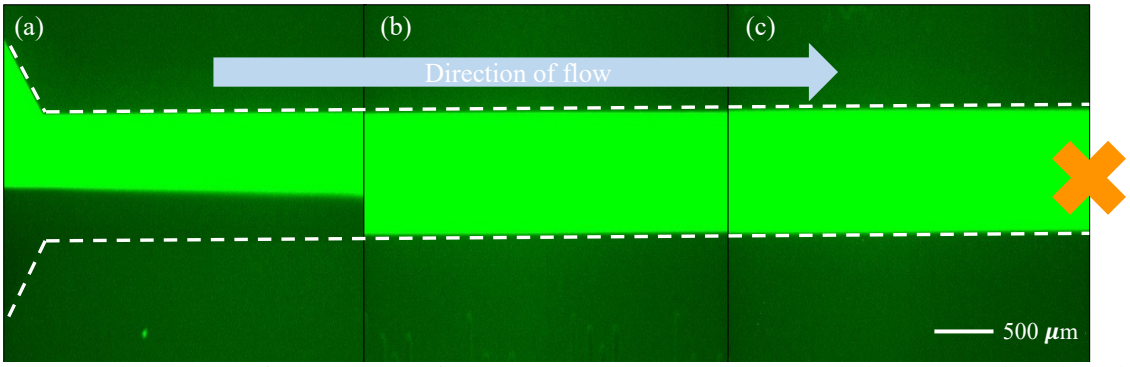

Figure 3-4 This sequence of images shows a fluorescent dye (neon green) and water (dark green) travelling through the microchannel. (a), (b) and (c) correspond to different positions along the channel. (a) shows the junction where the 2 liquids meet in the channel. (b) is a midpoint where the two fluids have diffused into each other and (c) is the end of the testing channel. White dashed lines have been added to the image to highlight the microchannel edges. Orange cross denotes the connection of the chip to the syringe pump. Fluorescent sample and water was stored in external reservoirs connected to the chip on the LHS, not shown above. Images were captured using an inverted Nikon Ti-E microscope. Flow rate was 0.1 µL/min.

The result of this investigation confirmed that the syringe pump maintained sufficient power to pull the samples through the microchannel for all of the flow rates investigated. The dimensions of the microchannel in *Figure 3-4* are as follows; (i) length = 30 mm, (ii)

width = 0.5 mm, and (iii) depth = 0.04 mm. An example of samples moving through the channel using fluorescent dye and water is shown above in *Figure 3-4*.

Although this initial step to investigate the use of negative displacement pumping for movement of fluid through the microchannel was successful, an issue was found concerning air entrapments within the channel. Air entrapments, bubbles, were problematic as their presence disturbed the smooth flow of cells through the channel, leading to turbulence and inconsistent test results.

Upon investigation, it appeared there were 2 factors which resulted in air leakage and entrapments in the channel. One element was the chip design which is discussed in detail in *Section 3.5*, and the second element was that the storage conditions of the chip naturally allowed air to reside in the channel. This required a system priming step to purge the channels of air using a priming solution.

(ii) Microfluidic circuit board for system priming

To accommodate the priming step, a second OEM pump was designed into the system. The purpose of this pump was to purge the microchannel of any air by infusing the channel with a priming solution at a high flow rate. The high flow rate of the solution through the microchannel forced the air out of the channel via the external reservoirs.

However, as there was only one connection from the chip to the syringe pump, the addition of a second pump required the development of microfluidic pathways with valves to direct fluid flow correctly through the system.

A microfluidic circuit board was designed in-house containing channel pathways, 2 non-return valves (Part no: 12130; Cambridge Reactor Design, UK) and an electric valve (Part no: 6724, Burkert, Germany). This circuit board setup ensured only one pump could control the fluid flow at any one time. A schematic of it is given below in *Figure 3-5*.

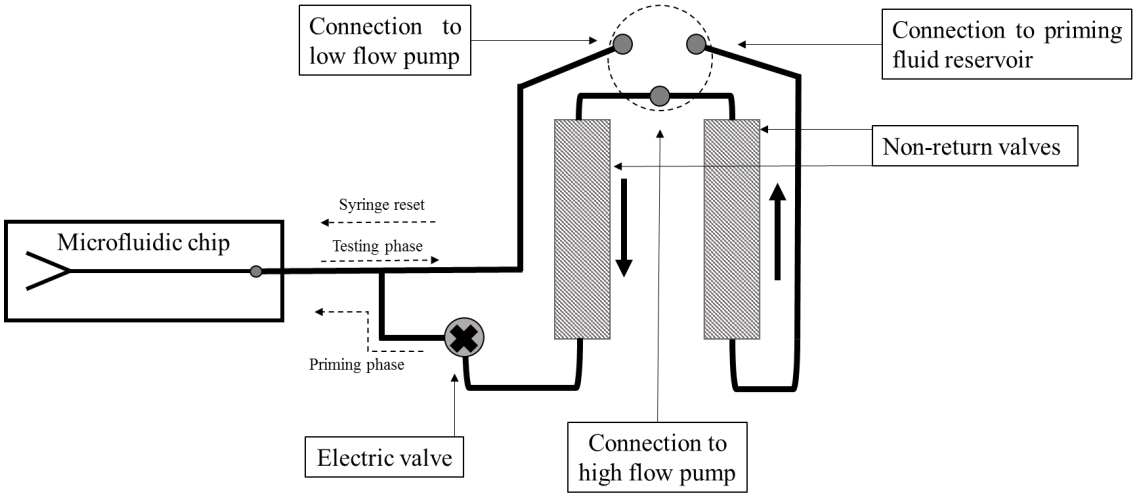

Figure 3-5 Microfluidic circuit board containing 2 non-return valves in opposing directions (direction of valve openings marked with arrow) and an electric valve.

The second pump was required to withdraw priming solution from an external reservoir and pump it through the circuit board via the valves to the microchannel. Although most system elasticity was removed through the use of glass syringes and PEEK (Polyetheretherketone) tubing instead of plastics, the higher flow rate utilised for priming (1.5 mL/min) had the potential to create pressure build-up within the microfluidic circuit board system. This pressure build-up would reduce to atmospheric pressure over time, however, to remove this variable an electronic valve was employed. The electronic valve physically prevented any connection between the high and low flow pumps. This ensured that the low flow pump was not influenced by any remaining pressure build-up from the high flow pump during testing.

The priming step could be repeated as many times as necessary to remove all air within the channel, although typically the air was removed by one purging sequence.

Figure 3-6 describes the new protocol sequence for the user based upon the addition of the priming step.

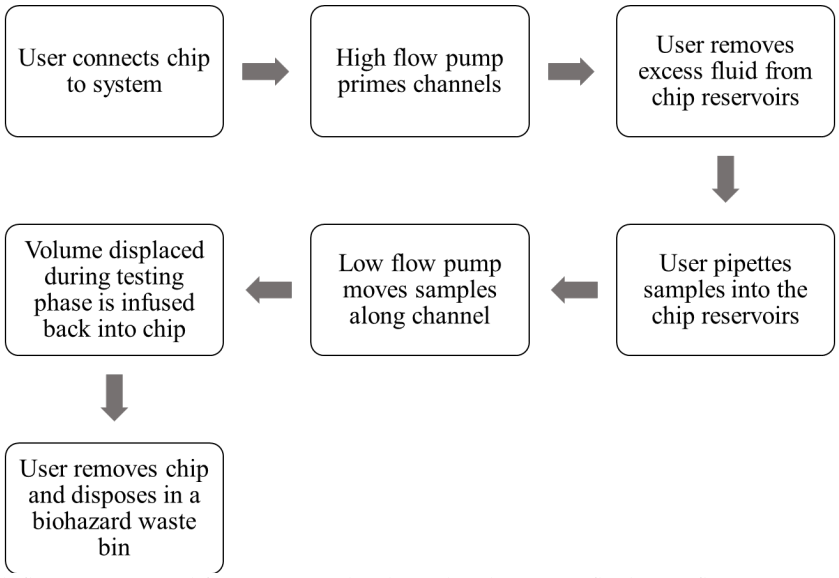

Figure 3-6 High flow pump is used for preparing the channel with priming fluid. Low flow pump controls the testing conditions under flow. Upon completion of the testing phase, the low flow pump infuses the sample fluid back into chip. Chip is then removed and disposed of in a biohazard bin.

A significant advantage of this system is the reduced user interaction with the instrument. The pumps withdraws and infuses the samples as required which eliminates the necessity for the user to regularly reload the syringes with a sample and clean the system.

The in-house development of the integrated fluidics system provided a specific path along which the fluid would flow and this was imperative for the instrument operation.

3.3.2 Imaging components

Traditionally, the well-established bench top microscope is the imaging technique of choice for microfluidic experimental setups. Other approaches have been developed as outlined in a review by *Wu et al.* including digital in-line holography, scanning based techniques and others.[201] Advances in the field of optical imaging techniques and data processing revolutionised microfluidic applications. However, it is up to the discretion of the user to decide the imaging system which is best suited to their application.

For this thesis, the ability to record populations of red blood cells travelling down a channel was imperative. Following on from that, it was advantageous for the components to be low-cost and readily available for implementation into the system.

(i) Camera

The first area of investigation was the camera for image and video capture. There are a wide variety of low-cost solutions for image capture. To allow for creative control over the user interface and imaging software, it was advantageous to choose a camera with programming capabilities. The camera of choice was the Raspberry Pi, V2 (RS Components, UK).

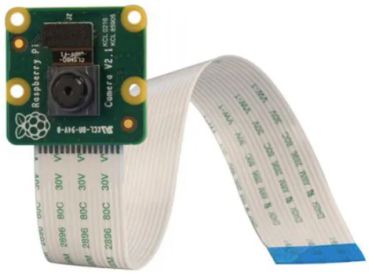

Figure 3-7 The compact size of the Raspberry Pi camera makes it an ideal choice of camera for integration into a portable system. The dimensions are 23.86 x 25 x 9mm with 8 megapixel resolution.

The Raspberry Pi camera module, with a frame rate of 15 FPS and pixel resolution of 3280 x 2464, could be operated in 2 modes; (i) continuous video mode, and (ii) snapshot mode. An advantage of using this camera was that it was possible to simultaneously record a video and capture images. This camera proved to be suitable producing very clear images and videos, see below in *Figure 3-8*, and was priced at ~ €40.

(ii) Magnification

The native magnification of the Raspberry Pi (RPi) camera was not adequate to view the RBCs moving along the microfluidic channel. For that reason, an objective lens (Nikon achromatic finite conjugate objective lens, 4x, NA: 0.10, Edmund Optics, UK) was required for higher magnification, priced at ~ €85.

The distance required between the RPi camera and the lens for optimal focusing of the microfluidic channel was 130 mm. Visual observation of the microchannel coming into focus on the live video feed informed on this optimal distance. A cylindrical holder was designed and manufactured for attachment of the camera and the lens. The holder was connected to a z-axis which was adjusted as necessary for fine focusing purposes.

(iii) Light

Illumination was provided by a white LED (H2A3-NW, 4.0 V; Roithner Laser, Austria) which was held in a fixed position above the microfluidic cartridge. To scatter the light

more evenly across the field of view of the camera, a diffuser lens (Ground glass diffuser, DG10-600; Thor Labs, UK) was positioned just below the LED. This was important for analysis of the images at a later stage. This is a very simple microscopy illumination system but was found to be adequate for our application.

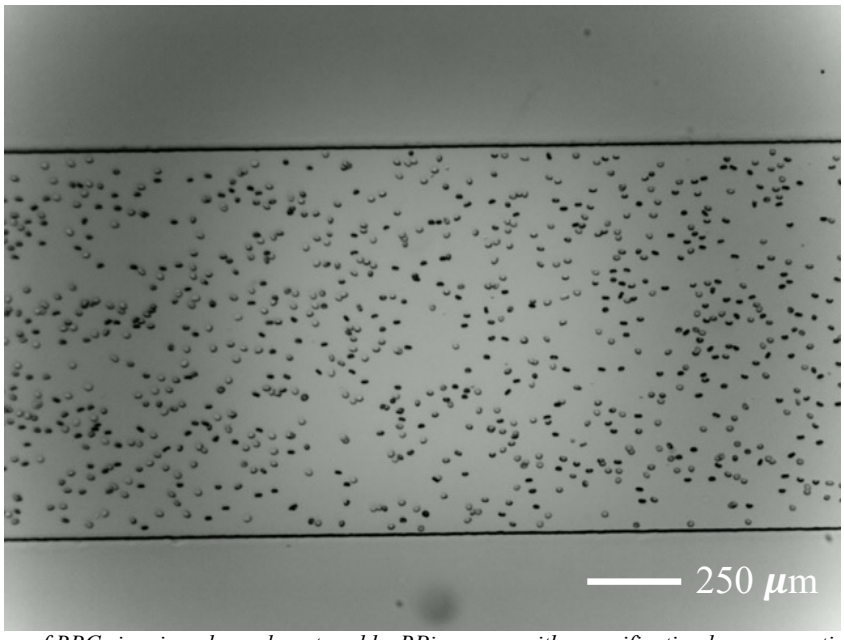

Figure 3-8 Image of RBCs in microchannel captured by RPi camera with magnification lens connection. Illumination was provided by the LED light with diffuser lens for smoothing of light. Visible black lines show channel edges.

(iv) Chip alignment

Alignment of microfluidic cartridge was achieved using a manual X-Y stage (Dino-lite rotational base, RS, UK) which included an internally manufactured holder specific to the design of the microfluidic cartridge. Following initial alignment, the Y-axis subsequently required minimal alignment.

Movement of the chip by the user in the X-axis was required to record observations at predefined positions along the microfluidic cartridge.

3.3.3 Electronic circuit board

Ease-of-use is an important factor to consider for the development of any instrument. To provide easy operation for the user, it is crucial for the device to be as convenient as possible. For this, an electronic circuit board was assembled in-house which supplied power and data transfer to the system. This allowed the user to control all aspects of the instrument via a specifically designed programme.

In this instrument, the syringe pumps, electronic valve, and light source were all controlled via the electronic circuit board, as shown below in *Figure 3-9*. The only interaction the user has with the electronics of the instrument is a common plug connection to a power outlet.

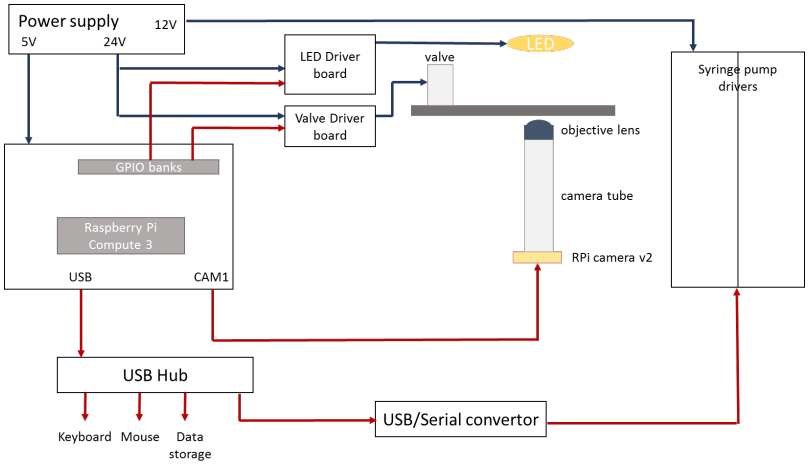

Figure 3-9 Schematic of the control setup for the instrument provided by Epigem. Red arrows indicate data transfer, black arrows indicate power.

3.3.4 High magnification imaging

For the diagnosis of rare anaemias, it is common practice that clinicians will observe a patient's blood smear under a microscope to investigate if there are any abnormal RBC shapes that may help in the diagnosis of the patient. The rationalisation for the development of high magnification imaging was based on the benefit of viewing RBCs for this shape analysis.

This was developed in conjunction to the primary instrument with intentions to integrate into the primary instrument at a later stage.

(i) Hardware and imaging

The components of the high magnification imaging system were similar to that of the primary instrument; (i) RPi camera with cylinder attachment to objective lens (Olympus 50 x, ULWD MSPLAN50) with a distance of 200 mm between camera and lens, (ii) LED in fixed position with diffuser lens, (iii) manual XY stage and Z-focusing, see schematic below in *Figure 3-10.* The casing to hold the imaging system together was made in-house.

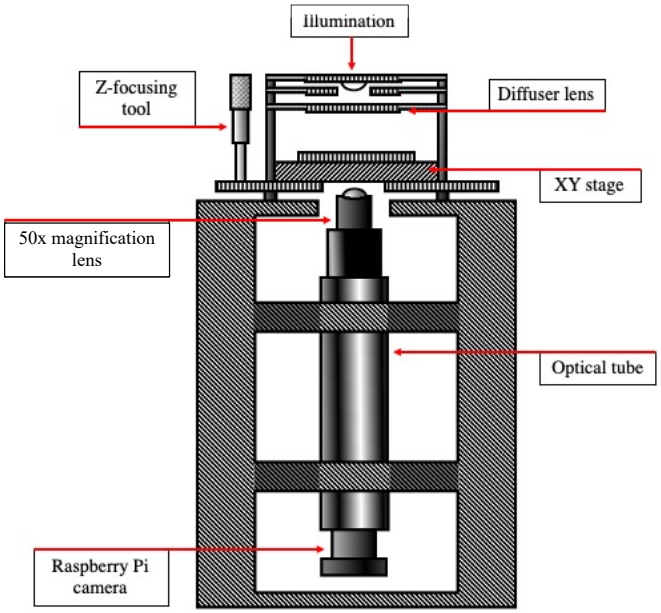

Figure 3-10 Schematic of the high magnification setup.

Due to its relatively simple setup, the high magnification system did not require too many optimisations prior to use. *Figure 3-11* shows the optimisation of the high magnification imaging setup.

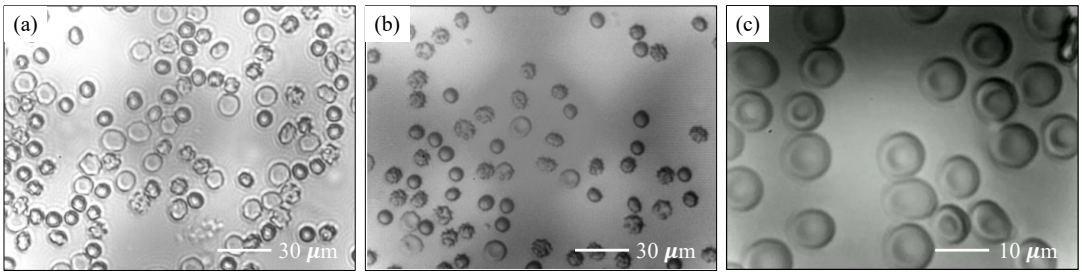

Figure 3-11 (a) insufficient magnification and poor lighting conditions made analysis of the image difficult, (b) addition of a diffuser lens greatly improved the image for analysis, however the magnification was much too small, and (c) a higher objective lens (50 x) produced much better quality images for shape analysis of the cells.

It was intended that this high magnification setup could be used for shape analysis of RBCs prior to and during the biochemical assay experiments.

3.3.5 Summary

The objective of *Section 3.3* was to design an instrument to which a microfluidic chip could easily be attached to run biochemical assays. *Section 3.3* highlights the development of the main instrument with imaging and flow capabilities, see *Figure 3-12*. It also describes an additional imaging tool – the high magnification setup, see *Figure 3-13.* This was not integrated into the primary instrument during the course of this thesis, but it will be integrated in future instrument iterations.

Considering the overall system (instrument, chip, and biochemical assay) was designed to use both mechanical (flow) and chemical (acid) stress to the cells, the primary instrument was termed **MeCheM**, and shall be referred to as MeCheM herein.

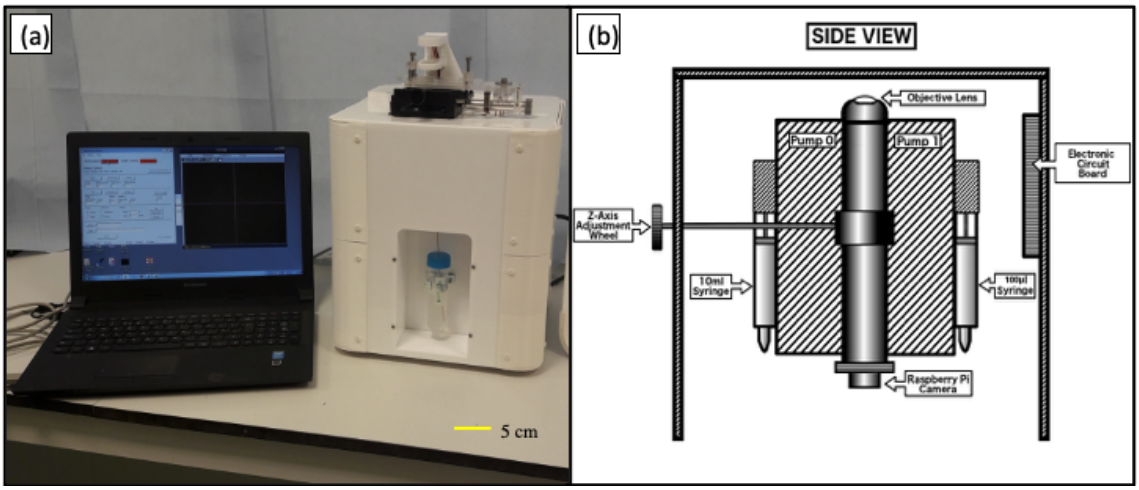

Figure 3-12 (a) shows MeCheM enclosed in a white outer casing. This casing was 3D printed by collaborators in Northumbria University. (b) a diagram of the internal components of MeCheM.

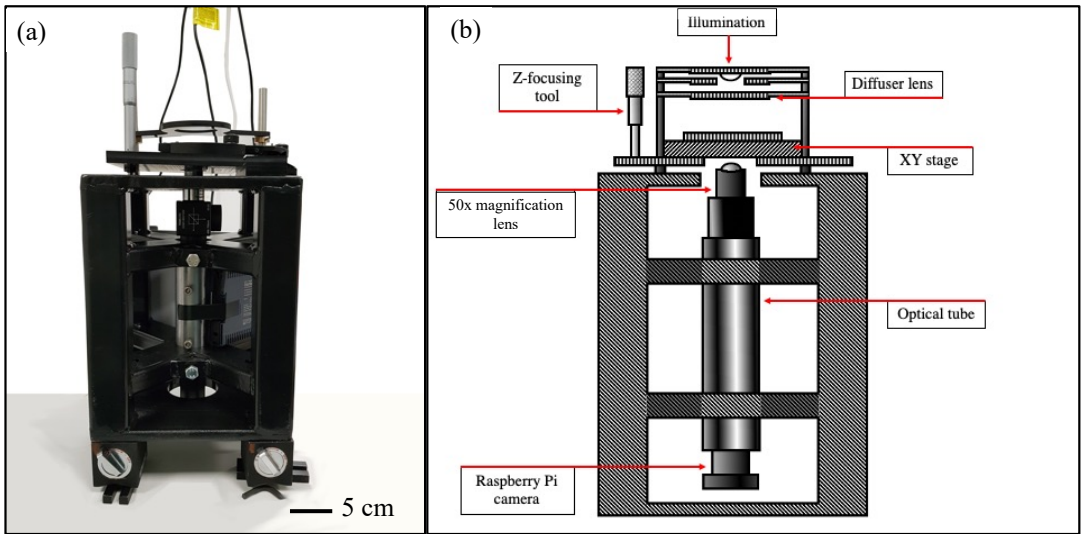

Figure 3-13 (a) shows the high magnification prototype, (b) diagram of the components of the high magnification system

3.4 User interface and data outputs

3.4.1 Interface for MeCheM and High Magnification setup

Similarly to the hardware, it was also of high importance to provide the user with an uncomplicated software for running the system. The requirements for MeCheM were that the user had full control over the pump flow rates, lighting parameters and image/video capture.

For the high magnification setup, all that was required was the ability to change lighting parameters and capture images and videos. A programme was developed in Python by *Epigem* containing all the necessary components required for the operation of MeCheM and the High Magnification test. The user could manually control these parameters, see below in *Figure 3-14.*

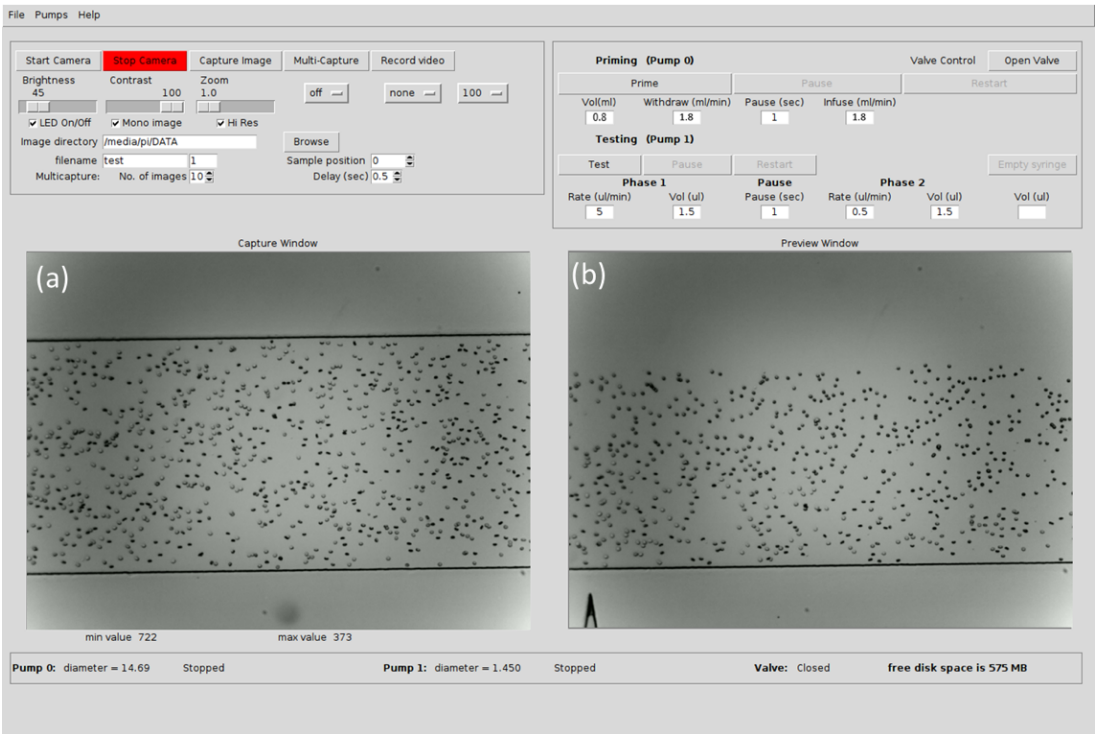

Figure 3-14 User interface for MeCheM shows lighting parameter options (top LHS) and syringe pump controls for the priming (Pump 0) and testing (Pump 1) pumps (top RHS). (b) displays the real-time test recording, and (a) shows the last image that has been captured.

(i) Pumping control

The user was required to input criterion for the flow rate and fluid volume withdrawn in the case of the priming and testing phases of the experiment.

The first function to be executed was the “Prime” function. This opened up the electronic valve to allow for the removal of a user-determined volume of priming solution at a set flow rate from the external reservoir. Upon completion, the electronic valve automatically closed preventing any interference from the priming pump throughout the duration of the test.

The second operation was to run the ‘Test’ function. Again, this followed the users pre-set conditions for flow rate and fluid volume removal.

After the test function has run its course, the user is required to implement the ‘Empty Syringe’ function. This resets the testing syringe back to its zero position by infusing the volume of fluid withdrawn during the test back into the chip for removal.

The pumping control was only required for the operation of MeCheM. This option could be disregarded if High Magnification System experimentation was being investigated.

(ii) Camera control

To accurately monitor cell flow through the channel and cell shape changes using the high magnification setup, it was necessary to observe the experiments in real-time. This was done via a real-time video capture that the user could see in a designated window within the programme. The ability to record the test was also available.

The video capture function was imperative to monitor shape changes of the RBCs over time in the high magnification setup. It was also useful in the case of MeCheM to highlight any unusual flow patterns of the RBCs in the channel which may have been caused by abnormal cell shapes (such as sickle). The video recordings were saved automatically to a previously assigned folder.

Camera setup

Prior to beginning the test, the user was required to turn on the camera using the ‘Start camera’ button. A preview window appeared and the user could use this to align the chip to the desired position and adjust the focus as desired.

Other parameters that could be adjusted at this point were; (i) brightness of the LED, (ii) image contrast, and (iii) the magnification.

The user then saved the files to their directory of choice by using the 'Browse' function which is typical of most applications.

Video recording

To commence video recording, the user implemented the 'Record video' function. This recorded a video continuously until otherwise commanded by the user. The video file was stored in the user-selected directory as previously described.

Image capture

Capture of images could be obtained in two different ways; (i) manual, or (ii) automatic. To obtain manual images, the user simply used the 'Capture image' function, which would capture one image. This function was frequently used for the high magnification setup to capture high magnification images of abnormal cells. It was also useful in the case of MeCheM function to capture any observed abnormalities within the microchannel, such as severe cell-surface adhesion.

The automatic capture of multiple images was a more controlled process of image capture and was used only with MeCheM during the flow analyses. With this function, the user defined the time points at which to take an image, (0.3 – 1.5 seconds) and the number of images taken at that position. The files were automatically stored with their position and image number reference, e.g. Position 0 Image 1 would be P0_1, and so forth.

For any given experiment, it was recommended to take 10 images at each position which totalled 140 images from Position 0 – Position 13. For this reason, the automatic multi-capture function was the preferred method of image capture.

3.4.2 MeCheM analysis software

An in-house analysis programmed termed *'MeCheM Cell Analysis'* was developed by Epigem for automated counting of RBCs in the microchannel and on a microscope slide. For the flow test, images were uploaded in the sequence they had been taken (i.e. from

the 0^{th} to the 13^{th} position). The software could analyse single and multiple images, and video recordings. The output was a .txt file with the number of cells counted with the associated image number and a raw graph with the data plotted. The .txt file could be opened within Microsoft Excel and GraphPad Prism for further analysis.

Parameters that influenced variation in particle counting included the 'zoom' of the image, minimum particle size, minimum separation and box size.

The default 'zoom' was pre-set specifically for images captured by imaging system in MeCheM thus changing the default parameters of this function was not required during the course of this work.

Minimum particle size relates to the minimum size of the smallest cell. If this parameter was set too high, the programme could not find all the cells within an image. Similarly, if it was set too low, the programme would detect smaller particles in the channel that were not cells (debris etc.). The user was required to monitor this parameter as it varied between different blood samples. Minimum separation is the minimum distance between cells. Again, setting this parameter too high or too low may result in inaccurate detection.

Box size is a function that allows the user to determine the region of interest for particle counting. For these experiments, the absolute image was taken into account for analysis, thus this function was not used.

To check the parameters for uploading multiple images, the user should first upload one image and check that all cells in the image are detected accurately. A black circle with a cross through it was added over each cell that was detected giving the user a visual of the detected cells, see *Figure 3-16(a)*. Once the satisfactory parameters had been established, the user then employed the multi-image analysis function.

The particles were counted and a raw graph output was displayed on screen, an example is shown below in *Figure 3-16 (b).* A data file was stored in .txt format and the user uploaded this to Microsoft Excel for further analysis. Below in *Figure 3-15*, a diagram of the analysis work flow is given.

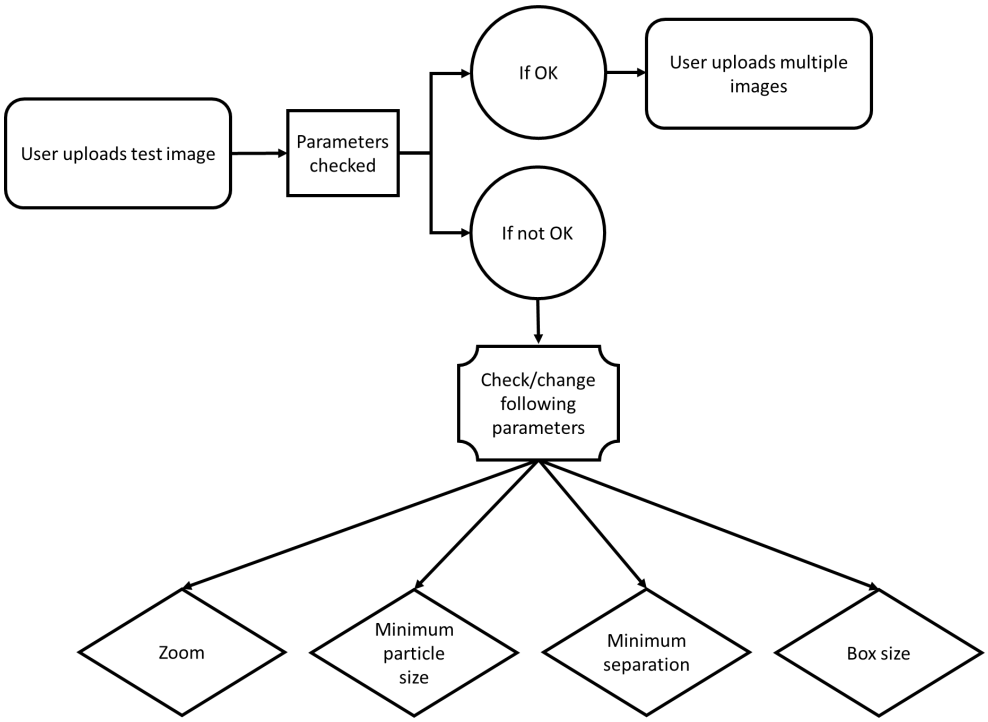

Figure 3-15 Typical workflow for the image analysis software

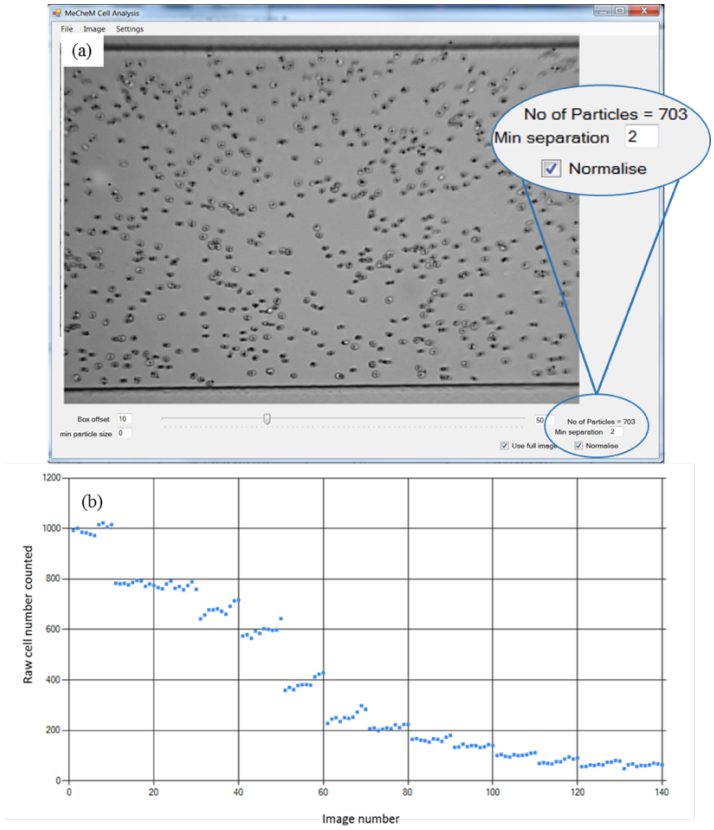

Figure 3-16 Data output of multiple flow test images. (a) MeCheM Cell analysis program counts the cell number in a field of view. User can manually adjust settings to ensure all cells have been located using the 'min particle size' and 'min separation' functions. (b) Output graph from program gives the raw cell count per image.

A template was designed using Microsoft Excel macros which quickly provided the average cell number for 10 images per position and output a graph with normalised cell population count as a function of position along channel.

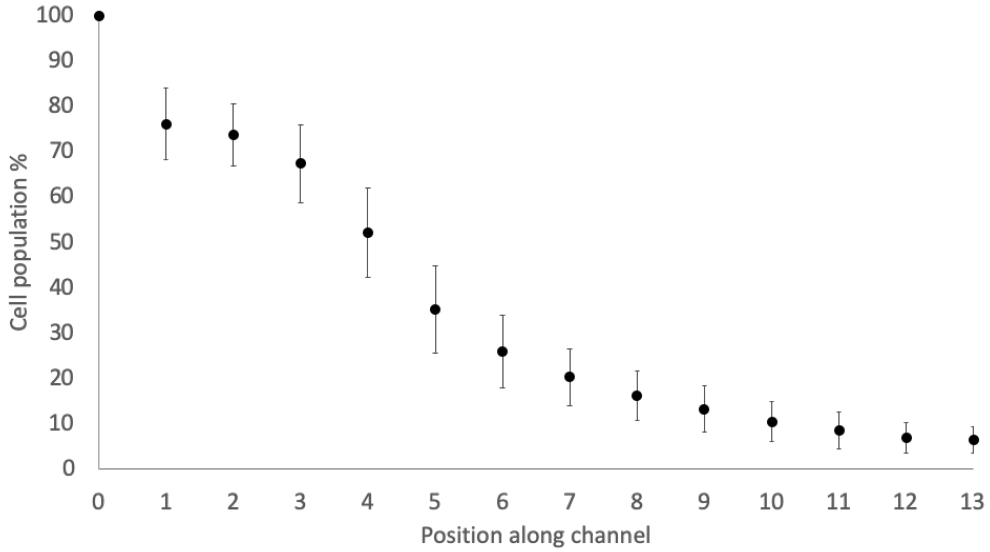

Figure 3-17 Example output image from Excel® showing the normalised cell count per position for 12 healthy samples obtained from University Medical Centre, Utrecht. The error bars are standard deviation.

3.4.3 High magnification analysis

The analysis program for the high magnification data was written in Python and developed between collaborators in the Technical University of Munich and Epigem. The interface for the high magnification system analysis was more rudimentary than the MeCheM analysis.

The data output obtained from the high magnification video analysis was cell lysis as a function of time, cell size distributions as a function of time, and cell size changes as a function of time. The output of this program were .csv and .xlsm files containing all the information relevant to the aforementioned parameters. These files were further analysed as required in Microsoft Excel and GraphPad Prism.

(i) Command Prompt for analysis

The Command Prompt application in Windows was used to execute the analysis. The user ran the following command ‘inferbatch_v2.py’ which called up the analysis programme. Once the programme commenced, a browser window appeared prompting the user to select the video for analysis, see visual in *Figure 3-18*.

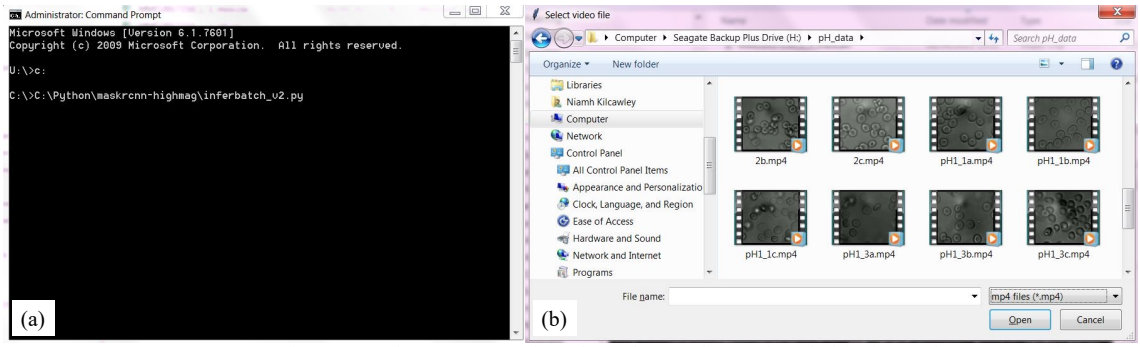

Figure 3-18 Using 'Command Prompt' the user can select the videos to be analysed. (a) shows the Command Prompt window where user will decide the programme, (b) upon selecting the 'inferbatch_v2.py' programme, a window will pop up allowing the user to select the videos for analysis.

Upon selection of a video, the programme requested the user to choose a starting frame. This gave the user the option of including or omitting the analysis of the first few frames of the video which corresponded to the time before acid addition. Following the starting frame decision, the user then had to decide how many frames to analyse. All frames in the video could be analysed, or the user could 'skip' a number of frames to speed up the analysis. It was found that important detail could be lost if the user skipped more than 5 frames for this analysis, thus, 5 frames was chosen as the maximum number of frames that could be omitted.

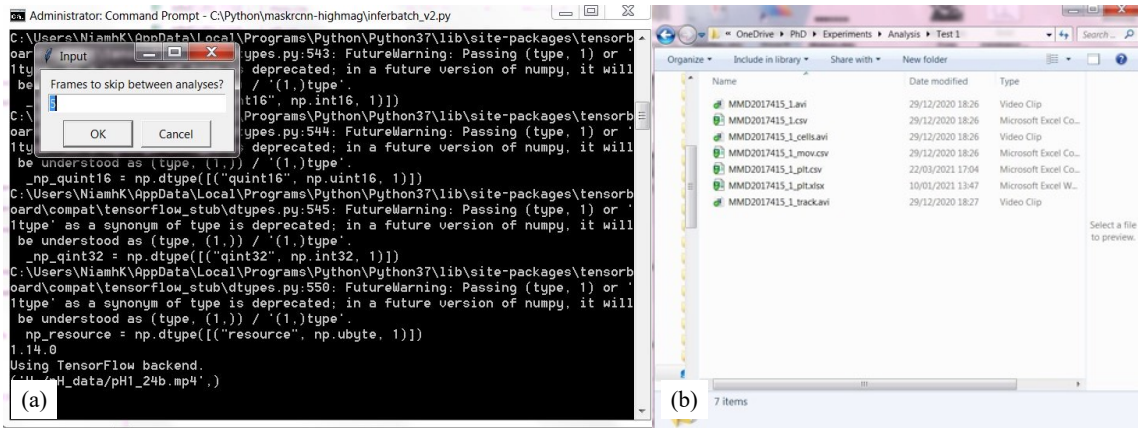

Figure 3-19 (a) user is given the choice to skip frames within the videos, (b) output files are recorded in a folder selected by the user.

Finally, the user was requested to choose a folder in which to save the output files. Once this was selected, the programme began analysing the frames until completion, the time for this typically took 15 minutes, although it varied for videos of different length.

(ii) Analysis programme data output

The data output from the inferbatch_v2.py programme were in the forms of; (i) a .plt.csv file containing data recording the cell count over time and the projected area measurements over time, and (ii) two .avi files, each highlighting different aspects; (1)

Figure 3-20 (b) displayed a brightly coloured blob over each cell detected, and (2) *Figure 3-21* shows a circle around each cell that increased or decreased in size with the cell over time.

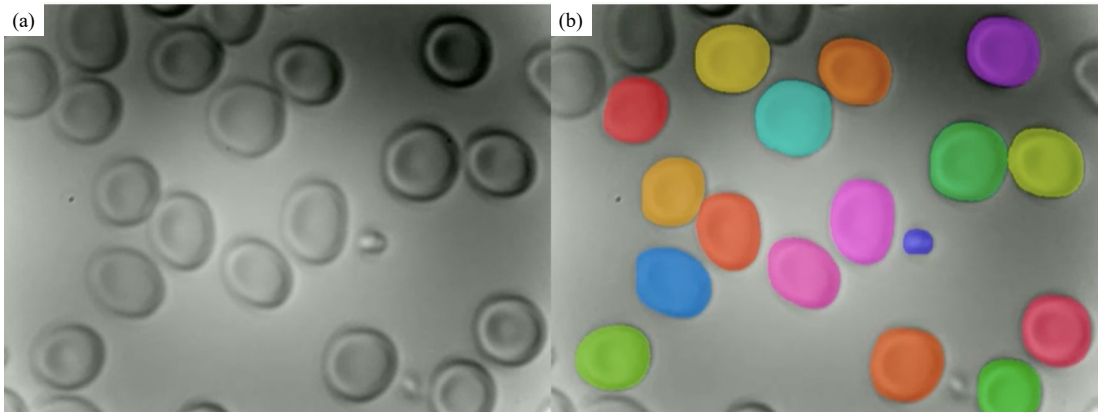

Figure 3-20 The recorded experimental video is shown in (a) and the blob detection analysis is shown in (b).

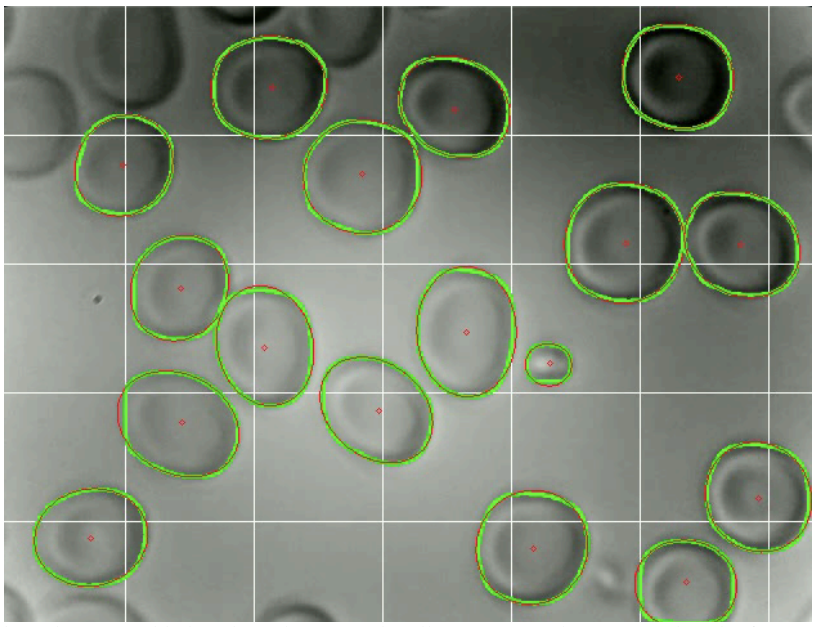

Figure 3-21 Grid marks were added to the video as each cell was given a location within the frame. This allowed the user to review specific cells based on their location from the excel spreadsheet. Green circles were drawn around the detected cells and the red dot corresponded to the centre of the cell.

(iii) Microsoft Excel compilation

A macro-enabled template was created in Excel which allowed the user to upload the .plt.csv files. As each test was carried out in triplicate, the template required the input of 3 .plt.csv files. The programme would automatically search for and determine the 'zero' point, that is, the point after acid addition. Due to the testing method procedure, the pipette tip required for acid addition would obscure the view of the camera and, typically, the frames would go dark until the pipette tip had been removed. This was logged on the

analysis programme as an error because the cells and their projected area could not be measured. In the Excel file, it was recorded as ‘ #N/A’.

The Excel programme would detect an influx of these ‘errors’ and use their location to set the zero point. The user could then confirm that the chosen zero point was correct. If it was correct, the user could then run the consolidate macro that consolidated the output graphs to the zero time point. If the zero point was chosen incorrectly by the excel programme, the user could manually change it to the correct zero point before running the consolidate macro, see sample data below in *Figure 3-22*.

Frame	Time	Cell count	584|381	351|77	579|185	521|52	212|60	485|189	77|408	207|270	297|312	415|414	98|123	361|254
0	-8.8	17												
1	-8.4	16												
2	-8	38												
3	-7.6	40	53.21999	49.69877	52.72345	52.89813	51.84864	64.53468	50.26822	49.59836	50.25997	58.36566	45.17207	55.86091
4	-7.2	41	53.1636	49.51171	52.77296	52.83486	51.80463	64.35586	50.19669	49.99175	49.95461	58.30239	45.30549	55.93244
5	-6.8	53	52.96828	49.63687	52.99717	52.73995	52.19389	64.33661	50.17331	50.49655	50.16231	58.09469	44.98088	56.2543
6	-6.4	52	52.80598	49.59011	52.872	52.63404	52.34657	64.36687	50.41127	50.56257	50.16231	57.85123	45.04003	56.72334
7	-6	54	52.69181	49.49107	52.71794	52.60378	52.84311	64.1124	50.48692	50.67811	50.12654	57.74119	45.14456	57.13185
8	-5.6	54	52.44422	49.49658	52.39196	52.74408	52.883	64.13166	50.38788	50.97384	50.00138	57.63528	45.37014	57.33267
9	-5.2	54	52.39196	49.41542	52.59965	52.77021	52.85137	64.02988	50.47729	50.83216	49.89546	57.87186	45.2436	57.73156
10	-4.8	55	52.30805	49.26549	52.22827	52.70832	53.07419	63.63924	50.21595	50.42502	49.97387	57.88699	45.22159	58.15383
11	-4.4	53	52.2324	49.17196	51.99444	52.7262	53.39055	63.73415	50.04264	50.18569	50.22558	57.99565	45.64111	58.21711
12	-4	53	52.19114	49.14583	51.63407	52.67943	53.49647	63.71489	49.96836	50.33287	49.90372	58.29688	46.15416	58.14283
13	-3.6	53	52.12786	49.10044	51.66708	52.4566	53.61751	63.4563	49.8597	50.39476	49.80056	58.43168	46.43889	58.26662
14	-3.2	51	51.93667	49.2036	51.56392	52.57902	53.58174	63.74928	49.74003	50.55844	49.96836	58.6435	46.65209	58.03967
15	-2.8	52	51.84864	49.22836	51.63407	52.66705	53.58725	63.47143	49.92848	50.83492	49.67401	58.65038	46.54205	57.89662
16	-2.4	52	51.83076	49.21185	51.52265	52.58177	53.83208	63.10005	49.82669	51.29432	49.75379	58.638	46.58056	57.75357
17	-2	52	51.84589	49.43055	51.65608	52.71657	53.80045	63.48931	49.80606	51.9518	49.66713	58.57748	46.94094	57.4152
18	-1.6	54	51.76336	49.54609	51.94355	52.63679	53.68078	63.32426	49.8487	52.39058	49.71665	58.44956	46.78413	57.45922
19	-1.2	53	51.7652	49.56351	51.98665	52.65421	53.64593	63.18281	49.91014	52.24501	49.70313	58.32691	46.63489	57.44271
20	-0.8	54	51.81783	49.50703	51.97766	52.83459	52.84036	63.34681	48.4723	52.27229	52.83876	58.28615	47.93793	57.21548
21	-0.4	54	51.88234	49.43915	52.13509	52.7513	52.6555	63.00067	48.1244	52.49856	53.25246	58.24427	47.85288	57.3705
22	2.55E-15	49	51.92567	49.40304	52.11182	52.55793	52.5467	58.67995	47.33295	52.93344	54.67697	58.20335	48.25727	57.34643

data 1 | data 2 | data 3 | consolidated | smoothed | Chart | smoothed chart | cell counts | average | average data | output charts | distribution | +

Figure 3-22 Example of the data output from the Python analysis programme. Each patient sample was run in triplicate and the respective video files were reported in the Excel file as ‘data1, data2, data3’. The information obtained from these videos was consolidated and raw charts were reported in the ‘output charts’ sheet.

The final macro to run was a data binning macro. This macro separated the projected area measurements into pre-determined projected area ranges for different time points throughout the experiments. The user could modify the time points via the Microsoft Excel template. For these experiments, the time points chosen were; (i) t = -5, (ii) t = 20, (iii) t = 40, (iv) t = -60, (v) t = 80, and (vi) t = 100, with t = -5 corresponding to 5 seconds before the addition of the acid. *Figure 3-23* shows the output graphs from the Microsoft Excel template.

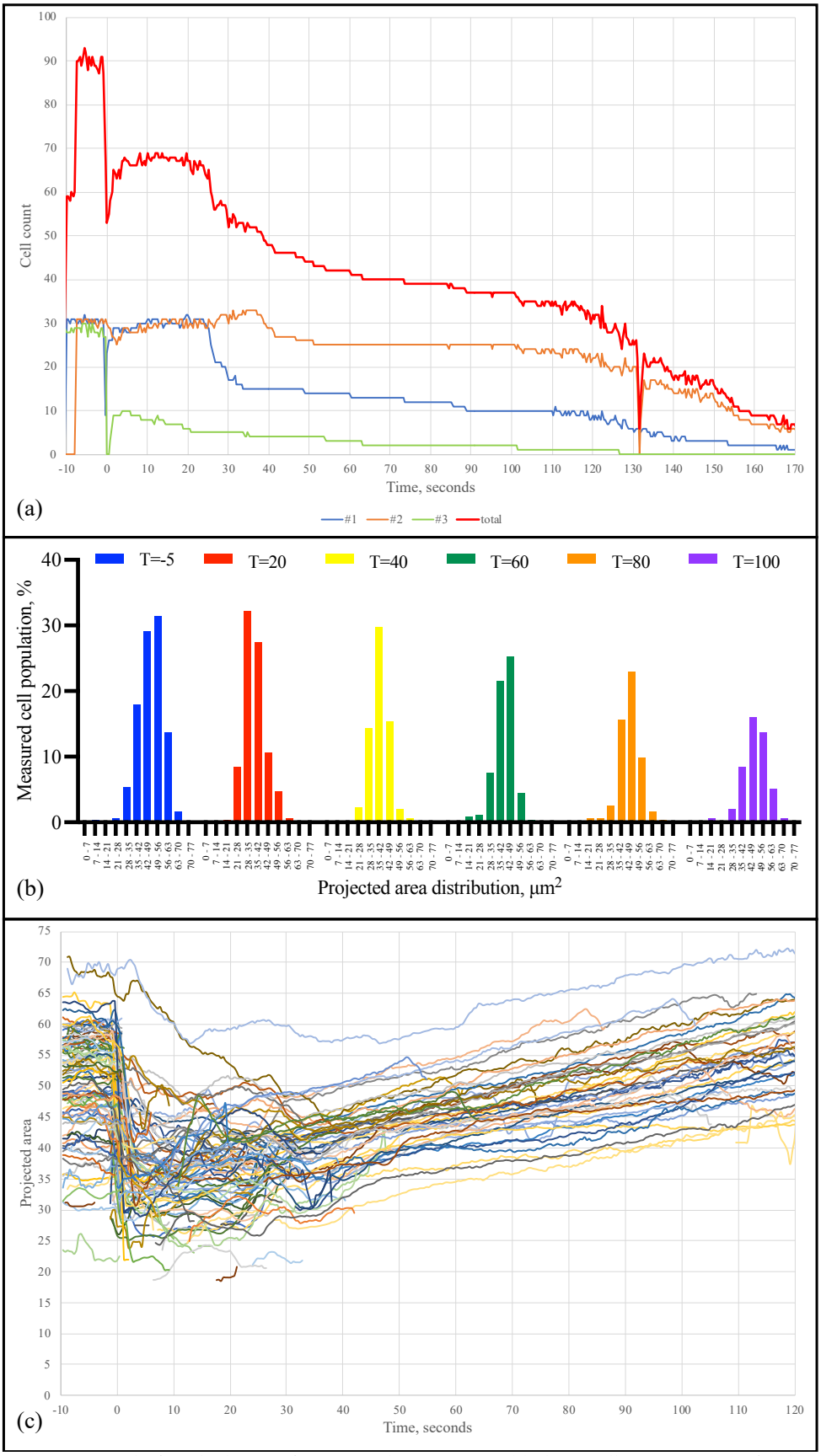

Figure 3-23 Output graphs from high magnification analysis program. (a) shows cell count over time for three runs on the same sample (#1 - #3) and their sum (total). Acid addition is at t=0, t<0 is pre-acid addition. (b) projected area distribution of cells at selected time intervals. -5=pre-acid addition, 20-100=post acid addition. (c) projected cell area over time for all cell tracks. A cell track is defined as a single cell that remains in the field of view of the camera throughout the test until lysis or test completion.

3.5 Microfluidic chip development

Whilst the protocol and chip development happened simultaneously, the design and optimisation of the microfluidic chip will be discussed first. All microfluidic chips were manufactured in-house by *Epigem* using both standard and proprietary photolithography methods.

3.5.1 Microfluidic chip design

The original design utilised 2 separate syringe connections to the chip. As previously discussed, one of the aims of MeCheM was to remove the need for syringe replacement or cleaning after each test.

(i) Version 1

Prior to the development of MeCheM, the microfluidic cartridges were manufactured for connection to an external syringe pump and monitored with an on-bench microscope. The first system optimisation was to use the syringe pump in withdrawal mode, meaning that only one syringe connection was required. Thus, the first chip design optimisation was to manufacture external reservoirs to store the samples and position the syringe connection at the end of the channel so the pump could withdraw samples from the external reservoirs through the channel, *Figure 3-24*.

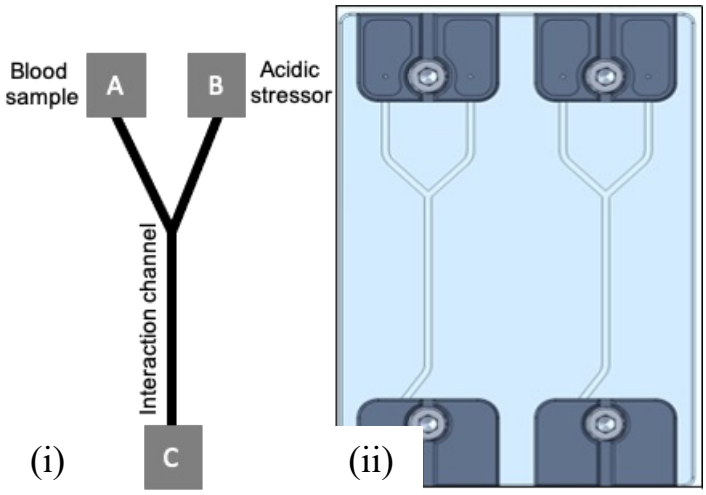

Figure 3-24 (i) Blood sample and acidic stressor were stored in their respective reservoirs; (A) and (B). The microfluidic chip was connected to the syringe pump via an attachment fitting at (C). Fluid from (A) and (B) travelled down their separate paths and merged in the interaction channel. (ii) The original design had 2 tests per chip. The microchannel was 1 mm in width and 20 μm in depth. The length of the testing channel was 30 mm . This image was designed using the 3D CAD software SolidWorks.

Challenges to overcome

The most concerning observation of this design was the propensity for air to become trapped within the microchannel, *Figure 3-25 (b)* and *(c)*.

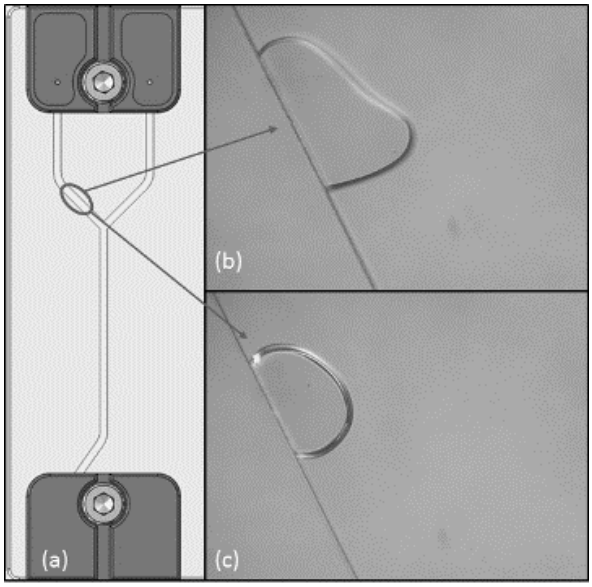

Figure 3-25 Bubbles attached to the wall of the microfluidic channel caused by air leakage around the reservoir connection point prevented stable flow of cells through the channels.

Rubber ferrules were used to seal the external reservoirs to the microchannel. However, they appeared to not have adequate sealing, leading to air leaking into the channel when the syringe was driving fluid. Leaking of air formed bubbles within the channel which affected the fluid flow. These bubbles, *Figure 3-25*, often adhered to the channel walls before or at the point of intersection and would sometimes release into the stream of fluid further along the testing channel. The formation of bubbles was problematic due to inconsistent flow of fluid around these air entrapments and would often cause incorrect software recognition of bubbles instead of cells.

A second issue was the direct connection of the sample channel to the syringe. For pumping in withdrawal to be beneficial, it was required that no sample would enter the syringe to contaminate it. *Version 1* of the chip design would only allow for a very short testing time before the samples would contaminate the syringe. Thus, it was decided that a ‘sample waste’ serpentine channel should be designed on to the chip that would store any of the waste samples on chip without concern about system contamination.

(ii) Version 2

With the advantage of the constant 'primed' state of the tubing within MeCheM, a significant reduction of air within the channels was observed. However, the external reservoirs on the chip remained an outstanding problem for air entrapments. As such, sample reservoirs were integrated into the chip design as shown below in *Figure 3-26*. These reservoirs were manufactured by drilling directly into the plastic casing of the chip before sealing it to the microchannel.

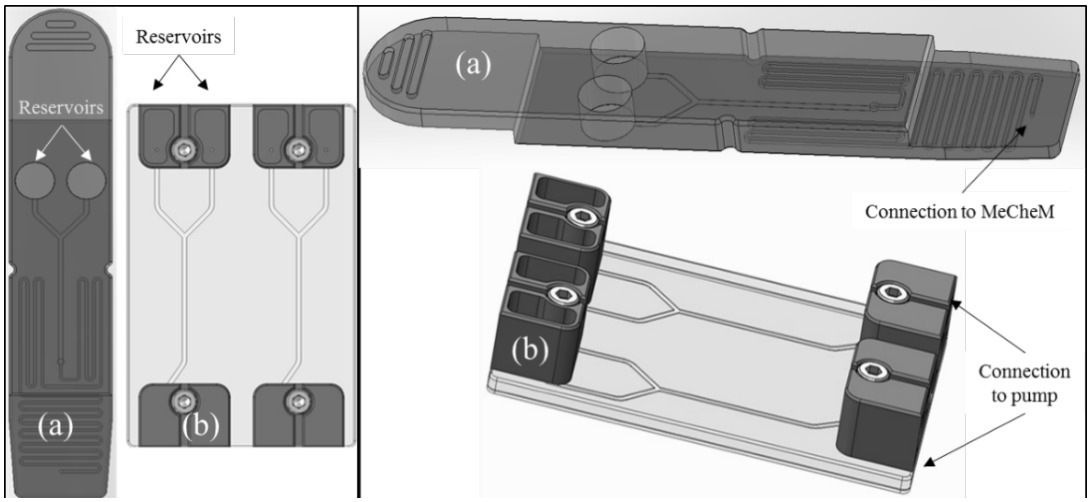

Figure 3-26 (a) optimised chip design with integrated sample reservoirs. (b) initial chip design with external reservoir fittings.

The design of the casing of the chip was altered to optimally secure into MeCheM instrument via a pressured O-ring connection. With this new design, bubbles within the channel were consistently removed with the priming step.

The geometry of the channel was designed to be as wide and as shallow as possible ensuring that all cells within the channel were in the field of view and field of depth of the camera. The length of the interaction channel was 30 mm. The channel depth was 20 µm with a width in the interaction channel of 1000 µm. This gave an aspect ratio of 50:1.

Challenges to overcome

With this high aspect ratio came significant issues for chip to chip reproducibility, *Figure 3-27*. During the manufacturing process, the bonding of the separate layers caused an irreparable buckling of the surface channel wall. This affected the flow within the channel and in more severe cases the surface channel would collapse thus preventing any fluid flow.

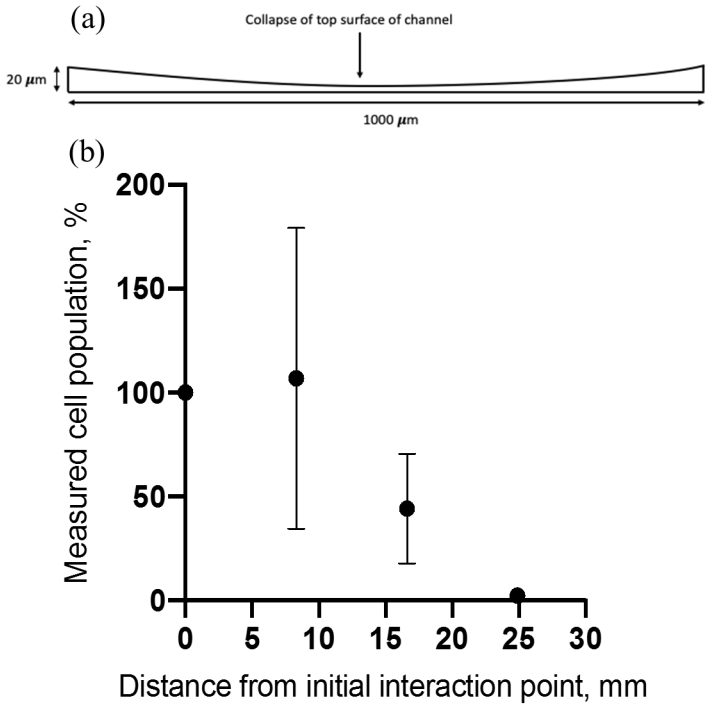

Figure 3-27 The initial high aspect ratio chip design had very low reproducibility. (a) shows a cross sectional schematic of the surface collapse of the channel. (b) The points on the graph represent the mean of the measured cell population (n=5) along 4 testing points in the channel. Error bars were calculated from the standard deviation.

The effect of this surface buckling could result in the measured cell population significantly increasing from position 1 to position 2 along the channel. This was due to blockages in the acid fluid pathway causing the blood sample pathway to dominate in the interaction channel leading to an influx of RBCs in the field of view (FOV).

It was also noted that there appeared to be disturbances of the RBC population around the joining of the sample channels to the testing channel. It was unclear whether this was caused by channel buckling or if it was a product of the channel design. This was under investigation in the next design iteration.

(iii) Version 3

The final optimisations were to eliminate channel blockages due to surface buckling and to remove any uneven flows within the channel. Surface buckling was caused by the high aspect ratio of the channel (50:1). Reduction of the high aspect ratio could be easily achieved by increasing the depth of the microchannel and decreasing the overall channel width. Uneven flow patterns within the channel were suspected to be a by-product of sample channel proportions and angles in relation to each other and the testing channel. This supposition required investigation.

The specifications for the chip were that a sufficient number RBCs (~ 500 cells) could be clearly observed in the microchannel, the flow of the cells was laminar, and the chip was reproducible.

Reduction of aspect ratio

Various configurations of channel depth and width were tested to determine the optimal channel geometry for reproducible clinical testing, see descriptions of chip designs tested below in *Table 3-2*.

The first design alteration reduced the channel width from 1 mm to 0.5 mm. The reduction of the channel width was investigated for a range of channel depths (20 – 100 μm).

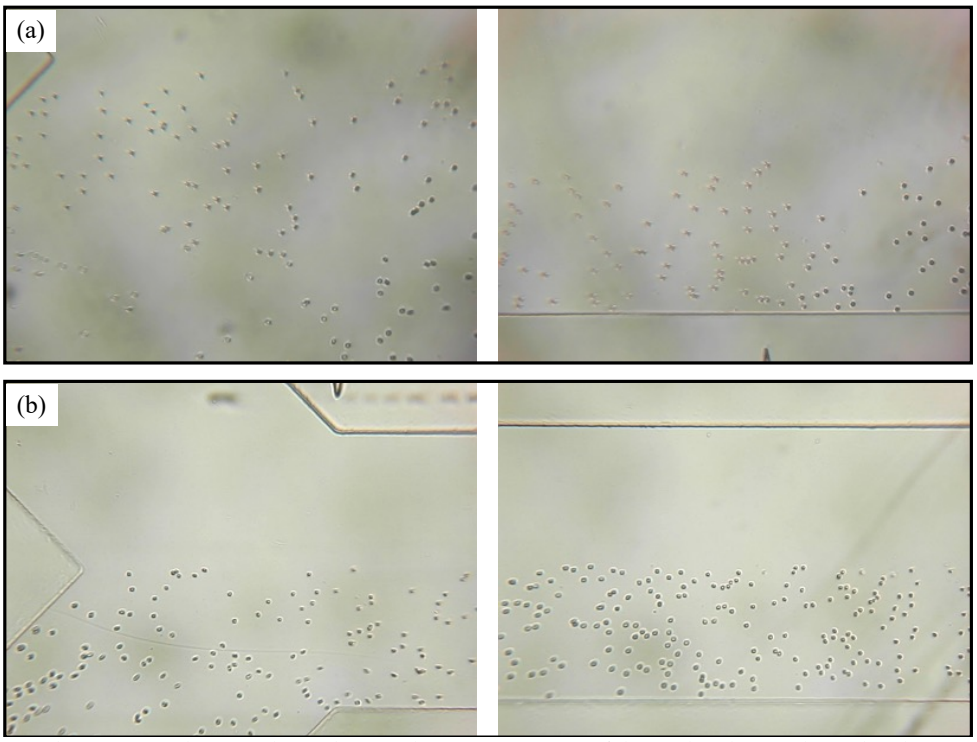

Figure 3-28 The image on the LHS shows the initial interaction point of the acid and RBC channels. The image on the RHS shows a point further down the channel in the 'testing' region. (a) FOV of the MeCheM imaging system for the original chip dimensions (1 mm width, 20 μm depth), (b) FOV of the MeCheM imaging system for the new chip dimensions (0.5 mm width, 40 μm depth).

It was found that the increased channel depth caused focusing issues for the camera, i.e. the camera could not observe all the cells flowing through the channel in the same field of focus. As such, the depth range for the channel was found to be between 20 and 40 μm.

Notwithstanding the reduction of the channel width, channel blockages were still observed for the 20 µm depth chips. Thus, it was decided to fix the channel depth at 40 µm for future chip variations.

Removal of channel turbulence

The issue of the channel turbulence and uneven flow patterns still remained. There appeared to be an almost reproducible pattern of a RBC velocity increase around the corner of the intersection channel for the cells closest to the channel wall.

To investigate the cause of this velocity increase, various chip designs were developed and tested including; (i) varying sample channel angles, and (ii) varying sample channel proportions.

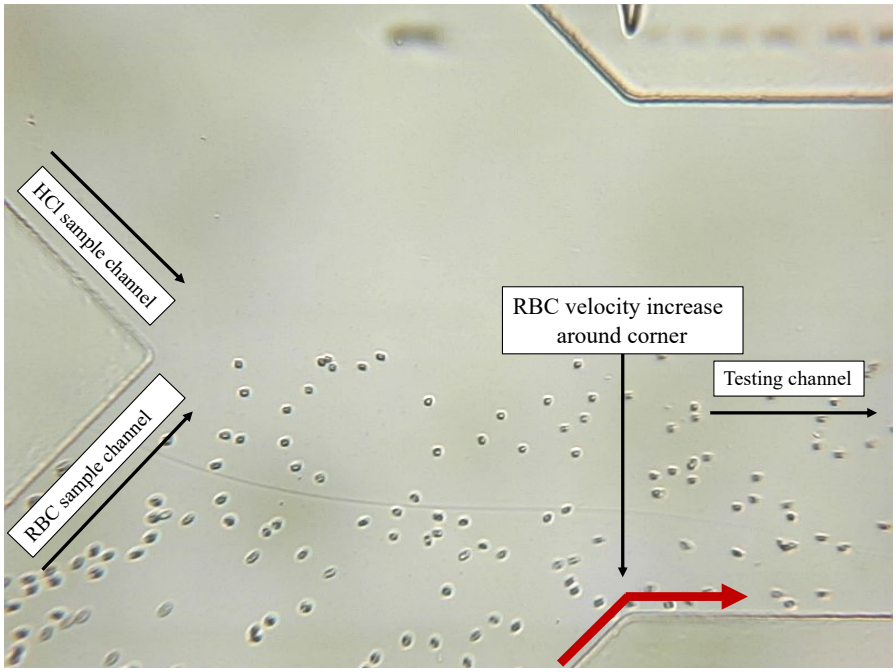

Figure 3-29 An increase in cell velocity around the corner of the channel was observed for all angle variations of the channel design. Here, the acid concentration is 0.25% HCl and the RBC sample was diluted to 15%.

The result of the sample channel angle variations was that for every angle > 0° tested, the increase in RBC velocity around the corner at the interaction of the sample channel and the testing channel remained. Thus, the optimal channel design for uniform velocity of cells was to remove all angles from the RBC sample channel, i.e. a straight pathway from RBC channel to testing channel.

Although designing a direct pathway from the RBC sample channel to testing channel removed the increased velocity of cells at the channel walls, the cell population still

appeared, albeit homogenously, to change velocity as they entered the testing channel. This was likely to be caused by fluid constriction as both 0.5 mm sample channels were flowing into one 0.5 mm testing channel. Various configurations of channel proportions were investigated, *Table 3-2 (C – F)*, and it was found that the optimal design for uniform velocity and sufficient cell numbers for observation was a blood sample channel width of 0.5 mm and an acid sample channel of 0.25 mm merging into a testing channel of 0.75 mm.

Iteration	Interaction channel width	Depth	Blood sample channel width	HCl sample channel width	Description	Comments
A	1mm	20 µm	1 mm	1 mm	Original y-channel with external reservoir block.	Many air entrapments from external block reservoirs and many channel blockages due to high aspect ratio chip design, not reproducible.
B	0.5 mm	20 µm	0.5 mm	0.5 mm	Y-channel design, integrated reservoirs, reduced overall size, new casing to fit and seal to MeCheM.	No air entrapments, flow around intersection seemed turbulent and unpredictable, some channel blockages observed, not reproducible.
C	0.5 mm	40 µm	0.5 mm	0.5 mm	Y-channel design, increased depth.	No air entrapments, no blockages, flow around intersection still unpredictable and turbulent, initial cell number very low (<300 cells in FOV), reproducible.
D	0.5 mm	40 µm	0.25 mm	0.25 mm	Y-channel design, sample channels reduced in width, interaction channel remained the same width as previous design.	No air entrapments, no blockages, flow appeared to be less erratic but still seemed to increase at the y-intersection, cell number very low (<300 cells in FOV), reproducible.
E	1 mm	40 µm	0.5 mm	0.5 mm	Ƴ-channel ("k-channel"), blood sample flowed down straight channel, acid sample interacted from the side, interaction channel width was increased to 1 mm.	No air entrapments, some blockages, flow less erratic. Cell count was increased (>500 cells in FOV), not reproducible.
F	0.75 mm	40 µm	0.5 mm	0.25 mm	Ƴ-channel, width of blood channel remained at 0.5 mm to allow the higher cell numbers in FOV, acid channel reduced to 0.25 mm to reduce channel blockages.	No air entrapments, no blockages, stable flow, cell count >500 in FOV, reproducible.

Table 3-2 Sample of microfluidic chip geometry variations during optimisation tests. Based on visual and graphical observations, the chip that was concluded to be the optimal design was iteration F. This chip was used for all flow tests unless otherwise stated.

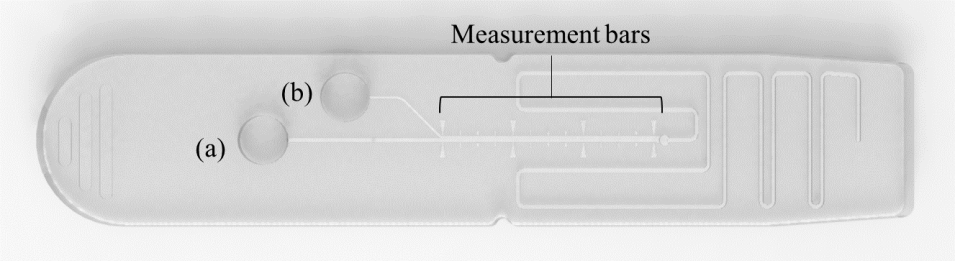

Figure 3-30 SolidWorks design of the optimal chip design for the flow test, iteration F, herein referred to as Ƴ-channel ("k-channel"). (a) integrated blood sample reservoir. (b) integrated acid sample reservoir. Measurement bars are marked along the interaction channel. Waste from test flows into the serpentine channel which is ~10 cm in length (full serpentine not shown in image) and can store a volume of up to 100 µL.

These chips were highly reproducible and all of the aforementioned issues were resolved with this design, *Figure 3-30*. Thus, it was chosen as the standard chip design for testing advancement. Additional markers were added along the outside of the channel to be used as reference points for imaging. This chip design is herein referred to as the Ƴ-channel ("k-channel"), alluding to its similarity to the symbol.

3.6 Development of experimental procedures

Prior to interrogation of the robustness of MeCheM and the High Magnification System, it was critical to develop a standard working protocol for the system. This section discusses the development of the experimental procedures that were brought forward for interrogation as discussed in the next chapter. Protocols for the developed methods can be found in *Chapter 2.7*.

3.6.1 MeCheM

The requirement for the flow test was that a measurable reaction (sufficient cell lysis ~ 80%) must be observable within the testing channel length (30 mm). To achieve this, the parameters that were varied; (i) flow rate, and (ii) acid concentration, are discussed below.

(i) Flow rate

The maximum experimental flow rate was determined by the frame rate of the camera. For these experiments, the camera frame rate was 15 frames per second (FPS). It was found that the camera could accurately image cells travelling through the channel at a flow rate of up to 1 μL/min, *Figure 3-31*.

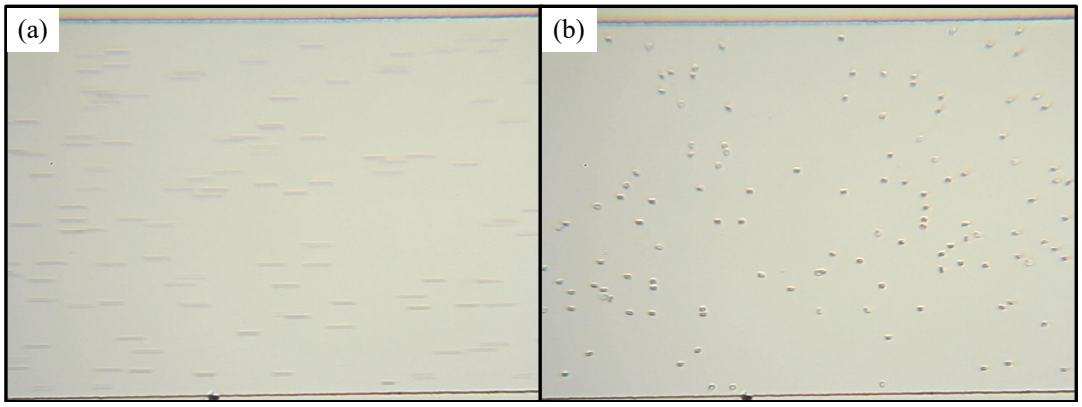

Figure 3-31 (a) cells travelling through channel at 1 μL/min. The image is unclear and the cells appear blurred. It was not possible to analyse this image using the particle counter programme. (b) cells travelling through channels at 0.5 μL/min. This image shows clear definition of each cell in the FOV.

The recognition of the maximum flow rate gave a range for flow rate analysis from 0.1 – 1 μL/min.

(ii) Flow stabilization

The initial experimental protocol commenced image capture of the channel immediately following the observation of cells in the channel. However, during the course of repeatability measurements, it was observed that the measured cell population appeared

to increase in the initial positions of the microfluidic channel where cell reduction due to acid lysis was the expected outcome, *Figure 3-32*.

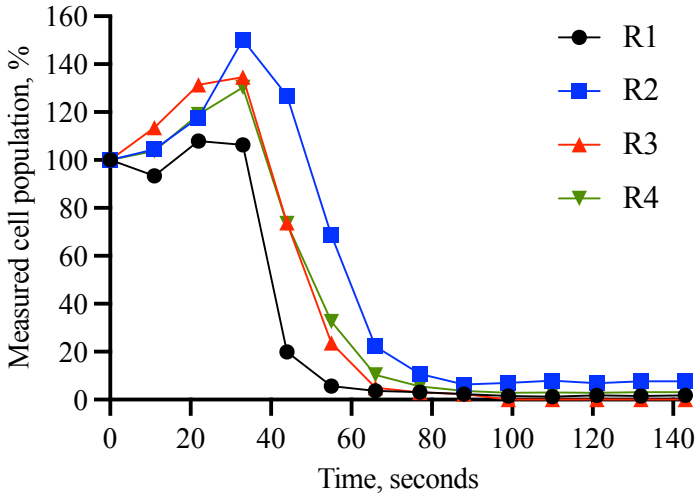

Figure 3-32 The initial position corresponding to t=0 on the x-axis was expected to show the highest number of cells. Cell count was normalised to the number of cells counted at this position. R1 – R4 indicates the test 'run'.

To investigate the apparent cell increases, an experiment was conducted using a control saline solution in the acid reservoir of the chip to monitor cell population fluctuations in one position over time, see *Figure 3-33*.

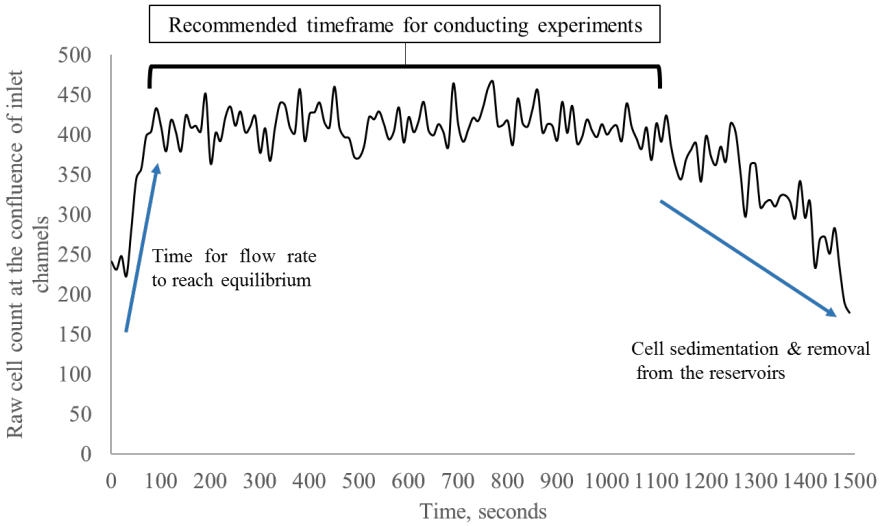

Figure 3-33 An image was recorded every 10 seconds for 25 minutes at the junction of the blood and acid channel. The results show a flow stabilization time of approximately 2 minutes, where the cell count increases up to that timepoint. The flow rate remained stable, albeit with cell fluctuations, between 120 and 1100 seconds. The recommended maximum test time for the Y-chip at 0.5 µl/min is therefore 18 minutes.

The results show that between 0 and 120 seconds the cell population increases as the flow stabilizes within the microchannel. There are further cell population fluctuations within the recommended testing timeframe of 18 minutes. These fluctuations in the plateau region are very likely to be statistical noise associated with the cell population varying in number for each image recorded. To account for these fluctuations, it was recommended

that the user took an average cell count of 10 images per position and used this average cell count for analysis. After ~18 minutes, the RBCs numbers began to decline due to cell sedimentation and emptying of the sample from the reservoir. Future tests were adjusted to take the optimal testing timeframe into consideration. The time required to allow flow stabilization in the channel was 120 seconds, thus, imaging and video recording did not commence before this time.

(iii) Acid concentration

Another consideration was to ensure that the acid was the correct concentration to allow for a measurable reaction within the length of the testing channel. The blood and acid samples flow through their respective channels, eventually combining at the interaction point. At this point, the samples begin to mix and this continues along the length of the testing channel.

As the reaction is both concentration and time-based, it follows that the flow rate and acid concentration could be adjusted separately to achieve the desired outcome. However, for the determination of the optimal acid concentration, it was decided to use a constant mid-point flow rate (0.5 μL/min). This flow rate was chosen to allow sufficient time to monitor the haemolysis trends of the cells within the channel with intentions to use the output curve shape as a distinguishing factor, thus it was a limiting factor.

Haemolysis caused by acid disruption had been originally investigated by *Bodansky* using a range of inorganic acids.[202] One of *Bodansky's* findings from that research was that low pH HCl (pH 1.3) had the most rapid RBC lysis time (0.43 minutes).

With the short testing channel length of the Y-chip, a lower pH acid was required to achieve sufficient lysis of cells within the time of exposure during the test. Given the rapid lysis described as per *Bodansky's* method, it was decided to investigate the efficiency of low pH surrounding the range of pH 1.3 for RBC haemolysis within the microchannel. The results of these experiments are shown below in *Figure 3-34 (a)*.

Interestingly, a sharp decrease followed by sudden increase in cell population was observed for pHs 1.47, 1.85 and 2.0. Upon further investigation, it was found that these

'increases' were caused by aggregation of cells RBCs which appear to be more resistant to lysis, see *Figure 3-34 (b)*. These aggregations would be move through the microchannel in flow and would sometimes adhere to the surface of the microchannel. However, the RBC aggregation in flow was not observed for pH 0.7.

RBCs maintain a negative surface charge which prevents cell adhesion under normal circumstances.[203] However, the introduction of the H^+ ions from the acidic stressor will cause the cells to move through their isoelectric point, changing their surface charge from negative to positive.[204,205] Due to the nature of the experimental setup, the cells nearest to the acid stream within the microfluidic chip will go through this charge change first, allowing for attraction of the oppositely charged RBC surfaces, thus causing cell adhesion or agglutination. The adhered cell-cell clusters moved more slowly through the channel thus an increase in cell numbers was recorded in the later observation points along the channel.

This was also observed in the lower pHs between the first and second marker, but the aggregates of the lower pHs showed a tendency to adhere to the surface of the microfluidic channel instead of in flow further along the channel thus the cell 'increase' for these pHs was rarely recorded.

The result of this set of experiments was that pH 0.7 displayed the most rapid haemolysis with the least disruptive cell adhesion within the microchannel.

(a)

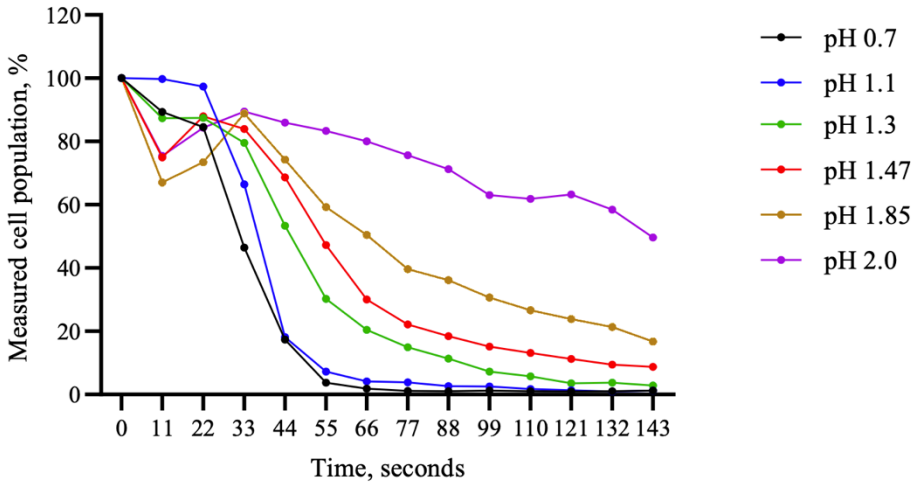

(b)

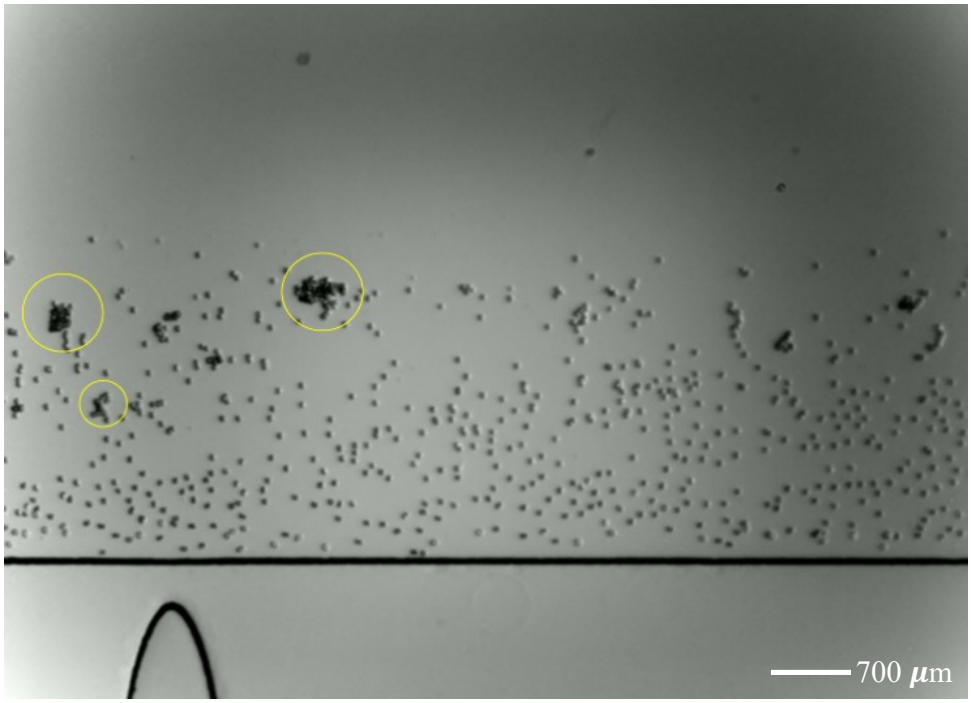

Figure 3-34 (a) The markers along the curves represent the position on the microfluidic channel where the images were taken for analysis. This was converted into time points post-analysis. For pH 0.7 $T_{50\%}$ was observed at 31.9 seconds. This was followed by 38.8 s for pH 1.1, 45.6 s for pH 1.3, 53.6 s for pH 1.47, 66.5 s for pH 1.85 and finally 142.5 s for pH 2.0. (b) Cell aggregates (highlighted with yellow circle) in flow at the 4th marker position along the channel (44 seconds) using the acid stressor at pH 1.85.

The results of varying the pH confirmed that lower pH will cause a more rapid haemolysis and this was optimal for the observable channel length. The seemingly rapid increase in resistance to lysis as pH is increased through the reported values is due to the logarithmic nature of the pH scale. An increase in 1 pH unit is a 10-fold difference. These investigations did not consider pH's below 0.7 as this pH already gave a measurable curve trend that may not have been observed if the haemolysis was initiated earlier in the channel.

Using pH 0.7 and a flow rate of 0.5 µL/min, a series of repeat experiments were conducted to determine the reproducibility of these parameters.

(iv) Blood dilution investigations

The number of blood cells contained in any one drop of blood varies between person to person within a healthy range. In the case of blood disorders, the number of RBCs per drop of blood can be significantly increased or decreased.[206] It was therefore important to establish a protocol that would take into consideration variations in RBC count.

To investigate the effects of an increased or decreased number of RBCs on the test outcome, whole blood was diluted in 1% BSA and 0.9% NaCl to 15%, 25%, 35% and 45%. Beyond 45%, there were typically too many RBCs present for accurate analysis due to overcrowding in the channel.

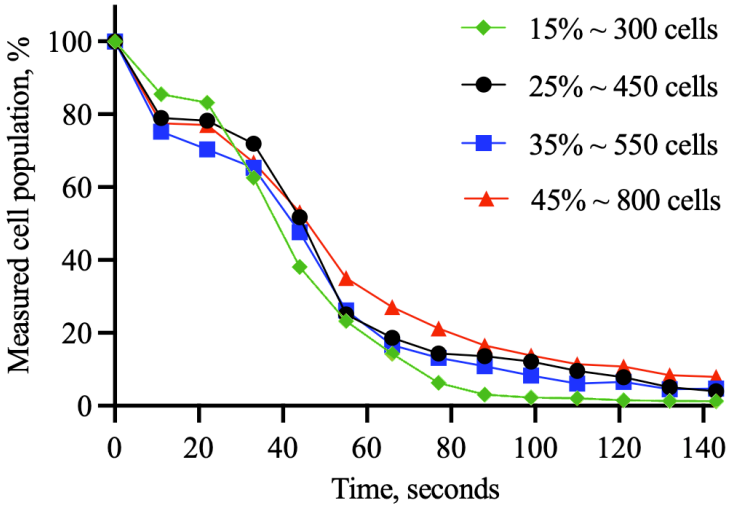

Figure 3-35 Resulting lysis curves for the blood dilutions showed that between 15 – 35% there were similarities in the curve trends. The curves produced for dilution of 45% appeared to be slightly more resistant to lysis.

Each blood dilution sample was taken from the same donor and run in duplicate. It was found that between dilutions of 15 – 35% the lysis trends were very similar. 45% (red) showed a slight increase in resistance to lysis from 55 seconds. It was considered that an explanation for the resistance to lysis may be that the increase in cell numbers could result in the strength of the HCl decreasing due to the H^+ ions reacting with a greater number of cells. Thus, fewer H^+ ions are acting on one cell.

Nonetheless, these experiments showed that between dilutions of 15 – 35% for a healthy sample, there appeared to be no significant differences in curve trends. In an effort to maintain small sample and reagent consumption, it was decided to work at the lower end of the workable range going forward.

(v) Summary of findings

(a) MeCheM flow protocol

The permitted range for the flow rate was between 0.1 and 1 μL/min. The flow rate was to remain constant throughout testing and the flow rate of 0.5 μL/min was the chosen constant. The HCl stressor was optimal for haemolysis in the channel at pH 0.7. The length of time required for flow stabilization was 2 minutes. The optimal blood dilution was 15%, but dilutions up to 35% were observed to be appropriate for testing.

(b) Additional MeCheM operation

A challenge of the High Magnification System, discussed in the following chapters, was the limited observable cell numbers due to the FOV of the camera. To overcome this constraint, it was considered that MeCheM could be used as a low magnification imaging system to supplement the lower cell numbers observed in the High Magnification System (~ 60 cells over triplicate runs).

A standard microscope slide could be placed on top of the chip holder and the camera could be refocussed to image cells in a droplet on the microscope slide without the requirement for any further system modifications. The average number of cells observed in the FOV was found to be ~ 830 for the dilution concentration of 15%. This application of MeCheM is referred to as the Low Magnification Drop Test (LMDT).

Although the LMDT experimental setup was relatively simple, there were a couple of procedural effects to note.

The first consideration was related to sample evaporation. Due to the very small volume of fluids being used, it was critical to conduct the experiment immediately following the cell sedimentation time. Failure to work quickly would result in blood sample evaporation which would leave an unusable crystalised residue on the microscope slide. Sample

evaporation would be completed in ~ 6 minutes thus the user had ~ 4.5 minutes to conduct the test following the cell sedimentation time of 1.5 minutes.

The second consideration was to note that when pipetting the HCl sample on top of the blood sample, the user could cause turbulence to the cells which would result in their movement. In the LMDT, turbulence rarely caused an issue unless the user introduced a bubble into the image that obscured the cameras view of the cells.

These biproducts of the LMDT experimental protocol were easily negated with precise execution of the developed protocol and care taken when pipetting the acid sample.

3.6.2 High Magnification System

The protocol for the High Magnification System (HMS) closely followed that of the LMDT with some minor modifications.

One of the considerations of the LMDT became increasingly more apparent upon viewing the cells in high magnification; turbulence to the cells upon introduction of acid to the droplet. Due to the much narrower FOV of the camera, any turbulence to the cells could cause cell migration out of the FOV entirely. Where it was the case that the cells were to monitored from pre to post-acid addition, losing cells of interest from the FOV could be critically detrimental to the analysis.

To help to overcome this issue, the investigations for the HMS were conducted in a standard clear, flat-bottomed 96-well plate which helped to contain the sample and also could be used as a guide for sample dispensing.

There were two dispensing techniques that were explored; (i) directly over the middle of the well reservoir, and (ii) angled pipette tip to the wall of the well reservoir. Dispensing the sample directly above the settled cells was more likely to cause cell turbulence. Whereas, angling the pipette tip to lightly touch the wall of the reservoir allowing the HCl sample to flow down the wall of the well created a much more gentle mix. This was chosen as the recommended pipetting technique going forward for the HMS.

A second modification was the sample volume size. The diameter of the well in the microtitre plate was 5 mm. The 5 µL droplet (as per the LMDT) did not cover the bottom of the well entirely, thus the decision was made to increase the volume of the blood and HCl samples accordingly.

3.7 Summary

The purpose of this chapter was to describe the development of the instrumentation used for the interrogation of a biochemical assay for the diagnosis of rare anaemias which is discussed in the following chapters.

The introduction of a novel microfluidic toolkit, MeCheM, and an additional image analysis platform, HMS, are outlined here with their working protocols and the development of those protocols. The 3 protocols discussed; (i) flow test, (ii) LMDT, and (iii) HMS, were brought forward to intense interrogation using healthy samples in the next chapter.

Chapter 4 Determination of technique repeatability

This chapter explores the use of the previously described methods to establish a baseline of the healthy population for future comparison with diseased samples. Here it is important to be critical of the pros and cons of the each of the developed methods. By the end of this chapter, a non-biased and critical review of each of the developed methods should highlight the reasoning for the chosen method recommendations for comparison against anaemic samples.

With the development of any new instrumentation, or experimental protocol, it is imperative that the instrument and/or protocol are subjected to error analysis. Investigating the range of experimental uncertainties and discerning between systematic and random errors are of critical importance in error analysis. The objective of error analysis is to reduce those errors, where possible, to increase the accuracy and precision of the experimental result, and to understand the ultimate instrument or protocol accuracy and repeatability.[207]

There are many different types of errors in measurement and, for this body of work, they can be classified into instrument variations and sample variations.

Instrument variations include everything related to the workings of MeCheM and the testing protocols. Sample variations relate to the diverse nature of blood and the discrepancies between healthy blood samples from different donors covering all aspects from the subject, through storage and transport and introduction into the instrument.

The aim of this chapter is to investigate the robustness of the developed protocols from *Chapter 3* and determine their repeatability with the view of recommending some or all of the developed protocols to be brought forward for comparison against rare anaemia samples.

4.1 Repeatability measurements

Variability within a single sample can be illustrated using standard deviation. The standard deviation, σ, calculation describes the range about the mean of a data set. It is determined using the following equation:

$$\sigma = \sqrt{\frac{\sum(x_i - \mu)^2}{N}}$$

where N is the population size, x_i is each value from the population, and μ is the population mean.

To determine the chip-chip repeatability, multiple tests were carried out using fresh blood from healthy donors for each of the developed protocols described in Chapter 3.

4.2 Low magnification drop test

4.2.1 Data normalisation

The low magnification drop test (LMDT) did not involve the flow of fluid thus it required the least amount of human-machine interaction. On this basis it was selected as the most user-friendly test to begin trend observations and analysis.

Whole blood was diluted as per the method described in *Chapter 2* and there were ~ 5 minutes between each test conducted. The diluted blood sample was stored in a fridge at 4ºC between tests.

The first consideration was the shape of the lysis curve that was produced using this method. A control graph plotting each of the triplicate runs for one sample is shown below in *Figure 4-1*.

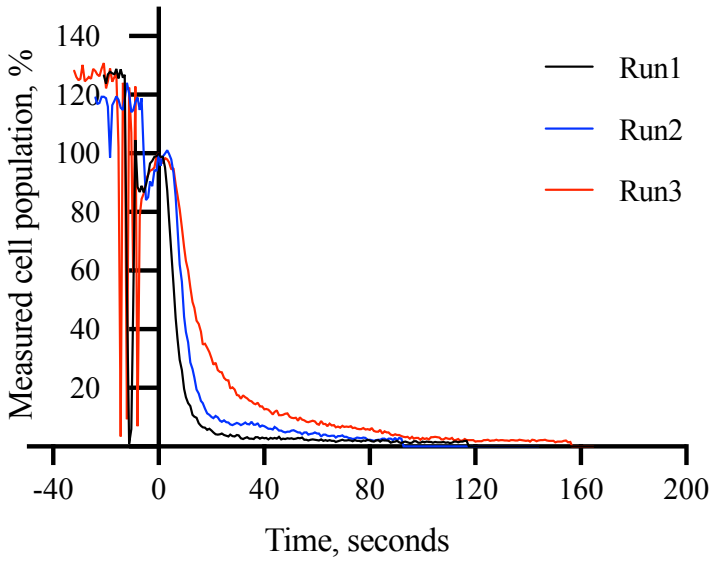

Figure 4-1 The LMDT was carried out in triplicate on the same healthy control sample. Run1 and Run2 follow similar trends, but Run3 (red curve) shows a notable delay in lysis as can been seen by the extended curve decline over time.

Data normalisation justification

The video recording was commenced prior to acid being added to the blood sample. This pre-acid addition time, $t < 0$, is depicted in *Figure 4-1* on the x-axis to the left of the origin. The large fluctuations in measured cell population were caused by 2 factors; (i) movement of the sample on the XY-stage to obtain the highest cell numbers in the FOV and (ii) obstruction of the FOV via pipette tip during addition of acid to the blood sample. The movement of the sample in the XY direction is depicted in the graph as minor fluctuations in measured cell population and the obstruction of FOV can be observed as the sharp decrease towards zero. As the pipette was removed, the cells came back into the FOV for measurement and this is shown in the graph above as an increase towards 100% of the measured cell population on the y-axis.

The data was normalised to the first frame where the observed image was no longer obstructed by the pipette tip and this time was selected as $t = 0$. This normalisation varied for each test as it was entirely dependent on the rate at which the user carried out the protocol, thus, each video recording had to be normalised independently.

The information collected at $t < 0$ was not required for these investigations, thus, all subsequent graphs will only show the measured cell population from the point of acid addition, $t = 0$.

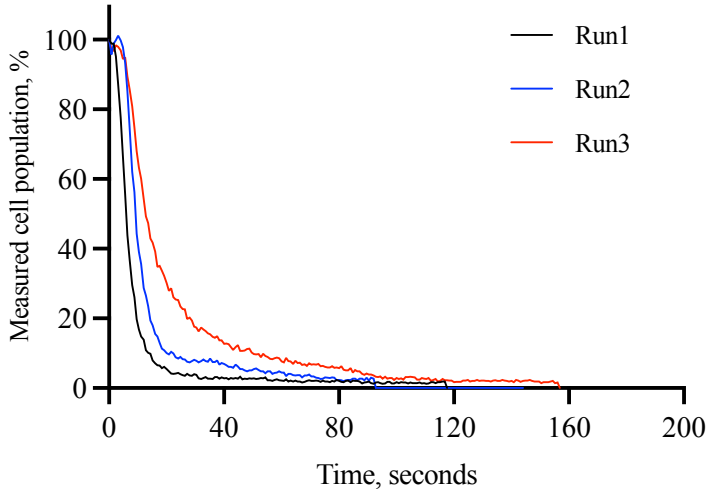

Figure 4-2 The results of the low magnification drop test with the removal of the pre-acid addition (t < 0) measurements.

As can be seen from the graph above, Run1 displayed the most rapid cell population decline, followed closely by Run2 and Run3. The results of the control repeatability test in *Figure 4-2* produced a declining non-linear curve for each run. For this sample, there was a rapid decline in cell population followed by a slower decline for each of the 3 runs. Analysis of the curves using the 'Two-Phase Decay' curve fit function in GraphPad Prism is shown below in *Figure 4-3*.

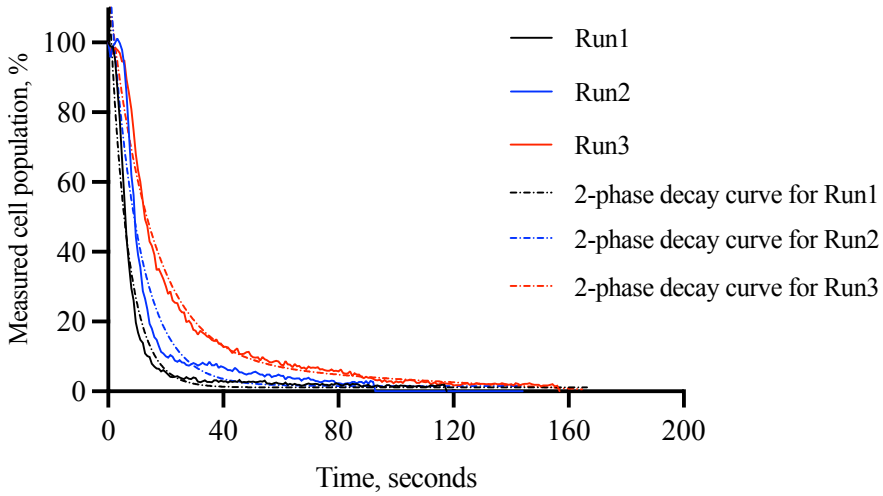

Figure 4-3 The curves produced from the low magnification drop test fitted closely with the 2-phase decay curve in GraphPad Prism, suggesting a biphasic response of the RBCs to the acid. The R^2 value, indicating goodness of fit, was 0.97, 0.95, and 0.98 for Run1, Run2 and Run3, respectively.

The bi-phasic response observed is likely due to a combination of the depletion of the RBCs over time and the dilution of the acid over time and distance. Investigation of the variability between the healthy control population is discussed in section 4.2.3.

4.2.2 Hypothesis for curve shape

The output graph in *Figure 4-2* shows a two-phase lysis trend with an initial rapid cell lysis followed by a slower decay of the cell population towards zero. There are two possible explanations for the two-phase shape of this curve.

The first is the way in which the acid is added to the blood sample. The acid droplet is pipetted directly over the blood droplet meaning that the red blood cells closest to the surface of the droplet will be exposed to the acid at its highest concentration.

Contrastingly, the cells that have settled nearer the microscope slide at the base of the droplet will be exposed to the acid after it diffuses from the surface. By the time the acid has reached these cells, it will also be diluted by the blood droplet, thus, the cells nearer the base of the droplet will be exposed to a lower concentration of acid. This delay in exposure and overall reduced acid concentration may result in the slower lysis of RBCs that is observed in the second phase of the haemolysis curve.

A second explanation for the shape of the curve is the heterogeneous nature of blood. Within any blood sample, there are cells that have just been released into circulation, and cells which are nearing the end of their 120 day sojourn around the body. As cells age, they lose volume, membrane and experience an increase in density[208,209]. These changes lead to a decrease in their deformability.

There is a method of separating RBCs based on their density, thus their age, using a density gradient medium, Percoll.[210] By separating the RBC sample into its sub-populations, it is possible to observe if there are differences in the shape of the haemolysis curve for the youngest and oldest subpopulations. *Figure 4-4* below shows the results of this investigation.

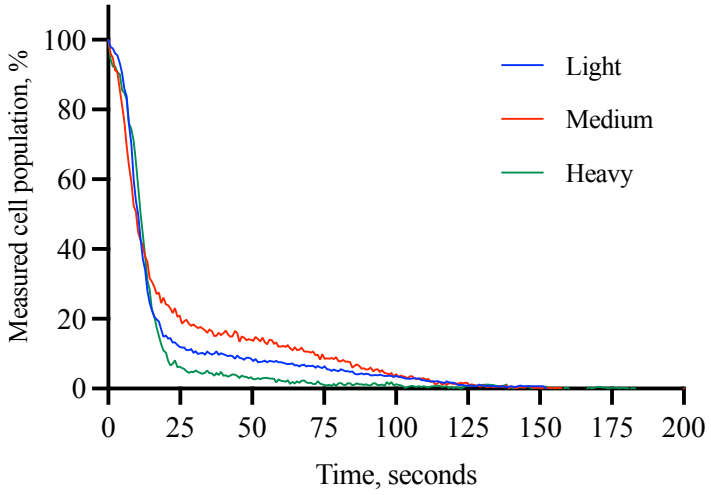

Figure 4-4 A whole blood sample was separated into its sub-populations based on cellular density using Percoll, a density gradient medium. The sub-populations were then investigated using the low magnification drop test to observe if there were differences in the shape of the haemolysis curve. The results show that although there are differences between the sub-populations, the shape of the curve remains bi-phasic for each density (light, medium and heavy).

The sub-population that has the lowest density corresponds to the youngest cells in the sample. These cells should exhibit the highest deformability of the 3 sub-populations. The medium and heavy fractions represent the middle-aged and oldest cells respectively. These cells should display reduced deformability.

The results shown above in *Figure 4-4* do report observable differences in the rate of haemolysis in the second phase of the curve between the 3 sub-fractions. However, the bi-phasic shape of the curve remains present for each sample. This suggests that the heterogeneity of the blood sample does not influence the shape of the haemolysis curve. Presently, the hypothesis for shape of the haemolysis curve has not been proven. However, it is suggested that the shape may be a result of the diffusion of the acid from a distance.

4.2.3 Investigation of procedure repeatability

To investigate repeatability between samples, the LMDT was carried out in triplicate for all healthy donor samples (n=6). The first sample is shown in *Figure 4-2* and the remaining 5 samples are shown below in *Figure 4-5*.

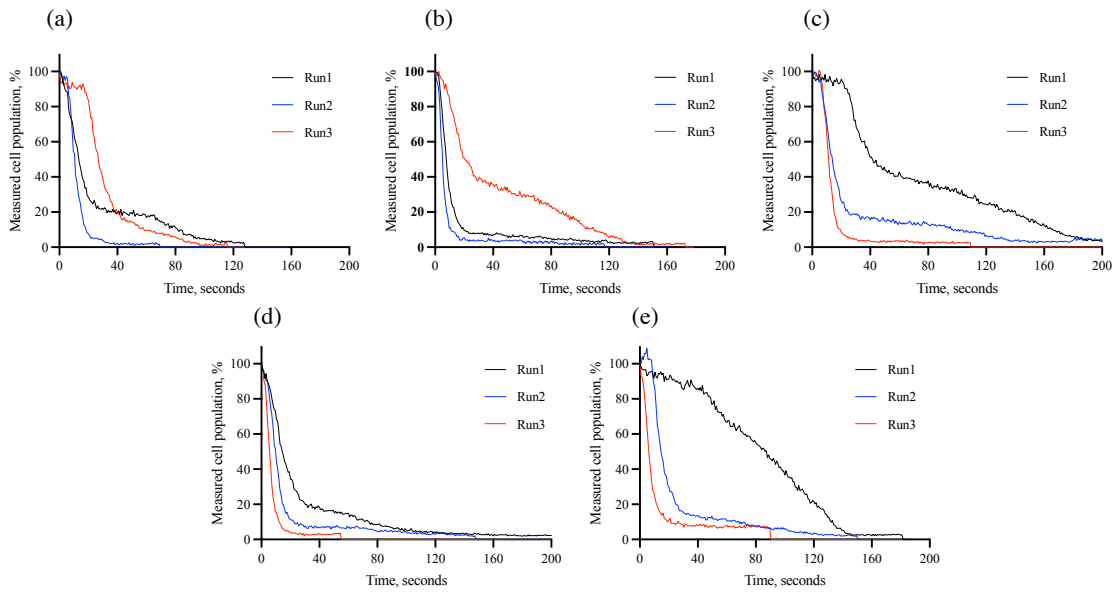

Figure 4-5 (a) –(e) show the results of the LMDT carried out in triplicate for each of the remaining control samples.

With the exception of sample *(e) Run1* it was clear that the LMDT protocol produced a bi-phasic curve for each healthy sample. Interestingly, it was also observed that the curves shifted along the x-axis, suggesting variability of lysis times within the same healthy sample and overall within the healthy population.

It was considered that this was an artefact of the testing protocol caused by the acid not being pipetted in the same location on the blood droplet each time.

Investigation of outlier curve

In the case of sample *(e) Run1*, the output curve gave a distinctively different result. To understand the cause of this result, the video recording for sample *(e) Run1* was investigated, along with a sample of the results that displayed the more common 2-phase lysis trend.

For the video recordings corresponding to the bi-phasic output curves, the addition of the acid to the RBC droplet appeared to almost instantaneously change the RBCs from their discocyte shape to a more spherical shape. However, this was not the case for the unique *(e) Run1* curve. Frames from this video are shown below in *Figure 4-6*.

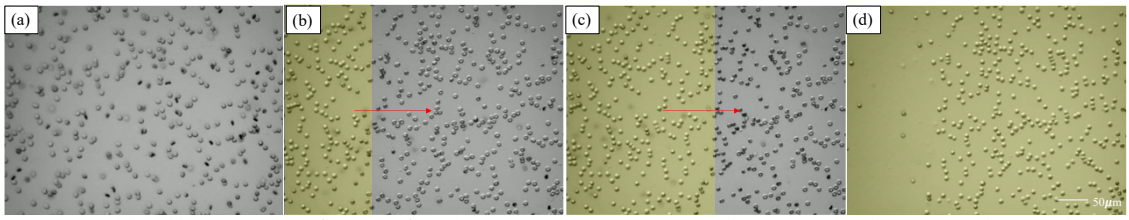

Figure 4-6 (a) – (d) shows the influence of acid on the RBCs over time, acid movement is depicted with the red arrow and the yellow box is symbolic of the area in the FOV that has been affected by the acid. In (a), the cells are in a physiological saline solution, unaffected by the acid. In (b) and (c), the acid is slowly moving into the FOV, and the affected cells lose their discocyte shape and start to appear spherical. In (d), cell lysis has already commenced while the acid is still moving across the FOV. The cell lysis is observed in the images as the reduction of visible cells on the LHS of (d).

It was clear from the video that the acid had been dispensed at a location away from the field of view of the camera. Instead of the almost instantaneous mixing of acid with the blood cells, the acid was observed to move in from the left hand side of the FOV, affecting the shape of the RBCs as it slowly moved across the population. The resulting effect of this much slower exposure to acid was a slower haemolysis of the RBC population with a much gentler slope in the output curve.

Although *(b) Run3* and *(c) Run1* were also outliers, these curves still displayed the bi-phasic fast and slow haemolysis, which appeared to be the common trend through the analysis of the LMDT results for the control samples.

The videos for these curves were also analysed in depth, in the case of *(b) Run3*, there did not appear to be any obvious differences that could be recognized from a frame by frame analysis of the video. However, for *(c) Run1*, the exposure of the RBCs to the acid was delayed from the time of pipetting to the time of observation on the video. It is assumed that this was a result of, again, the acid being dispensed in a location outside of the FOV of the camera, thus requiring a time before extending to the observation position.

4.2.4 Conclusions and recommendations

The average of these triplicate runs for the control population was plotted with error bars representing the standard deviation across the population, shown in *Figure 4-7*.

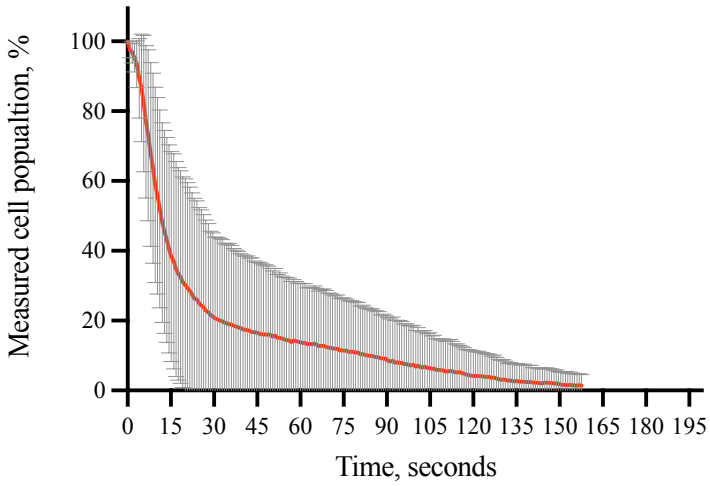

Figure 4-7 Compilation of triplicate runs for each healthy sample (n=6) including the defined outliers. The curve represents the mean of all the runs and the error bars are the standard deviation between the control population. The maximum standard deviation was found in the range of 8.8 – 25.6 seconds (with maximum standard deviation of 30.8% at 16.8 seconds)

From the graphs shown in *Figure 4-5* and *Figure 4-7*, it appears that in most cases the resulting curves produced a bi-phasic decline in cell populations. However, from the analysis of the outlier curves and their corresponding videos, it is evident that inconsistent positioning of the acid droplet over the blood droplet can create variations in the resulting output curves.

It is clear that without further refinement of this testing protocol one could create variations in the resulting curves suggesting a sample is of interest from a diagnostic perspective, whereas, the cause of the resulting curve could be due to human error. Further development of MeCheM to allow for high precision droplet dispensing would undoubtedly reduce that human error. However, the development of high precision dispensing as an additional MeCheM tool was not within the scope of this thesis. Consequently, given the clear concerns about protocol repeatability, this method was not recommended in its present form as a comparison tool between healthy and diseased samples.

4.3 High magnification drop test

The experimental method for the high magnification drop test (HMDT) was akin to that of the LMDT. The addition of the acid was prone to creating cell turbulence, and accurate positioning of the pipette tip was critical for reproducible results. A key difference between the two protocols, however, was that the HMDT used a well plate to contain the

blood droplet in a reservoir. This allowed the user to gently position the pipette tip against the side of the reservoir prior to releasing the acid into the blood sample. The addition of this step introduced a small protocol refinement.

As mentioned in the previous chapter, there were 3 output graphs from the HMDT experiment; (i) RBC population count, (ii) RBC size distribution, and (iii) RBC size measurement. The output curves and their repeatability will be discussed in this section.

4.3.1 RBC population count

RBC population count allows for the observation of cell lysis over the time the cells are exposed to acid. Similar to the LMDT, there was a 'pre-acid addition' time recorded, but it was not informative for this measurement. As such, the data was adjusted as described above for the LMDT and t=0 corresponds to the first frame where the image of the cells was not obscured by the pipette tip.

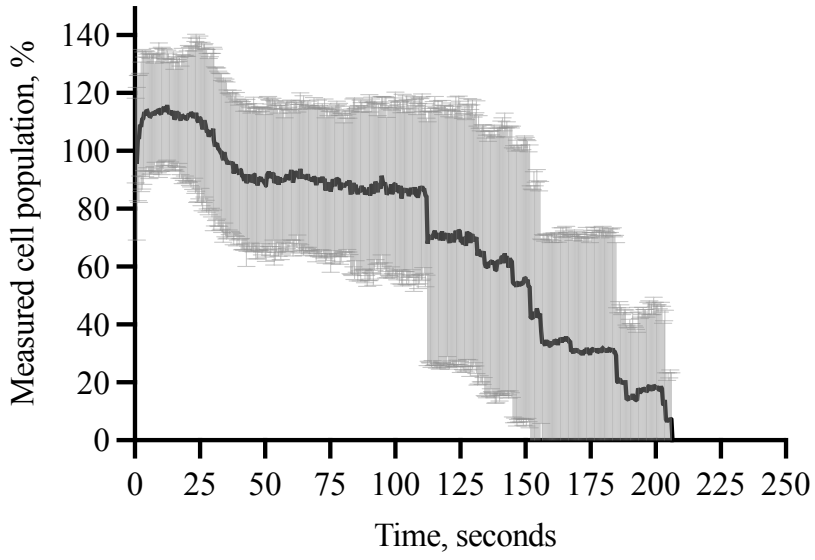

Figure 4-8 Compilation of the control samples (n=6) displaying the reduction of the cell population over time with exposure to acid. The error bars are standard deviation.

Due to small cell numbers (~ 360 cells in total) cell movement about the FOV created large increases/decreases in the observable cell population. The movement of cells was directly related to the addition of acid to the reservoir. Inspection of the high magnification videos and output graphs showed a tendency for more cells to move into the FOV and this can be seen in *Figure 4-8* as an increase in measured cell population from 100% to ~ 118%. This investigation was conducted on a relatively small sample

size, therefore it was not considered that this increase of cells after addition of acid would be a trend if a larger sample population was investigated.

As previously mentioned, the cell number available for observation in the high magnification setup was significantly less than that of the LMDT (~ 12500). Due to a much narrower depth of focus with the HMDT, the cells that were observed were only cells which had settled near the bottom of the reservoir on the well plate. Considering the hypothesis given for the biphasic shape of the curve produced by the LMDT, it was considered that the rate for lysis of the cells in the HMDT would be similar to the rate of lysis of the second phase of the curve in the LMDT. The rapid cell lysis begins to slow at ~ 25 seconds. This was chosen as the beginning of the second slower phase of the LMDT curve which continued over a period of ~ 3 minutes. The data from 25 seconds onwards was renormalised and plotted with the data from the HMDT. The results are shown below in *Figure 4-9*.

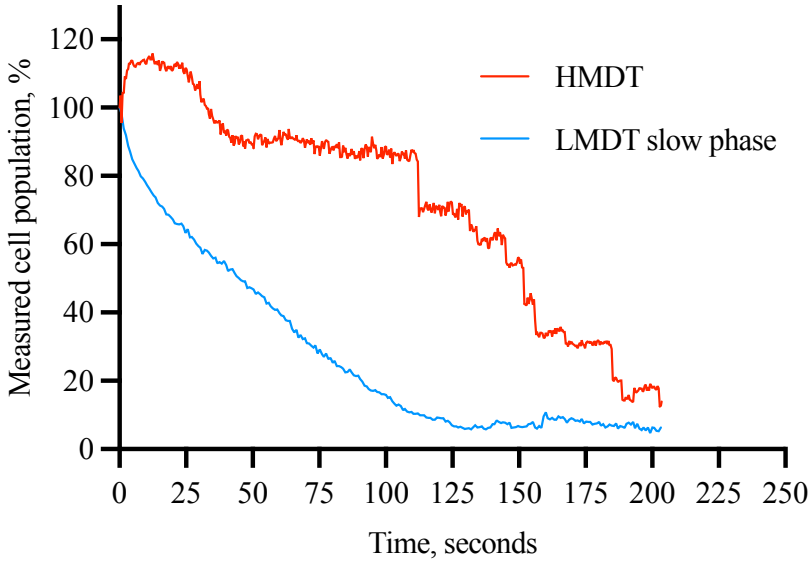

Figure 4-9 Comparison of the HMDT curve and the second phase of the LMDT curve showed suggested that the time to complete lysis was similar.

It is important to highlight the large difference in cell population size analysed between the low and high magnification drop tests. The sum of cells analysed for the LMDT was ~12,500. In contrast, only ~ 360 cells in total were analysed for the healthy HMDT. The smaller sample size for the HMDT drop test may account for the uneven appearance of the resulting curve. Interestingly, it appears that both curves approach zero around the 200 second mark. This may suggest that the second phase of the curve for the LMDT is a by-product of the diffusion profile of the acid through the blood droplet.

Given the large standard deviation between control samples (ranging between 14 – 50%), this method of high magnification population decline measurement was deemed not repeatable in its current form. Future work to improve this technique should focus on increasing number of cells measured and overall protocol repeatability with respect to high precision droplet dispensing.

4.3.2 RBC size distribution

Red blood cell distribution width (RDW) and mean corpuscular volume (MCV) are examples of tests within a complete blood count that are used as a first investigative tool to determine the health status of a blood sample.[110] The high magnification system has the ability to measure the XY-axis projection of RBCs during experimentation. The experimental protocol dictates that the video recording of the sample commences prior to the addition of acid. This allows the user to analyse projections of the RBCs in a physiological solution and then follow their evolution from acid addition to cell lysis. Unlike the previous investigations, the information obtained from the time prior to acid addition is of great importance here.

The average cell projected area for the healthy population was calculated in GraphPad Prism and found to be 48 ± 8 μm^2. The projected area of all cells in the healthy sample population were measured prior to acid addition and the size data recorded was binned into the following ranges; (i) 0 - 7 μm^2, (ii) 7 - 14 μm^2, (iii) 14 - 21 μm^2, (iv) 21 - 28 μm^2, (v) 28 - 35 μm^2, (vi) 35 - 42 μm^2, (vii) 42 - 49 μm^2, (viii) 49 - 56 μm^2, (ix) 56 - 63 μm^2, (x) 63 - 70 μm^2, and (xi) 70 - 77 μm^2.

The result of this analysis for the control population showed a Gaussian distribution with most RBC projected areas observed in the 42 - 49 and 49 - 56 intervals, see below in *Figure 4-10*.

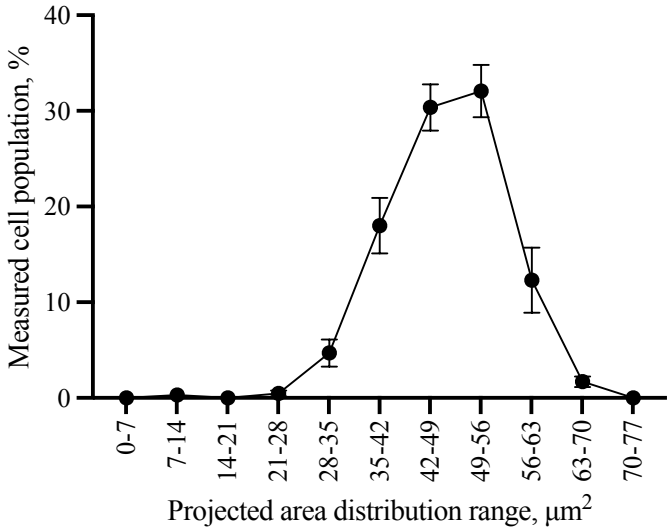

Figure 4-10 A compilation of all healthy control samples pre-acid addition shows that the majority of cells in the sample are found within the 42 - 56 µm² range.

The size variability of RBCs is affected by many factors within a healthy sample, thus, it was not expected that the projected area of the control population would fall neatly at a specific value. However, the results of this investigation did provide a range for the projected area of the healthy sample for comparison against rare anaemias. This will be investigated further in *Chapter 5*.

The healthy control samples were also measured at specified time ranges post-acid addition. The cell distributions at the following time stamps were recorded; (i) t = 20s, (ii) t = 40s, (iii) t = 60s, (iv) t = 80s, (v) t = 100s. The time is given in seconds, s. The compiled graph is shown below in *Figure 4-11*.

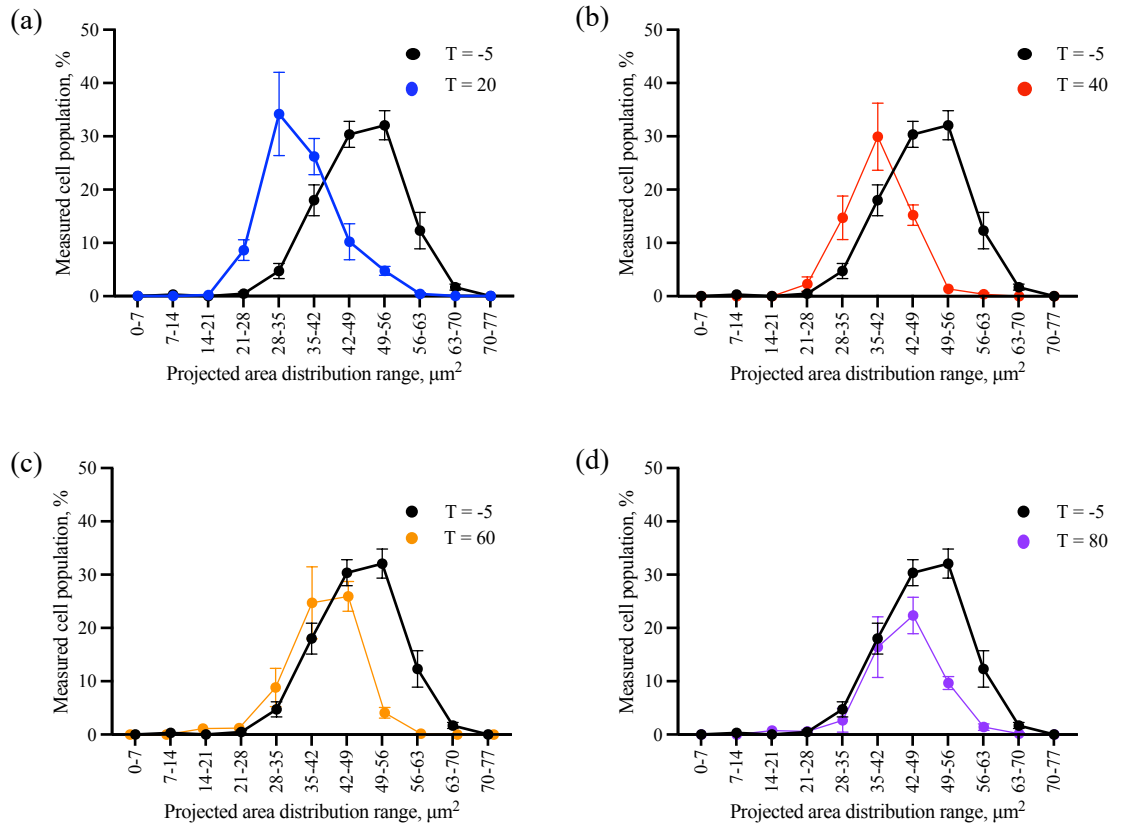

Figure 4-11 The series of graphs (a) – (d) display the projected area distributions from all healthy samples post-acid addition with the pre-acid addition measurement shown in black.

It is evident from *Figure 4-11* that the RBC projected area distributions reduce in size upon exposure to acid. This is shown in *Figure 4-11 (a)* by the increase in measured cell population for the smaller interval ranges for T=20.

The distributions then begin to increase for each measured time point, *Figure 4-11(b) – (d)*. Within the measured timepoints, the projected areas appear to almost return to their original 'pre-acid addition' measurement. Reduced cell numbers beyond T = 100 seconds made it difficult to analyse the projected area distributions at later time points.

It is important to note that the projected area of the RBCs is only recorded along the cells X and Y-axis, i.e. the measurements are 2-dimensional. However, the cell is 3-dimensional and the effects of the exposure of the cell to acid on the Z-axis is not reflected in these measurements. It has been previously described that the exposure is causing water to enter the cell, thus it is likely that the RBC is swelling in a 3-dimensional projection, see schematic of proposed reaction in *Figure 4-12*.

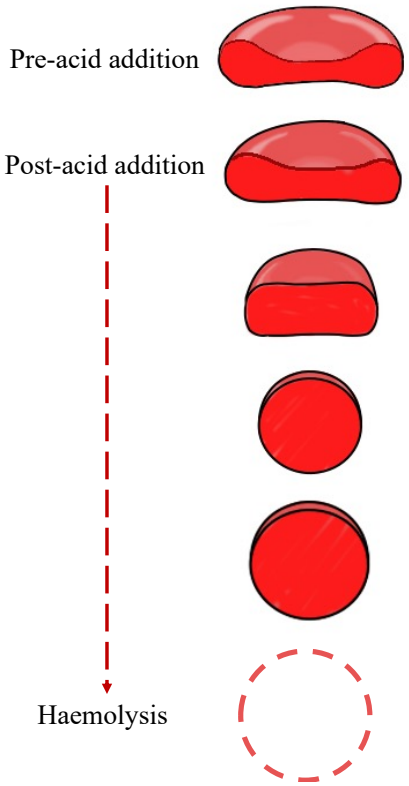

Figure 4-12 A 3-D schematic proposal of the effect of exposure to a low pH shock on the red blood cell. It is proposed that the RBC membrane is swelling in the X, Y and Z-directions, however this is not recorded in the 2-D measurements.

Frames extracted from a control sample video, *Figure 4-13*, show the cell projected area evolution throughout the experiment.

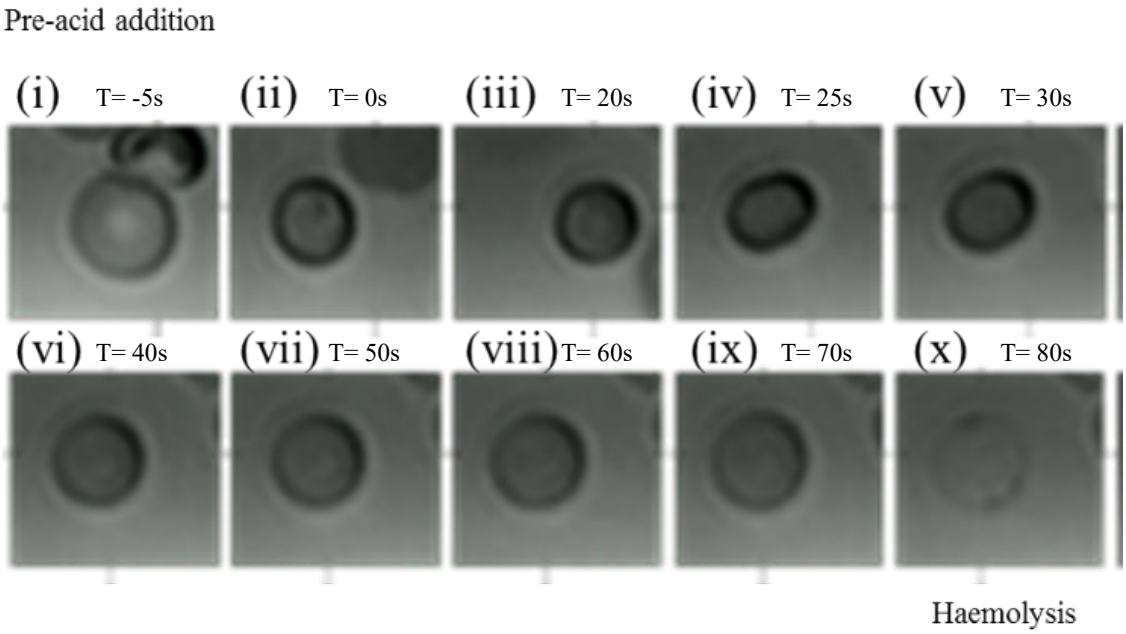

Figure 4-13 Images extracted of the HMDT from pre-acid addition shown in (i) to post-acid addition shown in (ii) and through to haemolysis (iii) – (x) with remaining membrane ghost shown in (x) for a healthy control sample. In response to the acid addition, the cell immediately appears to shrink (ii) and reaches its minimum projected area in (iii). From (iv) to (ix) the cell increases in projected area due to the influx of water caused by the low pH shock.

As can be seen in *Figure 4-13*, the observable changes in RBC size is relatively small. However, as mentioned in *Chapter 1*, the RBC can only increase to 4% in surface area prior to haemolysis, thus, large size increases were not expected to be observed.

Knowledge of RBC size has proven to be a useful tool for the diagnosis of rare anaemias. Correlation of RBC projected area as determined by the high magnification system with haematology indices such as RDW and MCV would be an ideal low-cost solution for first tier investigations. Correlation analysis is investigated in *Section 4.5*.

4.3.3 RBC size measurement

The final output graph of the high magnification system displayed the real-time response of cells to acid over time. The programme tracked single cells and recorded their projected area in real time. The graph below in *Figure 4-14* shows the average of the tracked cells in the control population from the moment of acid addition.

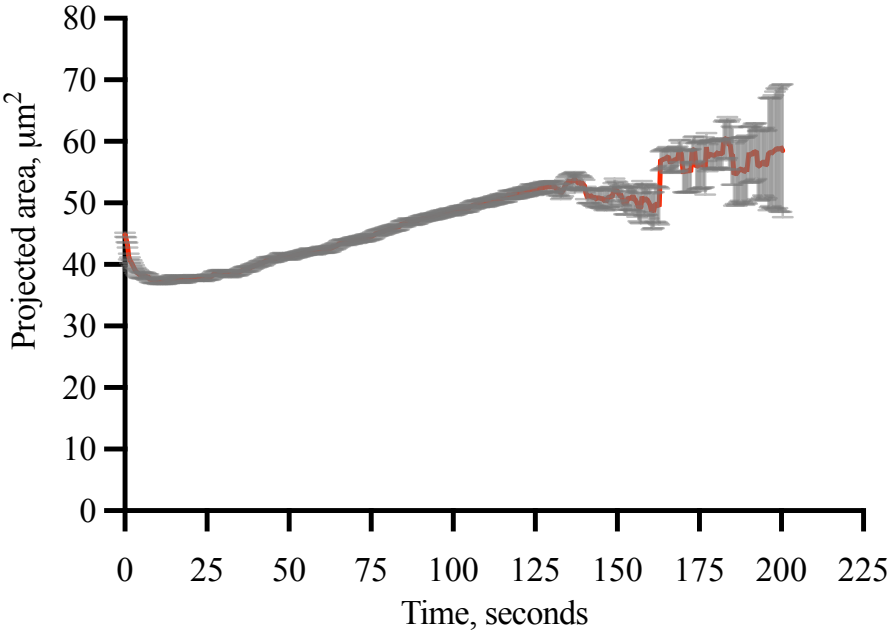

Figure 4-14 Changes in RBC projected area following exposure to acid. This graph shows an average of all healthy sample cell tracks over time. Error bars are standard error. Large standard errors after ~ 150 seconds are due to cell lysis. This was an expected result.

Prior to acid addition, each cell had a unique projected area measurement with the range of 7 – 77 µm^2. There is an initial decrease in projected area followed by a steady increase until the point of cell lysis, which is in agreement with the cell distribution data in *Figure 4-11*.

The increase in projected area measurements is relatively smooth until ~ 130 s, see *Figure 4-14*. Here, the haemolysis of the majority of the cell population can be observed. After 140 s, most of the cells have lysed and fluctuations in the curve are due to the small number of remaining cells, as confirmed by the large error bars.

This can be observed in the graph as a 'dip' in the projected area measurement. As cells are continuing to lyse from 144 s, the population is declining rapidly and the average may now contain outlier cells and anomalies, thus owing to the 'jagged' appearance of the curve.

However, the results of this graph give a further insight into the swelling capacity of the RBCs beyond 100 s and it was observed that the remaining cells also continue to increase in projected area over time until eventual lysis.

(i) Cell swelling capacity and sample resistance to lysis

The swelling capacity of the cell is defined here as the ability of the cell to increase from its minimum to maximum projected area. The RBC evidently experiences physical alterations to its shape during exposure to acid, as shown in *Figure 4-13*. The suggested mechanism for this swelling was previously described in *Section 1.5.1*. In summary, this reaction is caused by an influx of water into the cell in an attempt to maintain osmotic balance upon exposure acid. Initially, the RBC appears in its typical discocyte configuration. Following the addition of acid, it reduces in projected area and appears spherical and, finally, the 'swelling' of the RBC commences until its eventual lysis.

It is known that RBCs of patients suffering with various types of rare anaemia (Sickle Cell Disease, Spherocytosis) do not possess the same level of deformability when compared with a healthy sample.[48] Prior to comparison between healthy and diseased samples a healthy cell swelling capacity range must be determined. This information is easily obtained using the Microsoft Excel file output from the high magnification analysis programme. *Figure 4-15* shows the output graph of a sample of individual cell tracks and their projected area over time.

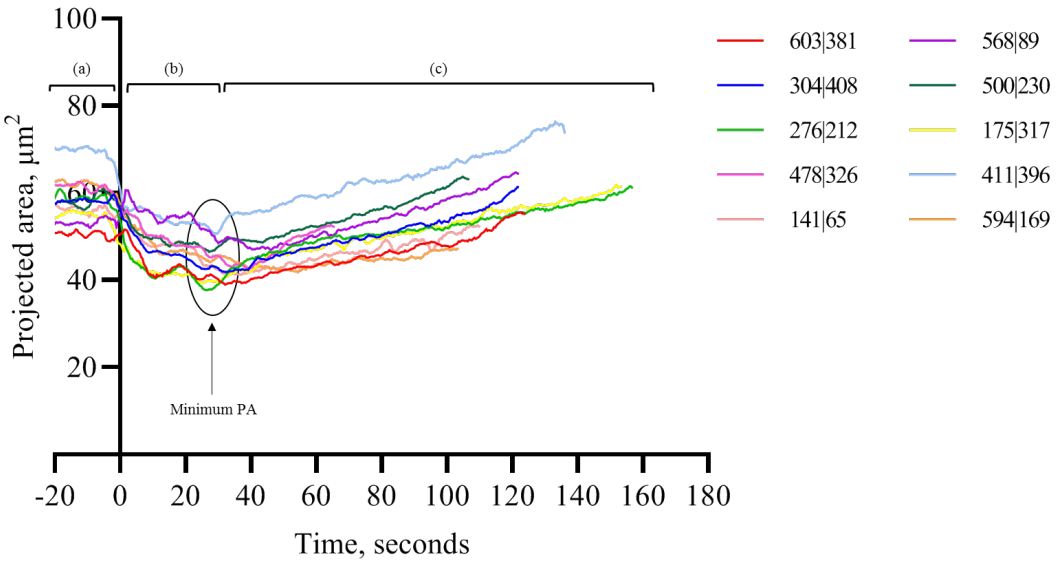

Figure 4-15 A selection of individual cell tracks from the healthy population. (a) the initial cell projected areas before acid addition, (b) projected area of cells changes rapidly in response to addition of acid and appears to reduce in size until the cell reaches its minimum projected area, (c) the, now spherical, cells will swell until they reach their maximum swelling capacity and lyse.

The minimum and maximum projected area for each track was found using the MIN and MAX functions in Microsoft Excel. The swelling capacity of each healthy sample was found using the following equation:

$$Cell\ swell, \% = \frac{(PA_{max} - PA_{min})}{PA_{max}} * 100 \qquad Equation\ 1$$

where PA_{max} is the maximum projected area and PA_{min} is the minimum projected area.

The results of this analysis showed that the average swelling capacity of the healthy cell population was 28.8 ± 4.99%, *Figure 4-16*.

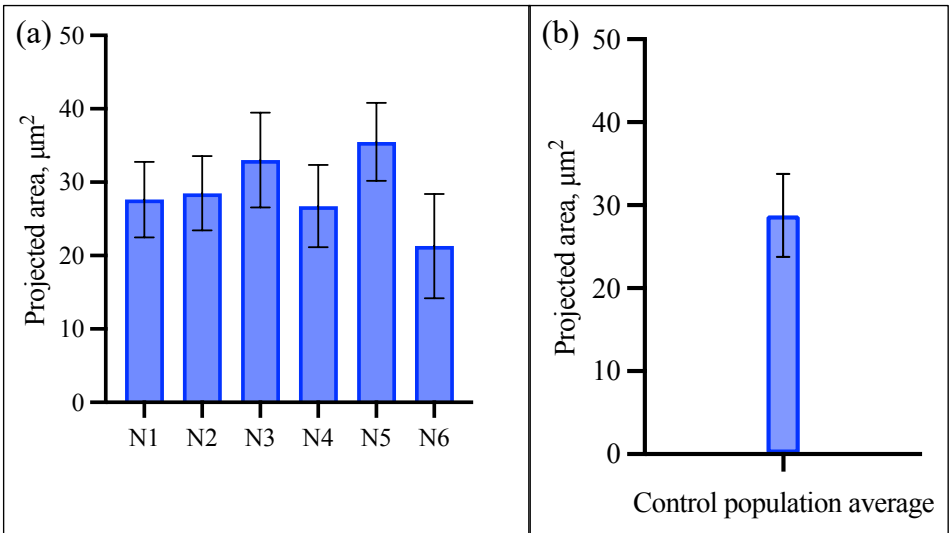

Figure 4-16 (a) shows the deviation between the swelling capacity within each healthy sample (N1 – N6). The standard deviation for each sample is ~ 5%. (b) The average swelling capacity of healthy cells over the entire control population.

This information can be used going forward for comparison of diseased blood samples with the control.

4.3.4 Conclusions and recommendations

The high magnification drop test gave significantly more insight into the effect of acid exposure on red blood cells, but there were also some drawbacks to this method.

The cell population decline displayed significant variations between healthy samples (~ 30%). Small cell numbers in the FOV are very likely to be the cause of the extent of the variations observed on the output graph. Following the present protocol, this method was not recommended for comparison of healthy and diseased blood sample. Similarly to the low magnification drop test, refinement of droplet dispensing may reduce some errors. Another improvement would be the ability to monitor more cells in the FOV with a wider angled camera.

The second method under investigation was the red blood cell projected area distribution graphs. This investigation showed that the population of red blood cells was normally distributed for each healthy sample. There were also two apparent trends among the healthy samples; (i) the projected area distribution of the majority of cells appeared to centre around 50 μm^2, and (ii) upon exposure to acid, the projected area distribution of the cells reduced initially and increased again over time. Considering that these trends

were true for each healthy sample, this method of investigation was recommended for comparison against rare anaemias.

The final method of investigation was the observation of the projected area measurement of singular cell tracks over time. Unbroken cell tracks were selected and plotted against time giving an overview of the average cell projected area development throughout the experiment. However, the information obtained by this output graph was limited by haemolysis reducing cell numbers over time. To account for this, a new parameter, cell swelling capacity, was developed. Identification of the minimum and maximum projected areas of unbroken cell tracks allowed for the cell swelling capacity to be calculated. The average deviation of this value between healthy samples was ~ 5%. In view of the general agreement of cell swelling capacity results between healthy samples, it was deemed an appropriate tool for comparison against rare anaemias.

4.4 Flow test

A clear advantage of the flow test was the reduced human interaction throughout experimentation. The flowrate of fluid within the microchannel was determined by the previously described protocol and remained constant throughout all experiments. The benefit of this protocol was the controlled manner in which the acid was introduced to the blood sample. Repeatability measurements were conducted in triplicate to determine chip-chip repeatability. Following this, all healthy samples were measured using the same technique and curve trends were established for the healthy population. The results of these investigations are discussed below.

4.4.1 Chip-chip repeatability measurements

The microfluidic chips were designed as single use to avoid contamination between samples. As such, it was required that there was good agreement between the manufactured chips.

The first point of measurement, 0 mm, relates to an unmarked position (termed position 0) on the microchannel along the RBC travel pathway prior to the introduction of the acid pathway, see *Figure 4-17*. The cell count at this point was used for normalisation of all images beyond this first position.

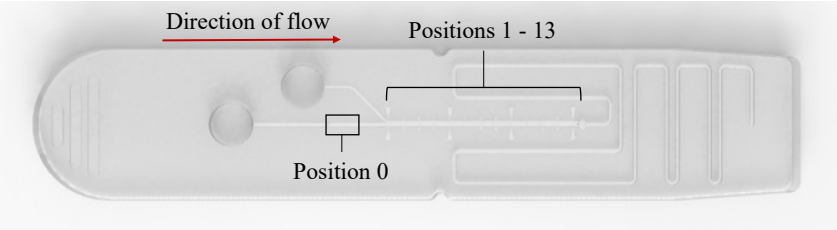

Figure 4-17 The first image was recorded at Position 0, labelled with black box. This position was location before the junction at which the acid was introduced. All distances are marked along the channel.

To investigate chip-chip repeatability, the same blood sample was used in 3 microfluidic chips using a flow rate of 0.5 µl/min and the resulting graph is shown below in *Figure 4-18.*

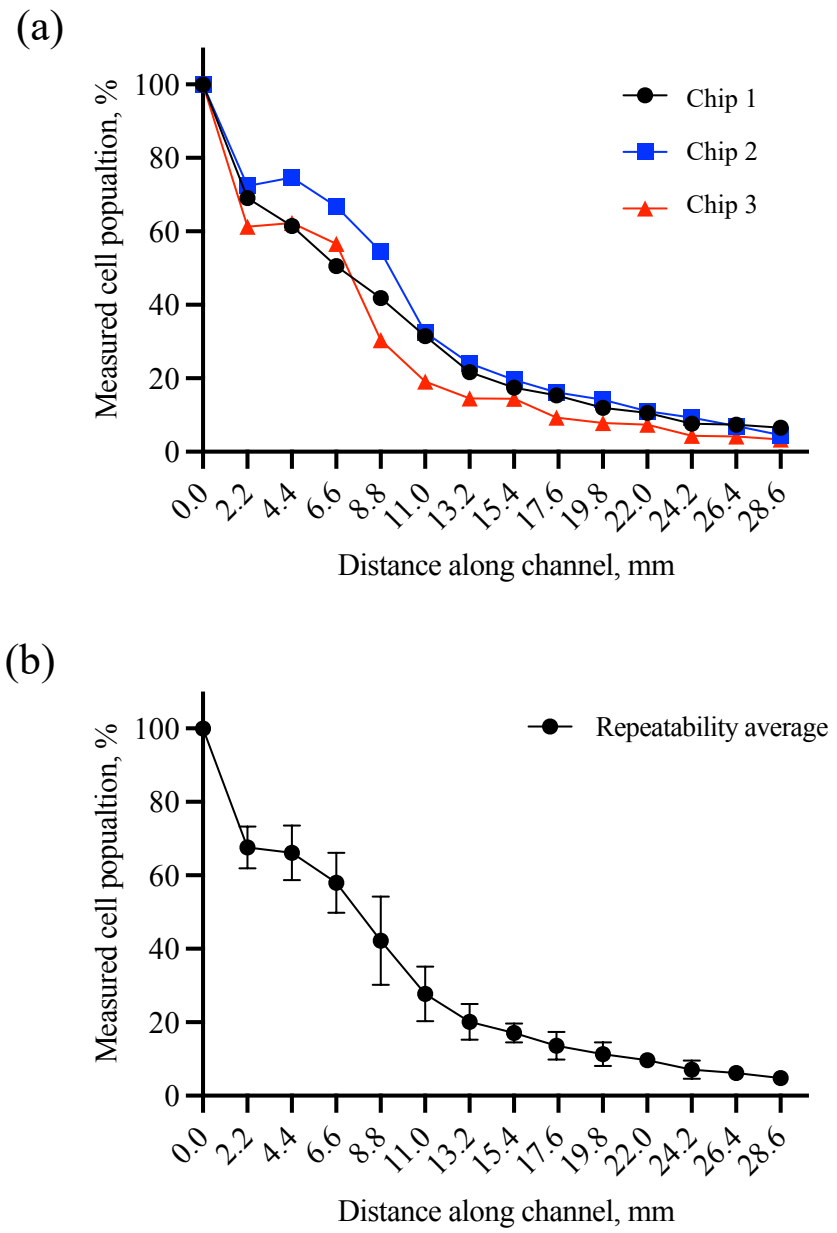

Figure 4-18 (a) Output curves of triplicate runs showed some variations between chips for the same healthy sample (b) The average of triplicate runs with standard deviation error bars. The largest error was ~ 12% at 8.8 mm along the microchannel.

The results in *Figure 4-18(a)* show that the curves appear to follow the same trend but there is some variation between the cell population decline. Further analysis of the variation between the triplicate samples showed that the largest variation was found to be ~ 12% at 8.8 mm along the microchannel, *Figure 4-18 (b)*.

The output curve for this healthy sample showed a significant decline of cell population from 0 – 2.2 mm along the channel and a two-phase reduction of cell population. To investigate if these curve traits were unique to this blood sample, the flow test was conducted using a larger population of healthy samples, shown in the following *Section 4.4.2*.

4.4.2 Control population characterisation

The flow test experiment was repeated on all healthy samples (n=9) and the following curve was obtained, *Figure 4-19*.

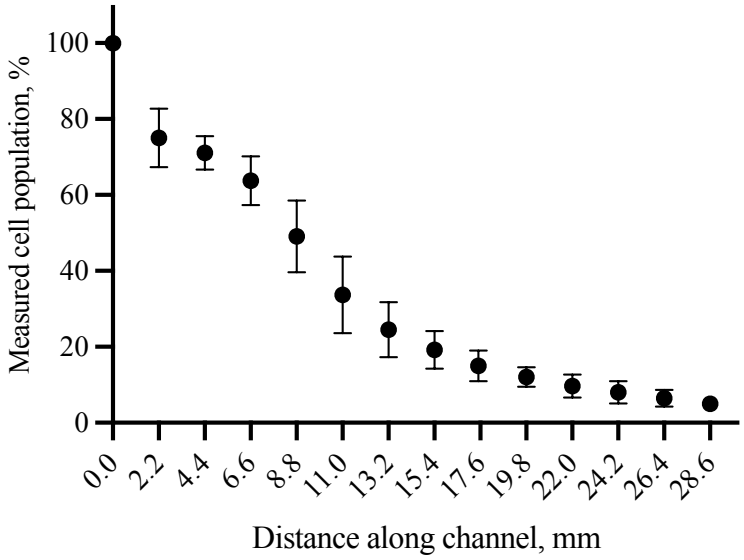

Figure 4-19 Graphical representation of the healthy subject characterisation (n=9) for the flow test investigations. The error bars are standard deviation with the largest error margin ~ 10% at 11 mm, the 6th imaging position along the microfluidic channel.

The initial drop in measured cell count from 0 mm to 2.2 mm that was apparent in the chip-chip repeatability measurements was consistent between all healthy samples investigated. The decline in cell population at this position was not observed to be a result of cell lysis. It is hypothesized that merging of the two channels at 2.2 mm may have caused a disturbance which pushed a proportion of cells out of the field of view and

further along the testing channel. This typically accounted for a loss of ~30% of the cell population, see *Figure 4-20*.

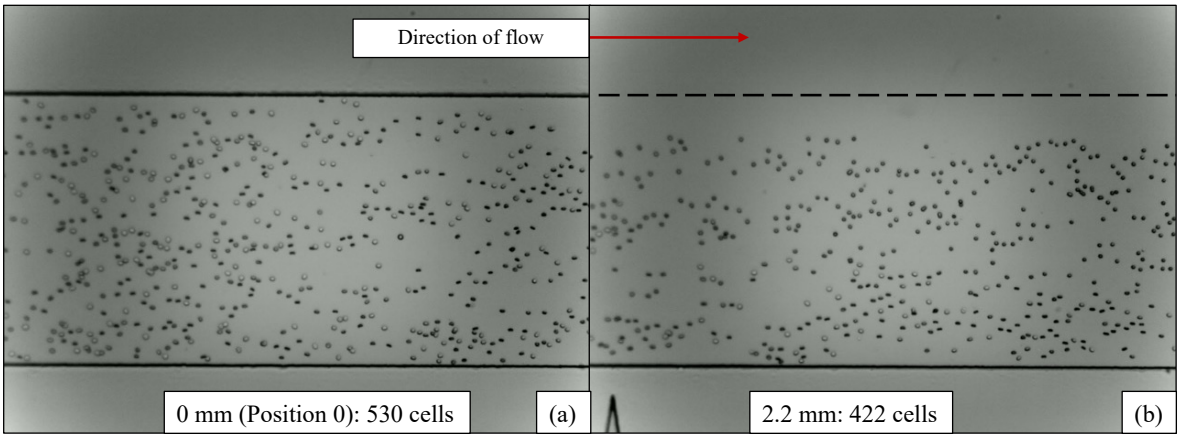

Figure 4-20 (a) 0 mm (Position 0) is located at a point along the channel prior to the introduction of the acid channel and is thus unaffected by any potential turbulence. The cell count at this position was 530 cells. (b) Removal of 108 cells likely caused by disturbance due to the introduction of the acid flow stream.

The shape of the output curve from 2.2 mm followed the weak biphasic population decline that was first observed in the earlier repeatability test. To compare this with the biphasic response of the LMDT, it was required to convert the units of the flow test from distance to time.

4.4.3 Comparison of flow and low magnification drop test

It was possible to determine the average velocity of a population of cells by analysing a selected group in a frame by frame manner using the image processing system *ImageJ*. Converting frames to time gave the average velocity at which cells were travelling in the channel (~ 0.2 mm/s). Knowledge of the velocity allowed for the conversion of distance along the channel to approximate time at the marked positions. The graphs of the LMDT and flow test were overlayed in GraphPad Prism, *Figure 4-21*.

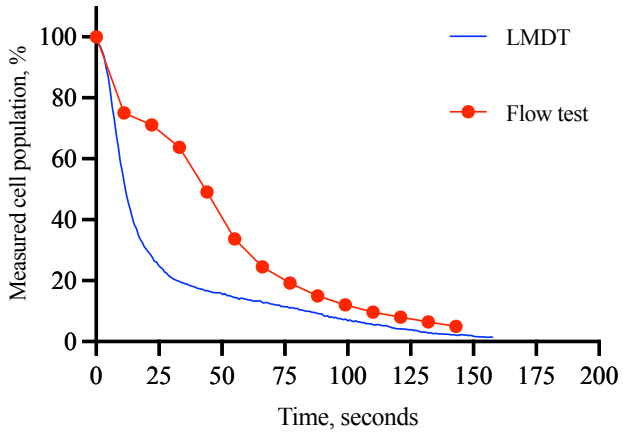

Figure 4-21 Comparison of curve shape from low magnification drop test (blue) and flow test (red) showed that both curves had a 2-phase decline of the cell population. The LMDT had a more extreme initial decline than the flow test.

Compared with the biphasic decline of the LMDT, the two phases of decline in the flow test took place over a longer time period. This is likely a result of the more controlled diffusion of the two samples within the microchannel.

4.4.4 Surface adhesion of cells

It was discovered after the completion of each test that there appeared to be cell cluster which adhered to the surface of the microchannel, *Figure 4-22*. This cell cluster adhesion presented at the first point of interaction of the acid and blood sample, however, it did not appear until approximately 90 seconds following the initiation of the low flow testing phase of the protocol.

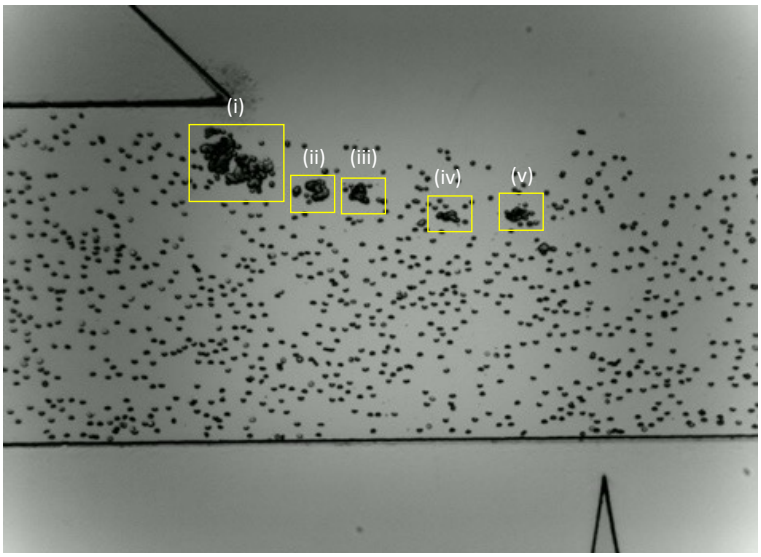

Figure 4-22 Build-up of RBCs adhering to the surface of the microchannel in yellow box ((i) – (v)). It is unclear whether this is the top or bottom surface of the channel.

The RBCs of patients suffering with Sickle Cell Disease typically present as 'sticky' under conditions of deoxygenation. This apparent 'stickiness' is due to a surface mutation changing a charged amino acid (glutamate) to a neutral amino acid (valine). The mutant modification from a charged to a neutral amino acid creates a sticky patch on the molecular surface of the RBC that causes aggregation upon deoxygenation.[211] Red blood cells release oxygen in the body when exposed to low pH environments.[212]

The nature of the developed protocols is exposure of RBCs to a low pH environment, thus it is assumed that the RBCs would be in a deoxygenated state during the experiment. As such, it was considered that the severity of cell-surface adhesion may be notably increased in samples that contained sickle cells. It was considered that this knowledge could be utilised as an additional diagnostic parameter.

(i) Measurement of cell-surface adhesion

Cell-surface adhesion is defined by the RBC clusters that have adhered to the surface of the microchannel. To determine the healthy range of cell-surface adhesion (RBC clusters), images were collected at the end of each test recording all cell-surface adhesion in the microchannel.

Adhered cell clusters were measured using the freehand tool in *ImageJ*. Within *ImageJ*, it was also possible to set the scale of the image using a known distance. The freehand tool allows for the conversion of measured pixels to the output measurement surface area, μm^2. All cell adhesion groups were measured and summed, thus the recorded measurement is representative of the total adhesion within the microchannel.

Analysis of the same healthy blood sample showed that the pattern and surface area of adhesion varied between triplicate runs, *Figure 4-23*.

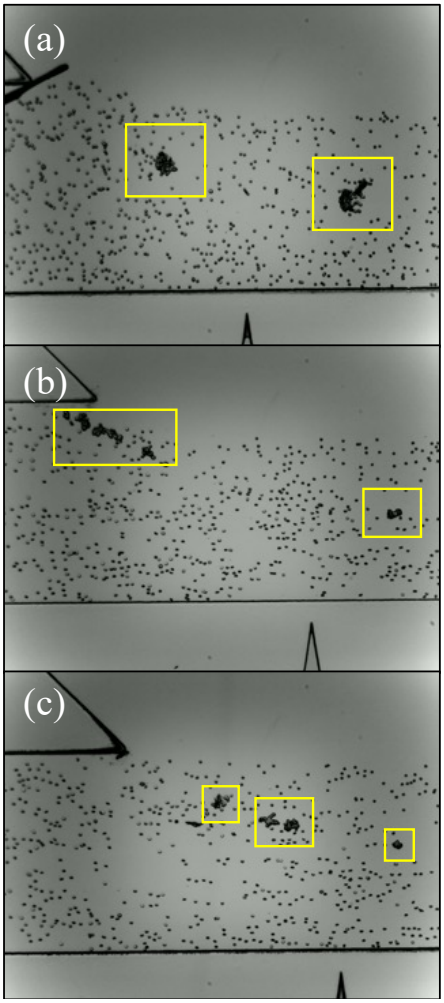

Figure 4-23 (a, (b) and (c) show different surface adhesion patterns for the same healthy sample using 3 single-use chips.

It is possible that cell-surface adhesion is random and it may rely on the accidental interaction of the RBC and the channel surface. It appeared that the adhesion of one cell to the surface of the microchannel caused the adhesion of other cells, creating a wall of cell aggregation within the channel.

All cell-surface adhesion for the control population was measured and the results are shown below in *Figure 4-24*.

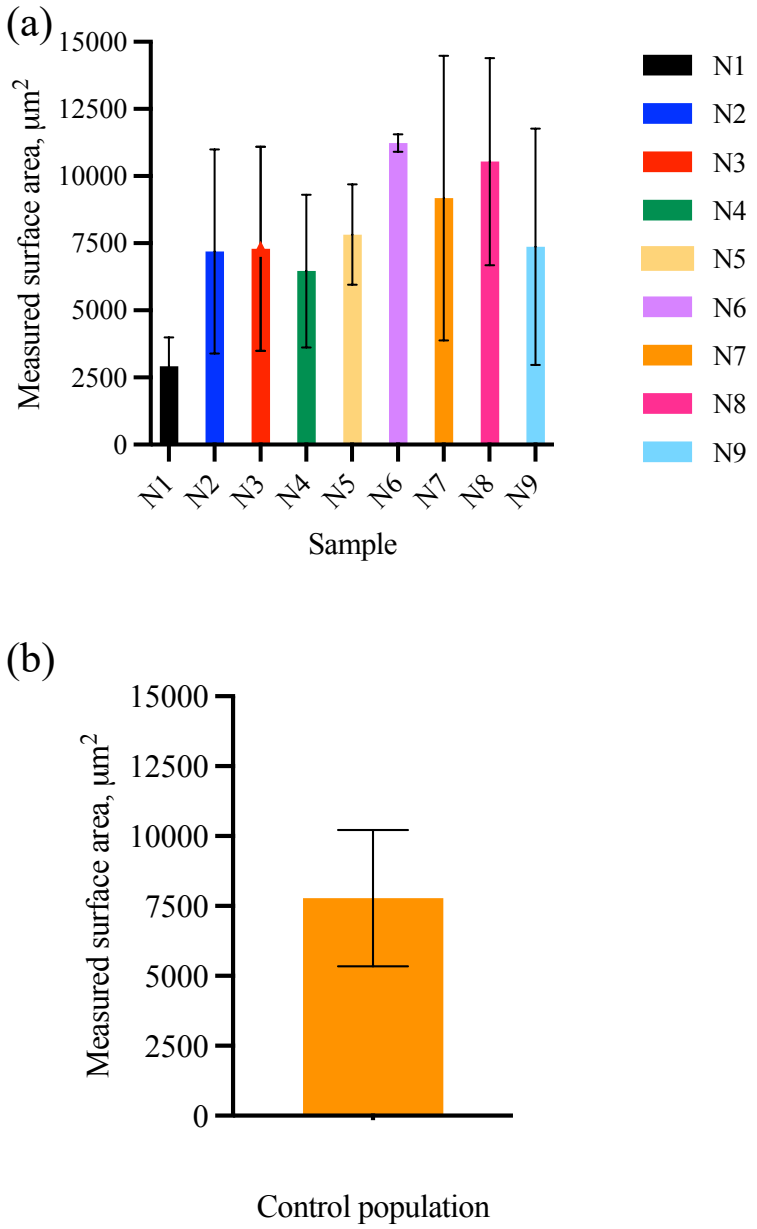

Figure 4-24 (a) shows the variation of measured cell-surface adhesion between the healthy samples. Error bars are standard deviation and were calculated from the average of 3 runs per sample. Samples are labelled N1 – N9. (b) the average deviation over all control samples.

It is clear from the large variations of measured cell-surface adhesion within the same sample that the results are not repeatable. However, it is possible that the measured cell-surface adhesion of the rare anaemia samples may exceed that of the control population, particularly in the case of Sickle Cell Disease. As such, this parameter was considered for comparison against rare anaemia samples, but the comparisons should be interpreted with caution. It is also important to note that these measurements were not executed by a programme thus error in precision is expected.

4.4.5 Conclusions and recommendations

The flow test had the unique advantage of a pre-determined flow rate (0.5 µl/min)which allowed for the controlled addition of acid to the blood sample. Investigation of the flow test demonstrated that it had good repeatability between healthy samples, with a maximum standard deviation of 10% over the total control population. Each healthy curve produced a similar two-phase decline trend.

The contrasting curve declines for the low magnification drop test and the flow test are likely a result of the differences in the protocols. More specifically, the flow test displayed greater control of diffusion of the acid with the blood sample.

Cell-surface adhesion was noted as a bi-product of the experimental protocol. Measurement of the cell aggregates formed on the surface of the channel showed large variations between triplicate runs of the same sample. However, it is possible that cell-surface adhesion of diseased blood samples may greatly exceed that of the control population, thus, it was cautiously considered as an option for comparison between control and diseased samples.

4.5 Haematological parameter correlative studies

A complete blood count is the first-tier investigation for diagnosis of a suspected rare anaemia. Although it is not the goal of this thesis to correlate the developed methods with current clinical practices, correlations would be of great benefit to any future user if access to a more expensive haematology analyser was not an option.

Considering the abilities of MeCheM and the developed protocols, a selection of haematology indices were chosen for correlation; (i) RBC count, (ii) haemoglobin variations, (iii) red cell volume and distribution width variations.

Simple linear regression analysis was carried out in GraphPad Prism to study the relationship between the variables obtained by MeCheM analysis and the gold standard haematology analyser. For this set of analyses, the values obtained from the haematology analyser were considered the dependent variable, and those from MeCheM were deemed the independent variable. The R^2 value will be used to determine how much variation of the dependable variables is explained by the independent variables. The categorization of the R^2 value generally follows that for; (i) $R^2 < 0.4$ = weak correlation, (ii) R^2 between 0.4 and 0.7 = good correlation, (iii) $R^2 > 0.7$ = high correlation, and (iv) $R^2 > 0.9$ very high correlation. However, due to small sample numbers and cell populations, the R^2 value should be considered with a degree of caution. The R^2 values were obtained from the output analysis sheet in GraphPad Prism.

Pearson correlation analysis was also conducted in GraphPad Prism and the P-value is reported for each correlation analysis. The P-value determines the probability that the null hypothesis is true. The significance level, α, was set to 0.05, meaning that there was only a possibility of 5% that the correlation observed between the variables being investigated occurred by chance.

A full account of all R^2 and p-values is given in tabulated form in *Appendix A.4*.

4.5.1 Cell count variations

The RBC count is a measure of number of red blood cells in the blood. One of the most common clinical features in patients suffering with anaemia is a low RBC count.[213] A low RBC count suggests that one of two situations are true; (i) the body is not creating sufficient numbers of RBCs, or (ii) the RBCs in circulation are being destroyed prematurely.[48]

To investigate whether fluctuations in RBC count could be observed using the methods developed within this body of work, the initial cell count, that is, the number of countable

cells in the FOV prior to addition of acid, for flow test were plotted against RBC count for each sample. 10 images were taken at Position 0 and the average cell count was recorded as the initial cell count for the test.

It was considered that a linear correlation may exist between the RBC count and the initial count of cells for the flow test given that each sample was diluted in the same manner prior to experimentation. It was expected that a correlation would be observed here as this is a like-like comparison. See results shown below in *Figure 4-25*.

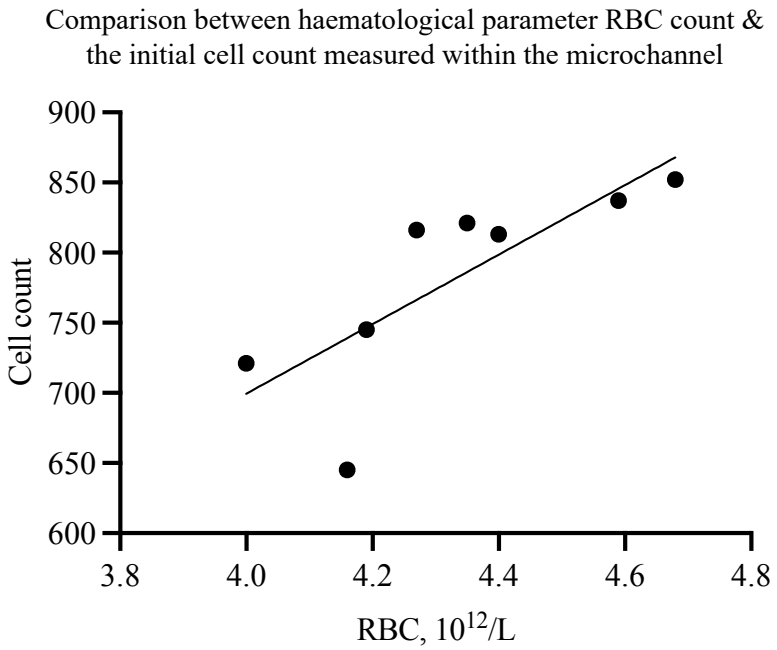

Figure 4-25 Here, initial cell count recorded within the channel prior to the junction where the acid is introduced is plotted against the RBC count measurements.

These preliminary results suggest that a linear correlation between RBC count and initial cell count for the flow test *may* exist. Simple linear regression analysis reported an R^2 value of 0.62, suggesting correlation between the variables *may* exist.

Applying the Pearson method, the correlations between initial cell count and RBC count were reported to be significant, with a p-value of 0.021.

Although these results suggest a correlation between initial cell count and RBC count may exist, given the small sample size used in this investigation, these preliminary results must be taken with a degree of caution.

4.5.2 Haemoglobin variations

The standard haematology indices for haemoglobin measurements are; (i) HGB, (ii) MCH, and (iii) MCHC. The haemoglobin test (HGB**)** measures the total amount of haemoglobin present in the blood sample. Mean corpuscular haemoglobin count (MCH) is a measure of the average amount of haemoglobin molecules present per RBC. This differs from the HGB parameter in that it is not dependent on the RBC count. Mean corpuscular haemoglobin concentration (MCHC) is a measure of the average concentration of haemoglobin per unit volume. This is dependent on the HGB value, thus affected by the RBC count.

Owing to the Bohr Effect, haemoglobin will bind H^+ ions in vivo in an effort to limit pH shifts in the body.[212,214] The buffering properties of haemoglobin have been widely reported in relation to the conversion of carbon dioxide into bicarbonate; $CO_2 + H_2O \rightarrow H_2CO_3 \rightarrow H^+ + HCO_3^-$. During this process, hydrogen ions are liberated, and the pH of the surrounding environment is lowered.

To maintain pH homeostasis, haemoglobin binds the free hydrogen ions raising the pH to the optimum level.[171,215] The hypothesis under consideration in this section is whether the RBCs with higher haemoglobin concentrations are afforded some protection from acid haemolysis due to haemoglobin 'buffering'. Thus, determining whether the acid resistance test could be used in absence of an expensive haematology analyser to monitor haemoglobin variations within a blood sample.

The haematological parameters of the control population are given in *Table 4-1*.

Sample	HGB, mmol/L	MCH, fmol	MCHC, mmol/L
N1	8.44	2.03	21.9
N2	7.76	1.94	21.8
N3	9.06	1.94	21.7
N4	7.32	1.71	20.2
N5	8.56	1.86	20.4
N6	8.02	1.93	20.7
N7	8.43	2.01	21.3
N8	7.78	1.79	21
N9	8.67	1.97	21.6

Table 4-1 Haematological values for the haemoglobin studies is included in this table. These values all fall within the recommended healthy ranges.

To determine whether correlations exist between the developed protocols and the haemoglobin measurements, comparison parameters within the developed tests had to be established.

For the flow test, it was decided that the time to achieve 50% lysis of the cell population, $T_{50\%}$, should be the parameter for comparison against the haemoglobin measurements. $T_{50\%}$ was calculated in Microsoft Excel using the TREND function. The population sample for the flow test was n=9.

For the high magnification drop test, the parameter chosen was the time taken for the cell to respond to the acid and reach its minimum projected area, i.e. the time required for the cell to become spherical. This was termed the 'activity time'. The activity time was calculated in Microsoft Excel by finding the minimum value of a cell track, post acid addition, and it's corresponding time point. The population sample size for the high magnification drop test was n=6.

It was considered that a later $T_{50\%}$ and activity time would be reported for samples with greater haemoglobin content.

Correlation analysis of gold standard haemoglobin parameters with the novel parameters developed within this thesis ($T_{50\%}$ & activity time)

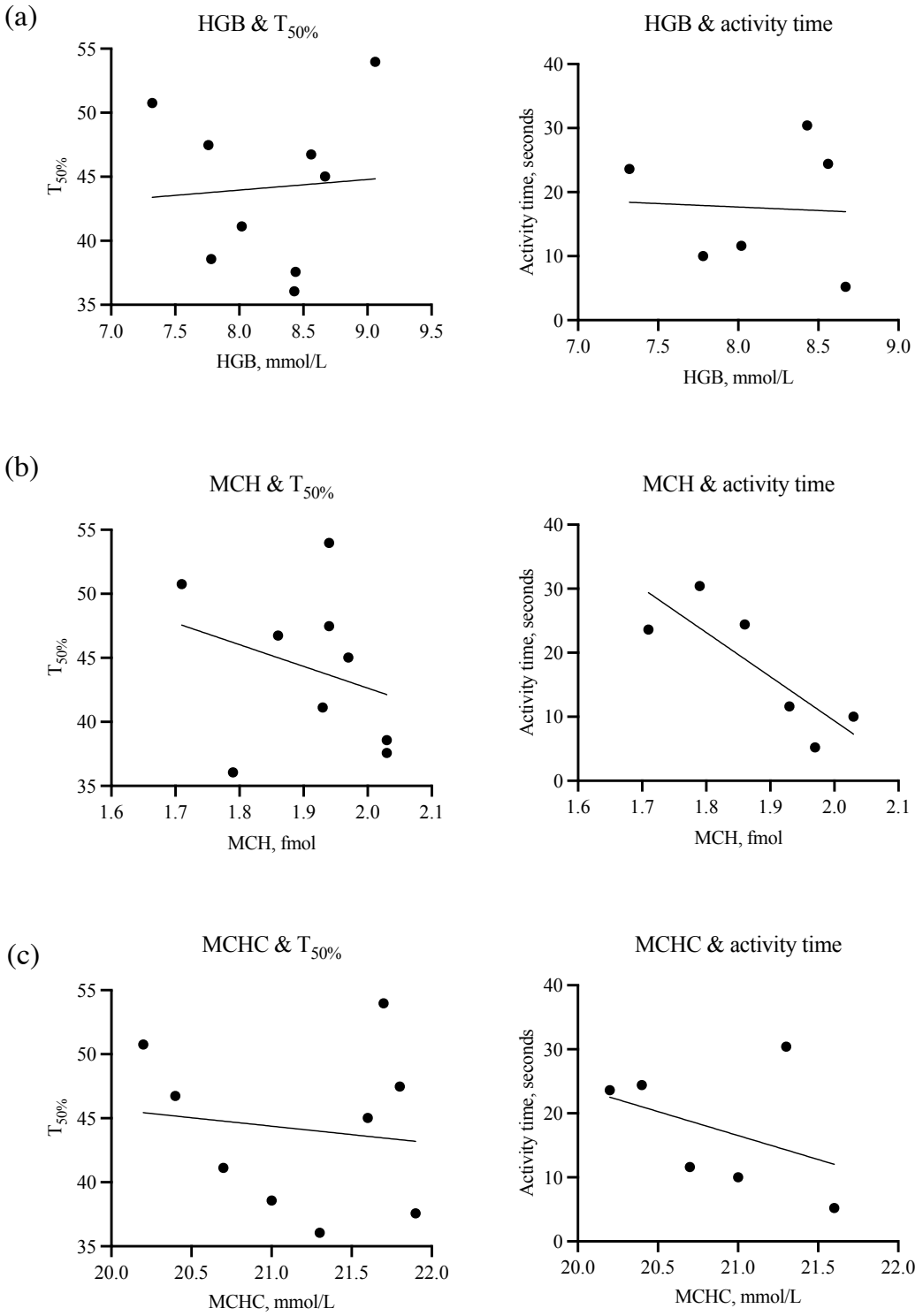

Figure 4-26 (a) Haemoglobin count with $T_{50\%}$ and activity time, (b) Mean corpuscular haemoglobin with $T_{50\%}$ and activity time, (c) Mean corpuscular haemoglobin concentration with $T_{50\%}$ and activity time.

The results from the analysis are shown above in *Figure 4-26*, and only one analysis, MCH and activity time for the HMDT, suggested any linear correlation (R^2 value 0.6799, p-value = 0.04). This suggested correlation is interesting because the MCH value is the only parameter from the selected group for analysis that is completely independent of other RBC values. HGB and MCHC are both dependent on the RBC count of the sample. It is also important to note that, given the small control sample size (n=6) for the activity time analysis, it is possible that this correlation is coincidental. Further investigations on a larger control sample population are required to confirm the apparent correlation.

Otherwise, the remaining set of analyses shows a lack of correlation between all other haemoglobin levels and the HMDT and flow test. This suggests that; (i) the haemoglobin content is not binding hydrogen ions in the acid haemolysis test, and/or (ii) the tests are not sufficiently sensitive to record variances in haemoglobin levels.

The conclusion of this set of analyses suggests that HGB and MCHC did not display any linear correlations with $T_{50\%}$ or activity time. A correlation appeared between the activity time and MCH, but this was not observed for MCH and $T_{50\%}$. There is an obvious need for larger control sample sizes which would prove or disprove any suggested correlations.

To use the $T_{50\%}$ as a variable for investigation, the protocol should be refined. A potential system optimisation would be to use a motorised XY-stage and to follow the same population of cells in the microchannel from beginning to end, ensuring that the correct and exact time point for $T_{50\%}$ is recorded. It is important to note that this correlation analysis is not comparing like-like data.

4.5.3 Cell volume and size variations

(i) Mean corpuscular volume

Mean corpuscular volume (MCV) describes the average size and volume of the RBCs in a sample. Low values for MCV are common in iron deficiency anaemia but can also be a clinical presentation of hereditary anaemias such as thalassaemia and spherocytosis.[76,195] These smaller RBCs are termed ‘microcytic’. The hypothesis under investigation in this section is that smaller cells are more fragile due to their reduced membrane, thus decreasing their resistance to lysis.

The aim of this section was to determine if the projected area measurements as given by MeCheM was comparable with the gold standard MCV parameter. This is a like-like correlation.

The variable that was under consideration for comparison against MCV values was the average cell projected area pre-acid addition for the healthy samples. Each healthy projected area measurement represents ~ 60 cells over triplicate runs, the standard deviation of cell projected areas within samples was between 1 – 2%. The results are shown below in *Figure 4-27*.

Correlation analysis between the gold standard MCV & the Projected Area measurement as determined by MeCheM

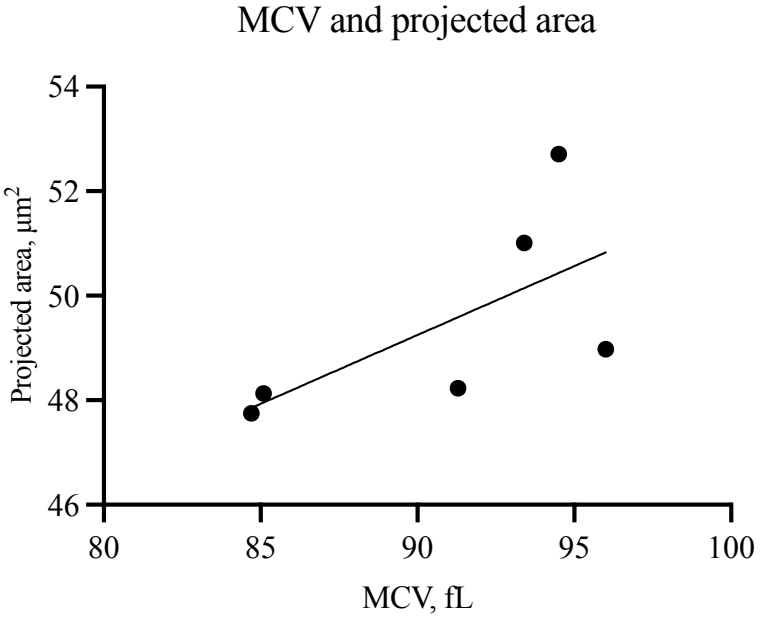

Figure 4-27 There does not appear to be a correlation between the projected area measurement from the HMDT and the MCV values.

The results from this analysis gave an R^2 value of 0.402. Given the small sample sizes, it is difficult to suggest whether a correlation might exist between average cell projected area pre-acid addition to MCV value. The p-value was reported to be 0.07, thus, not significant.

(ii) Red cell distribution width

The red cell distribution width (RDW) is a haematological parameter that represents the size variability of RBCs in circulation. The normal range for this parameter is 11.5 – 15.5%.[216] Values outside this parameter indicate a greater variation of cell size in the

sample population. This can be seen in inherited anaemias such as sickle cell disease, β-thalassaemia, and others which is caused by an increase in different cell types within the sample population.[114,217,218] Although RDW is not a diagnostic factor in itself, it is indicative of an underlying problem thus it is a valuable parameter for first-tier clinical investigations.

The value for RDW is calculated by the dividing the standard deviation of the MCV by the mean MCV and multiplying by 100.[219]

A comparable parameter developed within this thesis is the projected area distribution width (PDW) obtained from the HMDT. Using the RDW formula and applying it to the projected area measurements of the HMDT it is possible to compare these two parameters and investigate correlations, see results below in *Figure 4-28*.

$$PDW = \frac{Standard\ deviation\ of\ projected\ area}{Mean\ projected\ area}\ x\ 100$$

Correlation analysis between the gold standard RDW & the Projected Area Distribution Width as determined by MeCheM

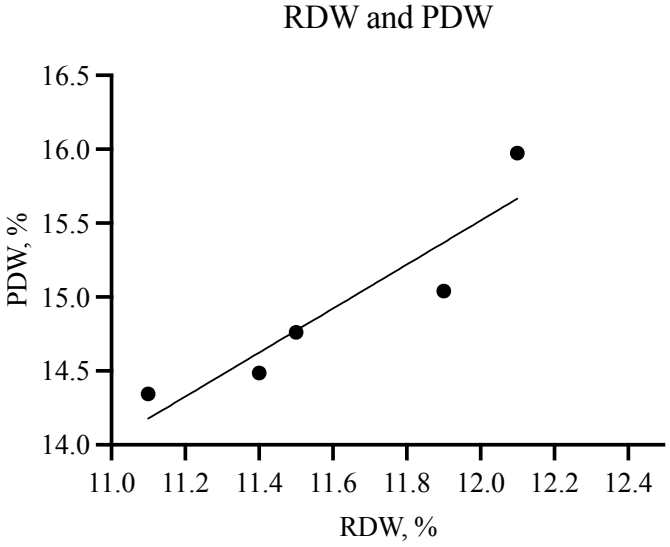

Figure 4-28 The R^2 value for linear correlation between RDW and PDW was found to be 0.8506, with p-value=0.02. This indicates that there may correlation between these variables.

It was expected, given the suggested correlation MCV and measured projected area, that there would be an observation linear correlation between RDW and PDW. With the

removal of one apparent outlier, (N3), the R^2 value for this correlation was 0.8056 which implies a correlation may exist for these parameters. The p-value was also reported to be significant at 0.02. This is a like-like comparison.

4.6 Method recommendations for further investigations with diseased blood

4.6.1 Low magnification drop test

The LMDT had the recognisable challenge of requiring considerable human interaction during the testing and analysis process. Due to its simple setup, user error was the main contributing factor to variation between samples. There were two factors that greatly reduced test reproducibility; (i) turbulence caused by the acid filled pipette tip coming into contact with the diluted blood sample, and (ii) inaccurate positioning of the acid drop causing the droplet to be dispensed away from the FOV of the camera.

Turbulence caused movement of cells within the droplet and in some cases that appeared on the LMDT output graph as a large drop in cell numbers. This perceived drop in cell numbers required visual observation of the video recording to determine the cause of the cell decrease. This requirement was an additional and timely step to the analysis of the LMDT.

Positioning of both the sample and the acid filled pipette tip accurately over the field of view of the camera proved to be the most difficult part of this test. If the acid was not added directly over the cells in the FOV of the camera, there would be a notable delay in the onset of haemolysis of the cells. The variation in acid drop position could result in curves with large differences in cell population decline between the same sample.

Due to the lack of test sensitivity, the LMDT was not recommended in its current state for comparison against diseased samples.

4.6.2 High magnification drop test

Similarly to the LMDT, user input was a highlighted challenge in the HMDT. The experimental protocol had a tendency to create movement of cells, and accurate

positioning of the pipette tip for acid dispensing was difficult to achieve. This created problems for test repeatability.

Using the HMDT, changes in cell projected areas in response to acid exposure over time can be tracked and recorded. Following the protocol, the cell projected areas are tracked from a time before acid exposure until eventual sample haemolysis.

The output graphs were; (i) RBC population count, (ii) RBC size distribution, and (iii) RBC size measurement.

The information obtained from the RBC population count was limited by very small cell numbers. Due to placement errors of the acid dispensing, the variations in curve shape between the healthy population were quite large, thus, this test was not recommended for comparison against diseased samples.

The RBC size distribution analysis showed a Gaussian distribution of the RBC population size with most cells centering around 50 μm^2. Upon exposure to acid, the RBC size distribution reduced initially and then increased for each measured increasing time point. This analysis gave a specific range for the healthy population and, as such, it was recommended for comparison against rare anaemia samples.

The final graphical output from the HMDT was RBC size measurement. This showed the changing cell projected area over time upon exposure to acid. There were large variations among the healthy population that were increased due to the occurrence of cell lysis with increasing test time. This direct measurement was not reliable for comparison against diseased samples. However, it was possible to obtain a cell swelling capacity, that is measurement of the swelling from the RBCs minimum to its maximum projected area. This analysis allowed for a healthy population cell swelling capacity to be determined which could be used for comparison against rare anaemia samples.

4.6.3 Flow test

The flow test required much less user input to the testing protocol which removed many of the variations observed in the LMDT and HMDT. The resulting curve for the flow test

was repeatable in terms of its general bi-phasic decline in cell population. The maximum error, standard deviation, for the control population was calculated to be ~ 10%.

Cell-surface adhesion was measured and it was considered that this could be used to compare against the cell-surface adhesion of rare anaemias, specifically Sickle Cell samples given the propensity for sticky cells among that disease.

4.6.4 Conclusion

The aim of this chapter was to investigate the repeatability of the developed methods, thus, their suitability going forward in the next chapter for comparison against rare anaemias. While not all of the methods are recommended in their current state, there is potential for system optimisation that would greatly increase their repeatability.

The methods that were deemed suitable for advancement for comparison against diseased samples in their current state are; (i) RBC size distribution pre-acid addition, (ii) RBC size distribution post acid addition, (iii) RBC swelling capacity, and (iv) flow test.

A secondary outcome of this chapter was the investigation of the developed methods with a complete blood count analysis for correlations. It was found that there appeared to be a correlation between; (i) MCH and activity time in the HMDT, and (ii) MCV and projected area of the HMDT. Due to the small cell number in the high magnification drop test this analysis could only suggest correlations, thus, further investigations are required to confirm the observed correlations.

Chapter 5 Application of MeCheM techniques as a potential diagnostic tool

The overarching goal of this thesis was to design a low-cost, user-friendly test for the diagnosis of rare anaemias. The previous chapters have described the development of the necessary elements of that test; a microfluidic instrument MeCheM, a microfluidic chip, a bioassay, and protocols. In this chapter, the diagnostic abilities of the developed methods are investigated.

The sample population sizes were quite limited due to the rare nature of these diseases. To avoid repetition at the conclusion of each section, it should be noted that **all results and correlations** were derived from limited anaemic samples and cell numbers, and future research should include a larger sample population.

Given the infrequency of rare anaemias, particularly in Northern Europe,[220] it was known that obtaining a large sample size for investigations would be a challenge. However, the purpose of this chapter was to conduct preliminary testing on any available samples with hopes that the results might highlight specific diseases or disease types to investigate in more depth.

5.1 A brief summation of rare anaemias

Rare anaemias are categorised according to the site of the mutations arising. The term ‘haemoglobinopathy’ refers to a group of rare anaemias that are caused by mutations in the haemoglobin molecule. The mutations in membranopathies are brought about by anomalies in the RBC membrane, including the cytoskeleton. Finally, enzymopathies describe the mutations that occur in the enzymes of red blood cells interfering with cellular metabolism. Although the mutations causing disease in each of these cases is different, the anaemias share some commonalities that suggest the developed testing methodologies have the potential to highlight these diseases for diagnostic purposes. The groups of hereditary anaemias that are investigated in this section are; (i) haemoglobinopathies, and (ii) membranopathies.

5.1.1 Haemoglobinopathies

Section *1.1* describes the importance of haemoglobin for oxygen delivery and the problems that arise when the haemoglobin is mutated. Haemoglobinopathies can be classified as; (i) Sickling disorders, and (ii) Thalassaemias.

Sickling disorders display several characteristics that could be used as differential factors in the employment of the previously described methodologies. The RBCs of patients with Sickle Cell Disease display reduced cellular deformability, increased red cell distribution width, and have a propensity for cellular adhesion.[52] Considering the recommended methods from *Chapter 4* it is hypothesized that the RBC size distribution may align with increased RDW. The reduced deformability of sickled cells may be demonstrated by the cell swelling capacity test and the predisposition for sickle cells to adhere may also be highlighted in the flow test.

Similarly, RDW can be elevated in Thalassaemia and patients often display a reduced MCV.[221] This may be highlighted in the RBC size distributions test as a shift to the left of the previously established control population histogram, thus, suggesting a higher number of cells are residing in the smaller interval ranges. Thalassaemic RBCs are typically more fragile than healthy RBCs meaning that samples may show decreased resistance to swelling and lysis in the cell swelling capacity and flow tests.

5.1.2 Membranopathies

Membranopathies are characterised by anomalies in the genes encoding the skeletal proteins which alter the membrane structure.[222] Among membranopathies, Hereditary Spherocytosis (HS) is the most common of the anaemias.[222] In HS, the molecular defects of the membrane proteins result in a loss of membrane surface area. This leads to fragile microcytic and spheroid RBCs which can be diagnosed using various haematological parameters.[223]

Other membranopathies may display similar defects or may have different characteristics that could be used for diagnostic purposes. Although disease heterogeneity proves a challenge for comparable RBC indices between Hereditary Xerocytosis (HX) patients, it

is typically reported that the RBCs are borderline macrocytic and characteristically dehydrated.[224,225]

Knowledge of the characteristics of the membranopathies allows hypotheses to be formed in respect of their anticipated responses to the developed methodologies. For HS, given the typical microcytic size of HS cells, it was expected that the RBC size distributions would demonstrate a shift to lower values on the control histogram. It was also hypothesized that the cells would exhibit a decrease in resistance to lysis which could be recorded using the flow test and the cell swelling capacity test. Contrastingly, for HX it was hypothesized that these cells would display an observable increase in resistance to cell lysis and swelling.

5.1.3 Overview of diseased samples

Samples were collected and tested on site in the University Medical Centre, Utrecht, over a 3-week period. *Table 5-1* below gives an overview of the samples that were investigated for diagnostic potential using the developed methods. In this section, samples that contained the same mutations were grouped together where appropriate. For example, samples S8 and S9 were both diagnosed as β-Thalassaemia Major, thus were categorised as 'BTM', etc.

Haemoglobinopathies	*Sickled diseases*		*Thalassaemias*		*Others*		**Membranopathies**	
HbSS	n=3	BTM	n=2	HbA/HbH	n=1	HS	n=2
HbS/BT	n=3	BTI	n=1	HbE/HbH	n=1	HX	n=2
HbSC	n=1	BT_m	n=1				
HbS/HbH	n=1	HbH	n=1				

Table 5-1 Overview of samples tested for comparison against the healthy control. Abbreviations are explained in the glossary.

Below in Table 5-2 to Table 5-4 is a compilation of haematological indices for the rare anaemia samples (coded S1 -S18).

(i) Haematological indices for haemoglobinopathies

	Sample code	*Disease*	*RBC, 10^{12}/L*	*MCV, fL*	*MCH, fmol*	*RDW, %*
Sickled diseases	S1	HbSS	4.74	58.1	1.17	22.1
	S2	HbSS	2.83	97.8	2.08	20.1
	S3	HbSS	3.46	80.5	1.69	24.4
	S4	HbS/BT	2.70	116.0	2.60	17.3
	S5	HbS/BT	2.88	86.9	1.69	28.7
	S6	HbS/BT	4.42	71.3	1.40	20.6
	S7	HbSC	4.75	64.9	1.43	19.1

Table 5-2 Haematological indices for Sickled diseases.

	Sample code	*Disease*	*RBC, 10^{12}/L*	*MCV, fL*	*MCH, fmol*	*RDW, %*
Thalassaemias	S8	BTM	3.01	84.6	1.74	15.6
	S9	BTM	3.1	76.2	1.73	24.5
	S10	BTI	2.42	83.9	1.59	28.1
	S11	BT_m	5.77	53.4	1.05	16.3
	S12	HbH	5.68	59.6	0.86	26.1
	S13	HbA/HbH	4.31	72.6	1.55	28.1
	S14	HbE/HbH	4.90	75.6	1.64	12.2

Table 5-3 Haematological indices for the Thalassaemias.

(ii) Haematological indices for membranopathies

	Sample code	*Disease*	*RBC, 10^{12}/L*	*MCV, fL*	*MCH, fmol*	*RDW, %*
Membranopathies	S15	HS	4.41	83.5	1.86	16.8
	S16	HS	3.20	82.0	1.79	21.6
	S17	HX	3.15	101.0	2.16	11.3
	S18	HX	4.25	87.7	2.04	12.9

Table 5-4 Haematological indices for Membranopathies.

(iii) Reference haematological indices

Healthy ranges for RBC indices			
RBC, 10^{12}/L	**MCV, fL**	**MCH, fmol**	**RDW, %**
3.8 - 5.9	80 - 100	1.7 - 2.0	11.8 - 16.1

Table 5-5 Haematological references ranges for healthy blood samples.

5.1.4 Summary of investigative parameters

The analyses considered for investigations of diagnostic potential using the rare anaemia samples could be categorized into; (i) flow analyses, (ii) high magnification analyses, and

(iii) haematological correlations. The tests for flow analyses were; (i) flow test, and (ii) cell-surface adhesion measurements. The analyses from the high magnification testing were; (i) RBC size distribution pre-acid addition, (ii) RBC size distribution post-acid addition, and (iii) RBC swelling capacity. The haematological parameters RBC count, RDW, MCH and MCV were chosen to investigate for correlations with the developed tests. RBC count was investigated for correlations with the initial cell count in the flow test. RDW was compared against the developed high magnification parameter Projected Area Distribution Width (PDW). MCH was investigated for correlation with the cell activity time, that is, the time required for the RBC to reach its minimum size following the introduction of acid. Finally, MCV and the average measured cell projected area values were compared for correlations. The results are discussed below in the following sections.

The results that will be discussed in this chapter are a sample of the experiments conducted and were chosen based on interesting experimental observations. The complete analysis for each sample and test type can be found in *Appendices A.1 – A.2*.

5.2 Results: Flow analyses

The analyses carried out under flow conditions were (i) the flow test, and (ii) cell-surface adhesion measurements. The flow test was the measure of cell population along the channel and the cell-surface adhesion was the measurement of the cell clusters that had adhered to the surfaces of the microchannel.

5.2.1 Flow test

(i) Haemoglobinopathies

Sickled disorders

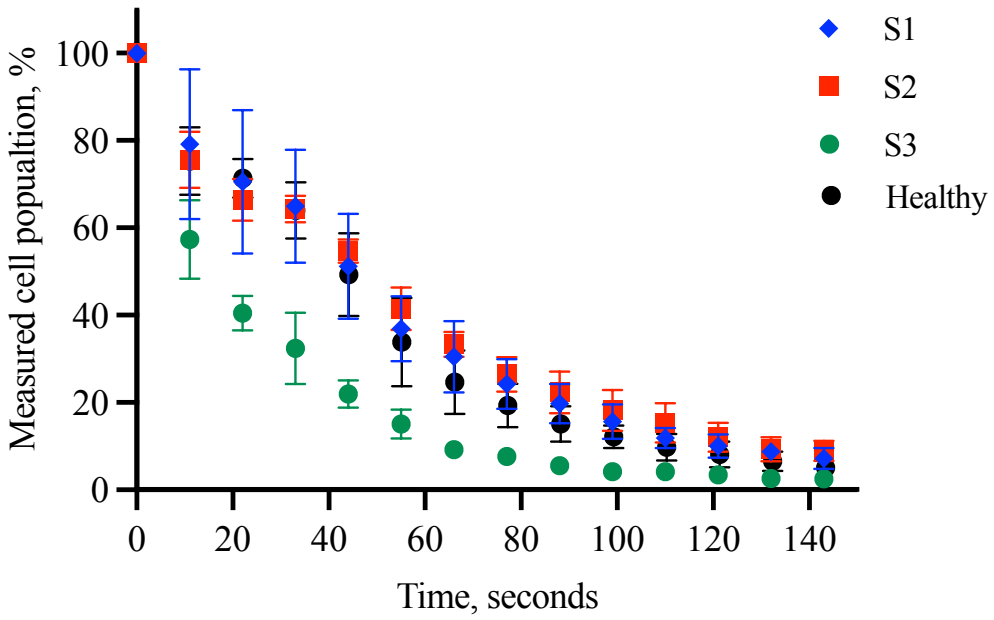

Figure 5-1 Flow test results for Homozygous Sickle Cell Disease (HbSS). Error bars are standard deviation.

The results shown in *Figure 5-1* for the homozygous sickle samples S1 – S3 suggest that, with the exception of rare anaemia sample S3, there were no clear differences for HbSS when compared with the healthy control population. A comparison of the haematological indices, see *Table 5-2*, for sample S3 with the healthy population showed a lower RBC count and a higher RDW. However, these values were also outside of the normal range for most of the other sickled samples. Therefore, the resulting curve could not obviously be attributed to these abnormal haematological values for sample S3. The standard deviation per position for sample S3 was not particularly large indicating that the sample behaved similarly for each triplicate run. However, the cause for apparent increased fragility of this sample was unknown.

The results of the flow test investigation reports that this assay was not sufficiently sensitive to highlight differences between healthy and sickled diseases in the case of 6 out of 7 samples, see *Appendix A.1* for further results.

Thalassaemias

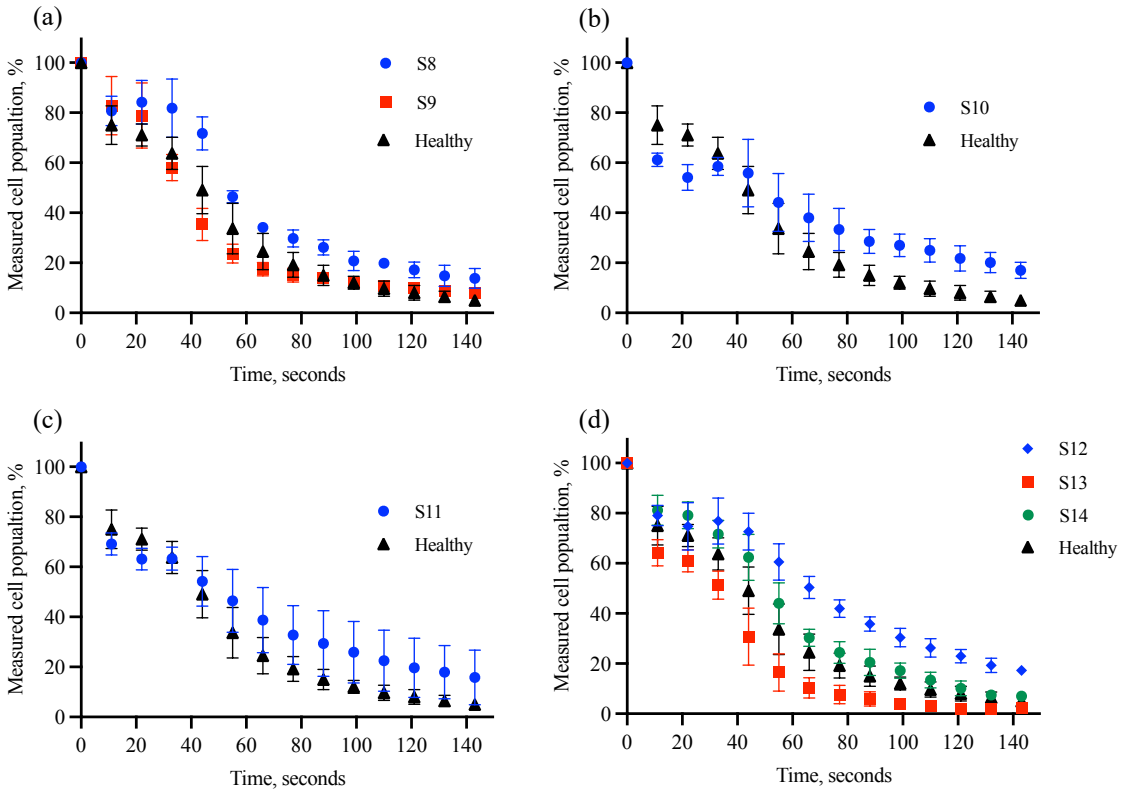

Figure 5-2 Flow test results for β-Thalassaemias is shown in (a) – (c), and the flow test results for α-Thalassaemias is shown in (d). Error bars are standard deviation.

Figure 5-2 (a) compares β-Thalassaemia major with the healthy result for the flow test. There appears to be a delay in lysis for sample S8, depicted by the rightward shift of the population decline curve. However, this was not observed for the second β-Thalassaemia major sample, S9 which appears to closely follow the shape of the control curve. It was known that there was a significant difference between patient sample S8 and S9 in that, patient sample S8 had undergone a splenectomy.

The primary function of the spleen is the removal of old and damaged red blood cells from circulation through phagocytosis which takes place in the macrophages of the spleen.[226] Other organs, such as the liver and bone marrow, also contain the macrophages required for red cell removal and these will work to remove old and damaged red blood cells in the absence of the spleen.[227] However, in severe rare anaemia cases like BTM, the production of mutated RBCs can be overwhelming to the splectomised system, thus, the mutated cells may be observed in circulation for longer periods of time.

Normal spleen function for patient S9 should remove many of the damaged and mutated red blood cells from circulation, meaning that the majority of the remaining cells, thus the cells under observation in the flow test, are the healthier cells. If this is the case, it would be expected that the patient sample would follow the control curve more closely.

A delay in the onset of haemolysis is observed for sample S8 and there is a higher percentage of surviving cells at the final imaging position compared to the control. It is possible that this could be caused by the disease mutations, however, it is not clearly distinguishable from the healthy control.

Figure 5-2 (b) shows that sample S10, β-Thalassaemia intermedia, initially appears to have faster cell lysis than the control curve. However, this haemolysis slows at ~ 55 seconds, and the remainder of the curve observes a decrease in haemolysis compared with the control curve.

Sample S11, β-Thalassaemia minor shown in *Figure 5-2 (c),* had the largest overall variation between triplicate runs. Although, on average it appeared that the sample S11 showed slower haemolysis in the microchannel, this was not the case for each experimental run. In one case, sample S11 appeared to align with the control curve which is concerning from a diagnostic perspective.

Finally, *Figure 5-2 (d)*, is a compilation of the α-Thalassaemia mutations. Sample S12, (HbH), displayed the clearest delay in haemolysis and there was little variation between triplicate runs in this case. Sample S13, (HbA/α-T), appeared to have faster haemolysis than the control curve. Sample S14, (HbE/α-T), did not appear to be distinguishable from the control curve.

Thalassaemic cells characteristically have excess membrane surface area and reduced membrane deformability.[228] This is interesting because, as confirmed by the high magnification tests in *Section 5.3.2*, the RBCs reduce in projected area upon exposure to acid prior to the initiation of the swelling phase. Reduced deformability may suggest that the Thalassaemic cell is reluctant to deform initially in response to acid. It could also suggest that the Thalassaemic cell has greater swelling capabilities than a healthy cell given its excessive membrane surface area – which may be observed in the flow test as a

resistance to lysis (samples S10, S11, and S12). Equally, a lack of deformability might suggest a decrease in resistance to haemolysis which could be characterised in the flow test as a more rapid haemolysis.

The results of the flow test appear to highlight differences in 5 out of the 7 Thalassaemic samples. Further investigations on larger population sizes may highlight potential diagnostic qualities for the Thalassaemic samples.

(ii) Membranopathies

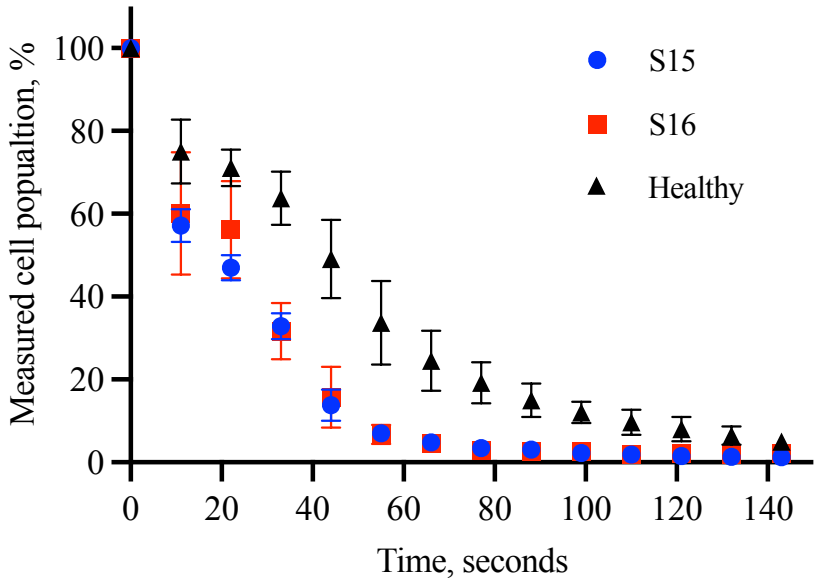

Figure 5-3 Flow test results for Hereditary Spherocytosis (S15 & S16. Error bars are standard deviation.

Figure 5-3 (a) shows the flow test results for HS which are clearly distinguishable from the healthy sample. A known characteristic of HS RBCs is their increased membrane fragility and this has been widely reported as a differentiating factor in the osmotic fragility test[229]. In HS, the RBC is typically microcytic and that may be described in haematology indices as a decreased MCV value. Whilst samples S15 and S16 did not highlight an abnormally low MCV value, the results of the flow test showed a decrease in resistance to lysis for both samples. The more rapid decline in cell population in the microchannel suggests that these cells are more fragile than the healthy population. The results also showed that the HS curves overlapped almost perfectly and the standard deviation of the triplicate measurements was much smaller than previously observed for the other rare anaemia types.

The HS samples are clearly distinguishable from the control curve. Although further research on larger sample populations is required, the preliminary results for the flow test suggest that there may be diagnostic potential for HS samples.

5.2.2 Cell-surface adhesion measurements

Cell-surface adhesion measurements are a measure of the total surface area of the cell 'cluster' that adhered to the surface of the microchannel.

The negative surface charge of the RBC prevents cell-cell and cell-surface adhesion under physiological conditions.[203] However, under these experimental conditions, the RBCs are exposed to H^+ ions from the acidic stressor causing the RBCs to move through their isoelectric point, changing their surface charge from negative to positive.[204,205] The RBCs that are nearest to the acidic stressor within the microchannel will move through this charge change before cells that are furthest away from the acid. This creates cell-cell and cell-surface attraction, thus measurable adhesion is observed.

Each cluster was measured individually and the value of the sum of all the clusters was recorded. The clusters varied in size and number across triplicate runs for the each patient sample. In some cases, only one small cluster would be observed within the microchannel and in contrast, for the same sample,6/7 clusters could be observed using a different chip. The chip-chip variation resulted in large standard deviations for this measurement.

(i) Haemoglobinopathies

Sickled disorders

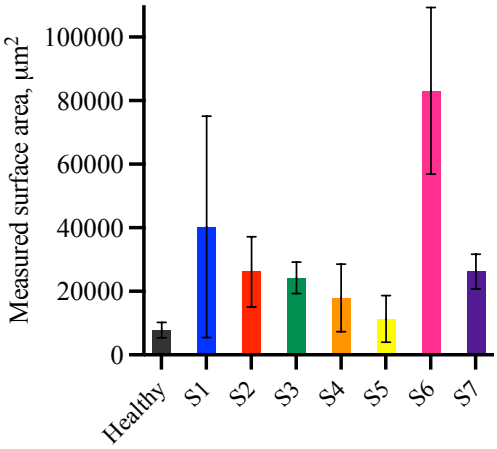

Figure 5-4 Measured cell-surface adhesion on the microchannel for each sickled disease (S1 – S7). Error bars are standard deviation.

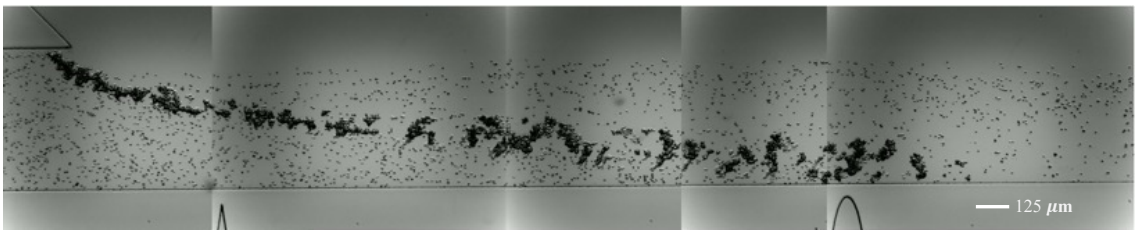

Figure 5-5 Cell-surface adhesion along the microchannel from sample S6 (HbSC) which had the largest measured adhesion from all the rare anaemias investigated.

The cell-surface adhesion measurements (*Figure 5-4)* showed that, in general, the average cell-surface adhesion for the sickled diseases was significantly increased when compared with the control.

However, as each test was investigated in triplicate, it was observed that there was a large degree of variation between the same samples. For example, the standard deviation of sample S1 in *Figure 5-4* shows that the measured cell-surface adhesion may fall within the healthy control population range.

Although this method seemed to highlight the sickled samples as more prone to cell-surface adhesion in most cases, there were inconsistencies among samples with the same mutation. As previously mentioned, samples S1 – S3 were homozygous HbSS. While samples S2 and S3 arguably fall within a similar cell-surface adhesion range, S1 appears to be an outlier.

To confirm whether the differences observed between the healthy and sickle cell-surface adhesion measurements were significant, an Unpaired T-Test was conducted in GraphPad Prism. The results from this showed that the sickle samples, with the exception of S5, showed significant differences to that of the healthy population, with p-values < 0.05 in all cases. Sample S5 did not show significant difference and the p-value was found to be > 0.05.

This investigation suggests that the adhesive properties of the sickled diseases *may* be detected by the cell-surface adhesion measurements, however, the accuracy of this measurement is not sufficient to highlight specific disease mutations, or even clearly distinguish between healthy and diseased samples at this point.

Thalassaemias

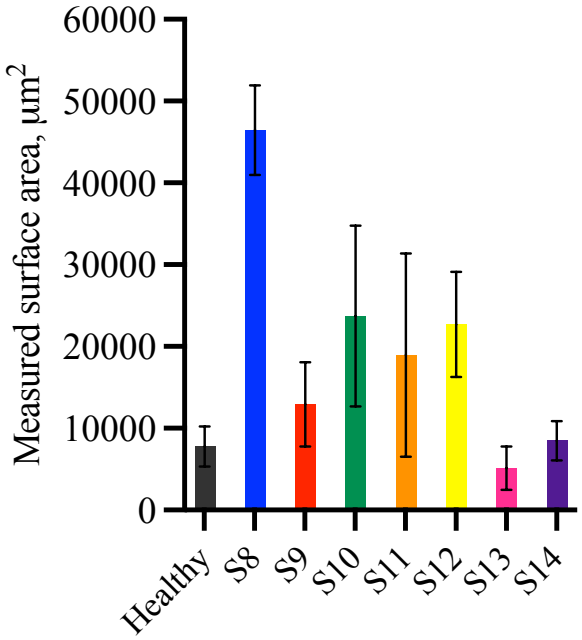

Figure 5-6 Aggregation analysis for the Thalassaemia diseases showed increased cell-surface adhesion in 5 of 7 disorders.

Although Thalassaemic cells are not known for their adhesive properties, significant cell-surface adhesion was observed in the flow test for samples S8, S10 and S12, *Figure 5-6*.

Interestingly, samples S8 and S9 (both β-Thalassaemia major) displayed substantially different cell-surface adhesion results. As mentioned in the previous section, patient sample S8 had undergone a splenectomy, meaning, that there was likely a higher percentage of abnormal cells in this sample. It is clear that high cell-surface adhesion was observed in the case of sample S8.

In contrast, patient sample S9 had not undergone a splenectomy, thus, the spleen would still be active in the role of removal of atypical cells resulting in the sample appearing closer to the control.

Samples S13 and S14 were heterozygous variations of α-Thalassaemia (HbA/α-T and HbE/α-T, respectively). The observed cell-surface adhesion for these samples was indistinguishable from the healthy samples. Upon subjecting S13 and S14 to an Unpaired T-Test, it was confirmed that these samples did not significantly differ from that of the healthy control, with P-values of 0.13 and 0.67, respectively.

Overall, this investigation suggests that upon subjecting Thalassaemic cells to low pH acid, significant differences from the control population (P-values < 0.05) were observed in adhesive properties of the cells were observed 5 of 7 cases; S8 – S12. It is possible that increased cell-surface adhesion *could* indicate the presence of unhealthy blood disorder. However, the result of this analysis has been variable and in some cases it has not been possible to distinguish healthy from diseased blood. This method is also not specific to a particular blood disorder, thus, should not be considered for diagnostic potential.

(ii) Membranopathies

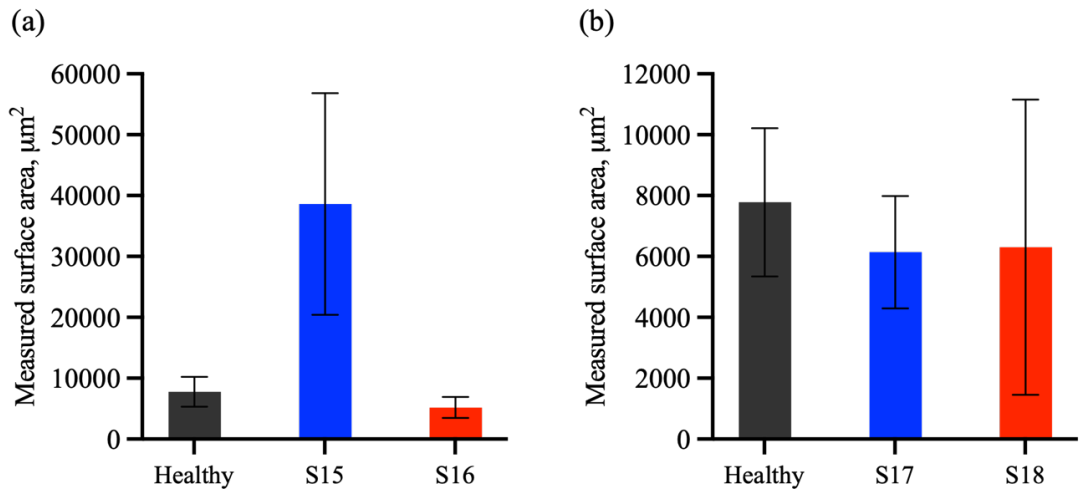

Figure 5-7 Cell surface adhesion measured for (a) Hereditary Spherocytosis samples, and (b) Hereditary Xerocytosis samples.

Like the Thalassaemias, HS and HX are also not known to have the same membrane adhesive properties as the sickled disorders. Measurement of the cell-surface adhesion of the samples confirmed a lack of adhesion to the microchannel in the case of three of the four samples investigated.

However, sample S15 (HS), shown in *Figure 5-7 (a)*, showed a significant amount of cell-surface adhesion. To provide a hypothesis for this increase in cell-surface adhesion for sample S15 an overview of the patient history could be useful, however, this was not available for investigation.

The measurement of cell-surface adhesion in the case of S16 – S18 did not appear to provide information that differentiate these rare anaemias from the control (with P-values of 0.1236, 0.1366, and 0.4881, respectively), thus, it was not recommended that this test is used for diagnostic purposes.

5.3 Results: High magnification testing

Red cell distribution width is a measure of sample heterogeneity. The range of size variation that should be observed in a healthy sample is between 11.8 and 16.1% for males and females.

The high magnification system measures the projected area of each cell in the field of view of the camera, thus, obtaining the sample size distribution. The resulting output is a histogram measuring the percentage of cells in each interval range. It was considered that the width of the projected area measurements could be correlated with the red cell distribution width parameter given by a haematology analyser. This hypothesis is investigated in the following sections.

The disorders chosen as representative for the high magnification testing protocols were the Thalassaemia disorders. The results from sickled and membrane disorders can be found in *Appendix A.2* for the pre-acid size distributions and *Appendix A.3* for the post-acid size distributions.

5.3.1 Pre-acid size distributions

(i) Haemoglobinopathies

(a) β-Thalassaemias

With the exception of BTM, which contained results from two subjects, each sample investigated was singular. The healthy data at T= -5 (black) was superimposed over the anaemic data for comparison.

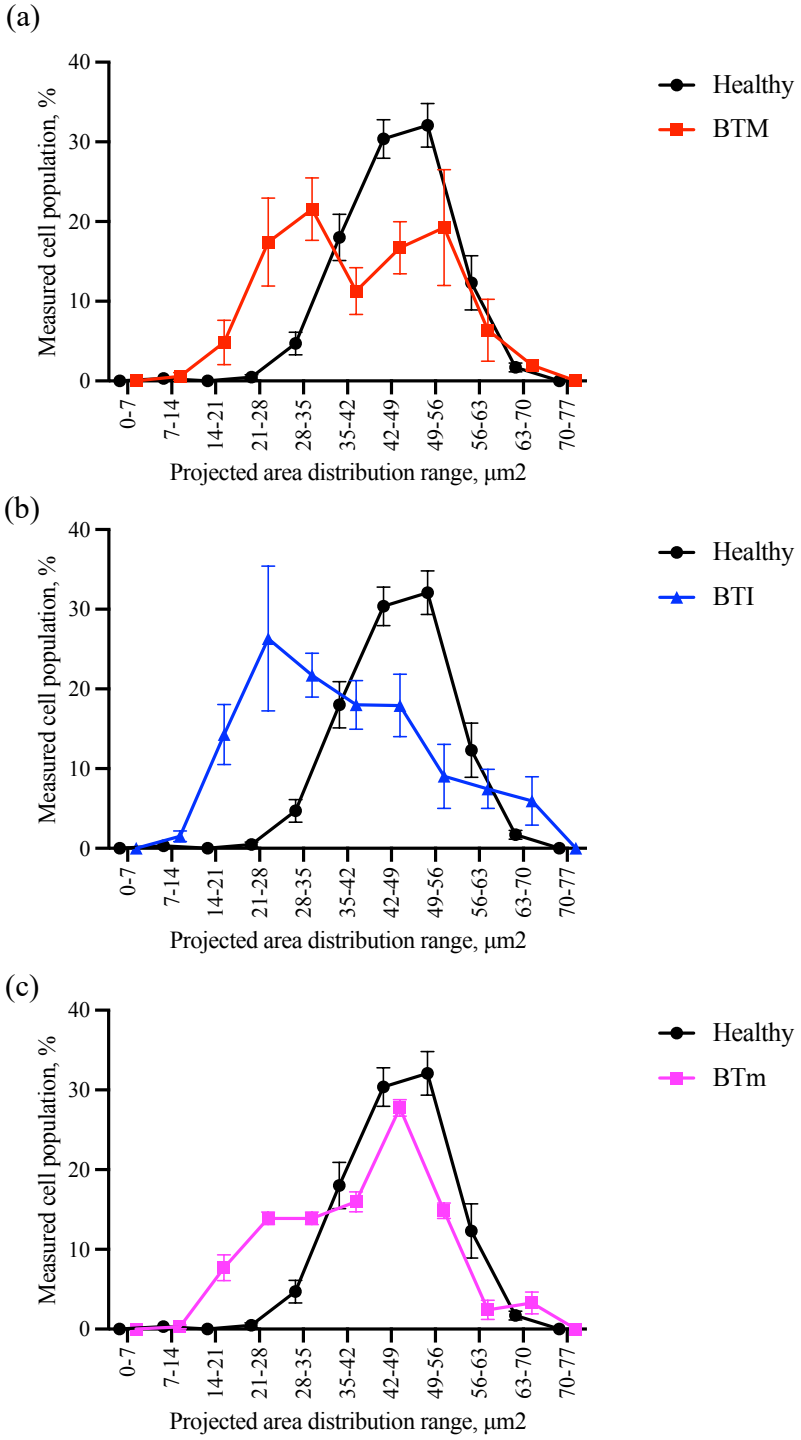

Figure 5-8 Projected area distributions pre-acid addition of (a) β-Thalassaemia Major, (b) β -Thalassaemia Intermedia, and (c) β-Thalassaemia Minor.

Red cell distribution width is often reported as increased in β-Thalassaemia blood samples. The majority of the cell population (~ 70%) for BTM is spread over 4 interval ranges and is weighted towards the smaller end of the measured projected areas.

The BTI sample appears to have a dip in cell population in the centre of the distribution. This could be an artefact of the test. As only one BTI sample was available for investigation, this perceived 'dip' cannot be considered characteristic of the BTI disorder. However, it is clear that BTI also has a wider span over the interval ranges, which is in agreement with the measured increase in the RDW parameter. 65% of the cell population is found within the interval ranges of 25 – 46 μm^2.

BTm reported a larger population of cells within a smaller range than compared with BTM and BTI. Approximately 48% of the cell population was observed within the 35 – 42 μm^2 and 42 - 49 μm^2 interval ranges with the rest of the cell population spread out across four further interval ranges.

For each of the β-Thalassaemias, it was found that the cell population percentage has a higher number of cells in the smaller interval ranges compared with the control. This indicates that the cells analysed were smaller in projected area indicating a decrease in MCV. It has been reported that the RBCs of patients with a β-Thalassaemia disorder may be microcytic, thus, a test that can highlight a reduction in cell size would be useful for screening blood samples for disease. See *Section 5.5* for this analysis.

A separate analysis was conducted on the BTM samples due to the differences observed between the splectomised patient sample S8 and the non-splenectomised patient sample S9.

The patient samples were analysed and plotted individually, see *Figure 5-9*.

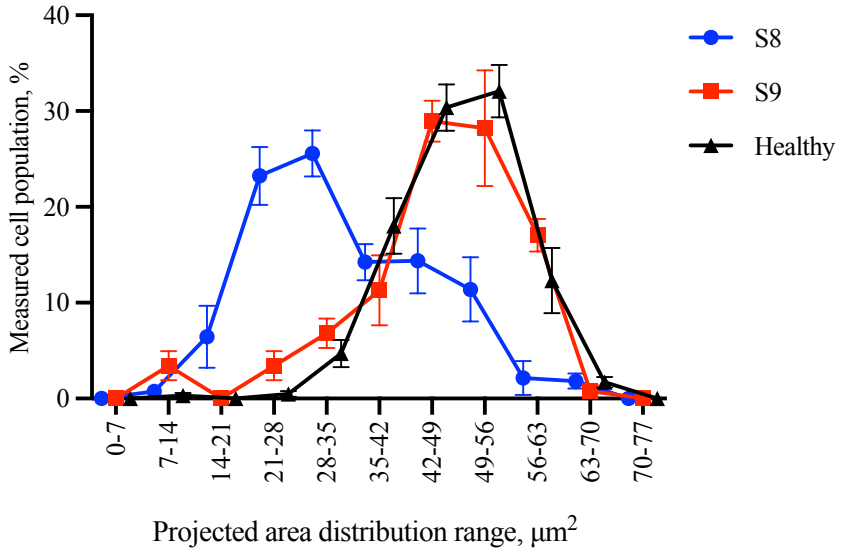

Figure 5-9 BTM samples S8 and S9 were separated and plotted individually which revealed that the distributions were quite different for the same disease.

There is a clear difference between patient S8 and patient S9 in their measured projected area distributions, *Figure 5-9*. Patient S9, non-splenectomised, appeared to more closely follow the distribution pattern of the control sample (black). Whereas, patient sample S8 is clearly distinguishable from the control. The cell population for S8 is also weighted towards the smaller intervals.

From these results, it would have been assumed that the RDW value for S8 would *exceed*, and for S9 may fall *within* the healthy range. However this was not found to be the case. In contrast, the haematological values report that the RDW for S8 was *within* the normal range and the RDW value for S9 *exceeded* the normal range for S9.

(b) α-Thalassaemias

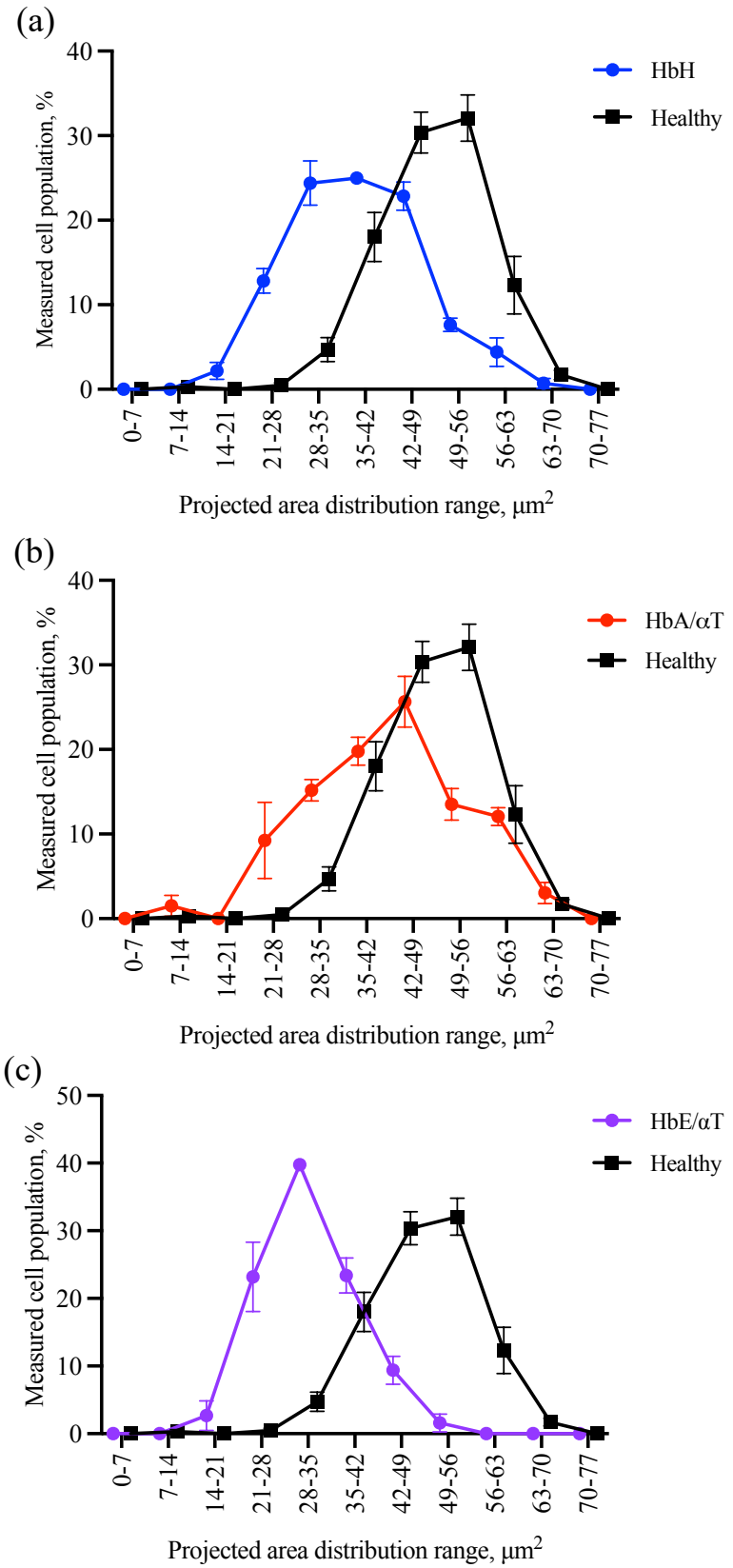

Figure 5-10 Projected area distributions pre-acid addition of (a) HbH, (b)HbA/α-Thalassaemia, and (c) HbE/ α-Thalassaemia.

Red cell distribution width has also been reported as increased for α-Thalassaemia blood disorders. Of the samples tested within this thesis, HbH and HbA/α-T report an increase in RDW values and HbE/α-T fell within normal ranges.

Referring to *Figure 5-10 (a) and (b)* it appears that both HbH and HbA/α-T show wider projected area distribution spans than the control population. This was not seen to be the case for HbE/α-T, *Figure 5-10 (c)*, thus in agreement with the haematological values. However, this agreement is taken with a degree of caution as this analysis was conducted on only one sample for each of the α-Thalassaemias.

HbH and HbA/α-T also report a shift to the left of the control for their observed distributions, suggesting that the cell population projected area is smaller than the control. This leftwards shift is not observed for HbE/α-T, however, there is a higher percentage of cells in the 35 -42 μm^2 interval band which weights the sample towards the smaller projected area distributions.

Summary

In conclusion, this investigation reported mixed results. It is very likely that the analysis requires larger cell numbers to more accurately predict the distribution width of the sample. In some cases, summing all the cells across the triplicate runs for the high magnification imaging test only resulted in the analysis of 60 cells in total for that sample. In comparison, a haematology analyser measures red blood cells in the range of 10^{12}.

Although in its current form this test is not sufficiently accurate to detect abnormal projected area distributions across a whole sample, it is possible that with protocol adjustment that this parameter could be comparable to the red cell distribution width of the haematology analyser. This is discussed in more depth in *Section 6.2.1*.

5.3.2 Post-acid size distributions

(i) Haemoglobinopathies

β-Thalassaemias

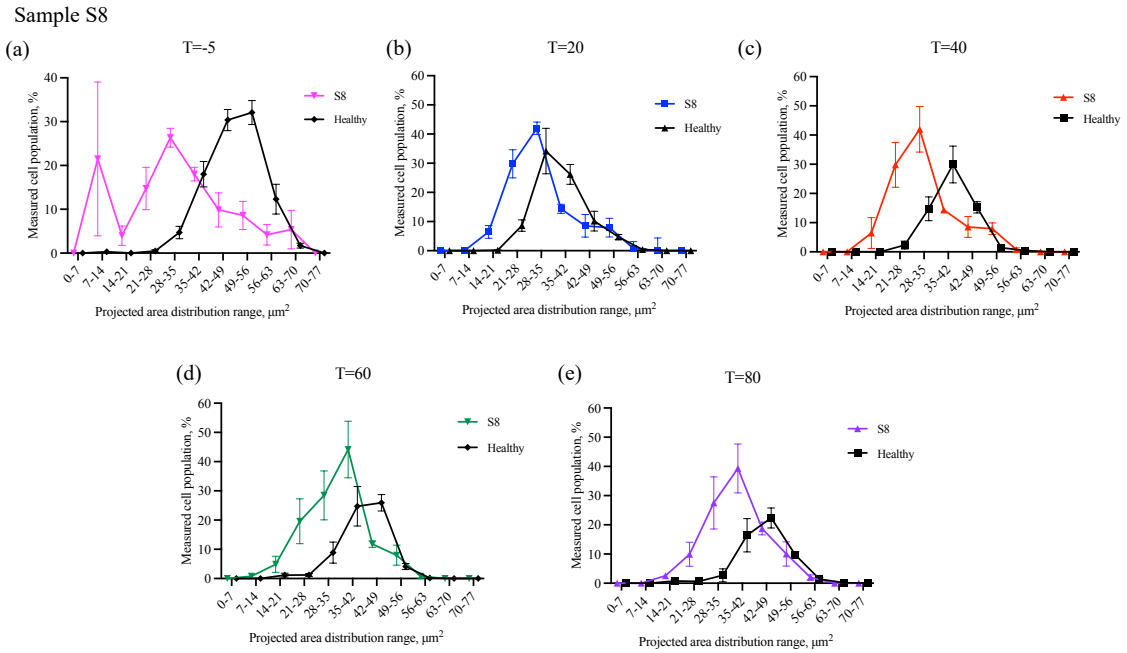

Figure 5-11 Projected area distribution ranges at specified time points in response to acid addition for β-Thalassaemia Major Sample S8. This patient had undergone splenectomy. It is clear that this sample responded significantly differently to the control.

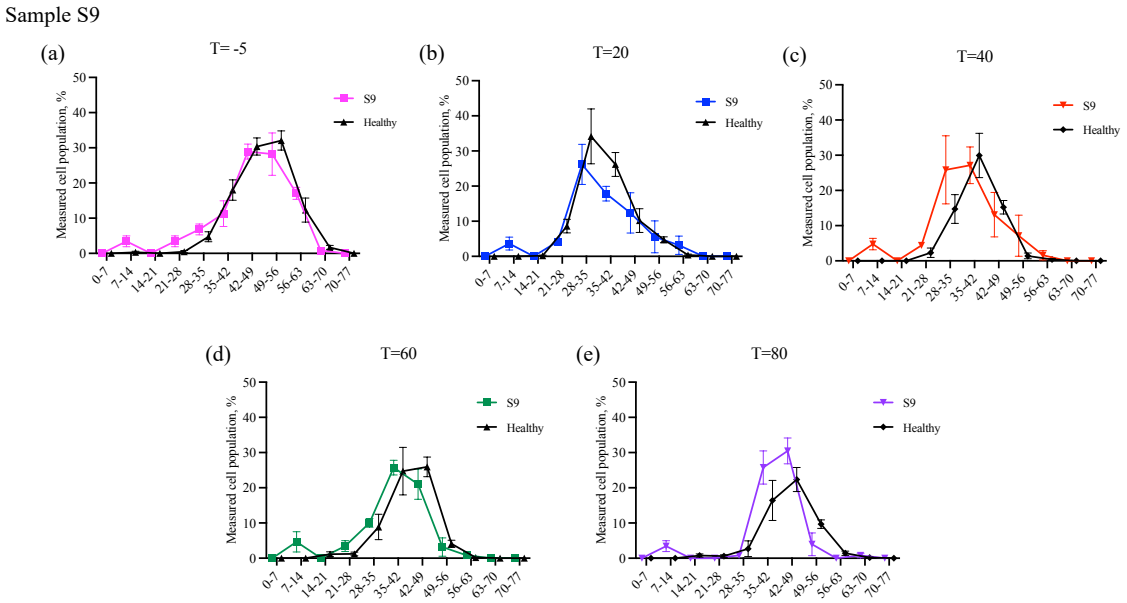

Figure 5-12 Projected area distribution ranges at specified time points in response to acid addition for β-Thalassaemia Major Sample S9. This patient had not had a splenectomy. Sample S9 responded in a very similar manner to the acidic stressor as the control samples.

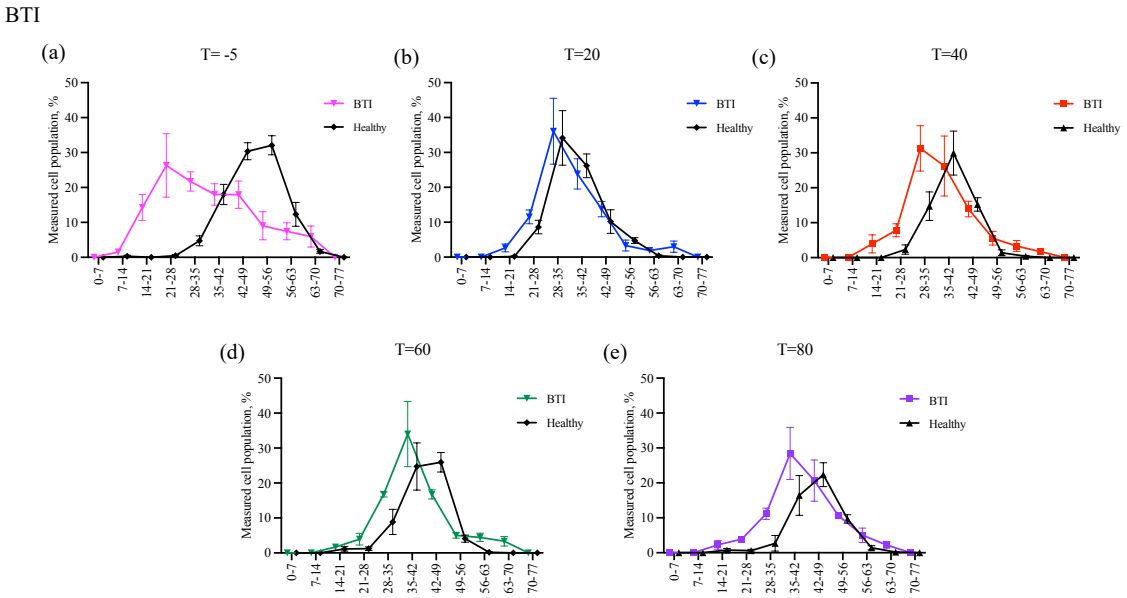

Figure 5-13 Projected area distribution ranges at specified time points in response to acid addition for β-Thalassaemia Intermedia.

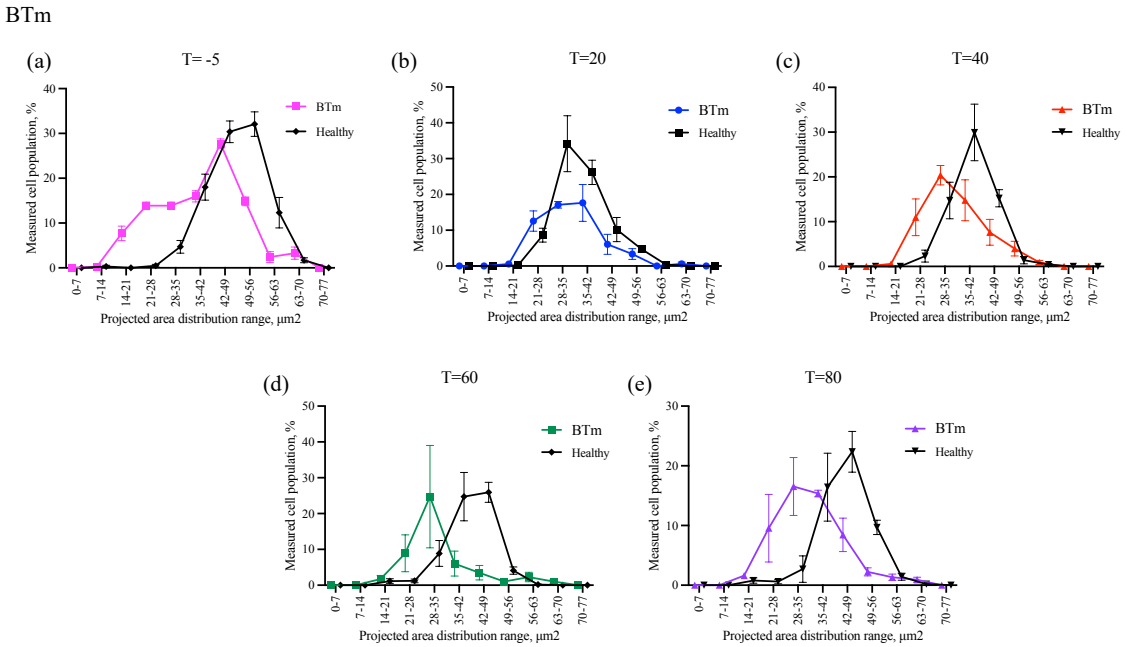

*Figure 5-14 Projected area distribution ranges at specified time points in response to acid addition for β-Thalassaemia Minor.**Error! Reference source not found.***

Sample	T=-5	T=20	T=40	T=60	T=80	T=100
Healthy	49 - 56	28 - 35	42 - 49	42 - 49	42 - 49	42 - 49
BTM: S8	28 - 35	21 - 28	28 - 35	35 - 42	35 - 42	35 - 42
BTM: S9	42 - 49	28 - 35	28 - 35	35 - 42	42 - 49	42 - 49
BTI	28 - 35	28 - 35*	28 - 35	35 - 42	35 - 42	35 - 42
BTm	42 - 49	28 - 35	28 - 35	28 - 35	28 - 35	35 - 42

*Table 5-6 Interval ranges with the majority of the cell population for each disease and the control. *Although a decrease to a smaller interval was not recorded for BTI, the cell population measurement was increased in the smaller interval ranges, see **Error! Reference source not found.** (b).*

The BTM patient samples were separated due to the differences between splectomised and non-splenectomised patients, shown in *Figure 5-11* and *Figure 5-12*.

BTM sample S9, non-splenectomised, followed a similar distribution pattern to the healthy control. There was a slight delay in swelling from the T=20 – T=40 timepoints but the majority of the cell population returned to the pre-acid addition projected area measurement by T=100.

Interestingly, sample S8 did appear to be observably different to the healthy distributions. The cells in the splectomised S8 sample initially report a majority in a smaller interval range for T=-5. The cells decrease as expected upon exposure to acid from T=-5 to T=20 and continue to increase in projected area until T=60 where the majority of cells reaches the 35 - 42 μm^2 interval range. The cell population majority remains at this interval range for T=80 and T=100. The percentage of cells observed at this interval was 38%, 35%, and 34% for T=60 – T=100, respectively. The reducing population in the previous 28 - 35 μm^2 interval range suggests that these cells are continuing to swell with time under acid exposure. The reason for the increase in projected area greater than the initial measurements is not fully understood.

It is not obviously clear from *Table 5-6* that the BTI sample decreases given the majority of the cell population remains within the same interval range (28 – 35 μm^2) as the previous time measurement. However, it can be seen from the graph, *Figure 5-13*, that the percentage of cells at the 28 – 35 μm^2 range increases (from 20% - 48%). The cell population continues to swell from T=40 – T=60 where it remains within the 35 - 42 μm^2 interval range. The BTI sample also reports an increase in projected area greater than the initial size measurements at T=-5.

BTm, *Figure 5-14*, follows the same trend of projected area distribution decrease from T=-5 to T=20. However, this sample displayed a long delay in increasing from the measured T=20 interval range (28 – 35 μm^2). In fact, the cell population majority remained at the 28 - 35 μm^2 interval range from T=20 – T=80. At T=100 the cell majority had increased to 35 – 42 μm^2 which was less than the initial majority projected area measurement of 42 – 49 μm^2.

Another observation of the β-Thalassaemia samples is the increase in measured cell population remaining at T=100 compared with the healthy sample. The total remaining cell population for the healthy sample at T=100 is ~ 29%. In contrast, the average remaining cell population at T=100 for all the β-Thalassaemias ~ 68%.

Similarly to the sickled disorders, the β-Thalassaemias are also reported to have decreased cellular deformability, which may be a result of reduced Band 3 function.[230] It is possible that the reluctance for the cells to increase in projected area upon exposure to acid is caused by reduced the Band 3 function, thus the RBC deformability.

α -Thalassaemias

HbH

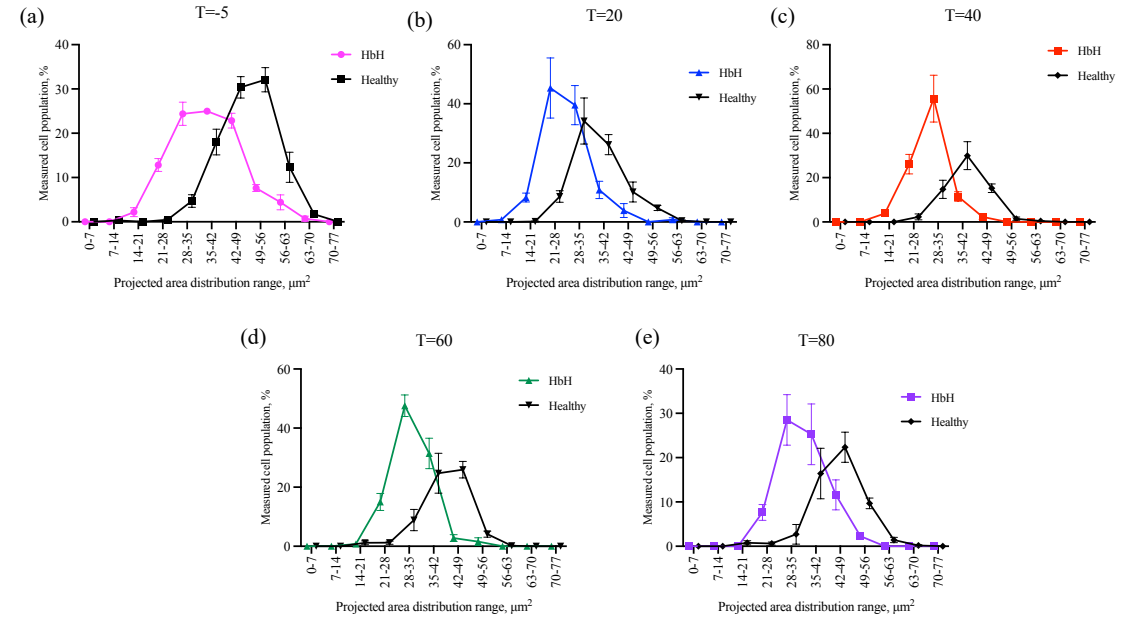

Figure 5-15 Projected area distribution ranges at specified time points in response to acid addition for HbH

HbA/**α**T

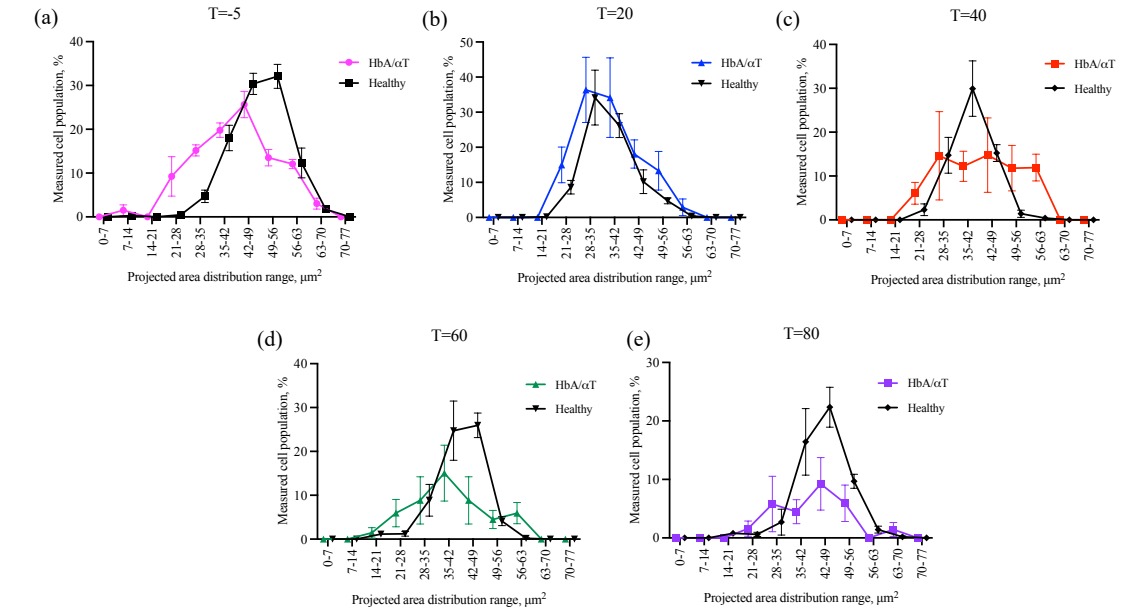

Figure 5-16 Projected area distribution ranges at specified time points in response to acid addition for HbA/αT

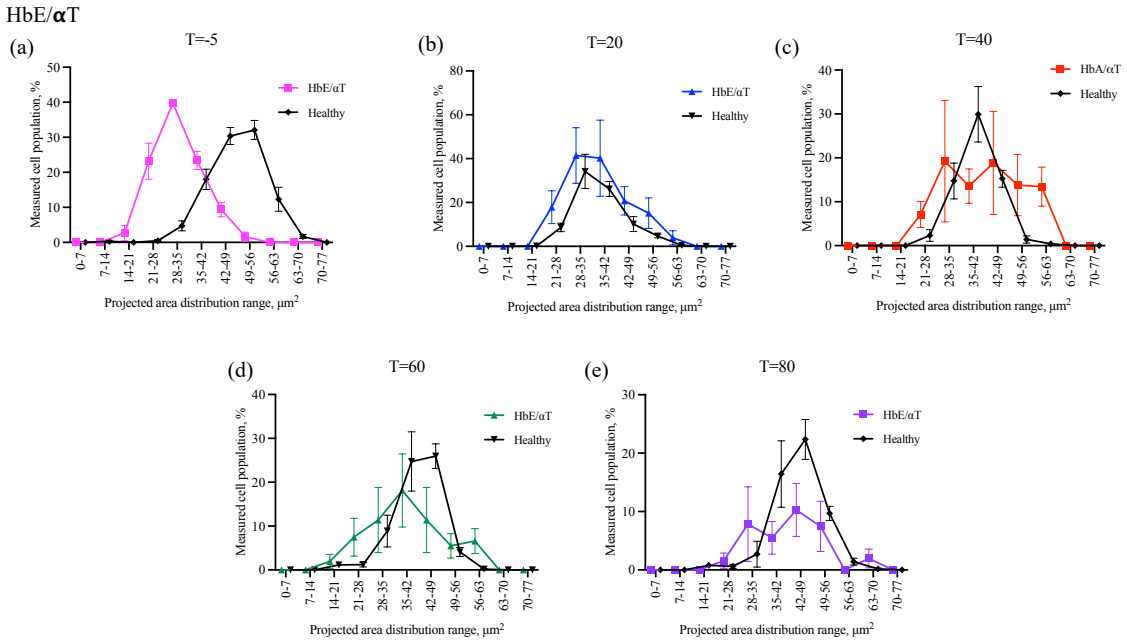

Figure 5-17 Projected area distribution ranges at specified time points in response to acid addition for HbE/αT

Sample	T=-5	T=20	T=40	T=60	T=80	T=100
Healthy	49 - 56	28 - 35	35 - 42	42 - 49	42 - 49	42 - 49
HbH	35 - 42	21 - 28	28 - 35	28 - 35	28 - 35	35 - 42
HbA/ α -T	42- 49	28 - 35	28 - 35	35 - 42	42- 49	42- 49
HbE/ α -T	35 - 42	28 - 35	28 - 35	35 - 42	35 - 42	35 - 42

Figure 5-18 Interval ranges with the majority of the cell population for each α-Thalassaemia disorder and the control.

All samples reported a decrease in projected area measurement from T=-5 to T=20. Following the initial decrease, each sample increased over time and eventually returned to the pre-acid addition measurement.

After the addition of acid for the HbH sample, high turbulence was observed which caused an increase in the apparent cell population, thus, the total cell population at T=20 for HbH was reported to be 106%. The high number of cells remained throughout the test with the final population at T=100 recorded as ~ 63%.

The graph shown in *Figure 5-16* shows that the cells in the HbA/ α -T undergo a much more rapid haemolysis than the control with only ~12% of the cell population remaining by T=100, compared with ~ 29% for the healthy population. This increase in cell haemolysis was also observed in the flow test, see sample S13 in the flow tests result *Figure 5-2 (d)*.

In contrast, the HbH and HbE/ α -T samples (*Figure 5-15* and *Figure 5-17*, respectively) retain 69% and 75% at T=100, respectively, and their resistance to lysis was also observed in the flow test results.

Summary

The overall conclusion of this section is that this post-acid addition test is not sufficiently accurate to detect differential trends between the healthy and Thalassaemic samples. As mentioned in the pre-acid addition test, the cell numbers in observation may be too small to detect population trends. It is interesting that all of the samples reported the decrease in projected area upon exposure to acid. However, this was also the case for the control samples, thus it is not a differential factor that could be used for diagnosis.

With respect to the cell population swelling from T=20 to T=100, this was observed for each of the rare anaemic samples. The samples did appear swell in a different manner to the control with most samples reporting a delay in the commencement of swelling. However, these differences were not clearly in correlation with any particular disease. Again, investigation of larger cell numbers *may* highlight trends that were not observable within the confines of the test designs for this thesis.

In conclusion, this test in its current form is not recommended for future diagnostic investigations.

5.4 Results: Haematological correlations

Please see *Appendix A.6* for a full report of R^2 and p-values for each correlation investigation.

5.4.1 Red blood cell count

A symptom of hereditary anaemias is chronic haemolytic anaemia which can be diagnosed clinically as a low RBC count,[231] 9 of the 18 samples investigated reported a low RBC count, see *Table 5-2* to *Table 5-4*.

The flow test has the capability to count RBCs in the channel prior to the addition of acid, thus, before the commencement of haemolysis. It was considered in the previous chapter that this 'cell count' could be utilized in absence of a haematology analyser. The cell count obtained from the flow test at the beginning of each experimental run was plotted against the RBC count value given by the haematology analyser. The results suggested a linear correlation between the two tests (R^2 = 0.6178). To investigate whether this correlation was true, the cell count values for the rare anaemia samples were plotted against the RBC count values. The results are shown below in *Figure 5-19.*

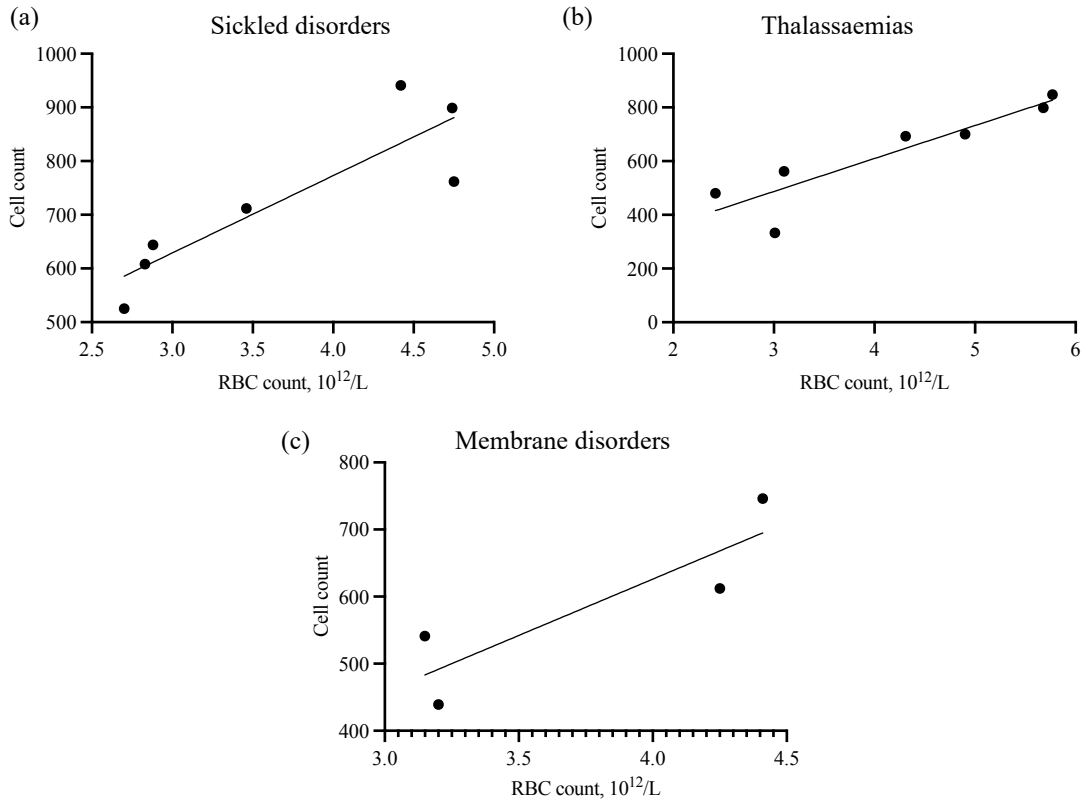

Figure 5-19 The anaemias were separated into their respective groups; (a) Sickled disorders, (b) Thalassaemias (α and β), and (c) Membrane disorders, and their cell counts were plotted against the RBC counts. The R^2 value for the sickled disorders showed good correlation; R^2=0.7755, p-value= 0.0089. The Thalassaemia group reported a strong correlation with an R^2 value of 0.8236 and p-value= 0.004. Finally, the membrane disorder group had a good correlation with an R^2 value of 0.7624, however, the p-value of 0.13 deemed this correlation not significant.

The R^2 and p-values for the sickled disorders, Thalassaemias and membranopathies were $R^2 = 0.7755$ and p-value = 0.0089, $R^2 = 0.8236$ and p-value = 0.004, and $R^2 = 0.7624$ and p-value =0.13, respectively. Overall, this suggests that there is a good linear correlation between the cell count in the flow test and the RBC count value from the haematology analyser for the sickled disorders and Thalassaemias. However, the Pearson analysis on the membrane disorders reported a non-significant result. This *could* be a result of small sample sizes in this group (n=4).

The variables that arise are likely caused by variations between blood dilutions during the preparation steps for the flow test. Each diluted sample contained the same volume of blood from a whole blood sample. It is possible that there was inefficient mixing of the whole blood sample prior to dilution. To reduce this potential variability, the whole blood

sample could be centrifuged down so that the user only dilutes RBCs instead of the whole blood sample.

Regardless of protocol improvements, this set of analysis suggests that the developed cell count parameter may be comparable with the gold standard RBC count, thus, suggesting it as a potential substitute for the RBC count.

5.4.2 Red cell distribution width

RDW is a measure of the variation of cell sizes in a sample. Within any blood sample, healthy or diseased, there will be a range of cell sizes due to the natural ageing process of the RBC.[232] However, it is widely reported that this range significantly increases in patients suffering with rare anaemias.[233] In the previous chapter, Projected area Distribution Width (PDW) was developed as a correlative parameter for RDW and the results with the control population showed strong linear correlation with an R^2 value of 0.8506.

The values for PDW of the anaemic samples were obtained using the formula described in *Chapter 4* and the results were plotted with their respective RDW values, *Figure 5-20*.

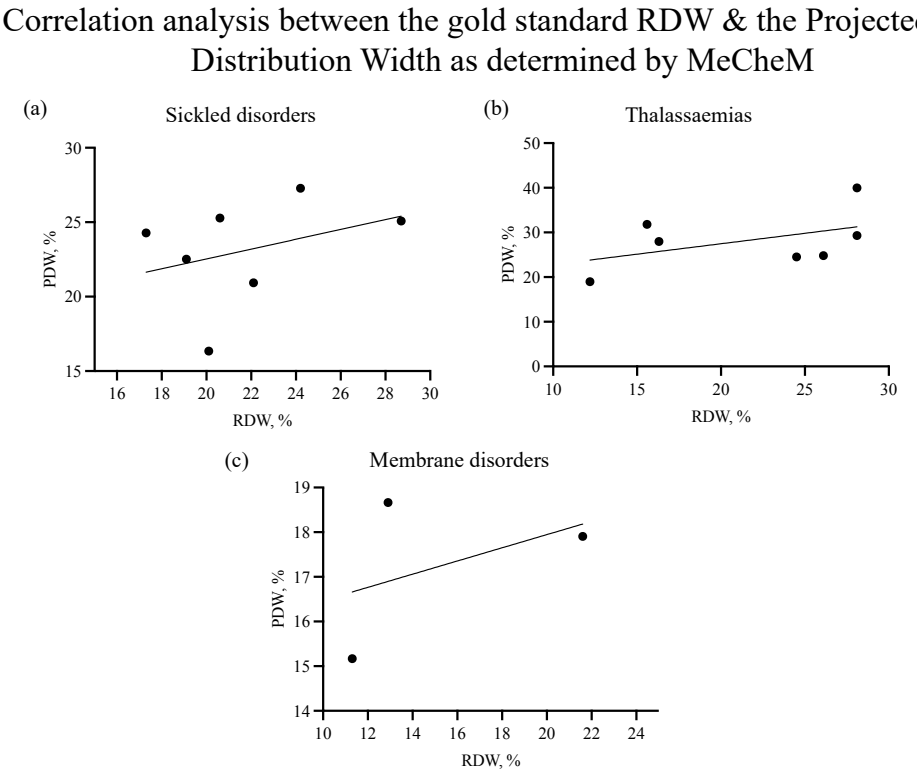

Figure 5-20 The gold standard RDW parameter was plotted against the developed PDW parameter for each of the disease groups and no linear correlation was observed.

The results of this investigation reported no linear correlations between RDW and PDW for the anaemic samples. The R^2 values for the sickled disorders, Thalassaemias, and membranopathies were 0.1189, 0.2205, and 0.1981 respectively. The p-values were all found to be not significant.

The obvious concern with small sample numbers is the dependability of any suggested correlations. The healthy population had an RDW value of 11.5 ± 0.33% which was significantly narrower than the rare anaemic RDW value of 20.3 ± 5.49%. This indicates that in any sample observed there is a smaller size variation of the healthy samples than in the rare anaemic samples. Thus, the healthy samples may appear to show a higher correlation between RDW and PDW values.

However, in the case of the rare anaemic samples, there was no correlation found between RDW and PDW values, thus, PDW is not suggested to be considered as an alternative parameter for RDW.

5.4.3 Mean corpuscular haemoglobin

MCH is a measure of the average amount of haemoglobin molecules present in a blood sample. In patients with rare anaemia, the levels of haemoglobin in their blood are often reported as lower than that of a healthy subject.

The parameter ‘activity time’ is defined as the time required for the cell to reach its minimum projection following the addition of acid to the sample. In the previous chapter, there was a good correlation ($R^2 = 0.6799$) between MCH and the activity times for the healthy samples. The hypothesis for this correlation was that haemoglobin may offer a buffering effect as it binds H^+ ions, reducing the overall extracellular pH, thus, slowing the effect of intracellular water uptake and increasing the activity time. Considering the hypothesis, samples with less haemoglobin present may not be afforded this same level of protection, thus, their activity time may be decreased. The average MCH values were 1.88 fmol for the healthy samples and 1.65 fmol for the rare anaemic samples. The results of this analysis are shown below in *Figure* 5-21.

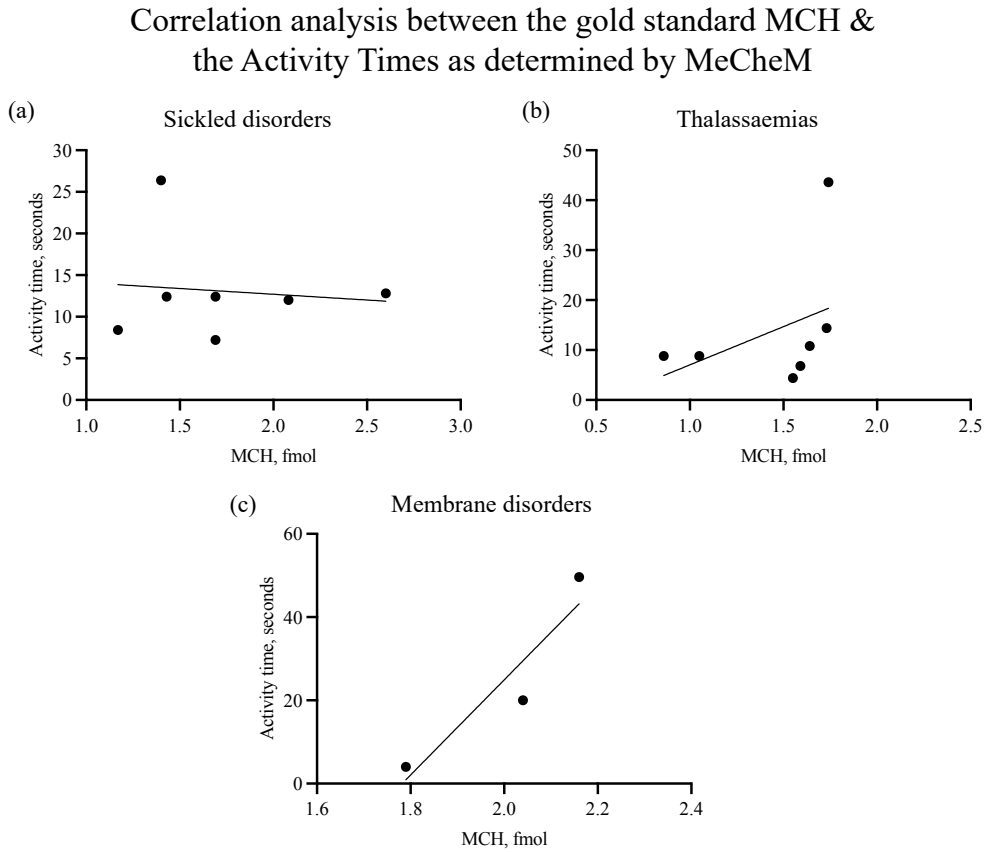

Figure 5-21 Comparing the MCH and activity times of the diseased samples did not suggest that there was any linear correlation between these parameters.

The results of this analysis did not indicate any correlation between MCH and activity time of the anaemic samples. The R^2 values for the sickled disorders, and Thalassaemias were 0.011 and 0.1590, respectively and all p-values were reported as not significant. There were too few points to provide indication of a correlation for the membranopathies.

A possible explanation for the lack of correlation observed with the anaemic samples is that, including MCH, there are myriad other factors to be considered when it comes to cell shape change. A critical factor is the deformability of the red blood cell.[234] Deformability of RBCs is required for the cells to pass through the narrow capillaries of the body. The high magnification tests provide data about the deformability of the sample under investigation. Cellular deformability in hereditary anaemia is widely reported as reduced when compared with healthy cells.[47] Due to increased cell size variation within anaemic samples, there will be a much greater variation in cell deformability than that observed in a healthy sample.

As previously defined, the activity time is given as the time for the cell to reach its minimum projected area. To achieve this, the cell must deform from its original configuration. With the knowledge that in an anaemic sample there will be a much greater range of cell deforming abilities, thus, varying activity times, this must be considered as a factor for the lack of correlations observed.

Given the small cell numbers that were observed during the high magnification investigations, it is possible that the previous healthy correlations were coincidental. It is also possible that there are too many conflicting factors in the mutated anaemic samples to allow for correlations.

The conclusion of this set of analysis is that MCH and activity time for the anaemic samples did not show any correlations, thus, it is not suggested as an alternative to the MCH parameter.

5.4.4 Mean corpuscular volume

MCV is a measure of the average RBC volume and thus size in a population sample. It was hypothesized that this parameter could be correlated to the average RBC projected area measurements which also give an insight into the size of the RBC albeit in a 2D manner.

In the previous chapter, the MCV and projected area measurements reported good linear correlation with an R^2 value of 0.7078. MCV was plotted against the projected area measurements of the anaemic samples, *Figure 5-22*.

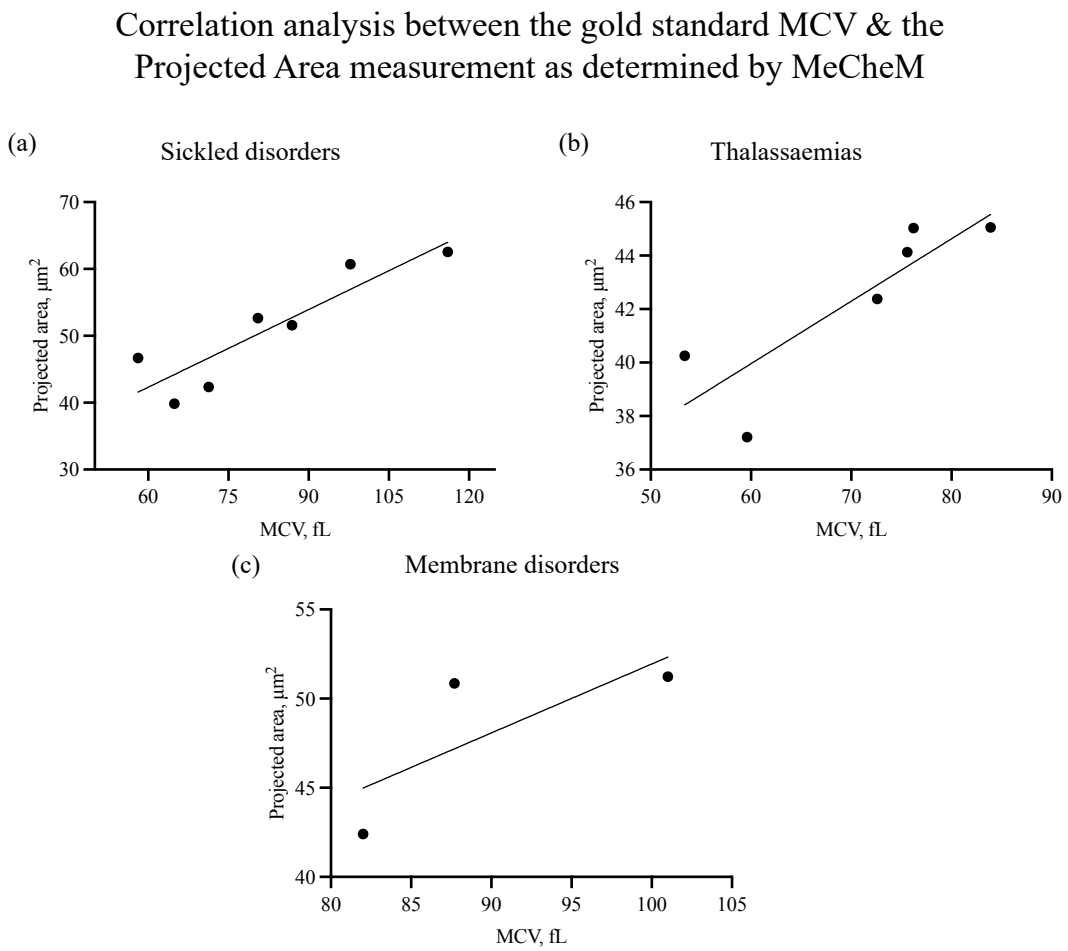

Figure 5-22 The comparison of MCV and projected area measurements from the high magnification test showed good linear correlation for each disease type. This result was expected following the good correlation result from the healthy samples.

The results shown above in *Figure 5-22* showed good correlation between MCV and projected area measurements. The sickled disorders and Thalassaemias showed R^2 values of 0.8050 and 0.7349, with p-values of 0.0061 and 0.029, respectively. The Thalassaemia group contained one outlier, sample S8 (β-Thalassaemia major), which was removed for this correlation. The membrane disorders had too few points to indicate a correlation, and the p-value was reported as insignificant.

Although the sample size is still quite small, this result suggests that it may be possible to use the projected area measurement parameter in the absence of a haematological analyser.

5.5 Summary

The overall conclusions for each parameter investigated are summarised here.

Flow analyses

The flow test did not report obvious deviations from the control curve in the case of the sickled samples, However, this test did highlight 5 of 7 samples in the Thalassaemia group and significant differences were observed in the membrane disorder group for Hereditary Spherocytosis. This was not found in the case of the second membrane disorder; Hereditary Xerocytosis. The results for the Thalassaemic and Hereditary Spherocytosis disorders suggest that this test has potential for sample screening in these cases. Of course, a larger investigation should be conducted with many more anaemic samples.

The cell-surface adhesion measurement highlighted significant adhesion for the sickled disorders group and in 5 of 7 cases in the Thalassaemia group. The samples that did not appear significantly different from the control were heterozygous α-Thalassaemias (HbA/α-T and HbE/α-T). In 3 of 4 of the membrane disorders, there was no observed differences in cell-surface adhesion. However, for Hereditary Spherocytosis sample S15, significant cell-surface adhesion was measured.

High magnification analyses

The pre-acid addition measurements of the projected area distributions appeared to highlight differences from the control distributions with most anaemic samples reporting a wider distribution range than the control. However, the small numbers of cells under observation for this test significantly reduces the impact of the results. This test *may* show potential as an alternative to the red cell distribution width parameter *if* cell numbers under investigation can be increased.

The post-acid addition measurements did not appear to be sufficiently different to the control. In all cases (anaemic and healthy) from T=-5 to T=20, the projected area distribution of the cell population decreased. Following that, from T=20 to T=100 the cell population was observed to be swelling, thus, an increase in projected area distributions was reported. Due to the small numbers of cells under investigation, any differences noted

between the healthy and anaemic samples were attributed to random variations. Thus, this test could not be considered for future diagnostic potential.

In all cases, it was found that the cell swelling capacity measurement was not sufficiently sensitive to detect deviations from the control results.

Haematology correlations

The initial RBC count prior to introduction of acid in the microchannel was investigated for correlations against the gold standard RBC count which counts the number of RBCs in a blood sample. The results suggest strong linear correlations in the case of each of the rare anaemias, with R^2 and p-values of 0.7755 and 0.0089, 0.8236 and 0.004, and 0.7624 and 0.13 for the sickled disorders, Thalassaemias, and membrane disorders, respectively.

No correlation was found between the projected area distribution width and the red cell distribution width. Similarly, there was also no correlation observed between time for the cell to reach its minimum projection (activity time) and the MCH value, suggesting that haemoglobin was not offering protection due to a buffering effect.

Finally, good correlation was found between MCV and average cell projected area in a sample. The R^2 and p-values were 0.8050 and 0.0061, and 0.7349 and 0.029 for the sickled disorders and Thalassaemias, respectively. There were not sufficient membrane disorders to observe a correlation.

The purpose of this chapter was to conduct preliminary investigations to determine whether the developed tests were successful at highlighting rare anaemic samples. The results suggest that differences between the diseased and healthy population may exist. Further research using larger sample and cell numbers may confirm the suggested correlations.

Chapter 6 Conclusions and future recommendations

6.1 Thesis overview

In summary, this thesis describes the application of microfluidic methods to investigate the diagnostic potential of an acid shock bioassay for rare anaemias.

Chapter 3 described the development of the novel microfluidic toolkit, MeCheM, comprising low magnification imaging analysis and flow, and a high magnification imaging system. MeCheM was designed to be user-friendly and relatively portable. The high magnification system was also manufactured considering these specifications. The optimisation of the microfluidic chip to achieve minimal requirements of blood sample and reagent volumes is discussed in this chapter.

The protocols that were developed were; (i) flow analyses, (ii) low magnification system, and (iii) high magnification system. Within these protocols the outputs for analysis were:

Flow analyses

- Cell count at predetermined positions along the microchannel.
- Cell-surface adhesion measurements.

Low magnification system

- Cell count as a function of time.

High magnification system

- Pre-acid addition average cell projected area.
- Pre-acid addition projected area distribution.
- Post-acid addition projected area distribution.
- Post-acid addition RBC size measurement.
- Cell swelling capacity.

In Chapter 4, the instruments and protocols were interrogated using healthy blood samples to determine the repeatability of the developed methods. The investigations

carried out in this chapter highlighted the protocols that proved to be repeatable for further analysis using rare anaemic samples. The successful protocols were; (i) RBC size distribution pre-acid addition, (ii) RBC size distribution post-acid addition, (iii) RBC swelling capacity, and (iv) flow analyses.

Although not all protocols were considered repeatable for comparison, curve trends were observed that were not insignificant. For example, in the low magnification drop test most of the curves displayed a bi-phasic cell population lysis with a rapid decline in the initial stages of the test followed by a slower population decline towards the end of the test. Also, for the size measurement parameter in the high magnification drop test, the curves followed a similar pattern with the projected area of the cell population initially reducing upon addition of acid followed by an increase until eventual lysis. Refinement of these methods may give greater testing repeatability, thus, these methods should not yet be completely disregarded.

A secondary outcome of Chapter 4 was the correlation of the developed methods with gold standard RBC indices. Correlations were observed for the following parameters: (i) Red blood cell count and initial cell count in the flow test, (ii) Red cell distribution width and projected area distribution width, (iii) Mean corpuscular haemoglobin and activity time, and (iv) Mean corpuscular volume and projected area measurements.

Finally, Chapter 5 investigated the methods that were determined as repeatable, as per the analysis in Chapter 4, for comparison against rare anaemic samples. The results from this chapter highlighted the flow analyses as the methods with the most potential for diagnostic purposes. The flow test reported observable differences for the Thalassaemia and Hereditary Spherocytosis disorders. The cell-surface adhesion measurements also highlighted the sickled disorders as significantly different from the control sample. *Table 6-1* below gives a brief overview of these results.

Disease group	Flow analyses			High magnification analyses		
		Flow test	*Cell-surface adhesion*	*Pre-acid addition*	*Post-acid addition*	*Cell swelling capacity*
	Sickle Diseases	No significant differences from control found.	Significant differences found in all cases.	No significant differences found.	No significant differences found.	No significant differences found.
	Thalassaemias	5 of 7 samples significantly different from control.	4 of 7 samples significantly different from control.	No significant differences found.	No significant differences found.	No significant differences found.
	Membrane Disorders	2 of 4 samples significantly different – both HS. No difference found for HX.	1 of 4 samples showed significant differences (HS).	No significant differences found.	No significant differences found.	No significant differences found.

Table 6-1 Overview of the results obtained from the flow and high magnification investigations for the rare anaemic samples.

Chapter 5 also investigated the haematology correlations and found that the parameters RBC count and initial RBC count in the microchannel, and MCV and average cell projected area pre-acid addition, maintained good correlations when considering the rare anaemic samples.

No correlation was found between the projected area distribution width and the red cell distribution width. Similarly, there was also no correlation observed between the activity time and the MCH value.

The aim of this thesis was to develop a user-friendly and low-cost method of diagnosis for rare anaemias. Overall, this work described the development of a novel microfluidic instrument and the investigation of an acid shock test for diagnostic potential. The findings suggest that the acid shock test highlights differences between a healthy and anaemic sample in some cases. This was observed in the case of the flow analyses for Hereditary Spherocytosis and the Thalassaemia disorders. The haematology correlations also suggest that the developed methods shows potential for use in the absence of a haematology analyser for the red blood cell count and mean corpuscular volume parameters.

A significant output from this body of work was the development of MeCheM, which could be used as a stand-alone research tool for many different assays by varying the footprint of the microfluidic chip.

The work carried out in this thesis provides researchers with novel methods and instrumentation for future diagnostic work. It also highlights some diseases for further preliminary research based on their response to the developed tests.

6.2 Future work

6.2.1 Refinement of drop test methodologies

The methods of low magnification drop test and cell size measurement (high magnification analysis) were both deemed unsuccessful due to their lack of repeatability in Chapter 4. However, the analysis of both of these methods showed that there were similar curve trends for each healthy sample investigated. The factors that seemed to cause the variation between the control samples were; (i) movement of cells in and out of the FOV caused by turbulence upon acid addition, and (ii) droplet dispensing outside of the FOV of the camera. These methods were both quite rudimentary and heavily relied on the precision and accuracy of the user.

Movement of the cells was largely caused by the penetration of the pipette tip into the sample droplet. Inaccurate droplet dispensing was a by-product of the 'blind' nature of the test. That is, the user could observe the cells without the knowledge of their location within the droplet. Automation of the drop tests could remove the large variations caused by these human errors. The implementation of a standard motorised XY-stage, for imaging at a pre-determined location, and an automated droplet dispensing machine would greatly reduce these variations.

6.2.2 Optimisation of MeCheM

For further system optimisation, it would be highly advantageous to integrate the high magnification system with MeCheM. To achieve this, a motorised microscope lens holder could be employed to secure both objective lenses of MeCheM and the high magnification system.

The addition of a motorised XY-stage would remove the requirement for the user to manually move the microfluidic chip to record images at each position. The motorised XY-stage could also be programmed to move at the same velocity as the cells within the

channel, thus, allowing for the analysis of a specific population of cells from initial interaction with acid to haemolysis.

Within the MeCheM analysis programme, the inclusion of a 'blob detection' image processing tool would allow for the automated measurement of the cell-surface adhesion which would significantly reduce the time required to complete this analysis.

Another future area for research is in the modification of the microchannel design. It would be simple to create narrow channel walls to 'squeeze' the red blood cells. This could potentially give information on the cellular deformability.

6.2.3 Expansion of sample populations sizes

As highlighted in *Section 5.1.3,* the sample sizes that were available for this body of work were quite limited due to the uncommon nature of rare anaemias. The challenge with small samples sizes is that the potential for the selected group to be populated with outliers and/or anomalies is quite high. It is generally accepted that a population of 100 samples is the minimum requirement for statistical analysis, although larger sample population sizes increase the likelihood of statistical significance.[235] However, within the confines of this body of work it was not possible to obtain the minimum sample requirements.

Study sizes for rare anaemia typically contain ~ 125 samples, with one report of only 369 samples obtained over an 11 year period.[233,236,237] To investigate the hypotheses of the correlations and diagnostic potential of the tests outlined in this thesis, a minimum sample size of 100 should be obtained.

6.2.4 Increasing sample cell numbers

In Chapter 5, the high magnification methods for measuring the projected area distributions of the sample populations in both a pre- and post-acid phase was discussed and the conclusion was that this method was not sufficiently sensitive for detection of rare anaemias. The pre-acid addition phase may have some success, however, if the number of cells analysed per sample could be increased.

As only the red blood cells in the FOV of the camera were measured, it is not known how many cells existed within the droplet in total for the high magnification analyses. However, for the low magnification drop test, the number of cells in the droplet on average was reported to be ~1000 cells, thus it is expected that the high magnification cell count would not be too dissimilar.

For the pre-acid addition measurement, the number of cells analysed could be easily increased by scanning through the sample and imaging at pre-determined locations. The data obtained from a larger population of cells may prove to be more comparable to the red cell distribution width parameter.

Similarly for the post-acid addition measurements, a larger number of cells analysed may highlight trends that have been concealed in this work due to the small number of cells analysed in a heterogeneous blood sample.

6.2.5 Stressor type variation

In *Section 3.6: (ii)*, the pH of the acid stressor (HCl) was varied from 0.7 – 2.0. Preliminary research into haemolysis by acidic stressor informed the approximate pH range to investigate - *Bodansky* recommended a pH of 1.3 for the most rapid haemolysis. However, it was required for the pH to be altered such that sufficient cell lysis (~80% of the population) could be observed within the testing channel length for this body of work.

One of the advantages of having MeCheM and microfluidic chip footprint design is that any stressor could be use in place of the HCl. For example, the blood disorder Glucose-6-Phosphase Dehydrogenase (G6PD) Deficiency decreases the resistance of the red blood cell to oxidative stress.[90] An oxidative stressor could be substituted for the acidic stressor to potentially detect the presences of a G6PD deficiency in the blood.

6.2.6 Other applications of MeCheM

Similarly, MeCheM could be used to detect the quality of transfused blood in storage. The haemolysis curves may be informative and the imaging from the high magnification system would allow clinicians to observe the average shape of cells in a sample the blood

population. Albeit, this is suggested with the caveat that the high magnification system does require a higher number of cells to be investigated.

6.2.6 Final considerations

It is submitted that what has been developed within this body of work is a stepping stone for future low-cost blood research. It is clear that the overall results were not in agreement with the original hypotheses and, at this time, the diagnostic potential of the acid stressor test is uncertain.

However, the potential for future research using the tools that have been developed within this thesis is not insignificant. MeCheM and the microfluidic chip as a toolkit will prove to be versatile to user requirements by modification of chip design, stressor and even channel flow rates.

I believe that the diagnosis of rare anaemias does not fall within the realm of ‘one-test-answers-all’. But I also believe that the MeCheM toolkit has the potential, through the modifications suggested previously, to provide a low cost solution for screening and diagnosis of blood disorders in areas that are under resourced due to lack of funding. It is my hope that the potential of MeCheM continues to be interrogated and explored in the future.

Appendices

A.1 Flow analyses

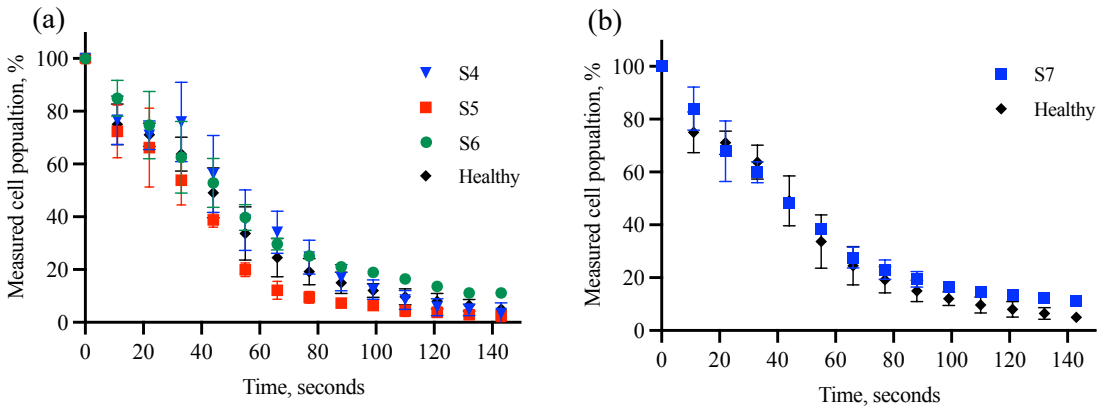

Figure A.1-1 Flow test results for: (a) Heterozygous Sickle Cell and β-thalassaemia (HbS/ βT), n=3, and (b) Heterozygous Sickle Cell and Haemoglobin C (HbSC), n=1. Error bars are standard deviation.

The flow test results for the remaining sickled disorders (HbS/βT and HbSC) are shown in the graphs above in *Figure A.1-1 (a)* and *(b)*. There appeared to be very little differentiation between these samples and the healthy control. For the HbS/βT group, *Figure A.1-1 (a)*, sample S5 appears to decline more rapidly than the control curve and the standard deviations were relatively small between triplicate runs. However, this was not observed for the other two HbS/βT samples (S4 and S6), thus could not be attributed as characteristic of this disease.

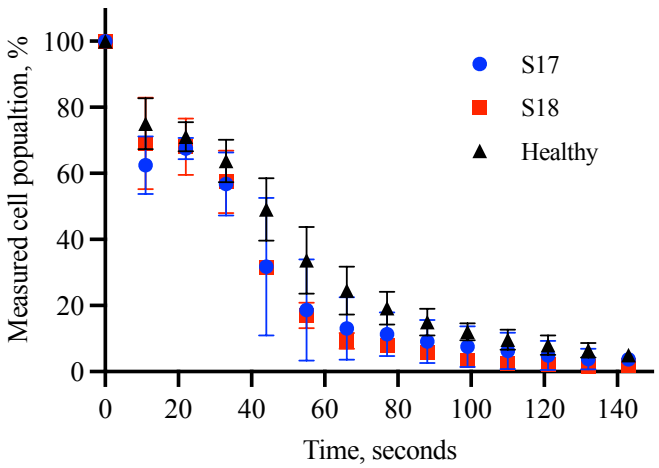

Figure A.1-2 Flow test results for Hereditary Xerocytosis (S17 & S18). Error bars are standard deviation.

The results for the Hereditary Xerocytosis (HX) samples, *Figure A.1-2*, follow the control curve trend much more closely. Similarly to HS, HX also characteristically displays membrane fragilty caused by reduced cellular deformability.[238] Therefore, it was expected that the reduced deformability would be observed in the flow test as a more

rapid cell decline when compared with the control curve. There appears to be a slight diversion of the average HX samples from the control curve suggesting a slight decrease in resistance to lysis. However, within the standard deviation errors, this could not be considered a distinctive feature of the HX samples.

A.2 High magnification testing: pre-acid addition

Sickled disorders

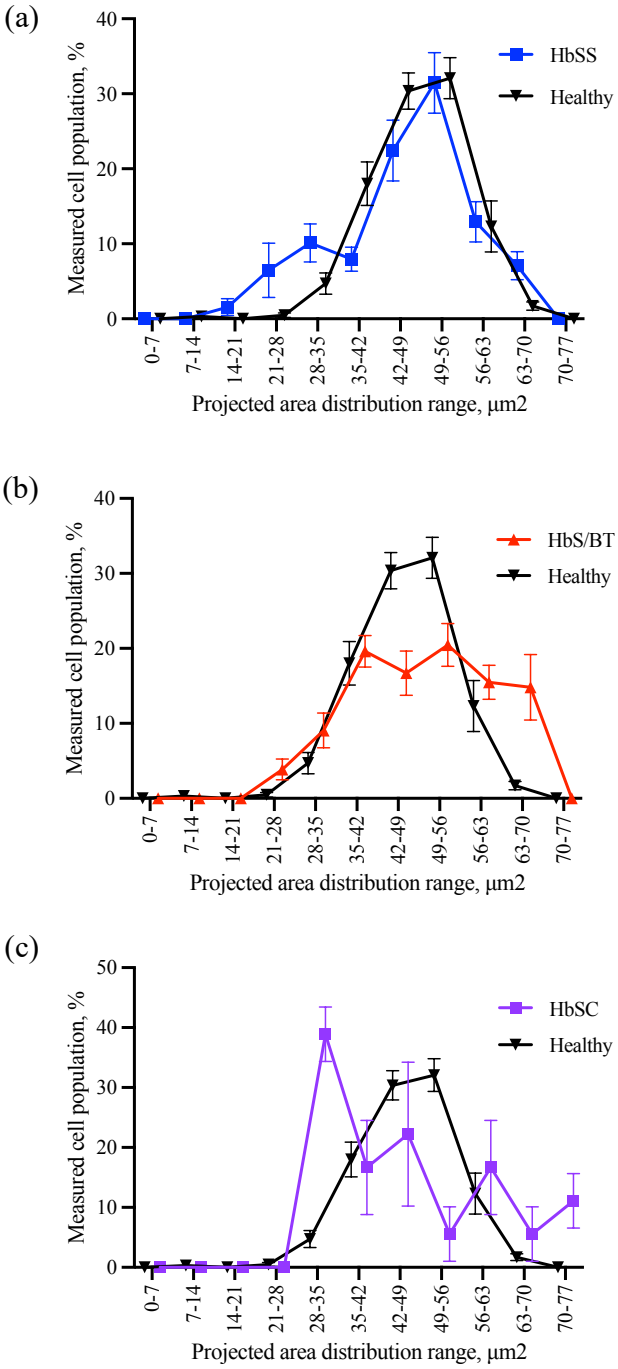

Figure A.2-1 Cell projected area distributions pre-acid addition. Samples containing the same mutation were grouped together. HbSS contained samples S1 – S3, HbS/ βT contained samples S4 – S6, HbSC was a singular sample. The pre-acid addition for the control population was overlaid in black.

It is known that blood samples with mutations, specifically HbS mutations, will have an increased red cell distribution width. The aim of this analysis was to investigate high magnification imaging on a small volume of diluted whole blood to determine if it could be used to detect increased/decreased red cell distribution width.

Figure A.2-1 shows the projected area distributions for the sickled samples and the healthy control (black). The total number of cells per sample pre-acid addition was used to normalise the populations. The samples were grouped according to their mutation, with the HbSS and HbS/βT groups containing 3 samples each and HbSC containing a singular sample.

The majority of the cell population for the control is found between 35 – 56 μm^2 range, *Figure A.2-1*.

For HbS/βT and HbSC, the majority of the cell population is spread over larger interval ranges, 35 – 63 μm^2 and 28 – 63 μm^2 respectively. For HbSS, the majority of the cell population is more focused and found within 42 – 56 μm^2.

Although, each of the samples in the sickled disorder group reported a high red cell distribution width, this was only observed in the high magnification imaging test for the HbS/βT and HbSC samples.

The HbSS sample highlights a potential increase in cell size with the highest cell population (38.5%) found at 49 – 56 μm^2. Mean corpuscular volume, the average volume of RBCs in a sample, is reported as increased or decreased in accordance with the average RBC size. It was considered that the projected area distributions may correlate to this haematological parameter. Correlation analysis between MCV and projected area measurements is reported in *Section 5.4.4*.

Overall, the results of this analysis suggest that the high magnification imaging set up is not sufficiently accurate to highlight abnormal red cell distribution widths for sickled samples.

Membrane disorders

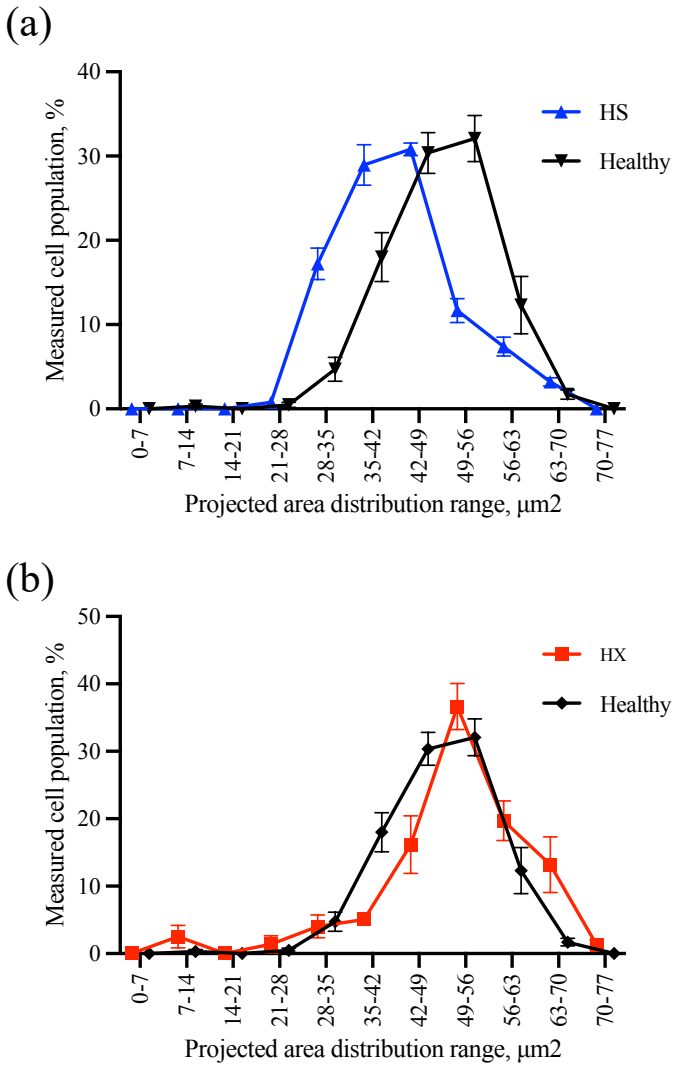

Figure A.2-2 Projected area distributions for Hereditary Spherocytosis (S16) and Hereditary Xerocytosis (S17 & S18).

To note, there was not sufficient sample volume for Hereditary Spherocytosis (HS) sample S15, thus, the measurements for HS are reported from one sample (S16). The Hereditary Xerocytosis (HX) group contained 2 samples (S17 and S18).

As can be seen from *Figure A.2-2,* the projected area distributions for HS is shifted left to the control distribution. In contrast, the HX sample was observed to have a shift to the right of the control distribution indicating an increase in measured projected area.

It is known that HS blood samples often display microcytic RBCs due to their fragile membrane[112]. It is also known that macrocytic RBCs are observed in HX blood samples[225]. The haematological parameter expected to correlate with an increase/decrease

in projected area measurements is Mean Corpuscular Volume. This is investigated in *Section 5.4.4*.

The spread of the distributions containing the majority of the cell population for HS and HX spans 3 interval ranges.

The RDW values for HX were not increased, thus, it was not expected to observe an increase in the spread of distributions across the interval ranges in this analysis. However, there was an increase in the RDW for the HS sample, see *Table 5-4* in *Chapter 5*. This was not observed in the projected area distributions where ~ 82% of the RBC population was observed within 3 interval ranges.

The high magnification imaging test pre-acid addition does seem to highlight samples that have an increase/decrease in projected area measurement, thus, size. However, it does not appear to be accurate in all cases for reporting an increase/decrease in the width of the distribution of a sample. For this purpose, this analysis in its current form is not recommended.

A.3 High magnification testing: post-acid addition

Sickled disorders

HbSS

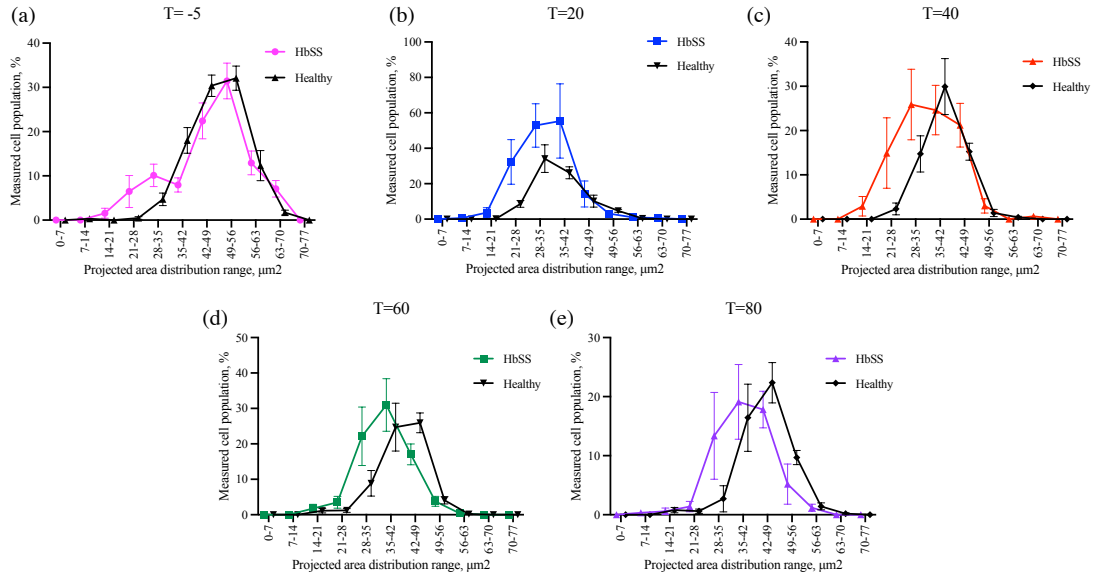

Figure A.3-1 Projected area distribution measurements for homozygous Sickle Cell Disease show that the swelling of the sickled disorders post acid addition is slower than that of the control (black).

HbS/BT

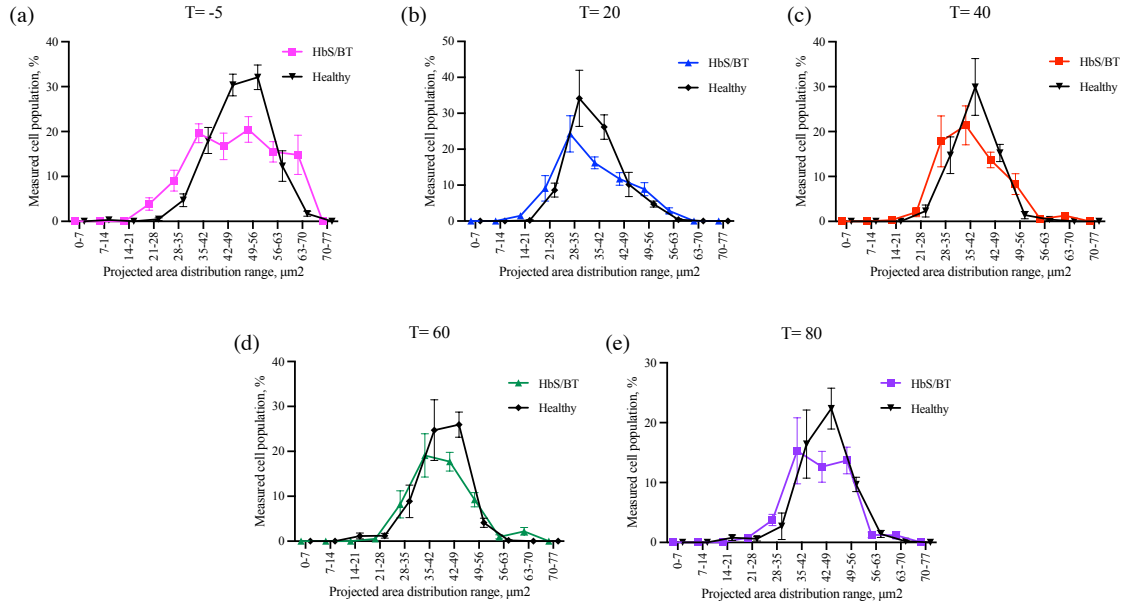

Figure A.3-2 Although the distribution of the heterozygous HbS/BT spans a wider range than the control, it appears that these samples follow the sweeling patterns of the control and reside within a similar range at T=80.

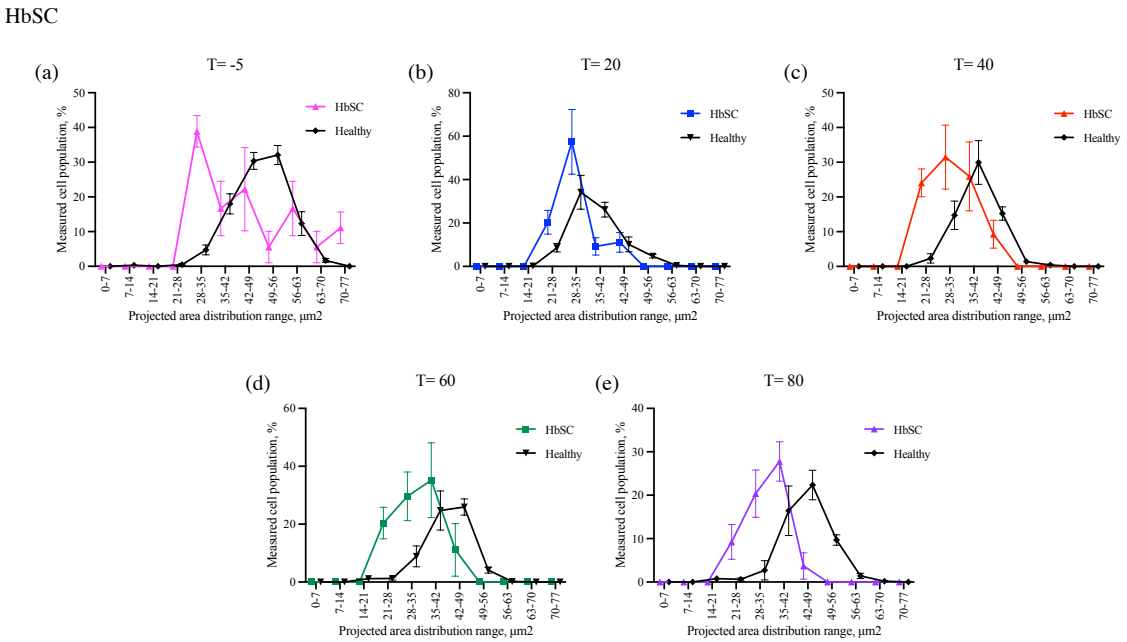

Figure A.3-3 HbSC showed the most sample distribution variation pre-acid addition and the most notable delay in swelling post acid addition.

Dehydration is a well-known characteristic of sickle cells which is caused by a loss of intracellular potassium and an increase in intracellular sodium.[239] It was assumed that the volume of water required to counterbalance the high levels of intracellular sodium ions in the sickled samples would be greater than the volume required in the case of the healthy population. Thus it was considered that this could be observed in the HMDT as a slower increase in projected area distribution.

Figure A.3-1 - *Figure A.3-3* shows the response of the sickled disorders to the addition of acid. For each disease there is a decrease in measured projected area from T=-5 to T=20. This was also found in the case of the control sample. The table below, *Table A*.6-1, reports the interval where most of the cell population was found for each time point and disease.

Sample	T=-5	T=20	T=40	T=60	T=80	T=100
Healthy	49 - 56	28 - 35	35 - 42	42 - 49	42 - 49	42 - 49
HbSS	49 - 56	28 -35	35 - 42	42 - 49	42 - 49	49 - 56
HbS/βT	35 - 42	28 -35	35 - 42	42 - 49	42 - 49	42 - 49
HbSC	28 -35	*28 -35	35 - 42	42 - 49	42 - 49	42 - 49

*Table A.6-1 Interval ranges with the majority of the cell population for each disease and the control. In each case, the projected area distribution of the cell decreases. *Although sample HbSC doesn't appear to decrease, the previous histogram reports an increase in cell population from 35% - 55% at this time point.*

For HbSS and HbS/βT, the majority of cells decrease by three and one interval ranges respectively, refer to *Table 4-1* in *Chapter 4* for the interval ranges. For HbSC, a decrease in projected area is not observed in the table. However, looking at the results in *Figure A.3-3*, it is clear that the percentage of cells that fall into the 28 - 35 μm^2 interval bracket increase (from 35% to 55%), suggesting that the cells *are* reducing in size, albeit not as dramatically as HbSS and HbS/βT.

For each sickled disease and the control at the time point T=40, the cell majority has increased to the next interval where it remains until the final measurement at T=100, except in the case of HbSS. HbSS has one final interval increase from T=80 to T=100 suggesting that cell swelling is still on-going at this point.

Considering only where the majority of the cell populations lie at the measured timepoints, it is very difficult to highlight distinct differences between the healthy and diseased populations. Although there are some differences in the spread of the cell population over the interval ranges, it is not sufficiently distinguishable to render this result as a potential diagnostic test.

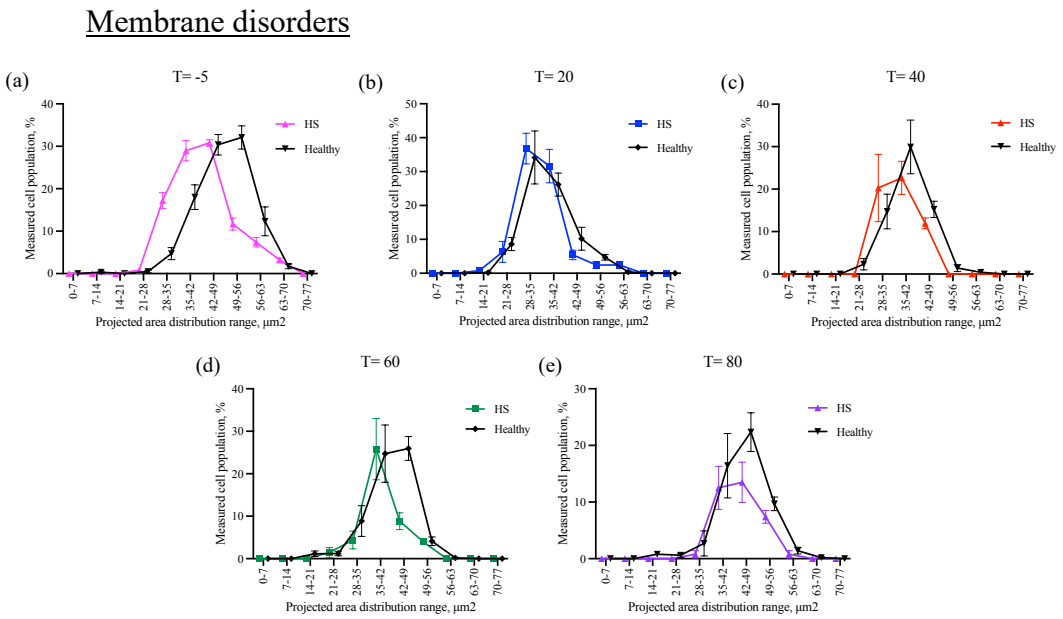

Figure A.3-4 The Hereditary Spherocytosis (S) samples clearly lie within a smaller projected area distribution range compared with the healthy samples for T=-5. Although the healthy and HS samples appear to align at T=20, the HS sample struggles to match the swelling of the healthy control for T=40 and T=60, with increased cell lysis evident in T=80.

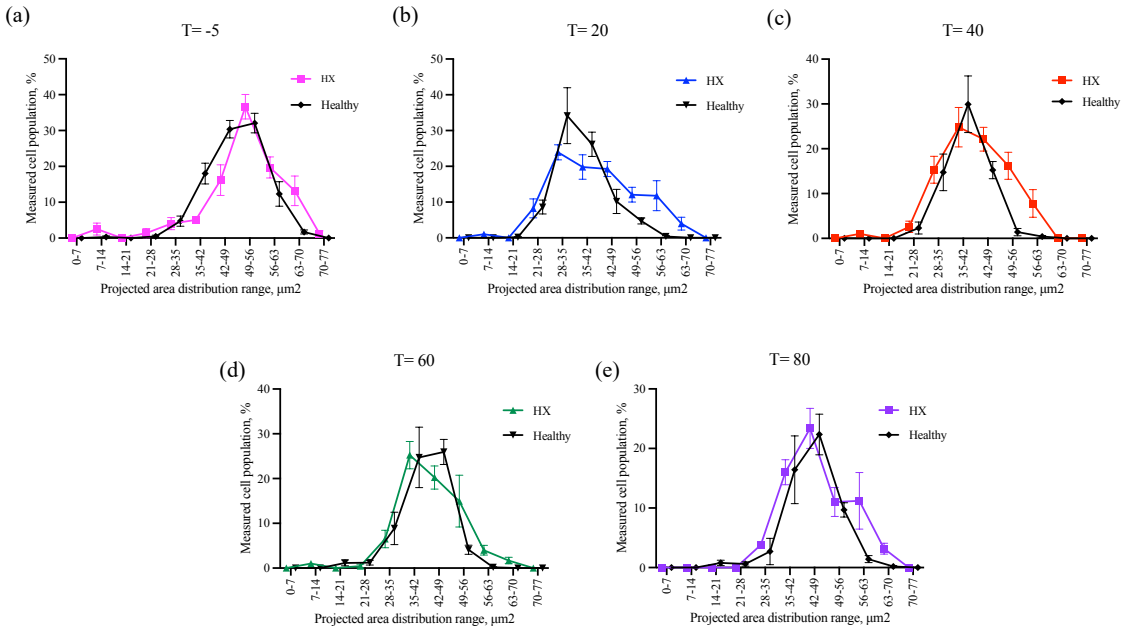

Figure A.3-5 The Hereditary Xerocytosis samples closely follow the projected area distributions of the healthy control. However, it is clear that there is larger variation in projected area sizes across the HX samples.

Sample	T=-5	T=20	T=40	T=60	T=80	T=100
Healthy	49 - 56	28 - 35	35 - 42	42 - 49	42 - 49	42 - 49
HS	42 - 49	28 - 35	28 - 35	35 - 42	35 - 42	42 - 49
HX	49 - 56	35 - 42	35 - 42	35 - 42	42 - 49	42 - 49

Table A.6-2 Interval ranges with the majority of the cell population for both membrane disorders and the control.

Both the HS and HX samples report a decrease in projected area measurement from T= -5 to T=20.

The HS sample has a delay in projected area increase and the majority of the cell population remains at the same interval (28 - 35 μm^2) for T=20 and T=40. The sample then increases to the 35 - 42 μm^2 range for T=60 and T=80 and finally reaching its pre-acid addition projected area interval range of 42 - 49 μm^2 at T=100.

It can be also seen in *Figure A.3-4* that the cell population is decreasing more rapidly over time than the control. This result was also observed in the HS sample for the flow test, see *Figure 5-3* in *Chapter 5*. The membrane of HS samples are known to be more fragile, thus, their ability to withstand deformation and swelling by pH shock would be reduced in comparison to a healthy sample.

The HX sample also shows a delay in projected area increase in comparison to the control. This delay is more pronounced than the HS sample as the majority of the cell population

remains in the 35 - 42 μm^2 interval range from T=20 to T=60. At T=80 the cell population majority shifts to the next interval (42 - 49 μm^2), indicating that population swelling is occurring, where it remains until the final timepoint. Unlike HS, the HX group did not reach the original measured projected area range (49 - 56 μm^2) by T=100.

The results that have been observed for the membranopathies, although dissimilar from the control, have not shown to be sufficiently unique for diagnostic purposes. It is also likely that the results will differ within even the same sample due to the heterogeneity of blood and the small population of cells within the field of view of the high magnification imaging system. As such, this test is not recommended in its current form for diagnostic purposes.

A.4 Correlation analysis

Simple linear correlation and Pearson correlation analysis was carried out for each correlation measurement for the control and diseased populations. *Table A.4-1* reports the R^2 and p-values for each correlation investigated for the control population, and *Table A.4-2* reports the R^2 and p-values for the diseased groups. Correlations that appear to be significant are highlighted in orange in the tables below.

Correlation	P – value		R^2
Cell count -v- RBC count	0.0021	**S**	0.617
HGB -v- $T_{50\%}$	0.852	**NS**	0.005
HGB -v- activity time	0.911	**NS**	0.003
MCH -v- $T_{50\%}$	0.451	**NS**	0.085
MCH -v- activity time	0.042	**S**	0.679
MCHC -v- $T_{50\%}$	0.733	**NS**	0.018
MCHC -v- activity time	0.431	**NS**	0.163
MCV -v- projected area	0.703	**NS**	0.707
RDW -v- PDW	0.021	**S**	0.851

Table A.4-1 The tests were investigated for correlations between the developed methods and the haematological parameters for the control population.

Correlation		P – value		R^2
Cell count -v- RBC count	*Sickled disorders*	0.0089	**S**	0.775
	Thalassaemias	0.004	**S**	0.823
	Membrane disorders	0.130	NS	0.762
RDW -v- PDW	*Sickled disorders*	0.452	NS	0.118
	Thalassaemias	0.282	NS	0.221
	Membrane disorders	0.713	NS	0.198
MCH -v- activity time	*Sickled disorders*	0.822	NS	0.011
	Thalassaemias	0.373	NS	0.159
	Membrane disorders	0.231	NS	0.868
MCV -v- PA	*Sickled disorders*	0.0061	**S**	0.805
	Thalassaemias	0.029	**S**	0.734
	Membrane disorders	0.451	NS	0.571

Table A.4-2 The tests were investigated for correlations between the developed methods and the haematological parameters for the diseased groups.

A.5 MeCheM patent

US 20200156066A1

(19) **United States**

(12) **Patent Application Publication** (10) **Pub. No.: US 2020/0156066 A1**

SUMMERSGILL et al. (43) **Pub. Date: May 21, 2020**

(54) **MICROFLUIDIC DEVICE AND APPARATUS**

(71) Applicant: **EPIGEM LIMITED**, Redcar Cleveland (GB)

(72) Inventors: **Philip SUMMERSGILL**, Redcar Cleveland (GB); **Simon ALLEN**, Yarm Yorkshire (GB); **Timothy George RYAN**, Middlesborough Cleveland (GB); **Niamh Aine KILCAWLEY**, Beaumont, Dublin (IE)

(21) Appl. No.: **16/604,400**

(22) PCT Filed: **Apr. 16, 2018**

(86) PCT No.: **PCT/GB2018/050992**

§ 371 (c)(1),
(2) Date: **Oct. 10, 2019**

(30) **Foreign Application Priority Data**

Apr. 26, 2017 (GB) 1706616.8

Publication Classification

(51) **Int. Cl.**
B01L 3/00 (2006.01)
C12Q 1/02 (2006.01)

(52) **U.S. Cl.**
CPC ***B01L 3/502715*** (2013.01); ***B01L 3/50273*** (2013.01); ***B01L 3/502761*** (2013.01); ***C12Q 1/02*** (2013.01); *B01L 2200/0647* (2013.01); *B01L 2400/049* (2013.01); *B01L 2300/06* (2013.01); *B01L 2300/0627* (2013.01); *B01L 2300/0883* (2013.01); *B01L 2300/047* (2013.01); *B01L 2200/16* (2013.01)

(57) **ABSTRACT**

A microfluidic test apparatus including a microfluidic device having a first reservoir for receiving a first fluid containing a sample of cells, a microfluidic test region, a first microfluidic pathway provided between the microfluidic test region and the first reservoir; and a port for connection to a pump, the apparatus including a first pump connected to the port and configured to pump a priming fluid into the port, a second pump connected to the port and configured to apply suction at the port when operated and a controller configured to control operation of the first and second pumps, where the controller operates the first pump to prime the microfluidic device and operates the second pump to draw a test volume from the first reservoir into the microfluidic test region.

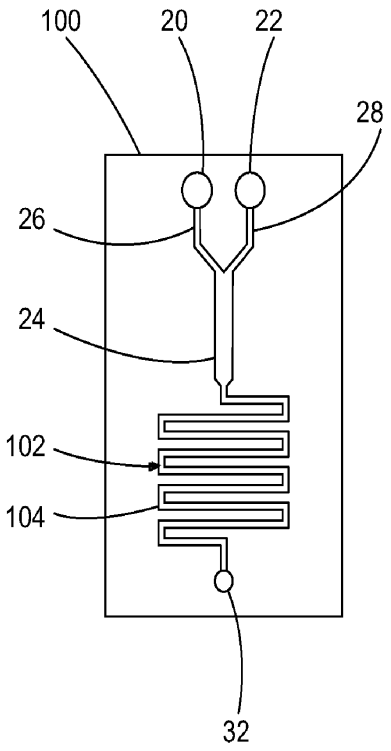

Patent Application Publication May 21, 2020 Sheet 1 of 9 US 2020/0156066 A1

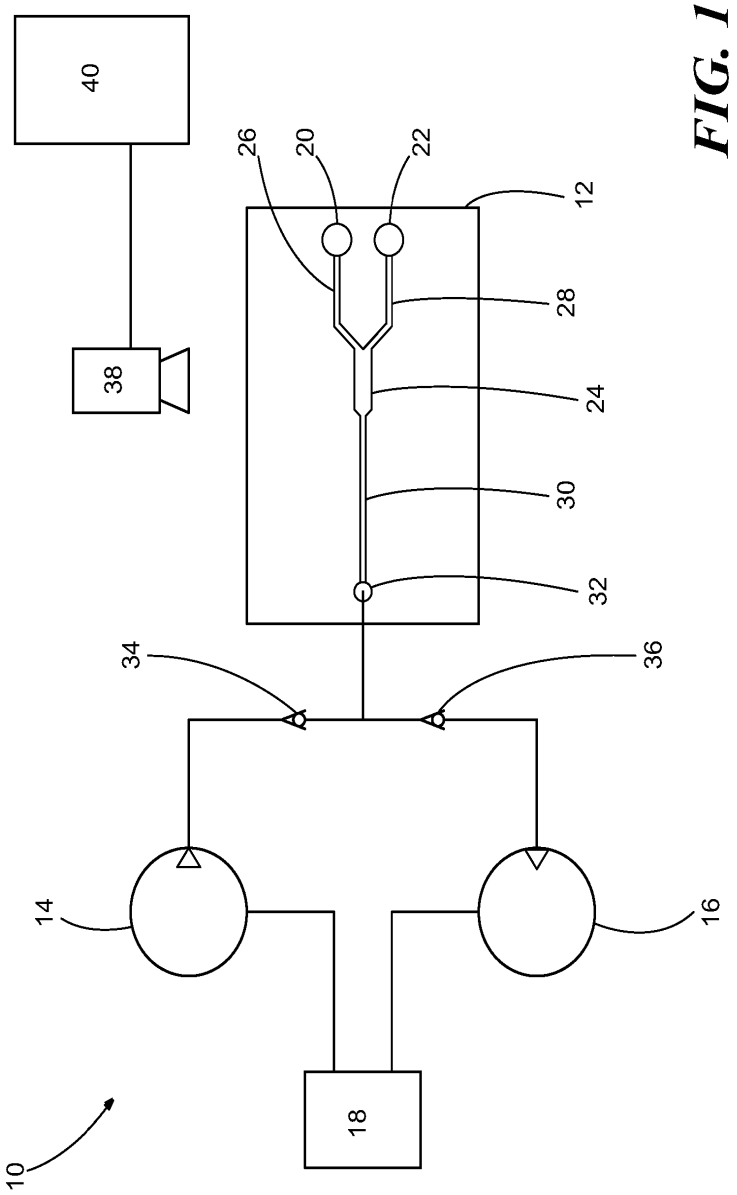

FIG. 1

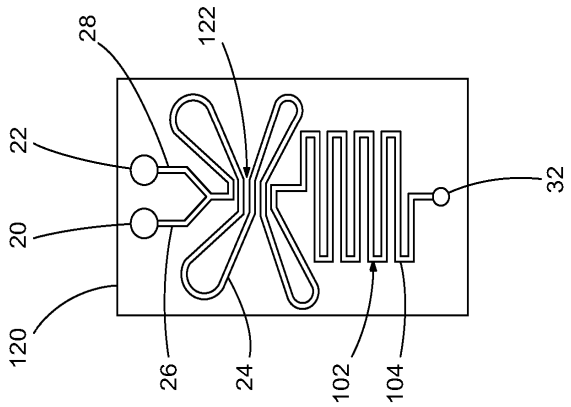

FIG. 2c

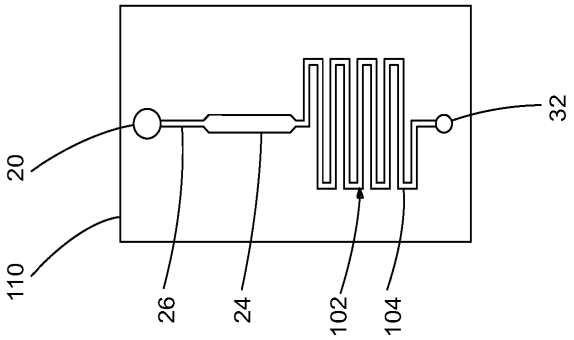

FIG. 2b

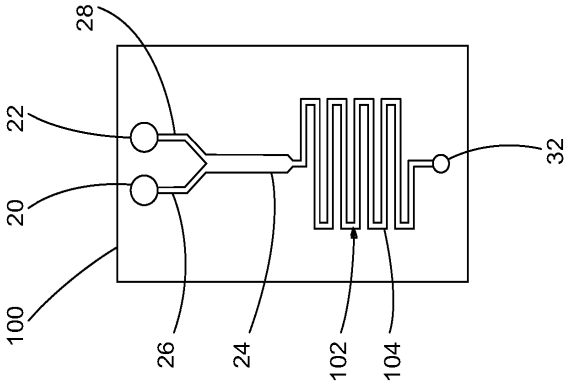

FIG. 2a

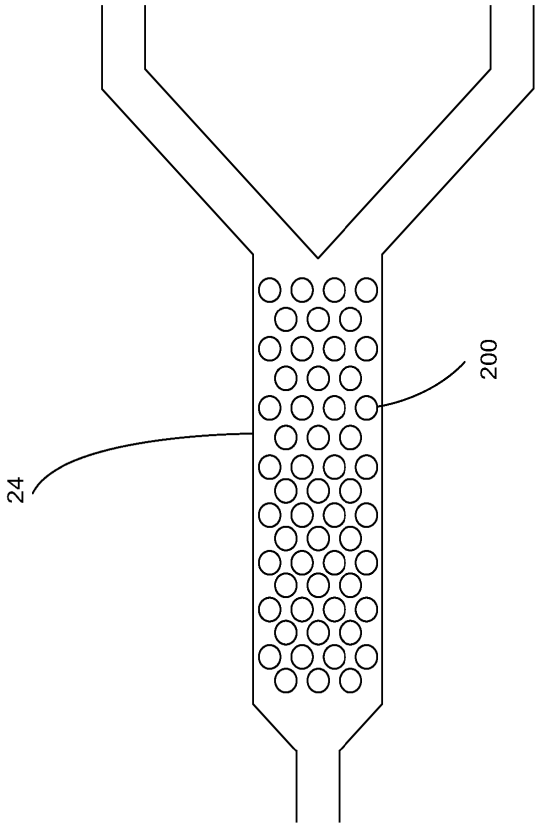

FIG. 3

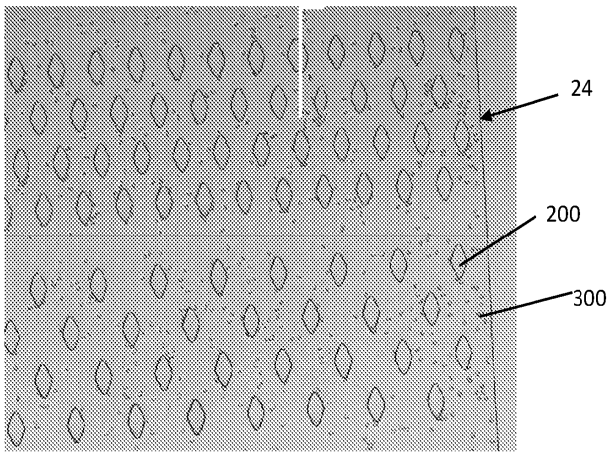

FIG. 4a

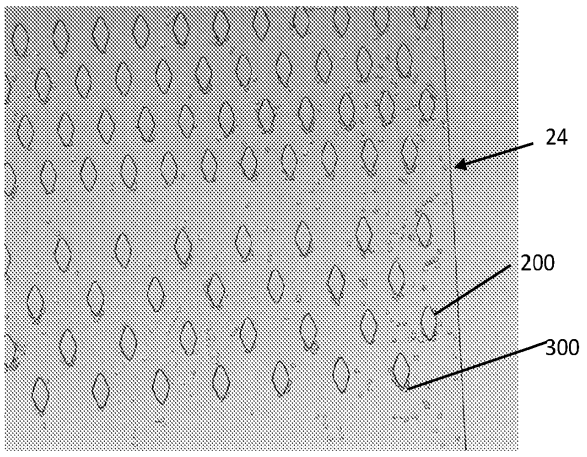

FIG. 4b

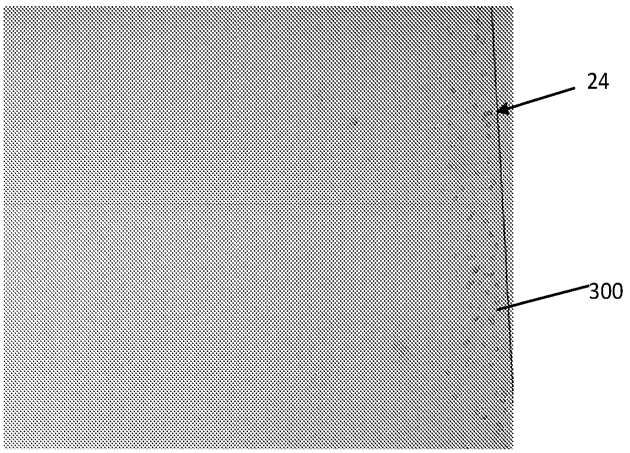

FIG. 5a

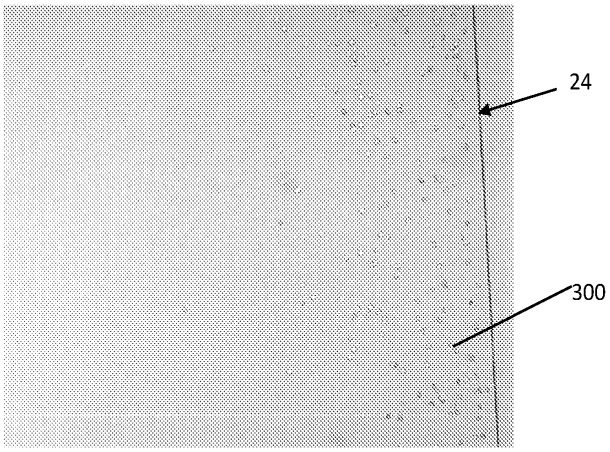

FIG. 5b

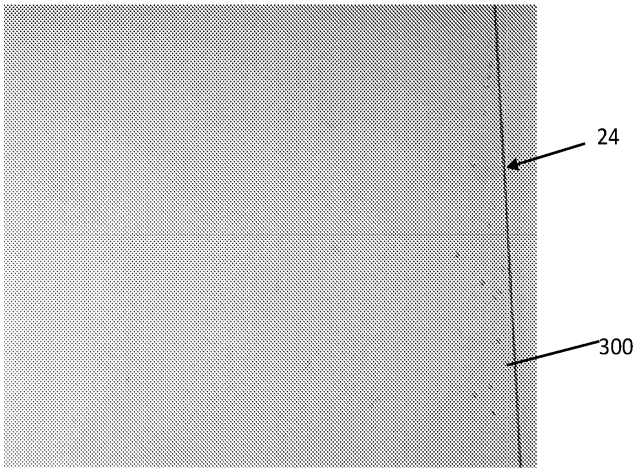

FIG. 6a

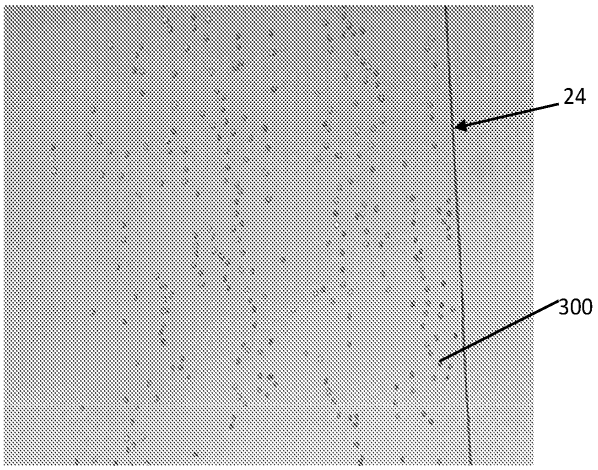

FIG. 6b

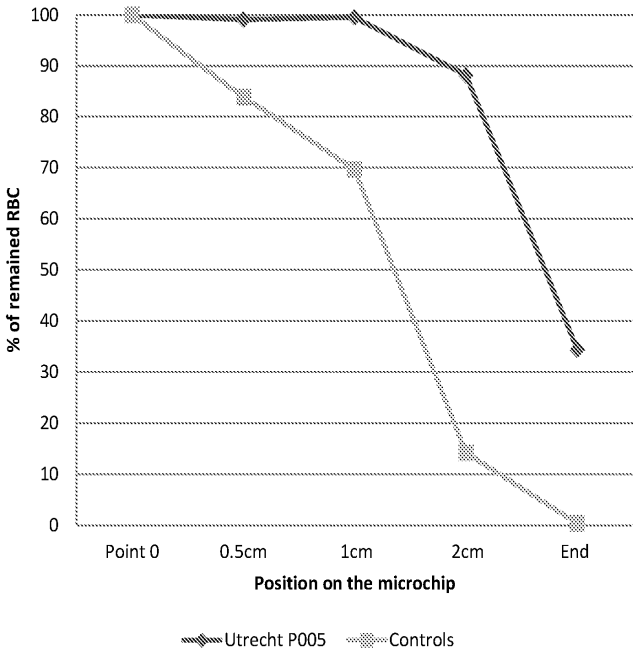
100
90
80
70
60
50
40
30
20
10
0
% of remained RBC
Point 0
0.5cm
1cm
2cm
End
Position on the microchip
Utrecht P005
Controls

FIG. 7

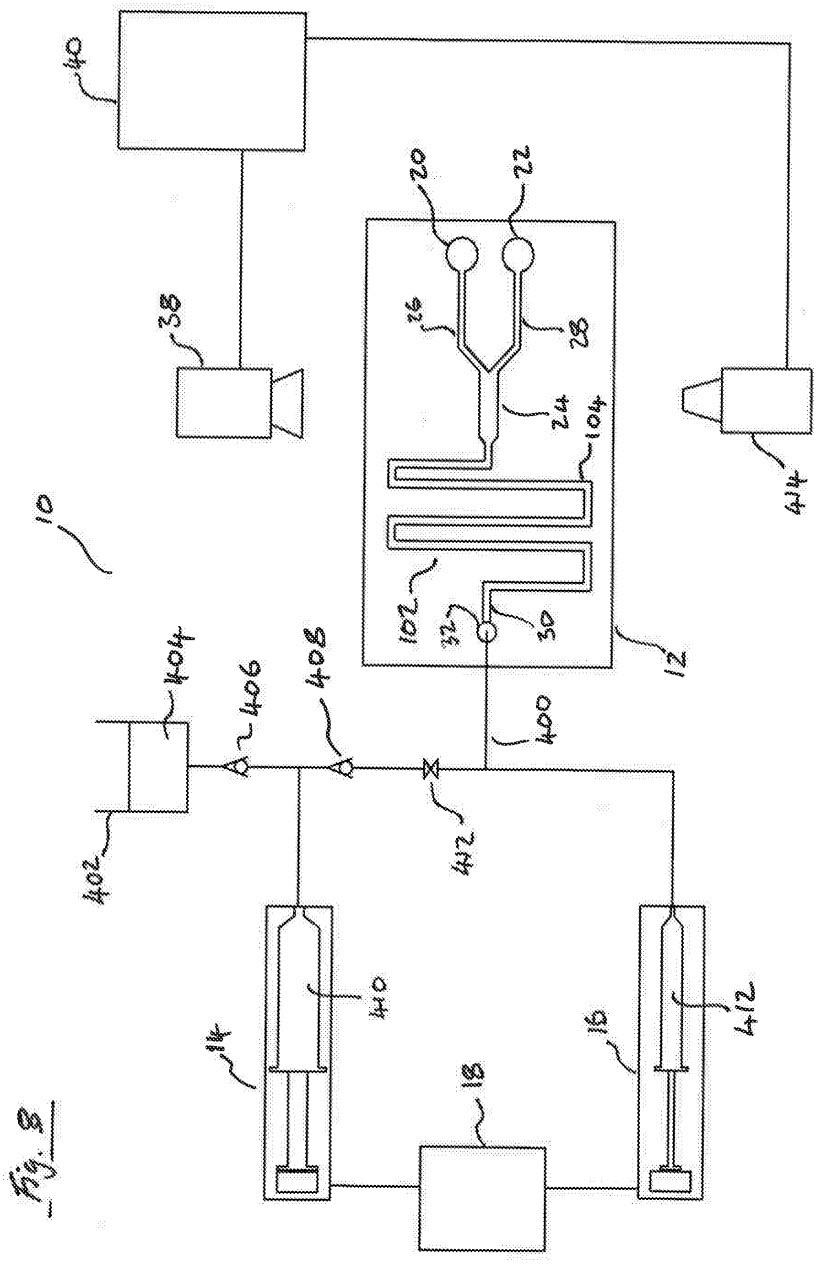
40
20
22
38
26
28
24
104
414
10
102
32
30
12
404
406
408
400
402
412
410
14
16
18

Fig. 8

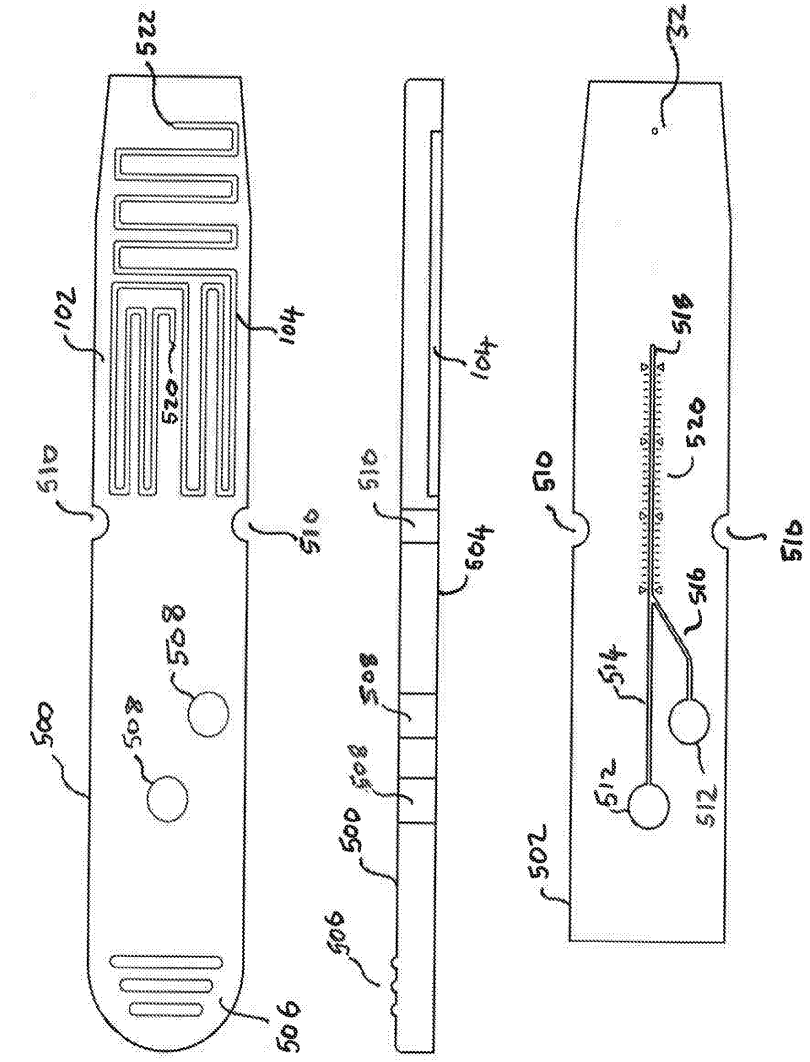

Fig. 9A Fig. 9B Fig. 9C

US 2020/0156066 A1 May 21, 2020

MICROFLUIDIC DEVICE AND APPARATUS

TECHNICAL FIELD

[0001] The present disclosure relates to a microfluidic device and to a microfluidic test apparatus. The microfluidic device and microfluidic test apparatus have particular utility in performing tests on fluid samples of cells.

BACKGROUND

[0002] Microfluidic devices are devices with very small features, typically in the μm range, which perform operations on very small fluid samples, typically in the μl range. The small volume of fluid required for use with a microfluidic device offers benefits in fields such as medicine, since only a very small blood sample is needed.

[0003] One such application of microfluidic devices is described by Lei Li et al. in "A microfluidic platform for osmotic fragility test of red blood cells", RSC Advances, 2012, 2, 7161-7165. Li describes the use of two syringe pumps to push a blood sample and pure water into a microfluidic device. The microfluidic device of Li consists of a Y junction at which the blood sample and pure water meet and form a laminar flow and a length of serpentine channel consisting of 40 square-wave structures. The blood sample and pure water pass along the channel and then exit the microfluidic device at a waste outlet. In the device of Li, the fragility of red blood cells are tested along the length of the channel. An image capture device captures images of the blood sample at several places along the channel, and these images are analysed to determine an osmotic fragility curve from the number of blood cells present at each place along the channel.

SUMMARY OF THE DISCLOSURE

[0004] In a first aspect of the present disclosure, a microfluidic test apparatus is provided, comprising a microfluidic device. The microfluidic device comprises a first reservoir for receiving a first fluid containing a sample of cells, a microfluidic test region, a first microfluidic pathway provided between the microfluidic test region and the first reservoir; a port. The microfluidic test apparatus further comprises a first pump connected to the port and configured to pump a priming fluid into the port, and a second pump connected to the port and configured to apply suction at the port when operated. A controller is provided, which is configured to control operation of the first and second pumps, wherein the controller operates the first pump to prime the microfluidic device and operates the second pump to draw a test volume from the first reservoir into the microfluidic test region.

[0005] In a second aspect of the present disclosure, a microfluidic device is provided, comprising a first reservoir for receiving a first fluid comprising a sample of cells and a microfluidic test region. A first microfluidic pathway is provided between the microfluidic test region and the first reservoir. The microfluidic device further comprises a port for connection to a pump, the pump in use applying suction at the port to draw a test volume from the first reservoir into the microfluidic test region. A microfluidic waste region is provided between the microfluidic test region and the port, wherein the microfluidic waste region defines a microfluidic volume commensurate with the test volume.

[0006] Other features and aspects of this disclosure will be apparent from the following description and the accompanying drawings.

BRIEF DESCRIPTION OF THE DRAWINGS

[0007] FIG. **1** is a schematic diagram of a microfluidic test apparatus according to one embodiment of the present disclosure;

[0008] FIGS. **2***a*, **2***b*, and **2***c* are schematic diagrams of microfluidic devices according to embodiments of the present disclosure;

[0009] FIG. **3** is an enlarged view of a microfluidic test region from a microfluidic device according to one embodiment of the present disclosure;

[0010] FIGS. **4***a* and **4***b* are images of red blood cells in a microfluidic test region from a microfluidic test apparatus for blood samples that are normal and that have sickle-cell disease, respectively;

[0011] FIGS. **5***a* and **5***b* are images of red blood cells in a microfluidic test region from a microfluidic test apparatus for blood samples that are normal and that have sickle-cell disease, respectively;

[0012] FIGS. **6***a* and **6***b* are images of red blood cells in a microfluidic test region from a microfluidic test apparatus for blood samples that are normal and that have hereditary spherocytosis, respectively;

[0013] FIG. **7** shows a red blood cell profile along a microfluidic test region from the test shown in FIGS. **6***a* and **6***b*.

[0014] FIG. **8** shows, schematically, a microfluidic test apparatus according to an embodiment of the disclosure; and

[0015] FIGS. **9**A-**9**C illustrate component parts of an embodiment of a microfluidic device of the disclosure.

DETAILED DESCRIPTION

[0016] Reference will now be made in detail to specific embodiments or features, examples of which are illustrated in the accompanying drawings. Wherever possible, corresponding or similar reference numbers will be used throughout the drawings to refer to the same or corresponding parts. Moreover, references to various elements described herein, are made collectively or individually when there may be more than one element of the same type. However, such references are merely exemplary in nature. It may be noted that any reference to elements in the singular may also be construed to relate to the plural and vice-versa without limiting the scope of the disclosure to the exact number or type of such elements unless set forth explicitly in the appended claims.

[0017] FIG. **1** is an illustrative schematic view of a microfluidic test apparatus **10** according to embodiments of the present disclosure. The microfluidic test apparatus **10** comprises a microfluidic device **12**, first and second pumps **14** and **16**, respectively, and a controller **18** that operates the pumps **14**, **16**.

[0018] The microfluidic device **12** comprises a first reservoir **20** and a second reservoir **22** for receiving a first fluid and a second fluid, respectively, and a microfluidic test region **24**. A first microfluidic pathway **26** is provided between the first reservoir **20** and the microfluidic test region **24**. A second microfluidic pathway **28** is provided between the second reservoir **22** and the microfluidic test region **24**. In the microfluidic device **12** illustrated in FIG. **1**, a further

microfluidic pathway **30** is provided between the microfluidic test region **24** and a port **32**.

[0019] The first pump **14** is connected to the port **32** via a valve **34**. The first pump **14** and valve **34** are arranged to pump a priming fluid into the port **32** when operated. The first pump **14** may be a syringe pump, in which the syringe filled with the priming fluid. The priming fluid may contain a wetting agent to reduce air being trapped in the microfluidic device **12**.

[0020] The second pump **16** is connected to the port **32** via a valve **36**. The second pump **16** and valve **36** are arranged to apply suction at the port **32** when operated and draw fluid therefrom. The valves **34** and **36** may take any suitable form, including a one-way valve, non-return valve, or an activated valve. In some embodiments the valves **34**, **36** may be omitted.

[0021] The controller **18** is configured to control operation of the first and second pumps **14** and **16**, and the valves **34**, **36** where the valves are activated. The controller **18** may be any suitable device such as a microcontroller, embedded controller, programmable logic controller (PLC), microprocessor, portable computing device or computer and may include a control program. The controller **18** is configured to operate the first pump **14** to prime the microfluidic device **12**. The first pump **14** preferably has a pump rate in the order of mL/second (e.g. 1-10 mL/s), and preferably mL/minute (e.g. in the range of 1-10, or 1-100, or 1-200 mL/min); this relatively high flow rate aids priming the microfluidic device **12** and reduces or eliminates air entrapment. The controller **18** operates the first pump **14** to pump priming fluid into the microfluidic device **12** such that priming fluid enters the reservoirs **20**, **22**.

[0022] After priming, the first and second fluids are then added to the reservoirs **20** and **22**, respectively. Where priming fluid has entered the reservoirs **20**, **22**, in some embodiments the priming fluid may be removed before the first and second fluids are added. The first fluid comprises a sample of cells. The second fluid is chosen according to the test requirements and may for example include a label and/or a stressor to the cells that cause a distinctive change in cells which may include cell lysis, aggregation, swelling, shrinkage, and/or shape change. In some embodiments, a series of second fluids may be added one by one to the second reservoir **22** as a test is performed, each second fluid having a different stressors, stressor concentration, and/or different labels. One example of a suitable label/dye is eosin-5-maleimide (EMA), which may be used for instance to stain band **3** proteins following shear stress.

[0023] The controller **18** is configured to operate the second pump **16** to draw a test volume of first fluid from the first reservoir **20** into the microfluidic test region **24**. A volume of second fluid will also be drawn from the second reservoir **22**, according to the dimensions of the microfluidic pathways **26**, **28**. Since the second pump **16** applies suction to the port **32**, pressure on the cells in the first fluid is limited. Using a pump to 'push' the first fluid through the microfluidic device **12** can result in higher pressure on the cells and cause cell ruptures, which may affect testing. It is preferred that the second pump **16** has a pump rate in the order of μL/minute (e.g. 10-100, or 10-200, or 10-500 μL/m) or μL/second (e.g. 1-10 μL/s, or 1-100 μL/s or 1-500 μL/s).

[0024] In the microfluidic device **12** shown in FIG. **1**, the microfluidic test region **24** comprises a microfluidic channel into which the first and second fluids flow. Other forms of microfluidic test region **24** may be employed; for instance, the microfluidic test region **24** may comprise a microfluidic channel formed into a spiral. Forming the microfluidic test region **24** in a spiral may permit the imaging device **38** to capture fluid flow at several locations along the microfluidic test region **24** in a small area covered by a single image. Other configurations of the microfluidic test region **24** are possible, one example of which is described below in relation to FIG. **2***c*. The dimensions of the microfluidic channel may be determined according to requirements, such as desired fluid flow rate, and test sample volume.

[0025] The microfluidic test apparatus **10** further comprises a sensor responsive to the microfluidic test region **24**. The sensor may be any form of sensor according to the test being performed. In the embodiment illustrated in FIG. **1**, the sensor comprises an imaging device **38**. The imaging device **38** captures images of the microfluidic test region **24** as the first and second fluids pass along it. In some embodiments, a region (not shown) of colour filter may be provided in the microfluidic test device **12** above the microfluidic test region **24**, which may improve contrast in the images captured by the imaging device **38**. A dye or marker may also be used, such as a fluorescent or chemiluminescent dye or marker. The test region may be configured for multiparameter testing to identify cell related differences and also serum related, including serology testing using antigen/antibody binding using a printed panel of antigens in the test region to recognise sought proteins in the serum or in the cell surface. Suitable surface chemistries may be used to prevent surface adhesion except in targeted areas in the sensor area of the test region by spotting or printing with specific molecular moieties for targeted molecular trapping or binding.

[0026] The microfluidic test apparatus **10** further comprises an image processor **40** that analyses images received from the imaging device **38**. The image processor **40** may be configured to perform one or more forms of analysis of images received form the imaging device **38**. Such analysis may include cell counts at locations along the microfluidic test region **24**, cell counts at one or more locations in the microfluidic test region **24** which may have an affinity substance applied thereto, cell shape, to name a few. Where the second fluid is a stressor to the cells, the image processor **40** may be configured to determine a cell lysis or cell shape change profile across the microfluidic test region **24**, and may also be configured to compare or display the cell lysis or shape change profile to one or more control profiles. The imaging device **38** can also be used as part of a control system to ensure that the rate of movement of cells within the test region **24** is kept constant for each test, such that the residence time in the test region **24** is monitored and controlled by control of pump **16**.

[0027] Referring now to FIG. **2***a*, a microfluidic device **100** according to another embodiment of the present disclosure is shown. The microfluidic device **100** is similar to the microfluidic device **12** shown in FIG. **1**, with like reference numerals denoting like parts. The microfluidic device **100** differs from the microfluidic device **12** in that the microfluidic device **100** is provided with a microfluidic waste region **102** provided between the microfluidic test region **24** and the port **32**. The microfluidic waste region **102** may comprise a circuitous microfluidic pathway **104**. While shown in two dimensions in the drawings for clarity it will be appreciated that the pathway **104** may be formed in three dimensions.

The microfluidic waste region **102** defines a microfluidic volume commensurate with the test volume to prevent the first or second fluids from reaching the port **32**. The microfluidic waste region **102** prevents the first or second fluid from leaving the microfluidic device **100**, thereby avoiding cross-contamination that would result if some of the first or second fluids were to leave the microfluidic device **12** and then subsequently be pumped into another microfluidic device during the priming thereof.

[0028] FIG. **2***b* shows a microfluidic device **110** according to a further embodiment of the present disclosure. The microfluidic device **110** is similar to the microfluidic device **100** shown in FIG. **2***a* with like reference numerals denoting like parts. The microfluidic device **110** differs from the microfluidic device **100** in that the microfluidic device **110** omits the second reservoir **22** and second microfluidic pathway **28**. The microfluidic device **110** may be used where a stressor has been added to the first sample or where mechanical stress is applied in the microfluidic device.

[0029] FIG. **2***c* shows a microfluidic device **120** according to a further embodiment of the present disclosure. The microfluidic device **120** is similar to the microfluidic device **100** shown in FIG. **2***a* with like reference numerals denoting like parts. The microfluidic device **120** differs from the microfluidic device **100** in the configuration of the microfluidic test region **24**. The microfluidic test region **24** of the microfluidic device **120** comprises a serpentine channel which passes back and forth through a central region **122**. The central region **122** provides a compact area that can be imaged by the imaging device **38** to capture information at several locations along the microfluidic test region **24** without requiring several imaging sensors.

[0030] Referring now to FIG. **3**, a microfluidic test region **24** from a microfluidic device **12** or **100** according to further embodiments of the invention is shown. The microfluidic test region **24** has a plurality of obstacles **200** formed therein. It will be appreciated that the size, shape, quantity and density of the obstacles **200** may be varied from what is shown, and further that the size, shape, quantity and density of the obstacles **200** may be varied along the microfluidic test region **24**. In some embodiments of the disclosure, a first affinity substance is formed on at least one of the obstacles **200**. In other embodiments of the present disclosure, a plurality of affinity substances are provided, each affinity substance being formed on a group of obstacles **200** associated therewith. The image processor **40** may then count cell affinity to obstacles or groups of obstacles to which an affinity substance has been applied. Any suitable affinity substances known to those skilled in the art may be used, including cationic or anionic polymers. Diffusive mixing under laminar flow conditions or mixing geometries that induce turbulent mixing may be used in the microfluidic test region **24**.

[0031] It will be appreciated that the foregoing examples of microfluidic devices are exemplary only, and that further configurations are possible according to test requirements. For instance, in some embodiments, more than one microfluidic test region may be provided, more than two reservoirs may be used. In other embodiments, the second microfluidic pathway **28** may include a junction to split into two pathways that sandwich the first microfluidic pathway **26**, one to either side, so that the first fluid has the second fluid on both side in the microfluidic test region.

EXAMPLES

[0032] FIGS. **4***a* and **4***b* are images from the image sensor **38** of a microfluidic test region **24** in which obstacles **200** are present which provide mechanical stress to cells passing through the test region **24**. The direction of fluid flow in FIGS. **4***a* and **4***b* is from the bottom of the image to the top of the image. FIG. **4***a* is an image showing red blood cells **300** from a healthy patient. FIG. **4***b* is an image showing red blood cells (RBC) **300** from a patient with sickle-cell disease. As can be seen, the RBC **300** in the patient in FIG. **4***b* have an increased tendency to adhere to the obstacles **200**. A microfluidic device, such as that shown in FIG. **2***b*, with a single reservoir was used for the tests shown in FIGS. **4***a* and **4***b* since stress was provided mechanically.

[0033] FIGS. **5***a* and **5***b* are images from the image sensor **38** of a microfluidic test region **24**. The second fluid used in this example was a stressor in the form of dilute HCl at 0.5% concentration by volume in buffer. As the first fluid containing red blood cells and the second fluid containing the dilute HCl enter the microfluidic test region **24**, a laminar flow results, with the HCl diffusing into the first fluid. Since the fluids are flowing along the microfluidic test region, a diffusion gradient forms along the length of the microfluidic test region **24**. In FIGS. **5***a* and **5***b* the HCl has diffused from left to right. The images in FIGS. **5***a* and **5***b* are taken at the same point along the microfluidic test region **24**. As would be appreciated, images may be take at several locations along the microfluidic test region **24** by the imaging device **38**, and the image processor **40** may then count RBC in each image to produce a lysis profile as the HCl diffuses and stresses the RBC. FIG. **5***a* is an image showing red blood cells **300** from a healthy patient. FIG. **5***b* is an image showing red blood cells (RBC) **300** from a patient with sickle-cell disease. As can be seen, RBC in patients with sickle-cell disease are more resistant to lysing from the HCl.

[0034] FIGS. **6***a* and **6***b* are images from the image sensor **38** of a microfluidic test region **24**. The second fluid used in this example was a stressor in the form of dilute HCl at 0.5% concentration by volume in buffer. FIG. **6***a* is an image showing red blood cells **300** from a healthy (control) patient. FIG. **6***b* is an image showing red blood cells (RBC) **300** from a patient with hereditary spherocytosis. As can be seen, RBC in patients with hereditary spherocytosis are more resistant to lysing from the HCl.

[0035] FIG. **7** is a profile of RBC count from the test shown in FIGS. **6***a* and **6***b*, as a percentage of a RBC count from an image taken at the start of the microfluidic test region **24**. Further images were taken at 0.5 cm, 1 cm, 2 cm and the end of the microfluidic test region **24**. In FIG. **7**, the curve labelled 'control' represents a RBC count from a healthy patient, while the curve labelled 'Utrecht P005' represents a RBC count from a patient with hereditary spherocytosis. As can be seen from FIG. **7**, the profile of RBC count along the microfluidic test region **24** is markedly different.

[0036] FIG. **8** illustrates a further preferred embodiment of a microfluidic test apparatus, generally indicated by **10**. The test apparatus comprises a microfluidic device **12** having first **20** and second **22** reservoirs for receiving a first and second fluid, respectively, a microfluidic test region **24** and a waste region **102**, preferably microfluidic, said waste region **102** comprising a circuitous pathway **104**. Again, a first microfluidic pathway **26** is provided between the first

reservoir **20** and the test region **24**, and a second microfluidic pathway **28** is provided between the second reservoir **22** and the test region **24**.

[0037] A microfluidic pathway **30** is also provided between the waste region **102** and the port **32**. In use, the port **32** is connectable to a fluid pathway **400** connecting the microfluidic device **12** to two pumps **14**, **16**, and priming reservoir **402** for holding priming fluid. The outlet of the reservoir **402** is provided with a valve **406** to allow priming fluid to leave the priming reservoir, but not to return. This may be achieved by use of a one-way valve, non-return valve, or an isolation valve, preferably controlled in tandem with the pumps **14**, **16**. A second such valve **408** may also be provided in the fluid pathway, with a connection to the pump **14** provided between the two valves **406**, **408**. In this preferred embodiment, the pump **14** is a syringe pump, of relatively large volume, e.g. at least as large as the total fluid volume of the microfluidic device **12** and the interconnecting fluid pathway **400**. The pump may be activated in a first mode to draw priming fluid **404** into the barrel **410** of the syringe pump **14**. The two valves **406**, **408** operate to ensure that the flow is from priming reservoir **402**, rather than from any connected microfluidic device **12**.

[0038] The pump **14** may then be operated in a second mode to push priming fluid through the fluid pathway, into the microfluidic device **12** and eventually into the reservoirs **20**, **22** as described above. A further isolation valve **412** may also be provided, either manually-operated, or controlled in tandem with the pump controls, to enable the priming fluid reservoir to be isolated from the microfluidic device and the second pump **16**. The priming reservoir **402** may be provided with a level sensor (not illustrated) to monitor the amount of priming fluid **404** available, and to raise a user alarm if more fluid **404** needs to be added.

[0039] Once the microfluidic device **12** has been primed, a sample (e.g. of cells, especially red blood cells) may be added to one of the reservoirs **20**, and a reagent (e.g. a stressor, or marker dye) may be added to the other reservoir **22**. The second pump **16** may then be activated to draw fluid through the microfluidic device **12**, as described above, for analysis. In this preferred embodiment, the second pump **16** is also a syringe pump, and is preferably configured such that the volume of its barrel **412** is less than the volume of the microfluidic waste region **102** of the microfluidic device **12**. This ensures that neither the fluid pathway **200** nor the pump **16** can be contaminated with any material introduced into the microfluidic device **12**.

[0040] As described above, the apparatus **10** also includes a controller, to control at least the operation of the pumps. The apparatus also includes an imaging device and an imaging processor **40**. For some applications, a fluorescent marker might be used in the analysis, and in this instance an illuminator **414** may be provided to illuminate the test area **24** with e.g. ultraviolet light.

[0041] FIGS. **9**A-**9**C illustrate component parts of a preferred microfluidic device **12** of the invention. The device **12** comprises an upper portion **500** and a lower portion **502**. In use, the two portions are joined together, e.g. with a thermoplastic adhesive, to form the microfluidic device. The upper portion **500**, which may conveniently be made of a material such as plastics, e.g. acrylic or polymethyl methacrylate is shown in plan and elevation view in FIGS. **9**A and **9**B respectively. Two through-holes **508** are provided, forming the first and second reservoirs **20**, **22** when the upper and lower portions are joined together. The upper portion **500** has a waste region **102** formed as a circuitous pathway, preferably a microfluidic pathway. The pathway comprises a continuous channel in the lower surface **504** of the upper portion. When the two portions are joined, the channel is sealed by the upper face of the lower portion **502** forming the pathway. A gripping portion **506** may also be provided, in the form e.g. of raised ribs or indentations, to allow a user to firmly hold the device for positioning in a test apparatus. Indentations **508** may also be provided on each edge of the device **12** to allow it to be positioned in a test apparatus relative to cooperating pins (not illustrated). The indentation may be formed by e.g. moulding, machining, etching or other such method.

[0042] The lower portion **502** of the device is illustrated in plan view in FIG. **9**C. This portion comprises the accurately-formed microfluidic flow paths, as described above, and may be most conveniently produced by e.g. photo-resist techniques, micro-machining or other such technique known in the art. The flow paths are again in the form of channels, or indentations, in the upper surface of the lower portion **502** which, when abutted to the upper portion **500** form a fluid-tight microfluidic pathway.

[0043] Two recessed circular regions **512** are provided that are positioned to interact with the through-holes in the upper region to form the reservoirs **20**, **22**. First and second recessed channels **514**, **516** are provided in fluid communication with each respective recessed circular regions **512** that, when covered by the upper portion **500**, form the first and second microfluidic pathways **26**, **28** described above. A third recessed channel **518** is also provided, which, when covered by the upper portion **500**, forms the microfluidic test region. The third recessed channel **518** is in fluid communication with both the first and second recessed channels **514**, **516** to allow two fluids therein to come into contact when the device is used as described herein. In a particularly preferred embodiment illustrated in FIG. **9**C, the first recessed channel **514** is co-linear with the third recessed channel **518**. In this way, if cells are put into the reservoir in fluid connection with the first microfluidic pathway **514**, their flow path is essentially linear. The inventor has found that this reduces unwanted mechanical damage to the cells when the device is in use. It is particularly also preferred that the transverse cross-sectional area of the third recessed channel **518** is equal to the sum of the transverse cross-sectional areas of the first and second recessed channels **514**, **516**. In this way, the fluid is not subjected to any acceleration when the two fluid streams meet, which might otherwise cause unwanted damage to cells under analysis. Such a feature is preferred for any microfluidic devices described herein.

[0044] Indicia **520** may also be provided adjacent the third recessed channel **518** to aid positioning and to provide a reference for the image analysis.

[0045] The end of the third recessed channel **518** is positioned such that it fluidly communicates with the proximal end **520** of the waste region. The distal end **522** of the waste region is positioned such that it fluidly communicates with a port **32** (e.g. a through-hole) in the lower portion **502** of the device.

[0046] It should be appreciated that the present disclosure is not limited to the foregoing examples. For instance, other stressors may be used, including stressors which induce shrinkage or oxidative stress in RBCs. Based on preliminary

test results, the microfluidic test apparatus **10** of the present disclosure may be a useful tool for diagnosis of a rare anaemias and other blood diseases, severity diagnosis, and assessment of the efficacy of treatment. Other tests may also be performed, including a rapid 'shrinkage' test for overhydrated RBCs, oxidation resistance tests, RBC membrane surface tests. The test apparatus **10** can be readily programmed for a simple or complex set of assay operations.

[0047] Various embodiments disclosed herein are to be taken in the illustrative and explanatory sense, and should in no way be construed as limiting of the present disclosure.

1. A microfluidic test apparatus, comprising:
a microfluidic device comprising:
a first reservoir for receiving a first fluid containing a sample of cells;
a microfluidic test region;
a first microfluidic pathway provided between the microfluidic test region and the first reservoir; and
a port for connection to a pump;
a first pump connected to the port and configured to pump a priming fluid into the port;
a second pump connected to the port and configured to apply suction at the port when operated; and
a controller configured to control operation of the first and second pumps, wherein the controller operates the first pump to prime the microfluidic device and operates the second pump to draw a test volume from the first reservoir into the microfluidic test region.

2. The microfluidic test apparatus of claim **1**, further comprising a sensor responsive to the microfluidic test region.

3. The microfluidic test apparatus of claim **2**, wherein the sensor comprises an imaging device.

4. The microfluidic test apparatus of claim **3**, further comprising an image processor that analyses images received from the imaging device.

5. The microfluidic test apparatus of claim **4**, wherein the image processor is configured to determine a cell shape change profile across the microfluidic test region.

6. The microfluidic test apparatus of claim **4**, wherein the image processor is configured to determine a count of cell affinity to one or more obstacles provided in the microfluidic test region.

7. The microfluidic test apparatus of claim **6**, wherein the image processor is configured to determine a count of cell affinity to one or more groups of obstacles or printed spots provided in the microfluidic test region.

8. The microfluidic test apparatus of claim **1**, wherein the microfluidic device further comprises a microfluidic waste region provided between the microfluidic test region and the port, wherein the microfluidic waste region defines a microfluidic volume commensurate with the test volume.

9. The microfluidic test apparatus of claim **1**, wherein the microfluidic device further comprises a second reservoir for receiving a second fluid.

10. The microfluidic test apparatus of claim **9**, wherein the second fluid is a stressor to the cells.

11. A microfluidic device, comprising:
a first reservoir for receiving a first fluid comprising a sample of cells;
a microfluidic test region;
first microfluidic pathway provided between the microfluidic test region and the first reservoirs;
a port for connection to a pump, the pump in use applying suction at the port to draw a test volume from the first reservoir into the microfluidic test region;
a microfluidic waste region provided between the microfluidic test region and the port, wherein the microfluidic waste region defines a microfluidic volume commensurate with the test volume.

12. The microfluidic device of claim **11**, further comprising a second reservoir for receiving a second fluid, and a second microfluidic pathway provided between the microfluidic test region and the second reservoirs.

13. The microfluidic device of claim **11**, wherein the microfluidic test region comprises a microfluidic channel.

14. The microfluidic device of claim **13**, wherein a plurality of obstacles are provided in the microfluidic channel.

15. The microfluidic device of claim **14**, wherein a density of the obstacles varies along the microfluidic channel.

16. The microfluidic device of claim **14**, wherein a first affinity substance is formed on at least one of the obstacles.

17. The microfluidic device of claim **14**, wherein a plurality of affinity substances are provided, each affinity substance being formed on a group of obstacles associated therewith.

18. The microfluidic device of claim **11**, wherein the microfluidic waste region comprises a circuitous microfluidic pathway.

* * * * *

A.6 Marie Skłodowska-Curie training and secondments

Courses and workshops	**Year**
Webinar EU Horizon ITN	2016
ESR training week Arivis AG	2017
Webinar GMP training	2019

EU Horizon ITN consortium training meetings	**Year**
RELEVANCE meeting, Heidelberg	2017
RELEVANCE meeting, Amsterdam	2017
RELEVANCE meeting, Paris	2018
RELEVANCE meeting, Zürich	2019
RELEVANCE meeting, Roscoff	2019

Conferences	**Year**
European Red Cell Society Meeting, Heidelberg	2017
Poster and oral presentation	
European School of Haematology, Amsterdam	2018
Poster presentation	
European Red Cell Society, Ascona	2019
Poster and oral presentation	

Secondments	**Year**
University of Zürich, Zürich	2017
Sanquin, Amsterdam	2018
Ha'Emek Medical Centre, Afula	2018
University of Zürich, Zürich	2018
University Medical Centre, Utrecht	2018

Bibliography

1. Kassebaum NJ, Fleming TD, Flaxman A, et al. The Global Burden of Anemia. *Hematol Oncol Clin North Am*. 2016;30(2):247-308. doi:10.1016/j.hoc.2015.11.002
2. Jimenez K, Kulnigg-Dabsch S, Gasche C. Management of iron deficiency Anemia. *Gastroenterol Hepatol*. 2015;11(4):241-250.
3. Bosch X, Montori E, Guerra-García M, et al. Haemoglobin responses to transfusion in severe iron deficiency anaemia: potential impact of gastrointestinal disorders. *Vox Sang*. 2017;112(3):257-267. doi:10.1111/vox.12491
4. Vives-Corrons J-L. The Rare Anaemias. *Rare Dis*. 2020;(2):1-26. doi:10.5772/intechopen.86986
5. Chourasia S, Kumar R, Singh MPSS, Vishwakarma C, Gupta AK, Shanmugam R. High Prevalence of Anemia and Inherited Hemoglobin Disorders in Tribal Populations of Madhya Pradesh State, India. *Hemoglobin*. 2020;44(6):391-396. doi:10.1080/03630269.2020.1848859
6. Andolfo I, Russo R, Gambale A, Iolascon A. New insights on hereditary erythrocyte membrane defects. *Haematologica*. 2016;101(11):1284-1294. doi:10.3324/haematol.2016.142463
7. Balarajan Y, Ramakrishnan U, Özaltin E, Shankar AH, Subramanian S V. Anaemia in low-income and middle-income countries. *Lancet*. 2011;378(9809):2123-2135. doi:10.1016/S0140-6736(10)62304-5
8. Osungbade, Kayode & Oladunjoye, Adeolu. (2012). Anaemia in Developing Countries: Burden and Prospects of Prevention and Control. doi:10.5772/29148
9. World Health Organization. Global health observatory. https://www.who.int/data/gho/data/indicators/indicator-details/GHO/prevalence-of-anaemia-in-women-of-reproductive-age-(-). Published 2021.
10. World Health Organization. Prevalence of Anaemia in women of reproductive age. https://www.who.int/data/gho/data/indicators/indicator-details/GHO/prevalence-of-anaemia-in-women-of-reproductive-age-(-). Accessed June 7, 2021.
11. Elguero E, Délicat-Loembet LM, Rougeron V, et al. Malaria continues to select for sickle cell trait in Central Africa. *Proc Natl Acad Sci U S A*. 2015;112(22):7051-7054. doi:10.1073/pnas.1505665112
12. Balgir RS. Contribution of marital distance to community inbreeding, homozygosis, and reproductive wastage for recessively inherited genetic disorders in Madhya Pradesh, India. *Mediterr J Hematol Infect Dis*. 2013;5(1):1-5. doi:10.4084/MJHID.2013.063
13. Merten M. Keeping it in the family: Consanguineous marriage and genetic disorders, from Islamabad to Bradford. *BMJ*. 2019;365(April):2-4. doi:10.1136/bmj.l1851
14. Shawky RM, Elsayed SM, Zaki ME, Nour El-Din SM, Kamal FM. Consanguinity and its relevance to clinical genetics. *Egypt J Med Hum Genet*. 2013;14(2):157-164. doi:10.1016/j.ejmhg.2013.01.002
15. Anwar WA, Khyatti M, Hemminki K. Consanguinity and genetic diseases in North Africa and immigrants to Europe. *Eur J Public Health*. 2014;24(SUPPL.1):57-63. doi:10.1093/eurpub/cku104
16. Bittles AH, Black ML. Consanguinity, human evolution, and complex diseases. *Proc Natl Acad Sci U S A*. 2010;107(SUPPL. 1):1779-1786.

doi:10.1073/pnas.0906079106
17. Phillips MA, Burrows JN, Manyando C, Van Huijsduijnen RH, Van Voorhis WC, Wells TNC. Malaria. *Nat Rev Dis Prim*. 2017;3. doi:10.1038/nrdp.2017.50
18. WHO Africa. *World Malaria Report 2019*.; 2019. https://www.who.int/news-room/fact-sheets/detail/malaria.
19. Kato GJ, Piel FB, Reid CD, et al. Sickle cell disease. *Nat Rev Dis Prim*. 2018;4:1-22. doi:10.1038/nrdp.2018.10
20. Eridani S. Sickle cell protection from malaria. *Hematol Rep*. 2011;3(3). doi:10.4081/hr.2011.e24
21. Archer NM, Petersen N, Clark MA, Buckee CO, Childs LM, Duraisingh MT. Resistance to Plasmodium falciparum in sickle cell trait erythrocytes is driven by oxygen-dependent growth inhibition. *Proc Natl Acad Sci U S A*. 2018;115(28):7350-7355. doi:10.1073/pnas.1804388115
22. Aidoo M, Terlouw DJ, Kolczak MS, et al. Protective effects of the sickle cell gene against malaria morbidity and mortality. *Lancet*. 2002;359(9314):1311-1312. doi:10.1016/S0140-6736(02)08273-9
23. Luzzatto L. Sickle cell anaemia and malaria. *Mediterr J Hematol Infect Dis*. 2012;4(1). doi:10.4084/MJHID.2012.065
24. Szczesny-malysiak E, Dybas J, Blat A, et al. *BBA - Molecular Cell Research* Irreversible alterations in the hemoglobin structure affect oxygen binding in human packed red blood cells. 2020;1867; 11(7). doi:10.1016/j.bbamcr.2020.118803
25. Liu J, Konermann L. Assembly of hemoglobin from denatured monomeric subunits: heme ligation effects and off-pathway intermediates studied by electrospray mass spectrometry. Biochemistry. 2013 Mar 12;52(10):1717-24. doi: 10.1021/bi301693g.
26. D'Alessandro A, Dzieciatkowska M, Nemkov T, Hansen KC. Red blood cell proteomics update: Is there more to discover? *Blood Transfus*. 2017;15(2):182-187. doi:10.2450/2017.0293-16.
27. Kim Y, Park J, Kim M. Diagnostic approaches for inherited hemolytic anemia in the genetic era. Blood Res. 2017 Jun;52(2):84-94. doi: 10.5045/br.2017.52.2.84.
28. Weatherall DJ, Provan AB. Red cells I: Inherited anaemias. *Lancet*. 2000;355(9210):1169-1175. doi:10.1016/S0140-6736(00)02073-0
29. Farashi S, Harteveld CL. Molecular basis of α-thalassemia. *Blood Cells, Mol Dis*. 2018;70(September 2017):43-53. doi:10.1016/j.bcmd.2017.09.004
30. S. Akers A, Howard D, Ford J. Distinguishing iron deficiency anaemia from thalassemia trait in clinical obstetric practice. *J Pregnancy Reprod*. 2018;2(1):1-6. doi:10.15761/jpr.1000125
31. State Department of Health - Newborn Screening Program W. Hemoglobin Bart's and Alpha Thalassemia Fact Sheet - Washington State Dept of Health. http://www.doh.wa.gov/Portals/1/Documents/5220/HbBartFactSheet.pdf.
32. Hanprasertpong T, Kor-Anantakul O, Leetanaporn R, et al. Pregnancy outcomes amongst thalassemia traits. *Arch Gynecol Obstet*. 2013;288(5):1051-1054. doi:10.1007/s00404-013-2886-9
33. Galanello R, Origa R. Beta-thalassemia. 2010:1-15.
34. Cao A, Galanello R. Beta-thalassemia. *Genet Med*. 2010;12(2):61-76. doi:10.1097/GIM.0b013e3181cd68ed
35. Choudhry VP. Thalassemia Minor and Major: Current Management. *Indian J Pediatr*. 2017;84(8):607-611. doi:10.1007/s12098-017-2325-1
36. Abu-Shaheen A, Heena H, Nofal A, et al. Epidemiology of thalassemia in Gulf

Cooperation Council countries: A systematic review. *Biomed Res Int*. 2020;2020. doi:10.1155/2020/1509501
37. Angelini C. Calpainopathy. 2005 May 10 [Updated 2022 Dec 1]. In: Adam MP, Mirzaa GM, Pagon RA, et al., editors. GeneReviews® [Internet]. Seattle (WA): University of Washington, Seattle; 1993-2023. Available from: https://www.ncbi.nlm.nih.gov/books/NBK1313/
38. Inati A, Noureldine MA, Mansour A, Abbas HA. Endocrine and bone complications in β -thalassemia intermedia: Current understanding and treatment. *Biomed Res Int*. 2015;2015. doi:10.1155/2015/813098
39. Borgna-Pignatti C. Modern treatment of thalassaemia intermedia. *Br J Haematol*. 2007;138(3):291-304. doi:10.1111/j.1365-2141.2007.06654.x
40. Dhanya R, Sedai A, Ankita K, et al. Life expectancy and risk factors for early death in patients with severe thalassemia syndromes in South India. *Blood Adv*. 2020;4(7):1448-1457. doi:10.1182/bloodadvances.2019000760
41. Borgna-Pignatti C, Cappellini MD, De Stefano P, et al. Taher A.T., Saliba A.N.: Iron overload in thalassemia: different organs at different rates. Hematology Am Soc Hematol Educ Program, 2017, 2017(1): 265–271. *Cold Spring Harb Perspect Med*. 2013;2(5):31-37. http://www.ojrd.com/content/5/1/11.
42. Li CK, Chik KW, Lam CWK, et al. Liver disease in transfusion dependent thalassaemia major. *Arch Dis Child*. 2002;86(5):344-347. doi:10.1136/adc.86.5.344
43. Sharma P, Nutritional HÁ, Red Á. Summary and Review of the Abstracts on Disorders of Red Cells and Erythropoiesis Presented at Haematocon 2016 – 2017. *Indian J Hematol Blood Transfus*. 2018;34(1):8-12. doi:10.1007/s12288-017-0912-y
44. Kingsmore, S.F., Lantos, J.D., Dinwiddie, D.L. et al. Next-generation community genetics for low- and middle-income countries. Genome Med 4, 25 (2012). https://doi.org/10.1186/gm324
45. Amin SK. Prevention of Thalassaemia by Genetic Counseling. *Anwer Khan Mod Med Coll J*. 1970;2(2):26-28. doi:10.3329/akmmcj.v2i2.8169
46. Lücker A, Weber B, Jenny P. A dynamic model of oxygen transport from capillaries to tissue with moving red blood cells. *Am J Physiol - Hear Circ Physiol*. 2015;308(3):H206-H216. doi:10.1152/ajpheart.00447.2014
47. Narla J, Mohandas N. Red cell membrane disorders. *Int J Lab Hematol*. 2017;39(February):47-52. doi:10.1111/ijlh.12657
48. Huisjes R, Bogdanova A, van Solinge WW, Schiffelers RM, Kaestner L, van Wijk R. Squeezing for life - Properties of red blood cell deformability. *Front Physiol*. 2018;9(JUN):1-22. doi:10.3389/fphys.2018.00656
49. Savitt TL, Goldberg MF. Herrick's 1910 case report of sickle cell anemia. The rest of the story. JAMA. 1989 Jan 13;261(2):266-71. PMID: 2642320.
50. Rab MAE, van Oirschot BA, Bos J, et al. Rapid and reproducible characterization of sickling during automated deoxygenation in sickle cell disease patients. *Am J Hematol*. 2019;94(5):575-584. doi:10.1002/ajh.25443
51. Abay A, Simionato G, Chachanidze R, et al. Glutaraldehyde - A subtle tool in the investigation of healthy and pathologic red blood cells. *Front Physiol*. 2019;10(MAY):1-14. doi:10.3389/fphys.2019.00514
52. Alapan Y, Matsuyama Y, Little JA, Gurkan UA. Dynamic deformability of sickle red blood cells in microphysiological flow. *Technology*. 2016;04(02):71-79. doi:10.1142/s2339547816400045
53. Huang Z, Hearne L, Irby CE, King SB, Ballas SK, Kim-Shapiro DB. Kinetics of

increased deformability of deoxygenated sickle cells upon oxygenation. *Biophys J*. 2003;85(4):2374-2383. doi:10.1016/S0006-3495(03)74661-X
54. Abboud MR. Standard management of sickle cell disease complications. *Hematol Oncol Stem Cell Ther*. 2020;13(2):85-90. doi:10.1016/j.hemonc.2019.12.007
55. Rhodes M, Akohoue SA, Shankar SM, et al. Growth patterns in children with sickle cell anemia during puberty. *Pediatr Blood Cancer*. 2009;53(4):635-641. doi:10.1002/pbc.22137
56. Strouse JJ, Lanzkron S, Urrutia V. The epidemiology, evaluation and treatment of stroke in adults with sickle cell disease. *Expert Rev Hematol*. 2011;4(6):597-606. doi:10.1586/ehm.11.61
57. Wilson M, Forsyth P, Whiteside J. Haemoglobinopathy and sickle cell disease. *Contin Educ Anaesthesia, Crit Care Pain*. 2009;10(1):24-28. doi:10.1093/bjaceaccp/mkp038
58. Khoriaty E, Halaby R, Berro M, Sweid A, Abbas HA, Inati A. Incidence of sickle cell disease and other hemoglobin variants in 10,095 Lebanese neonates. *PLoS One*. 2014;9(9). doi:10.1371/journal.pone.0105109
59. Aslam HM, Yousuf S, Kassim A, Iqbal SM, Hashmi SK. Hematopoietic stem cell transplantation for adult sickle cell disease in the era of universal donor availibility. *Bone Marrow Transplant*. 2018;53(11):1390-1400. doi:10.1038/s41409-018-0193-6
60. Al-Khabori M, Al-Huneini M, Al-Rawas A. Stem Cell Transplantation in Patients with Sickle Cell Disease. *Sick Cell Dis - Pain Common Chronic Complicat*. 2016. doi:10.5772/64917
61. Krishnamurti L. Hematopoietic Cell Transplantation for Sickle Cell Disease. Front Pediatr. 2021 Jan 5;8:551170. doi: 10.3389/fped.2020.551170.
62. Shenoy S, Eapen M, Panepinto JA, et al. A trial of unrelated donor marrow transplantation for children with severe sickle cell disease. *Blood*. 2016;128(21):2561-2567. doi:10.1182/blood-2016-05-715870
63. Williams TN. An accurate and affordable test for the rapid diagnosis of sickle cell disease could revolutionize the outlook for affected children born in resource-limited settings. *BMC Med*. 2015;13(1):1-3. doi:10.1186/s12916-015-0483-4
64. Aneke J, Okocha C. Sickle cell disease genetic counseling and testing: A review. *Arch Med Heal Sci*. 2016;4(1):50. doi:10.4103/2321-4848.183342
65. Ware RE, Odame I. Newborn screening with sickle cell point of care: A valuable resource in low-income settings. *Pediatrics*. 2019;144(4). doi:10.1542/peds.2019-1681
66. Kinnunen M, Kauppila A, Karmenyan A, Myllylä R. Effect of the size and shape of a red blood cell on elastic light scattering properties at the single-cell level. *Biomed Opt Express*. 2011;2(7):1803. doi:10.1364/boe.2.001803
67. Mesarec L, Góźdź W, Iglič A, Kralj-Iglič V, Virga EG, Kralj S. Normal red blood cells' shape stabilized by membrane's in-plane ordering. *Sci Rep*. 2019;9(1):1-11. doi:10.1038/s41598-019-56128-0
68. Mohandas N, Gallagher PG. Red cell membrane: Past, present, and future. *Blood*. 2008;112(10):3939-3948. doi:10.1182/blood-2008-07-161166
69. Li H, Lykotrafitis G. Erythrocyte membrane model with explicit description of the lipid bilayer and the spectrin network. *Biophys J*. 2014;107(3):642-653. doi:10.1016/j.bpj.2014.06.031
70. Barbalato L, Pillarisetty LS. Histology, Red Blood Cell. https://www.ncbi.nlm.nih.gov/books/NBK539702/.

71. Pretini V, Koenen MH, Kaestner L, et al. Red Blood Cells : Chasing Interactions. 2019;10(July):1-17. doi:10.3389/fphys.2019.00945
72. Paradkar S, Gambhire P. The Role of Cytoskeleton of a Red Blood Cell in Its Deformability. *J Indian Inst Sci*. 2021;101(1):39-46. doi:10.1007/s41745-020-00221-1
73. Oliveira S De, Saldanha C. An overview about erythrocyte membrane. 2010;44:63-74. doi:10.3233/CH-2010-1253
74. Red T, Membrane C. Advances in hematology. 2014;12(8):533-535.
75. Butler J, Mohandas N, Waugh RE. Integral Protein Linkage and the Bilayer-Skeletal Separation Energy in Red Blood Cells. 2008;95(August):1826-1836. doi:10.1529/biophysj.108.129163
76. King MJ, Zanella A. Hereditary red cell membrane disorders and laboratory diagnostic testing. *Int J Lab Hematol*. 2013;35(3):237-243. doi:10.1111/ijlh.12070
77. Peters LL, Jindel HK, Gwynn B, et al. Mild spherocytosis and altered red cell ion transport in protein 4.2- null mice. *J Clin Invest*. 1999;103(11):1527-1537. doi:10.1172/JCI5766
78. Wang C, Cui Y, Li Y, Liu X, Han J. A systematic review of hereditary spherocytosis reported in Chinese biomedical journals from 1978 to 2013 and estimation of the prevalence of the disease using a disease model. *Intractable Rare Dis Res*. 2015;4(2):76-81. doi:10.5582/irdr.2015.01002
79. Wager MGT and JFS. Traditional Laboratory Measures of Cardiovascular Risk in Hereditary Spherocytosis. *Bone*. 2011;23(1):1-7. doi:10.1002/pbc.22640.Traditional
80. Perrotta S, Gallagher PG, Mohandas N. Hereditary spherocytosis. *Lancet*. 2008;372(9647):1411-1426. doi:10.1016/S0140-6736(08)61588-3
81. Ciepiela O. Old and new insights into the diagnosis of hereditary spherocytosis. *Ann Transl Med*. 2018;6(17):339-339. doi:10.21037/atm.2018.07.35
82. Farias MG. Advances in laboratory diagnosis of hereditary spherocytosis. *Clin Chem Lab Med*. 2017;55(7):944-948. doi:10.1515/cclm-2016-0738
83. Da Costa L, Galimand J, Fenneteau O, Mohandas N. Hereditary spherocytosis, elliptocytosis, and other red cell membrane disorders. *Blood Rev*. 2013;27(4):167-178. doi:10.1016/j.blre.2013.04.003
84. Mentzer WC, Iarocci TA, Mohandas N, et al. Modulation of erythrocyte membrane mechanical stability by 2,3-diphosphoglycerate in the neonatal poikilocytosis/elliptocytosis syndrome. *J Clin Invest*. 1987;79(3):943-949. doi:10.1172/JCI112905
85. Mahapatra M. Red Blood Cell Enzyme Defects. *PG Textb Pediatr Infect Syst Disord (Volume 2)*. 2015;17:1704-1704. doi:10.5005/jp/books/12854_142
86. Yoshida T, Shevkoplyas SS. Anaerobic storage of red blood cells. *Blood Transfus*. 2010;8(4):220-236. doi:10.2450/2010.0022-10
87. Fibach E. The Redox Balance and Membrane Shedding in RBC Production, Maturation, and Senescence. *Front Physiol*. 2021;12(February):1-10. doi:10.3389/fphys.2021.604738
88. Mohanty JG, Nagababu E, Rifkind JM. Red blood cell oxidative stress impairs oxygen delivery and induces red blood cell aging. *Front Physiol*. 2014;5 FEB(February):1-6. doi:10.3389/fphys.2014.00084
89. Hess JR, Beyer GM. Red Blood Cell Metabolism during Storage: Basic Principles and Practical Aspects. Blood Banking and Transfusion Medicine. Elsevier; 2007. pp. 205-11. [DOI: 10.1016/b978-0-443-06981-9.50018-1.

90. Koralkova P, Van Solinge WW, Van Wijk R. Rare hereditary red blood cell enzymopathies associated with hemolytic anemia - pathophysiology, clinical aspects, and laboratory diagnosis. *Int J Lab Hematol*. 2014;36(3):388-397. doi:10.1111/ijlh.12223
91. Roper D, Layton M, Rees D, et al. Laboratory diagnosis of G6PD deficiency. A British Society for Haematology Guideline. *Br J Haematol*. 2020;189(1):24-38. doi:10.1111/bjh.16366
92. Agarwal AM, Nussenzveig RH, Reading NS, et al. Clinical utility of next-generation sequencing in the diagnosis of hereditary haemolytic anaemias. *Br J Haematol*. 2016;174(5):806-814. doi:10.1111/bjh.14131
93. Van Wijk R, Huizinga EG, Van Wesel ACW, Van Oirschot BA, Hadders MA, Van Solinge WW. Fifteen novel mutations in PKLR associated with pyruvate kinase (PK) deficiency: Structural implications of amino acid substitutions in PK. *Hum Mutat*. 2009;30(3):446-453. doi:10.1002/humu.20915
94. Grace RF, Barcellini W. Management of pyruvate kinase deficiency in children and adults. *Blood*. 2020;136(11):1241-1249. doi:10.1182/blood.2019000945
95. Al-Samkari H, van Beers EJ, Kuo KHM, et al. The variable manifestations of disease in pyruvate kinase deficiency and their management. *Haematologica*. 2020;105(9):2229-2239. doi:10.3324/haematol.2019.240846
96. Mouna J, Nadia H, Leila C, et al. Phenotypic and molecular genetic analysis of Pyruvate Kinase deficiency in a Tunisian family. *Egypt J Med Hum Genet*. 2016;17(3):265-270. doi:10.1016/j.ejmhg.2015.09.001
97. Bianchi P, Fermo E. Molecular heterogeneity of pyruvate kinase deficiency. *Haematologica*. 2020;105(9):2218-2228. doi:10.3324/haematol.2019.241141
98. Zanella A, Bianchi P. Red cell pyruvate kinase deficiency: From genetics to clinical manifestations. *Best Pract Res Clin Haematol*. 2000;13(1):57-81. doi:10.1053/beha.1999.0057
99. Bianchi P, Fermo E, Glader B, et al. Addressing the diagnostic gaps in pyruvate kinase deficiency: Consensus recommendations on the diagnosis of pyruvate kinase deficiency. *Am J Hematol*. 2019;94(1):149-161. doi:10.1002/ajh.25325
100. Laas C, Lambert C, Senior McKenzie T, et al. Improving the laboratory diagnosis of pyruvate kinase deficiency. *Br J Haematol*. 2021:994-1000. doi:10.1111/bjh.17483
101. Russo R, Marra R, Rosato BE, Iolascon A, Andolfo I, Perkins AC. Genetics and Genomics Approaches for Diagnosis and Research Into Hereditary Anemias. 2020;11(December):1-11. doi:10.3389/fphys.2020.613559
102. Shefer Averbuch N, Steinberg-Shemer O, Dgany O, et al. Targeted next generation sequencing for the diagnosis of patients with rare congenital anemias. *Eur J Haematol*. 2018;101(3):297-304. doi:10.1111/ejh.13097
103. Fermo E, Vercellati C, Bianchi P. Screening tools for hereditary hemolytic anemia: new concepts and strategies. *Expert Rev Hematol*. 2021;14(3):281-292. doi:10.1080/17474086.2021.1886919
104. Mansour-Hendili L, Aissat A, Badaoui B, et al. Exome sequencing for diagnosis of congenital hemolytic anemia. *Orphanet J Rare Dis*. 2020;15(1):1-15. doi:10.1186/s13023-020-01425-5
105. Notaro R. Glucose-6-Phosphate Dehydrogenase Deficiency Running title : Glucose-6-Phosphate Dehydrogenase Deficiency Scientific heading : Red Cells Glucose-6-Phosphate Dehydrogenase Deficiency 3 Laboratory of Cancer Genetics and Gene Transfer , Core Research Laborat. *Blood*. 2021;prepublica.
106. Frank JE. Diagnosis and management of G6PD deficiency. *Am Fam Physician*.

2005;72(7):1277-1282. doi:10.1016/j.beha.2004.08.022
107. Russo R, Manna F, Gambale A, et al. Multi-gene panel testing improves diagnosis and management of patients with hereditary anemias. 2018;(January):672-682. doi:10.1002/ajh.25058
108. Jahangiri M, Rahim F, Malehi AS. Diagnostic performance of hematological discrimination indices to discriminate between β eta thalassemia trait and iron deficiency anemia and using cluster analysis : Introducing two new indices tested in Iranian population. *Sci Rep*. 2019:1-13. doi:10.1038/s41598-019-54575-3
109. J. M. Pekelharing, O. Hauss, R. de Jonge, J. Lokhoff, J. Sodikromo, M. Spaans, R. Brouwer, S. de Lathouder, Hinzmann R. Haematology reference intervals for established and novel parameters in healthy adults. *Diagnostic Perspect*. 2010;1:1-11.
110. World Health Organization. Haemoglobin concentrations for the diagnosis of anaemia and assessment of severity. 2011:1-6. http://www.who.int/vmnis/indicators/haemoglobin.%0Apdf.
111. Vranken MVAN. Evaluation of Microcytosis. 2010;3:1117-1122.
112. Liao L, Xu Y, Wei H, et al. Blood cell parameters for screening and diagnosis of hereditary spherocytosis. 2019;(November 2018):1-6. doi:10.1002/jcla.22844
113. Journal B, Coura-vital W, Carvalho G. Revista Brasileira de Hematologia e Hemoterapia Original article A new index to discriminate between iron deficiency anemia and thalassemia trait. *Rev Bras Hematol Hemoter*. 2016;38(3):214-219. doi:10.1016/j.bjhh.2016.05.011
114. Webster P, Castro O. Red cell distribution width in sickle cell disease. Ann Clin Lab Sci. 1986 Jul-Aug;16(4):274-7. PMID: 3740796..
115. Mukhopadhyay M, Ghosh UU, Sarkar D, Dasgupta S. Surface property induced morphological alterations of human erythrocytes. *Soft Matter*. 2018;14(36):7335-7346. doi:10.1039/c8sm01146j
116. Nair SB. Potential Pithfalls in Using HPLC and its Interpretation in Diagnosing HbS. 2018;3:9-12.
117. Andrew, Okwi & Byarugaba, Wilson & Parkes, Arthur & Ocaido, Michael. (2010). The Reliability of Sickling and Solubility Tests and Peripheral Blood Film Method for Sickle Cell Disease Screening at District Health Centers in Uganda. Clinics in Mother and Child Health. 7. 1-5. 10.4303/cmch/C101947.
118. Wajcman H MK. Abnormal haemoglobins: detection & characterization. *Indian J Med Res*. 2011;134(4):538-546. https://www.ncbi.nlm.nih.gov/pmc/articles/PMC3237254/.
119. Andres O, Eber S, Speer CP. Early postnatal diagnosis of hereditary spherocytosis by combining light microscopy , acidified glycerol lysis test and eosin-5 ′ -maleimide binding assay. 2015:1959-1964. doi:10.1007/s00277-015-2491-z
120. Parpart AK, Lorenz PB, Parpart ER, Gregg JR, Chase AM. the Osmotic Resistance (Fragility) of Human. 1946:636-640.
121. Pribush A, Hatskelzon L, Kapelushnik J, Meyerstein N. Osmotic swelling and hole formation in membranes of thalassemic and spherocytic erythrocytes. Blood Cells Mol Dis. 2003 Jul-Aug;31(1):43-7. doi: 10.1016/s1079-9796(03)00122-0.
122. ChromSystems. Hemoglobin Variants. https://chromsystems.com/en/hemoglobin-variants-hplc-15330.html.
123. Ou C, Rognerud CL. Diagnosis of hemoglobinopathies : electrophoresis vs . HPLC. 2001:187-194.
124. Waterfall CM, Cobb BD, Sensing M, Park CB, Road B, Sn W. Single tube

genotyping of sickle cell anaemia using PCR-based SNP analysis. 2001;29(23).
125. Yue L, Lin M, Chen JT, et al. Rapid screening for sickle cell disease by polymerase chain reaction-high resolution melting analysis. *Mol Med Rep*. 2014;9(6):2479-2484. doi:10.3892/mmr.2014.2130
126. Alekseyev YO, Fazeli R, Yang S, et al. A next-generation sequencing primer—how does it work and what can it do? *Acad Pathol*. 2018;5:1-11. doi:10.1177/2374289518766521
127. National Laboratory of Enteric Pathogens, Bureau of Microbiology, Laboratory Centre for Disease Control. The polymerase chain reaction: An overview and development of diagnostic PCR protocols at the LCDC. Can J Infect Dis. 1991 Summer;2(2):89-91. doi: 10.1155/1991/580478.128. Kadri K. Polymerase Chain Reaction (PCR): Principle and Applications. :1-17.
129. Decorte R, Cassiman J. Forensic medicine and the polymerase chain reaction technique. 1993:625-633.
130. Ewalt MD, West H, Aisner DL. Next Generation Sequencing - Testing Multiple Genetic Markers at Once. *JAMA Oncol*. 2019;5(7):1076. doi:10.1001/jamaoncol.2019.0453
131. Schwarze K, Buchanan J, Fermont JM, et al. The complete costs of genome sequencing: a microcosting study in cancer and rare diseases from a single center in the United Kingdom. *Genet Med*. 2020;22(1):85-94. doi:10.1038/s41436-019-0618-7
132. Helmy M, Awad M, Mosa KA. Limited resources of genome sequencing in developing countries: Challenges and solutions. *Appl Transl Genomics*. 2016;9:15-19. doi:10.1016/j.atg.2016.03.003
133. Germain ARD levine susan hanson maureen. 乳鼠心肌提取 Cess. *Physiol Behav*. 2017;176(3):139-148. doi:10.1111/nyas.14092.Anemia
134. Hossain MS, Raheem E, Sultana TA, et al. Thalassemias in South Asia: clinical lessons learnt from Bangladesh. *Orphanet J Rare Dis*. 2017;12(1):1-9. doi:10.1186/s13023-017-0643-z
135. Kaestner L, Bianchi P. Trends in the Development of Diagnostic Tools for Red Blood Cell-Related Diseases and Anemias. *Front Physiol*. 2020;11(May):1-7. doi:10.3389/fphys.2020.00387
136. McGann Patrick T. HC. The Pressing Need for Point-of-Care Diagnostics for Sickle Cell Disease: A Review of Current and Future Technologies. 2017;(513):104-113. doi:10.1016/j.bcmd.2017.08.010.The
137. Max Roser (2014) - "Human Development Index (HDI)". Published online at OurWorldInData.org. Retrieved from: 'https://ourworldindata.org/human-development-index
138. eidt B, Siqueira WF, Eersels K, Diliën H, van Grinsven B, Fujiwara RT, Cleij TJ. Point of Care Diagnostics in Resource-Limited Settings: A Review of the Present and Future of PoC in Its Most Needed Environment. Biosensors (Basel). 2020 Sep 24;10(10):133. doi: 10.3390/bios10100133.
139. Weigl BH, Neogi T, McGuire H. Point-of-Care Diagnostics in Low-Resource Settings and Their Impact on Care in the Age of the Noncommunicable and Chronic Disease Epidemic. J Lab Autom. 2014 Jun;19(3):248-57. doi: 10.1177/2211068213515246.
140. Estrela P, Kennedy RO. Point-of-Care Diagnostics in Low Resource Settings: Present Status and Future Role of Microfluidics. 2015:577-601. doi:10.3390/bios5030577
141. Alapan Y, Fraiwan A, Kucukal E, et al. Emerging point-of-care technologies for

sickle cell disease screening and monitoring. *Expert Rev Med Devices*. 2016;13(12):1073-1093. doi:10.1080/17434440.2016.1254038
142. Adachi K, Asakura T. The solubility of sickle and non-sickle hemoglobins in concentrated phosphate buffer. *J Biol Chem*. 1979;254(10):4079-4084. doi:10.1016/s0021-9258(18)50698-0
143. Yang X, Kanter J, Piety NZ, Benton MS, Vignes SM, Shevkoplyas SS. A simple, rapid, low-cost diagnostic test for sickle cell disease. *Lab Chip*. 2013;13(8):1464-1467. doi:10.1039/c3lc41302k
144. Henriques G, Phommasone K, Tripura R, et al. Comparison of glucose-6 phosphate dehydrogenase status by fluorescent spot test and rapid diagnostic test in Lao PDR and Cambodia. *Malar J*. 2018;17(1):1-7. doi:10.1186/s12936-018-2390-6
145. Mohapatra R, Warang P, Ghosh K, Colah R. Hemoglobinopathy screening by osmotic fragility test based on flow cytometer or naked eye. *Cytom Part B - Clin Cytom*. 2016;90(3):279-284. doi:10.1002/cyto.b.21205
146. Manglani M, Lokeshwar MR, Vani VG, Bhatia N, Mhaskar V. 'nestroft'-an effective screening test for beta thalassemia trait. 1997;34(August).
147. Piety NZ, Yang X, Lezzar D, George A, Shevkoplyas SS. A rapid paper-based test for quantifying sickle hemoglobin in blood samples from patients with sickle cell disease. *Am J Hematol*. 2015;90(6):478-482. doi:10.1002/ajh.23980
148. S.P.Shewale D. Study of Effectiveness of NESTROFT and Solubility Test as a Screening Test for the Detection of Haemoglobin Disorder at Nanded Region of Maharashtra. -. *Int J Heal Sci Res*. 2014;4(9):49-54.
149. Cole LA. The hCG assay or pregnancy test. *Clin Chem Lab Med*. 2012;50(4):617-630. doi:10.1515/cclm.2011.808
150. Mak WC, Beni V, Turner APF. Lateral-flow technology: From visual to instrumental. *TrAC - Trends Anal Chem*. 2016;79:297-305. doi:10.1016/j.trac.2015.10.017
151. Mcgann PT, Schaefer BA, Paniagua M, Howard TA, Ware RE. Characteristics of a rapid, point-of-care lateral flow immunoassay for the diagnosis of sickle cell disease. *Am J Hematol*. 2016;91(2):205-210. doi:10.1002/ajh.24232
152. Hewson W. On the figure and composition of the red particles of the blood, commonly called the red globules. *Philos Trans R Soc London*. 1773;63:303-323.
153. Lombard J. Once upon a time the cell membranes: 175 years of cell boundary research. *Biol Direct*. 2014;9(1):1-35. doi:10.1186/s13062-014-0032-7
154. I Shehadul Islam, M., Aryasomayajula, A., & Selvaganapathy, P.R. (2017). A Review on Macroscale and Microscale Cell Lysis Methods. Micromachines, 8. doi:10.3390/mi8030083
155. Parpart AK, Lorenz PB, Parpart ER, Gregg JR, Chase AM. THE OSMOTIC RESISTANCE (FRAGILITY) OF HUMAN RED CELLS . *J Clin Invest*. 1947;26(4):636-640.
156. Kattamis C, Efremov G, Pootrakul S. Effectiveness of one tube osmotic fragility screening in detecting β-thalassaemia trait. *J Med Genet*. 1981;18(4):266-270. doi:10.1136/jmg.18.4.266
157. Sumera A, Ahmed S, Ali SA, Khanani R. Evaluation of NESTROFT as a marker of differentiation between β- thalassemia trait & iron deficiency anemia. *Int J Collab Res Intern Med Public Heal*. 2012;4(8):1560-1566.
158. Piplani S, Manan R, Lalit M, Manjari M, Bhasin T, Bawa J. NESTROFT - A valuable, cost effective screening test for beta thalassemia traitin north indian punjabi population. *J Clin Diagnostic Res*. 2013;7(12):2784-2787.

doi:10.7860/JCDR/2013/6834.3759
159. Paleari R, Mosca A. Controversies on the osmotic fragility test. *Enerca News*. 2008;(September):3-5. doi:10.1016/S0954-349X(99)00004-1
160. Weatherall DJ, Clegg JB. Inherited haemoglobin disorders: An increasing global health problem. *Bull World Health Organ*. 2001;79(8):704-712.
161. Mindukshev I V., Krivoshlyk V V., Ermolaeva EE, et al. Necrotic and apoptotic volume changes of red blood cells investigated by low-angle light scattering technique. *Spectroscopy*. 2007;21(2):105-120. doi:10.1155/2007/629870
162. Remigante A, Morabito R, Marino A. Natural Antioxidants Beneficial Effects on Anion Exchange through Band 3 Protein in Human Erythrocytes. Antioxidants (Basel). 2019 Dec 26;9(1):25. doi: 10.3390/antiox9010025.
163. Hsu K, Bruce LJ. Exploring the Potential Roles of Band 3 and Aquaporin-1 in Blood CO 2 Transport – Inspired by Comparative Studies of Glycophorin B-A-B Hybrid Protein GP . Mur. 2018;9(June):1-10. doi:10.3389/fphys.2018.00733
164. Saradhadevi V, Sakthivel R, Selvam R, Parinandi N. Alterations in band 3 protein and anion exchange in red blood cells of renal failure patients. 2005;(August 2014):10-24. doi:10.1007/s11010-005-5904-9
165. Bonar PT, Casey JR, Bonar PT, Casey JR. Structure , mechanism and physiology Plasma membrane Cl - / HCO 3- exchangers Structure , mechanism and physiology. 2008;6950. doi:10.4161/chan.2.5.6899
166. Häusser, M. The Hodgkin-Huxley theory of the action potential. Nat Neurosci 3 (Suppl 11), 1165 (2000). https://doi.org/10.1038/81426
167. Association AH. An official journal of the American Heart Association Cell Swelling. 1973;XLVIII(3);48:455–458; doi.10.1161/01.CIR.48.3.455.
168. Gallagher PG. Review Article Disorders of erythrocyte hydration. 2017;130(25):2699-2708. doi:10.1182/blood-2017-04-590810
169. Miller, Margaret & Zachary, James. (2017). Mechanisms and Morphology of Cellular Injury, Adaptation, and Death11For a glossary of abbreviations and terms used in this chapter see E-Glossary 1-1. doi: 10.1016/B978-0-323-35775-3.00001-1.
170. Ivanov IT. Low pH-induced hemolysis of erythrocytes is related to the entry of the acid into cytosole and oxidative stress on cellular membranes. *Biochim Biophys Acta - Biomembr*. 1999;1415(2):349-360. doi:10.1016/S0005-2736(98)00202-8
171. Swietach P, Tiffert T, Mauritz JMA, et al. Hydrogen ion dynamics in human red blood cells. 2010;24:4995-5014. doi:10.1113/jphysiol.2010.197392
172. Introini V, Marin-Menendez A, Nettesheim G, et al. The erythrocyte membrane properties of beta thalassaemia heterozygotes and their consequences for Plasmodium falciparum invasion. *Sci Rep*. 2022;12(1):1-14. doi:10.1038/s41598-022-12060-4
173. Fujimoto. Band 3 Catalyzes Sickle Hemoglobin Polymerization. *Bone*. 2008;23(1):1-7. doi:10.1016/j.bpc.2009.10.004.Band
174. Ribeiro ML, Alloisio N, Almeida H, et al. Severe hereditary spherocytosis and distal renal tubular acidosis associated with the total absence of band 3. *Blood*. 2000;96(4):1602-1604.
175. Convery N, Gadegaard N. 30 Years of Microfluidics. *Micro Nano Eng*. 2019;2(May 2018):76-91. doi:10.1016/j.mne.2019.01.003
176. Madou M, Zoval J, Jia G, Kido H, Kim J, Kim N. Lab on a Cd. *Annu Rev Biomed Eng*. 2006;8(1):601-628. doi:10.1146/annurev.bioeng.8.061505.095758
177. Kinahan DJ, Early PL, Vembadi A, et al. From chip-in-a-lab to lab-on-a-chip:

towards a single handheld electronic system for multiple application-specific lab-on-a-chip (ASLOC). 2014;16. doi:10.1039/c6lc00568c
178. Teh S, Lin R, Hung L, Lee AP. Droplet microfluidics. 2008:198-220. doi:10.1039/b715524g
179. Bouza E, Sousa D, Rodrı M, Garcı J, Mun P. Is the Volume of Blood Cultured Still a Significant Factor in the Diagnosis of Bloodstream Infections ? □. 2007;45(9):2765-2769. doi:10.1128/JCM.00140-07
180. Ellett, F., Jorgensen, J., Marand, A.L. et al. Diagnosis of sepsis from a drop of blood by measurement of spontaneous neutrophil motility in a microfluidic assay. Nat Biomed Eng 2, 207–214 (2018). https://doi.org/10.1038/s41551-018-0208-z
181. Smet D De, Moer G Van, Martens GA, Nanos N. Use of the Cell-Dyn Sapphire Hematology Analyzer for Automated Counting of Blood Cells in Body Fluids. 2010:291-299. doi:10.1309/AJCPY7J7OLASZAPC
182. Sharma R, Sharma S. Physiology, Blood Volume. 2022 Apr 14. In: StatPearls [Internet]. Treasure Island (FL): StatPearls Publishing; 2022 Jan–. PMID: 30252333.
183. Sista, & Ng, & Nuffer, & Basmajian, & Coyne, Jacob & Elderbroom, & Hull, & Kay, & Krishnamurthy, & Roberts, & Wu, & Kennedy, & Singh, Raj & Srinivasan, & Pamula, Vamsee. (2020). Digital Microfluidic Platform to Maximize Diagnostic Tests with Low Sample Volumes from Newborns and Pediatric Patients. Diagnostics. 10. 21. 10.3390/diagnostics10010021.
184. Iakovlev AP, Erofeev AS, Gorelkin P V. Novel Pumping Methods for Microfluidic Devices: A Comprehensive Review. *Biosensors*. 2022;12(11). doi:10.3390/bios12110956
185. Chiu DT, Andrew J, Carlo D Di, et al. Small but Perfectly Formed ? Successes , Challenges , and Opportunities for Microfluidics in the Chemical and Biological Sciences. *CHEMPR*. 2017;2(2):201-223. doi:10.1016/j.chempr.2017.01.009
186. Cardoso R. Fabrication of low-cost peripherals for the operation of microfluidic devices. 2019.
187. Yager P, Edwards T, Fu E, et al. Microfluidic diagnostic technologies for global public health. *Nature*. 2006;442(7101):412-418. doi:10.1038/nature05064
188. Whitesides GM. The origins and the future of microfluidics. *Nature*. 2006;442(7101):368-373. doi:10.1038/nature05058
189. Chirag M Lakhani1 2, Arjun K Manrai1, 3, Jian Yang4, 5, Peter M Visscher#4, 5,*, and Chirag J Patel#1, 1Department BTT. 乳鼠心肌提取 HHS Public Access. *Physiol Behav*. 2019;176(3):139-148. doi:10.1016/j.physbeh.2017.03.040
190. Mao X, Huang TJ. HHS Public Access. 2019;12(8):1412-1416. doi:10.1039/c2lc90022j.Microfluidic
191. Kumar S, Bhushan P, Agarwal AK. Chapter 1 A Historical Perspective on Paper Micro fl uidic Based Point-of-Care Diagnostics. :1-5.
192. Andryukov BG. Six decades of lateral flow immunoassay: From determining metabolic markers to diagnosing covid-19. *AIMS Microbiol*. 2020;6(3):280-304. doi:10.3934/microbiol.2020018
193. Chiu DT, deMello AJ, Di Carlo D, et al. Small but Perfectly Formed? Successes, Challenges, and Opportunities for Microfluidics in the Chemical and Biological Sciences. *Chem*. 2017;2(2):201-223. doi:10.1016/j.chempr.2017.01.009
194. McNerney R. Diagnostics for developing countries. *Diagnostics*. 2015;5(2):200-209. doi:10.3390/diagnostics5020200
195. Brancaleoni V, Di Pierro E, Motta I, Cappellini MD. Laboratory diagnosis of

thalassemia. *Int J Lab Hematol*. 2016;38:32-40. doi:10.1111/ijlh.12527
196. Lazzari MA. Developing a Standard Protocol for the Introduction of New Testing Into a Clinical Laboratory: Appendix 1. *Lab Med*. 2009;40(7):389-393. doi:10.1309/lmqe6ij6r0vuvjhh
197. Society R, Sciences B. Laboratory Support for Rural Health Care [and Discussion] Author(s): S. S. Brown Source: Proceedings of the Royal Society of London . Series B , Biological Sciences , Vol . 209 , No . 1174 , More Technologies for Rural Health (Jul . 28 , 1980), pp . 119. 2019;209(1174):31-36.
198. Ward T, Faivre M, Abkarian M, Stone HA. Microfluidic flow focusing: Drop size and scaling in pressure versus flow-rate-driven pumping. *Electrophoresis*. 2005;26(19):3716-3724. doi:10.1002/elps.200500173
199. Byun CK, Abi-Samra K, Cho YK, Takayama S. Pumps for microfluidic cell culture. *Electrophoresis*. 2014;35(2-3):245-257. doi:10.1002/elps.201300205
200. Juarez A, Maynard K, Skerrett E, et al. AutoSyP: A low-cost, low-power syringe pump for use in low-resource settings. *Am J Trop Med Hyg*. 2016;95(4):964-969. doi:10.4269/ajtmh.16-0285
201. Wu J, Zheng G, Lee LM. Optical imaging techniques in microfluidics and their applications. *Lab Chip*. 2012;12(19):3566-3575. doi:10.1039/c2lc40517b
202. Bodansky M. Hemolytic Action of Inorganic Acids. *J Biol Chem*. 1928;79(1):229-239.
203. Fernandes HP, Cesar CL, Barjas-Castro M de L. Electrical properties of the red blood cell membrane and immunohematological investigation. *Rev Bras Hematol Hemoter*. 2011;33(4):297-301. doi:10.5581/1516-8484.20110080
204. Novák P, Havlíček V. Protein Extraction and Precipitation. *Proteomic Profiling Anal Chem Crossroads Second Ed*. 2016:52-62. doi:10.1016/B978-0-444-63688-1.00004-5
205. Holik H, Heß H, Müller W, Lüdtke O. Unit Operations. *Handb Pap Board Second Ed*. 2013;1:351-472. doi:10.1002/9783527652495.ch7
206. Sadjadian P, Wille K, Griesshammer M. Ruxolitinib-associated infections in polycythemia vera: Review of the literature, clinical significance, and recommendations. *Cancers (Basel)*. 2020;12(11):1-14. doi:10.3390/cancers12113132
207. Hughes I, Hase T. *Measurements and Their Uncertainties*. Oxford University Press; 2010.
208. Huang YX, Wu ZJ, Mehrishi J, et al. Human red blood cell aging: Correlative changes in surface charge and cell properties. *J Cell Mol Med*. 2011;15(12):2634-2642. doi:10.1111/j.1582-4934.2011.01310.x
209. Thiagarajan P, Parker CJ, Prchal JT. How Do Red Blood Cells Die? *Front Physiol*. 2021;12(March):8-10. doi:10.3389/fphys.2021.655393
210. D'Alessandro A, Blasi B, D'Amici GM, Marrocco C, Zolla L. Red blood cell subpopulations in freshly drawn blood: Application of proteomics and metabolomics to a decades-long biological issue. *Blood Transfus*. 2013;11(1):75-87. doi:10.2450/2012.0164-11
211. Diez-Silva M, Dao M, Han J, Lim C-T, Suresh S. Shape and Biomechanical Characteristics of Human Red Blood Cells in Health and Disease. *MRS Bull*. 2010;35(5):382-388. doi:10.1557/mrs2010.571
212. Thomas C, Chb MB, Lumb AB, Bs MB. Physiology of haemoglobin. 2012;12(5):251-256. doi:10.1093/bjaceaccp/mks025
213. Thurnham D, Northrop-Clewes C. Biomarkers for the differentiation of anemia

and their clinical usefulness. *J Blood Med*. 2013:11. doi:10.2147/jbm.s29212
214. Benner A, Patel AK, Singh K, Dua A. Physiology, Bohr Effect. 2022 Aug 8. In: StatPearls [Internet]. Treasure Island (FL): StatPearls Publishing; 2022 Jan–. PMID: 30252284.
215. Doyle J, Cooper JS. Physiology, Carbon Dioxide Transport. [Updated 2022 Jul 5]. In: StatPearls [Internet]. Treasure Island (FL): StatPearls Publishing; 2022 Jan-.https://www.ncbi.nlm.nih.gov/books/NBK532988/.
216. Martínez-Velilla N, Ibáñez B, Cambra K, Alonso-Renedo J. Red blood cell distribution width, multimorbidity, and the risk of death in hospitalized older patients. *Age (Omaha)*. 2012;34(3):717-723. doi:10.1007/s11357-011-9254-0
217. Nishad AAN, De Silva IS, Perera HL, Pathmeswaran A, Kastutiratne KTAA, Premawardhena AP. Role of red cell distribution width in screening for Hb E trait in population screening for hemoglobin disorders. *J Pediatr Hematol Oncol*. 2014;36(8):e490-e492. doi:10.1097/MPH.0000000000000052
218. Walker HK, Hall WD, Hurst JW, editors. Clinical Methods: The History, Physical, and Laboratory Examinations. 3rd ed. Boston: Butterworths; 1990. PMID: 21250045.
219. Li N, Zhou H, Tang Q. Review Article Red Blood Cell Distribution Width : A Novel Predictive Indicator for Cardiovascular and Cerebrovascular Diseases. 2017;2017(Mcv). doi:10.1155/2017/7089493
220. Eleftheriou A. HAEMOGLOBIN DISORDERS IN EUROPE: A SYSTEMATIC EFFORT OF IDENTIFYING AND ADDRESSING UNMET NEEDS AND CHALLENGES BY THE THALASSAEMIA INTERNATIONAL FEDERATION. 2021:1-15.
221. Akhavan-Niaki H, Youssefi Kamangari R, Banihashemi A, et al. Hematologic features of alpha thalassemia carriers. *Int J Mol Cell Med*. 2012;1(3):162-167. http://www.ncbi.nlm.nih.gov/pubmed/24551772%0Ahttp://www.pubmedcentral.nih.gov/articlerender.fcgi?artid=PMC3920506.
222. Vives-Corrons JL, Krishnevskaya E, Rodriguez IH, Ancochea A. Characterization of hereditary red blood cell membranopathies using combined targeted next-generation sequencing and osmotic gradient ektacytometry. Int J Hematol. 2021 Feb;113(2):163-174. doi: 10.1007/s12185-020-03010-
223. Barcellini W, Bianchi P, Fermo E, et al. Hereditary red cell membrane defects: Diagnostic and clinical aspects. *Blood Transfus*. 2011;9(3):274-277. doi:10.2450/2011.0086-10
224. Maciak K, Adamowicz-Salach A, Siwicka A, et al. Hereditary xerocytosis - spectrum and clinical manifestations of variants in the PIEZO1 gene, including co-occurrence with a novel β-globin mutation. *Blood Cells, Mol Dis*. 2020;80(October 2019):102378. doi:10.1016/j.bcmd.2019.102378
225. Archer N, Shmukler BE, Andolfo I, et al. Hereditary Xerocytosis Revistited. *Am J Hematol*. 2014;89(12). doi:10.1002/ajh.23799
226. Dean L. 1 Blood and the cells it contains. In: *Blood Groups and Red Cell Antigens*. ; 2005:1-8.
227. Gottlieb Y, Topaz O, Cohen LA, et al. Physiologically aged red blood cells undergo erythrophagocytosis in vivo but not in vitro. *Haematologica*. 2012;97(7):994-1002. doi:10.3324/haematol.2011.057620
228. Bunyaratvej A, Butthep P, Sae-Ung N, Fucharoen S, Yuthavong Y. Reduced deformability of thalassemic erythrocytes and erythrocytes with abnormal hemoglobins and relation with susceptibility to Plasmodium falciparum invasion. *Blood*. 1992;79(9):2460-2463. doi:10.1182/blood.v79.9.2460.2460

229. Emilse LAM, Cecilia H, María TM, Eugenia MM, Alicia IB, Lazarte SS. Cryohemolysis, erythrocyte osmotic fragility, and supplementary hematimetric indices in the diagnosis of hereditary spherocytosis. *Blood Res*. 2018;53(1):10-17. doi:10.5045/br.2018.53.1.10
230. Méndez-Mora L, Cabello-Fusarés M, Ferré-Torres J, et al. Blood Rheological Characterization of β-Thalassemia Trait and Iron Deficiency Anemia Using Front Microrheometry. *Front Physiol*. 2021;12(October):1-13. doi:10.3389/fphys.2021.761411
231. Kato GJ, Steinberg MH, Gladwin MT. Intravascular hemolysis and the pathophysiology of sickle cell disease. *J Clin Invest*. 2017;127(3):750-760. doi:10.1172/JCI89741
232. Bogdanova A, Kaestner L, Simionato G, Wickrema A, Makhro A. Heterogeneity of Red Blood Cells: Causes and Consequences. *Front Physiol*. 2020;11(May):1-11. doi:10.3389/fphys.2020.00392
233. Qurtom HA, Al-Saleh QA, Lubani MM, et al. The value of red cell distribution width in the diagnosis of anaemia in children. *Eur J Pediatr*. 1989;148(8):745-748. doi:10.1007/BF00443100
234. Kim J, Lee H, Shin S. Advances in the measurement of red blood cell deformability: A brief review. *J Cell Biotechnol*. 2015;1(1):63-79. doi:10.3233/jcb-15007
235. Andrade C. Sample Size and its Importance in Research. *Indian J Psychol Med*. 2020;41. doi:10.4103/IJPSYM.IJPSYM
236. Shim YJ, Jung HL, Shin HY, et al. Epidemiological study of hereditary hemolytic anemia in the Korean pediatric population during 1997-2016: A nationwide retrospective cohort study. *J Korean Med Sci*. 2020;35(33):1-14. doi:10.3346/JKMS.2020.35.E279
237. Andolfo I, Martone S, Rosato BE, et al. Complex modes of inheritance in hereditary red blood cell disorders: A case series study of 155 patients. *Genes (Basel)*. 2021;12(7):1-15. doi:10.3390/genes12070958
238. Mohandas N. | HEMOLYTIC ANEMIA: A CORNUCOPIA OF CAUSES | Inherited hemolytic anemia: a possessive beginner's guide. 2018:377-381.
239. Brugnara C. Sickle cell dehydration: Pathophysiology and therapeutic applications. *Clin Hemorheol Microcirc*. 2018;68(2-3):187-204. doi:10.3233/CH-189007

- END -